2008

Systematic analysis of structure-function relationships of conserved sequence motifs in the NADH-binding lobe of cytochrome b5 reductase

Glenn W. Roma
University of South Florida

Systematic Analysis of Structure-Function Relationships of Conserved Sequence Motifs in the NADH-Binding Lobe of Cytochrome b_5 Reductase

by

Glenn W. Roma

A dissertation submitted in partial fulfillment
of the requirements for the degree of
Doctor of Philosophy
Department of Biochemistry and Molecular Biology
College of Medicine
University of South Florida

Major Professor: Michael J. Barber, D.Phil.
Ronald K. Keller, Ph.D.
Duane Eichler, Ph.D.
Eric S. Bennett, Ph.D.

Date of Approval:
July 15, 2008

Keywords: flavoprotein, transhydrogenases, oxidoreductases, methemoglobinemia, mutagenesis.

This work is dedicated to my mother, Linda Roma and my father, Ralph Roma. Thank you for a life time of support and belief.

ACKNOWLEDGEMENTS

I would like to thank Professor Michael J. Barber, D.Phil. for offering me the opportunity to achieve this goal. His guidance, input, direction, and, most importantly, his support, have allowed me to succeed. A special thank you to my dissertation committee members, Professor Duane C Eichler, Ph.D., Professor Larry P. Solomonson, Ph.D., Professor Eric Bennett, Ph.D., and my committee chairperson Professor Ronald K. Keller, Ph.D., for all of your instruction, constructive criticism, ideas, input, and always offering your encouragement to me. To my friend and former lab mate, Louis J Crowley PhD., for your guidance and assistance when I first entered the lab, and your input and honesty in professional and personal matters. To Joshua Smith, for your invaluable assistance in keeping the lab working efficiently, helping keep me sane when things became hectic and overwhelming, and for being a true friend and brother. To Jamie Melichar, for your assistance in running experiments and collecting valuable data. To my parents, Linda and Ralph Roma, for your constant love, vigilance, support, and belief in me my whole life, and for providing an environment that helped encourage and push me on to accomplish all that I can. And to my wonderful girlfriend, Jessica Provenzano, for you constant support and interest in my confusing science world and for the love and companionship you have given me over the years and that I look forward to enjoying for the rest of our lives.

TABLE OF CONTENTS

LIST OF TABLES

LIST OF FIGURES

LIST OF ABBREVIATIONS

A	alanine
Å	angstrom (1Å = 0.1 nm)
ADP	adenosine-5'-diphosphate
ADP-ribose	adenosine-5'-diphosphoribose
Amp	ampicillin
$APAD^+$	3-acetylpyridine adenine dinucleotide (oxidized)
$APHD^+$	acetylpyridine hypoxanthine dinucleotide (oxidized)
ATP	adenosine-5'-triphosphate
bp	base pair
C	cysteine
$CaCl_2$	calcium chloride
cb5	cytochrome b_5
cb5r	cytochrome b_5 reductase
CD	circular dichroism
CPK	Corey, Pauling, and Kultun (molecular coloring scheme)
D	aspartate
DEAE	diethylaminoethyl
E	glutamate

EDTA	ethylenediaminetetraacetic acid
EtBr	ethidium bromide
F	phenylalanine
FAD	flavin adenine dinucleotide
$FADH^{\bullet-}$	flavin adenine dinucleotide, semiquinone
$FADH_2$	flavin adenine dinucleotide, dihydroquinone
FMN	flavin mononucleotide
FNR	ferredoxin:$NADP^+$ reductase
FPLC	fast protein liquid chromatography
g	gram
G	glycine
H	histidine
H_4NAD	tetrahydronicotinamide adenine dinucleotide
I	isoleucine
IPTG	isopropyl-thio-β-galactoside
IR	infrared
K	lysine
k_{cat}	turnover number
K_d	dissociation constant
K_m	Michaelis constant, pseudo-first order binding constant
K_s	spectral binding constant
Kan	kanamycin
KPi	potassium phosphate

L	leucine
LB	Luria broth
M	methionine
MALDI-TOF	matrix-assisted laser desorption ionization-time of flight
metHb	methemoglobin
$MgCl_2$	magnesium chloride
MOPS	3-(*N*-Morpholino) propanesulfonic acid
mV	millivolt
MW	molecular weight
m/z	mass/charge ratio
μM	micro molar
N	asparagine
NaCl	sodium chloride
NAD^+	β-nicotinamide adenine dinucleotide (oxidized)
α-NAD^+	α-nicotinamide adenine dinucleotide (oxidized)
ε-NAD^+	1,N6-ethenonicotinamide adenine dinucleotide (oxidized)
o-NAD^+	nicotinamide adenine dinucleotide bis(dialdehyde) (oxidized)
NADH	β-nicotinamide adenine dinucleotide (reduced)
NADH:BR	NADH:cytochrome b_5 reductase
NADH:FR	NADH:ferricyanide reductase
NHD^+	3-nicotinamide hypoxanthine dinucleotide
nm	nanometer

NR	nitrate reductase
OH	hydroxyl group
P	proline
$PAAD^+$	3-pyridinealdehyde adenine dinucleotide
PAGE	polyacrylamide gel electrophoresis
PCA^+	3-pyridine carboxylic acid (oxidizied)
PCR	polymerase chain reaction
PDR	phthalate dioxygenase reductase
Pfu	*Pyrococcus furiosus*
PMSF	phenylmethylsulfonyl fluoride
Q	glutamine
R	arginine
S	serine
SDS	sodium dodecyl sulfate
SHE	standard hydrogen electrode
SOB	sterile osmotic broth
T	threonine
TB	terrific broth
T_{50}	thermal stability constant
$TNAD^+$	thionicotinamide adenine dinucleotide
Tris-HCl	tris(hydroxymethyl) aminomethane-hydrochloric acid
UV	ultraviolet
V	valine

W	tryptophan
WT	wild type
Y	tyrosine

Systematic Analysis of Structure-Function Relationships of

Conserved Sequence Motifs in the NADH-Binding

Lobe of Cytochrome b_5 Reductase

Glenn W. Roma

ABSTRACT

NADH:Cytochrome b_5 Reductase (cb5r) catalyzes the reduction of the ferric iron (Fe^{3+}) atom of the heme cofactor found within cytochrome b_5 (cb5) by the reduction of the FAD cofactor of cb_5r from reducing equivalents of the physiological electron donor, reduced nicotinamide adenine dinucleotide (NADH). Cb5r is characterized by the presence of two domains necessary for proper enzyme function: a flavin-binding domain and a pyridine nucleotide-binding domain. Within these domains are highly conserved "motifs" necessary for the correct binding and orientation of both the NADH coenzyme and the FAD cofactor.

To address the importance of these conserved motifs, site-directed mutagenesis was utilized to generate a series of variants of residues located within the motifs to allow for the full characterizations. Second, naturally occurring recessive congenital methemoglobinemia (RCM) mutants found in proximity to these highly conserved motifs were analyzed utilizing site-directed mutagenesis. In addition, a canine variant of the cb5r soluble domain was cloned, generated and characterized and

compared with the WT rat domain.

The canine construct showed a high degree of sequence homology to that of the corresponding human and rat sequences. Characterization of the canine variant indicated that it possessed comparable functional characteristics to the rat variant.

Investigation of the pyrophosphate-associating residues, Y112 and Q210, indicated that each played a role in the proper association and anchoring of NADH to the enzyme. The RCM type I mutants, T116S and E212K, caused a moderate decrease in efficiency of the enzyme. The presence of both mutations interact synergistically to generate a more substantially decreased function.

Analysis of the "^{180}GtGitP^{185}" NADH-binding motif and the preceding residue G179 revealed that these residues are vital in enabling proper NADH association. The residues of this motif were shown to be important in determining nucleotide specificity and properly positioning the NADH and flavin cofactor for efficient electron transfer. RCM variants A178T and A178V were shown to decrease catalytic efficiency or protein stability respectively, leading to disease phenotype.

Analysis of the NADH-binding motif "^{273}CGxxxM^{278}" indicated that this motif facilitates electron transfer from substrate to cofactor and is important in release of NAD^+ from the enzyme after electron transfer.

1. INTRODUCTION

Electron Transfer

Electron transfer is the process by which one electron moves from one atom or molecule to another. It is a mechanistic representation of the thermodynamic principle of oxidation-reduction. Numerous biological processes are dependent upon the proper transfer of electrons, including photosynthesis and respiration. Additionally, pathways involved in metabolism and detoxification are dependent upon appropriate electron transfer reactions. Regardless of the intended function, the ability of the cell to harness the energy from dietary and storage molecules is dependent upon converting energetic raw materials of macromolecules to a usable form. To this end, cells use a limited number of molecules to couple reactions. Most notable of these molecules are nucleotides such as ATP/ADP, NAD(P)/NADP(H), and FAD/$FADH_2$. The reducing power of these latter molecules is used to drive many reactions in anabolic pathways in the cell that would not normally occur due to unfavorable energy requirements.

In biological systems, the majority of enzymes involved in electron transfer reactions do so by the use of cofactor molecules and coenzymes which alter the electrostatic potential of the enzymes active site. These components span a large range of redox potentials, enabling them to carry out a large variety of processes within and equally widely varied number of environments and conditions. Electron transfer

reactions often utilize transition metal complexes, though many examples of organic molecules are now known. Common cofactors utilized to carry out electron transfer in cells include metal compounds such as Fe-S clusters, hemes and other porphyrin ring structures, and highly conjugated ring like those present in flavin nucleotides. Many complex electron transfer systems maximize the ability to move energy by clustering several such cofactors within a multi-center complex. Electrons are free to move through the electrochemical gradient by passing from one factor to the next. In other cases, systems show less efficiency by having separate compartments, but are able to interact with a variety of donor and acceptor molecules. Multiple examples of enzymes of each condition exist. Indeed, the list would be quite long. Virtually every oxidation or reduction reaction that occurs in the cell is catalyzed and regulated by an electron transfer protein. In general, electron transfer proteins serve to couple energetically unfavorable endergonic reactions to energy releasing exergonic reactions.

Methemoglobin

Methemoglobin is the form of hemoglobin in which the iron atom of the heme prosthetic group is present in the oxidized, or ferric (Fe^{3+}) state, compared to the reduced, or ferrous (Fe^{2+}) state found in normal hemoglobin. For tetrameric hemoglobin, this corresponds to a four-electron loss. Since methemoglobin is incapable of binding molecular oxygen this results in a loss of biological function of the hemoglobin molecule.

Observations from as early as the nineteenth century showed that methemoglobin could be generated in red blood cells in a variety of ways. Table I illustrates the assortment of toxic compounds that, when ingested, generate varying levels of

methemoglobin depending on the nature of the compound. This is typical in third-world countries where poor water supplies and living conditions often lead to high levels of nitrates in common well water sources [1]. Methemoglobin is also generated as a result of a reaction to certain drugs that are used in treating patients for various conditions including dapsone, local anesthetics, and anti-malarial drugs [2]. Additionally, methemoglobin is produced as a result of certain hereditary disorders.

Table I. Compounds Capable of Generating Methemoglobin.

Acetanlid	Chlorates	Lidocaine Hydrochloride	Phenacitin
Alloxan	Chloroquine	Naphthalene	Phenytoin
Aniline dyes	Dapsone	Nitrates	Pyridium
Aromantic Amines	Dimethyl Sulfoxide	Nitric Oxide	Resorcinol
Arsine	Dimethyltoluidine	Nitrites	Rifampin
Benzene Derivatives	Dinitrophenol	Nitrofuran	Silver Nitrate
Benzocaine	Ferricyanide	Nitroglycerine	Sulfasalazine
Bivalent Copper	Flutamide	Nitrophenol	Sulfonamides
Bismuth Subnitrate	Hydroxylamine	Nitrosobenzene	Trinitrotoluene

The steady-state levels of methemoglobin within normal erythrocytes is very low, corresponding to <1% total hemoglobin, indicating that the capacity to reduce methemoglobin far exceeds the rate of hemoglobin oxidation [3]. Methemoglobin homeostasis shows that electrons for methemoglobin reduction are generated in a variety of reactions. Primarily amongst these is the glycolytic pathway, which generates reducing equivalents in the form of NADH. However, the rapid reduction of methemoglobin by non-glycolytic substrates suggests that additional pathways may be involved with the generation of NADH, perhaps in response to elevate levels of methemoglobin. The steady-state levels of methemoglobin are a consequence of the methemoglobin-reducing reactions as well as the methemoglobin-generating reactions in erythrocytes.

Concentrations of methemoglobin in erythrocytes can become elevated as a result of accelerated oxidation or decreased reduction resulting from either environmental factors such as those described earlier or from hereditary abnormalities. The most frequent cause of methemoglobinemia is rapid oxidation resulting from ingestion of toxic compounds which are oxidants, or give rise to oxidants, such as peroxide and oxygen radicals, during their metabolism [3]. Methemoglobinemia also arises from oxidation of mutant hemoglobin belonging to the hemoglobin M class [4]. Methemoglobinemia resulting from decreased rates of reduction is most commonly the result of a deficiency in cytochrome b_5 reductase (cb5r) found in circulating erythrocytes. The most infrequent cause of decreased methemoglobin reduction has been attributed to deficiency in cytochrome b_5 (cb5) [5]. These latter two cases form the basis of the disease known as recessive congenital methemoglobinemia (RCM).

History of Methemoglobinemia

Methemoglobinemia stemming from decreased functionality of cb5r, now known as recessive congenital methemoglobinemia (RCM), is an extremely rare disorder that has been under investigation for over one year and the French physician, Francios, detailed an individual with long-standing cyanosis lacking any obvious signs of cardiac or pulmonary abnormalities [6]. Another vital piece of the puzzle was determined in 1891 when it was first suggested that methemoglobin was reduced to hemoglobin in circulating erythrocytes [7]. Forty years later, while describing a familial incidence of idiopathic cyanosis, Hitzenberger suggested the possibility of congenital, familial methemoglobinemia [8].

These key findings and others culminated in the classic investigations performed by Quentin Gibson at Queen's University, Belfast. Gibson's patients were two brothers, Russell and Fred Martin from Banbridge in Northern Ireland. The brothers presented with a blue appearance. At the time, Dr. James Deeny, a local physician, advocated the use of ascorbic acid in the treatment of heart disease, and his work demonstrated the benefits of vitamin C [9]. When Russell was treated with vitamin C, the cyanosis was ameliorated and he turned pink. Although Deeny assumed that he had corrected an underlying heart condition, cardiologists could find no cardiac abnormality in either brother. The physiologist Henry Barcroft carried out a detailed study of these cases during treatment and found elevated levels of methemoglobin [10]. Following this, Quentin Gibson conducted further work which correctly identified the pathway involved in the reduction of methemoglobin. This was the first description of an hereditary trait involving a specific enzyme deficiency [11]

In 1959, Scott and Griffith identified a normal human erythrocitic enzyme that catalyzed methemoglobin reduction in the presence of reduced nicotinamide adenine dinucleotide (NADH). They called this enzyme "diaphorase" [12]. Following further analyses, this enzyme was given additional names, including NADH-dehydrogenase, NADH-methemoglobin reductase, NADH-methemoglobin-ferricyanide reductase, or NADH-ferricyanide reductase. It was also demonstrated at this time that a deficiency in this enzyme resulted in hereditary methemoglobinemia. This deficiency was observed in diverse populations including Athabaskan Indians (Eskimos) of Alaska [13] and Navajo Indians [14], as well as an isolated community, the 'blue Fugates' living in the Blue-Ridge Mountains of Kentucky [15]. It was later demonstrated that a generalized

deficiency of cb5r occurred in cases of methemoglobinemia with mental retardation. The enzyme may be identical to NADH diaphorase. Leukocytes of patients with neurological disorder lack cb5r, whereas the enzyme is normal in others. [16]. Previously, NADH-cb5r (cb5r) and was shown to be involved, with the participation of cytochrome b_5, in methemoglobin reduction within erythrocytes [17]. The combined cb5r -cb_5 redox system is the most important for the conversion of methemoglobin to hemoglobin in circulating erythrocytes, and the activity of this system is dramatically reduced in the erythrocytes of patients described with enzymopenic hereditary methemoglobinemia, or RCM.

Cytochrome b_5 Reductase

NADH:Cytochrome b_5 reductase (cb5r, EC 1.6.6.2) is a member of the ferredoxin:$NADP^+$ reductase super-family of flavoprotein transhydrogenases [18] which catalyze the transfer of reducing equivalents between nicotinamide dinucleotides and one electron carriers. Notable members of this family include ferredoxin:$NADP^+$ reductase (FNR) [19], plant and fungal NAD(P)H:nitrate reductase [20], NADPH: cytochrome P450 reductase [21], NADPH:sulphite reductase, phthalate dioxygenase reductase [22], and nitric oxide synthase [23]. The enzymes found within this flavoprotein family have been demonstrated to possess distinct structural domains responsible for flavin-binding and pyridine nucleotide-binding. Cytochrome b_5 reductase catalyzes the single electron reduction of ferricytochrome b_5 to ferrocytochrome b_5 using the reduced pyridine nucleotide NADH as the physiological electron donor. The rate-limiting step in catalysis has been identified as a hydride ion transfer step involving the donation of one proton and two electrons from the nicotinamide moiety of NADH to the oxidized FAD prosthetic

group of cb5r [24]. Additionally, in mammalian species, microsomal and cytosolic cb5r isozymes provide reducing equivalents for a variety of physiologically important metabolic processes that include methemoglobin reduction [17, 25], fatty acid elongation and desaturation [26], cholesterol biosynthesis [27] and the cytochrome P450-mediated hydroxylations of steroid hormones and xenobiotics [28], such as the reaction catalyzed by cytochrome P450 3A4 [29] and the reduction of *N*-hydroxylamine [30]. Recently, it has been shown to be part of the microsomal cytochrome b_5 reductase-cytochrome b_5 pathway directly involved in the reductive detoxification of arylhydroxylamine carcinogens in human liver [31].

Cytochrome b_5 reductase is encoded by the *DIA1* gene (Figure 1), located on the human chromosome 22q13-qter [33, 34]. It transcribes two isoforms of cb5r by the use of alternative promoters [16, 35]. Each isoform is localized to separate regions of the cell and thus perform separate functions. The first isoform is the microsomal isozyme generated through the transcription of all 9 exons of the *DIA1* gene. The microsomal isozyme comprises 300 amino acid residues with a molecular weight of ~34 kDa. This isozyme, primarily localized to the cytosolic face of the endoplasmic reticulum, is also found associated with the mitochondrial, nuclear, and plasma membranes of somatic cells. The amino terminal 25 amino acids of the isozyme are primarily hydrophobic [36, 37] allowing for the microsomal association. Additionally, a myristoylation signature sequence has been shown to be present in this 25 amino acid region, believed to be involved in cb5r's membrane association [38]. The microsomal form of the enzyme accounts for the majority of the transcribed protein and is responsible for the majority of the electron transfer reactions described above, excluding methemoglobin reduction.

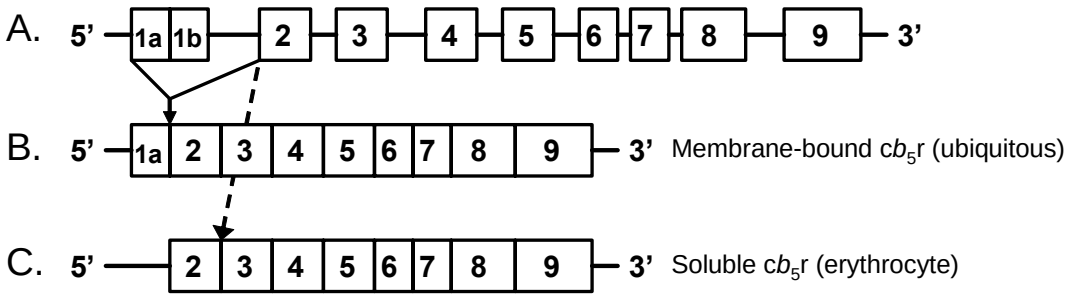

Figure 1. Structure of the Human *DIA1* Gene that Encodes Cytochrome b_5 Reductase. The *DIA1* gene (A) is composed of exons 1-9 [32]. There are two alternate transcription start sites, 1a and 1b, which yield the two isoforms of cb5r. (B) Represents the membrane-bound cb5r isoform containing exon 1a-9, but not 1b, and consists of 300 amino acids (**GAQL→CFVF**), including the myristoylation signature in exon 1a. (C) Represents the soluble cb5r isoform containing exons 2-9, but not exon 1, and consisting of the 275 amino acids that comprise the diaphorase domain (**LFQR→CFVF**).

The second isoform corresponds to the soluble, truncated form of cb5r. It is comprised of only exons 2-9 of the *DIA1* gene producing a 275 amino acid residue soluble form of cb5r, having a mass of ~31kDa. It is this form that is found primarily in circulating erythrocytes and is responsible, via interaction with cb5, for the reduction of methemoglobin to hemoglobin [17, 39]. In 1992, it was demonstrated that this truncated isoform is produced by the use of alternative promoter/alternate exons: the full length membrane-binding transcript is generated from an upstream housekeeping promoter, while the erythrocyte transcript originates from a downstream, erythroid-specific promoter [40]. Later, it was shown that the soluble form contains a non-coding new first exon located between the first 2 exons of the human cb5r gene previously identified. In addition, this new first exon shares 62% homology with the first exon and its 3-prime-flanking intron sequences of rat erythroid-specific b5R mRNA, whereas the 5-prime flanking region of the new first exon possesses features of a housekeeping gene [41].

The mechanism of electron transfer for the soluble form of cb5r from the physiological substrate, NADH and the FAD cofactor of cb5r is shown in Figure 2. In this schematic, two electrons are first transferred from NADH to FAD by a hydride ion

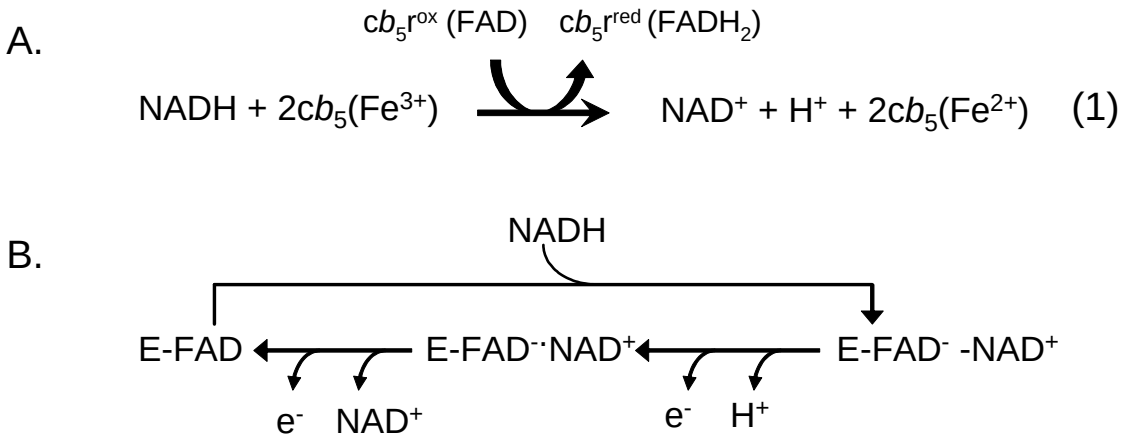

Figure 2. Mechanism of Cytochrome b_5 Reductase Mediated Cytochrome b_5 Reduction. (A) represents the chemical reaction (equation 1) catalyzed by cb5r . (B) illustrates the mechanism of cb5r transfer where each electron (e^-) reduces one molecule of cb_5 [42].

(H^-) transfer. The two-electron reduced enzyme-NAD^+ complex (E-FADH—NAD^+) then transfers one electron to each of two separate molecules of cb5 (E-$FAD^{\cdot-}$ - NAD^+), which returns the reduced enzyme to its oxidized state [43]. The reduction of FAD by NADH has been determined to be the rate-limiting step in the electron transfer process catalyzed by cb5r [44-46]. In the porcine variant of cb5r , it was also determined that the binding of NAD^+ stabilized the anionic red semiquinone of FAD [47, 48]. Further studies by Meyer *et al.* showed that binding of NAD^+ also modulates the electron transfer to cb5 [49], demonstrating the importance of the anionic red semiquinone form of cb5r (E-$FAD^{\cdot-}$ - NAD^+) in the catalytic process. Recent studies by Iyanagi *et al*. generated a

new scheme for the electron transfer sequence of cb5r involving the neutral blue semiquinone form and the oxidized enzyme-NADH-NAD^+ ternary complex (Figure 3) [43].

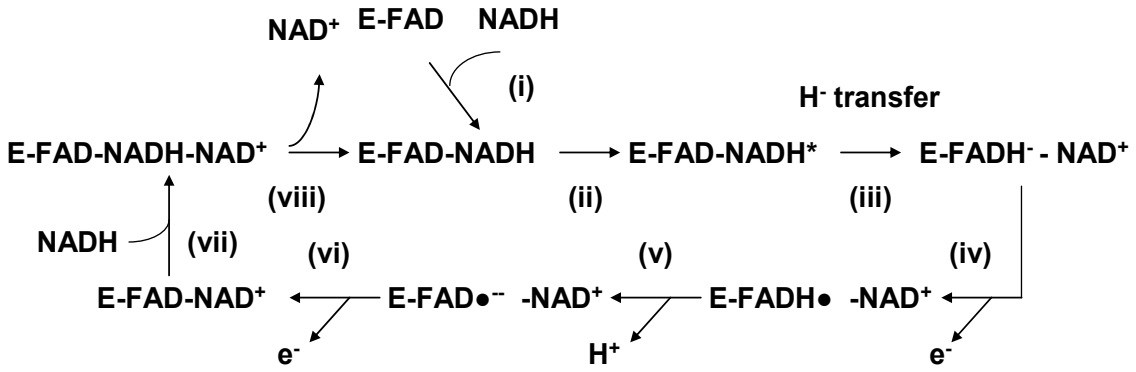

Figure 3. New Model of the Reaction Sequence of Cytochrome b_5 Reductase. This new model represents the reaction sequence of cytochrome b_5 reductase containing the neutral blue semi-quinone form and the oxidized enzyme-NADH-NAD^+ ternary complex as intermediates [43].

This scheme involves the following seven-step process: (i) formation of the oxidized enzyme-NADH complex (E-FAD-NADH), (ii) conversion of E-FAD-NADH to a form that has the ability to transfer a hydride ion (E-FAD-NADH), (iii) hydride (H^-) transfer from NADH to FAD, (iv) the first one-electron transfer from the two-electron reduced enzyme complex (E-$FADH^-$-NAD^+), (v) rapid conversion of the neutral blue semiquinone form (E-$FADH\cdot^-$-NAD^+) to the anionic red semiquinone form (E-$FAD\cdot^-$-NAD^+), (vi) the second one-electron transfer from E-$FAD\cdot^-$-NAD^+, (vii) formation of the oxidized enzyme-NADH-NAD^+ ternary complex (E-FAD-NADH-NAD^+) by binding of NADH, and finally (viii) release of NAD^+.

Recessive Congenital Methemoglobinemia

The efficiency of oxygen transport from the lungs to the extremities cannot occur without a properly functioning cb5r –cb5 electron transport system. A result of alterations to this system causes a deficiency in methemoglobin reduction and leads to the manifestation of the disease methemoglobinemia. The first sign of the onset of this disease is the characteristic bluish coloration of the skin illustrated in Figure 4. This coloration is common in newborns since the methemoglobin reducing capacity of their erythrocytes is only 50-60% that of an adult and this medical condition is commonly known as "blue baby syndrome". The disease can arise from various environmental as well as genetic factors.

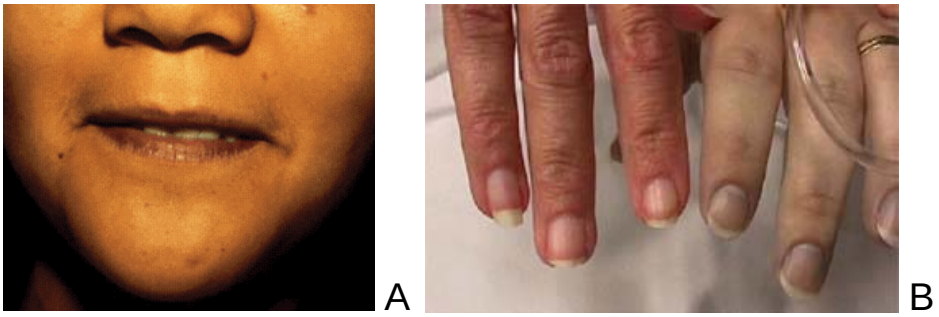

Figure 4. Clinical Indications of Cyanosis as a Result of Increased Levels of Methemoglobin in the Blood (A) This patient has the characteristic darkened or "chocolate brown" lips, which occurs when methemoglobin levels reach 10-20% total hemoglobin [50]. (B) A patient with drug-induced methemoglobinemia causing the noticeable bluish coloration of the skin (right) [51].

This disease, now classified as recessive congenital methemoglobinemia (RCM, OMIM 250800), arises from defects related to cb5r functionality and was the first disease to be directly associated with enzyme deficiency [52]. The most common cause of

recessive congenital methemoglobinemia (RCM) is a deficiency in the function of cb5r. This function is critical since elevated levels of methemoglobinemia give rise to cellular hypoxia, which results in death when levels of methemoglobin reach 70% or greater. Levels of methemoglobin concentration with corresponding symptoms are shown in Table II. Individuals with RCM are unable to effectively control the increasing levels of reduced methemoglobin continuously being formed through the deoxygenation of hemoglobin in circulating erythrocytes. Defects in the expression of cb5r give rise to two major clinical-biochemical classifications of methemoglobinemia, simply known as type I and type II, which are classified based on the patient pathophysiology.

Type I RCM, exhibited by the majority of patients, is due primarily to a deficiency of the soluble form of cb5r found in circulating erythrocytes. This form of methemoglobinemia is inherited in an autosomal recessive pattern. Though exhibited worldwide, type I RCM has been shown to be endemic in certain populations including the Athabaskan Alaskans, Navajo Indians, and Yakutsk natives of Siberia. Those individuals with type I RCM have methemoglobin concentrations ranging between 10 to 40%. The predominant symptom of type I RCM is a well-tolerated cyanosis that may result in additional mild complaints such as headaches, fatigue, and shortness of breath during exercise. Life expectancy of these patients is unaffected.

Type II RCM represents a significantly more severe form of the disorder and occurs in less than 10-15% of patients where the defect is attributed to a generalized cb5r deficiency, which includes the membrane-associated form present in somatic cells [3]. Type II RCM results in severe developmental abnormalities including mental retardation, microcephaly, opisthotonus, strabismus, and generalized hypertonia often leading to

premature death [12, 53, and 54]. A third form of RCM, type III, which occurs with a substantially lower frequency, has been associated with a deficiency of cb_5 (OMIM 250790) [5].

Table II. Levels of Methemoglobin Concentration and Symptoms.

% Methemoglobin	Diagnosis
0-3%	Normal
3-10%	Possible slight discoloration of skin.
10-20%	Relatively asymptomatic, cyanosis is prevalent.
30-40%	Constant headache, lightheadedness, weakness, and confusion.
40-50%	Dyspnea, Lethargy, palpitations. and chest pain.
50-60	Acidosis, arrhythmias, bradycardia, hypoxia, seizures, and coma.
>70%	Death

Both forms of RCM stem from the transcript of one gene, the *DIA1* gene, coding for cb5r. Due to this fact, the difference in severity of the resultant phenotypes of type I and type II must be due to the underlying effect that the mutation has on the function of the mature protein. It is because of this that it is believed that patients presenting with the less severe type I methemoglobinemia are producing the gene product at a normal rate, however the resulting protein is unstable. Since mature red blood cells cannot synthesize proteins, they are affected, whereas other somatic cells are able to continuously replace the cb5r as it degrades in the cell. Mutations that give rise to type I RCM tend to be single amino acid substitutions. Conversely, in patients expressing type II, mutations in the *DIA1* gene tend to introduce premature stops or deletions of amino acids or even an entire exon. These alterations give rise to decreased expression or reduced catalytic activity of cytochrome b_5 reductase and the deficiency is ubiquitous. Thus far, about 40

amino acid mutations have been identified within the *DIA1* gene giving rise to either type I or type II methemoglobinemia [35, 42, 55-57].

Crystal Structure of Cytochrome b_5 Reductase

High resolution crystal structures of the soluble, diaphorase domain of *R. norvegicus* cb5r have been solved in both the absence (2.0 Å, PDB 1I7P) and presence (2.3 Å, PDB 1IB0) of bound NAD^+ [58] (Figure 5). The structures possessed a classical two domain arrangement, containing an amino terminal FAD-binding lobe (amino acid residues I33-R142) and a carboxy-terminal NADH-binding lobe (amino acid residues K172-F300). Residues G148-V171 comprise the "linker" or "hinge" region, a 28 amino acid residue segment that forms a three stranded, anti parallel β-sheet demonstrated to be of critical importance in determining correct orientation of the two lobes and modulation of electron transfer between that of the FAD- and NADH-binding domain [59, 60].

The amino-terminal FAD-binding domain (Figure 6) is comprised of a seven-stranded anti-parallel β-barrel, labeled as Fβ1-Fβ7, oriented towards the *si*-face of the flavin isoalloxazine ring and capped by a single α-helix found in the FAD-binding domain. A majority of the interactions with the FAD- prosthetic group occur via the adenine dinucleotide moiety of the flavin and with a long loop of the FAD-binding domain which is comprised of amino acid residues K110-K125 forming a "lid" and is situated between Fβ6 and the α-helix.

The "hinge" or "linker" region (Figure 7) is situated between the FAD-binding and NADH-binding domains and is comprised of a three-stranded anti-parallel β-sheet structure designated as Hβ1-Hβ3. Studies of this linker region by Davis *et al.* [60]

demonstrated that it is this "linker" region which is actively involved in properly orienting the FAD- and NADH-binding lobes of cb5r for efficient electron transfer and suggested that any disruption within the conformation of the β-sheet architecture would lead to a significant decrease in catalysis.

The NADH binding domain (Figure 8) is composed of a canonical Rossman fold [61] formed by 3 α/β/α layers arranged into a five-stranded parallel β-sheet that is oriented towards the *re*-face of the isoalloxazine ring of the FAD prosthetic group. The isoalloxazine ring is the only region of the FAD- cofactor that forms interactions via hydrogen bonds between the NADH-binding site and the isoalloxazine ring. This occurs through the FAD-binding domain loop strands Fβ3 and Fβ4 (amino acid residues P92-K110) and the NADH-binding domain Nβ1-NαA (amino acid residues T181-T184).

Cytochrome b_5 Reductase Sequence Homology

Cytochrome b_5 reductase sequences, or those of closely related homologs, have been identified within the genomes of a diverse array of eukaryotic organisms that include fungi (*M. alpine*) [62], yeast (*S. cerevisiae*) [63], plants (*A. thaliana*) [64], nematodes (*C. elegans*) [65] insects (*D. melogaster*) [66], fish (*D. rerio*) [67], amphibians (*X. laevis*) [68], birds (*G. gallus*) [69] and mammals (*R. norvegicus*) [70]. Multiple sequence alignments have revealed extensive primary structure conservation within cb5r homologs with the most diverse sequences, corresponding to those of *H. sapiens* [71] and *P. yoelii* [23], retaining approximately 25% sequence identity.

Cytochrome b_5 reductase variants have been isolated from a limited number of eukaryotic sources. The majority of the early studies utilized enzymes isolated from

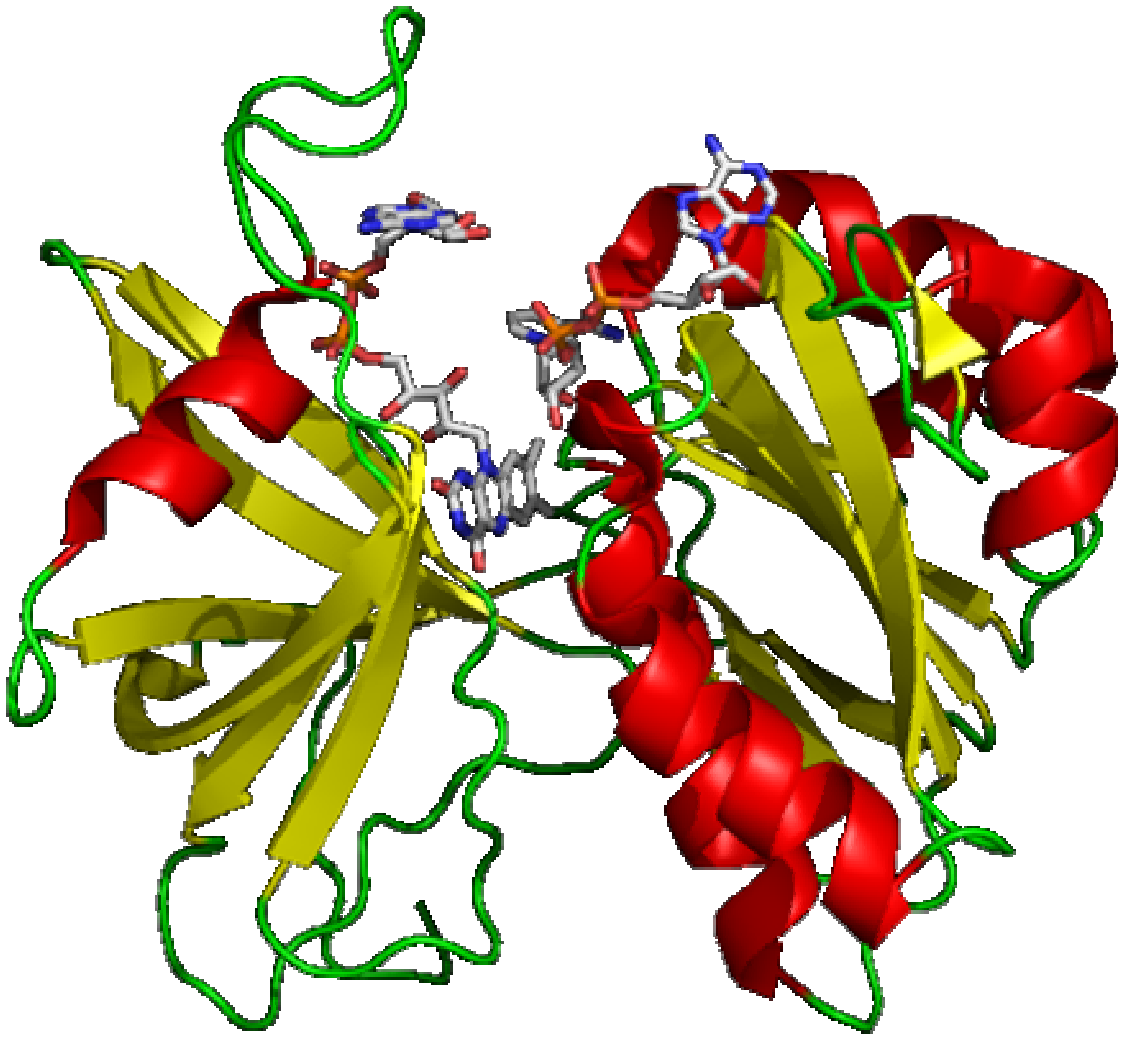

Figure 5. The Tertiary Structure of Rat Cytochrome b_5 Reductase. The 2.0Å resolution X-ray crystal structure derived from soluble recombinant rat liver cb5r (PDB 1IB0) [58] is illustrated as a schematic model where the red portions represent α-helices, the yellow ribbons with directional arrows represent β-sheet structures, and the green tubes are indicative of random coils and flexible loop structures. The FAD cofactor (left) and NAD^+ (right) are shown in stick configurations with standard CPK coloration.

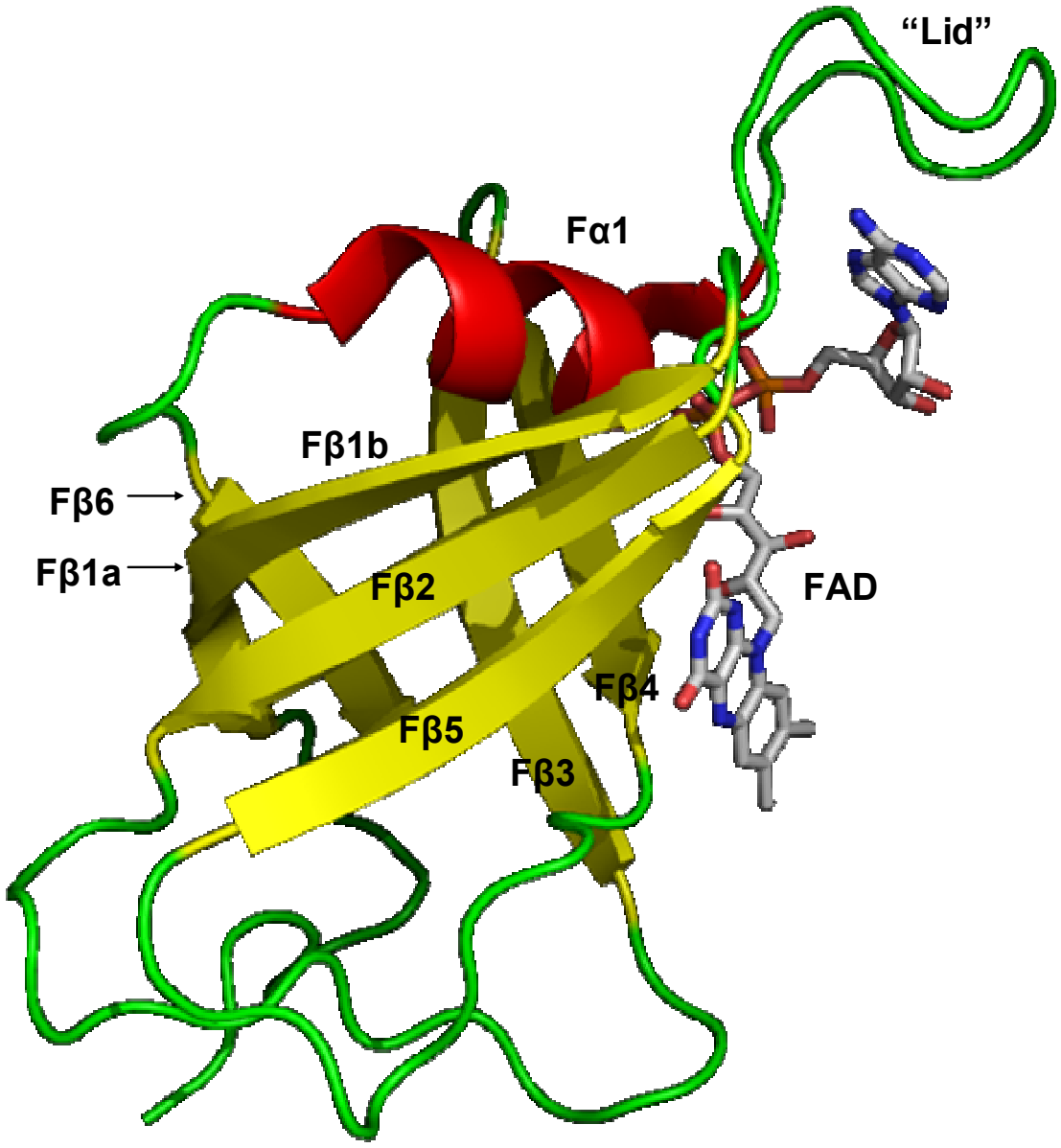

Figure 6. The Structure of the FAD-Binding Domain of Cytochrome b_5 Reductase. A view of the N-terminal FAD-binding domain of rat cb5r (PDB 1IB0) [58] with FAD bound. The *re*-face of the isoalloxazine ring faces towards the right. FAD is shown in stick configuration with standard CPK coloration. The polypeptide backbone is shown in green with the single α-helix in red and β-sheets colored yellow and are labeled accordingly.

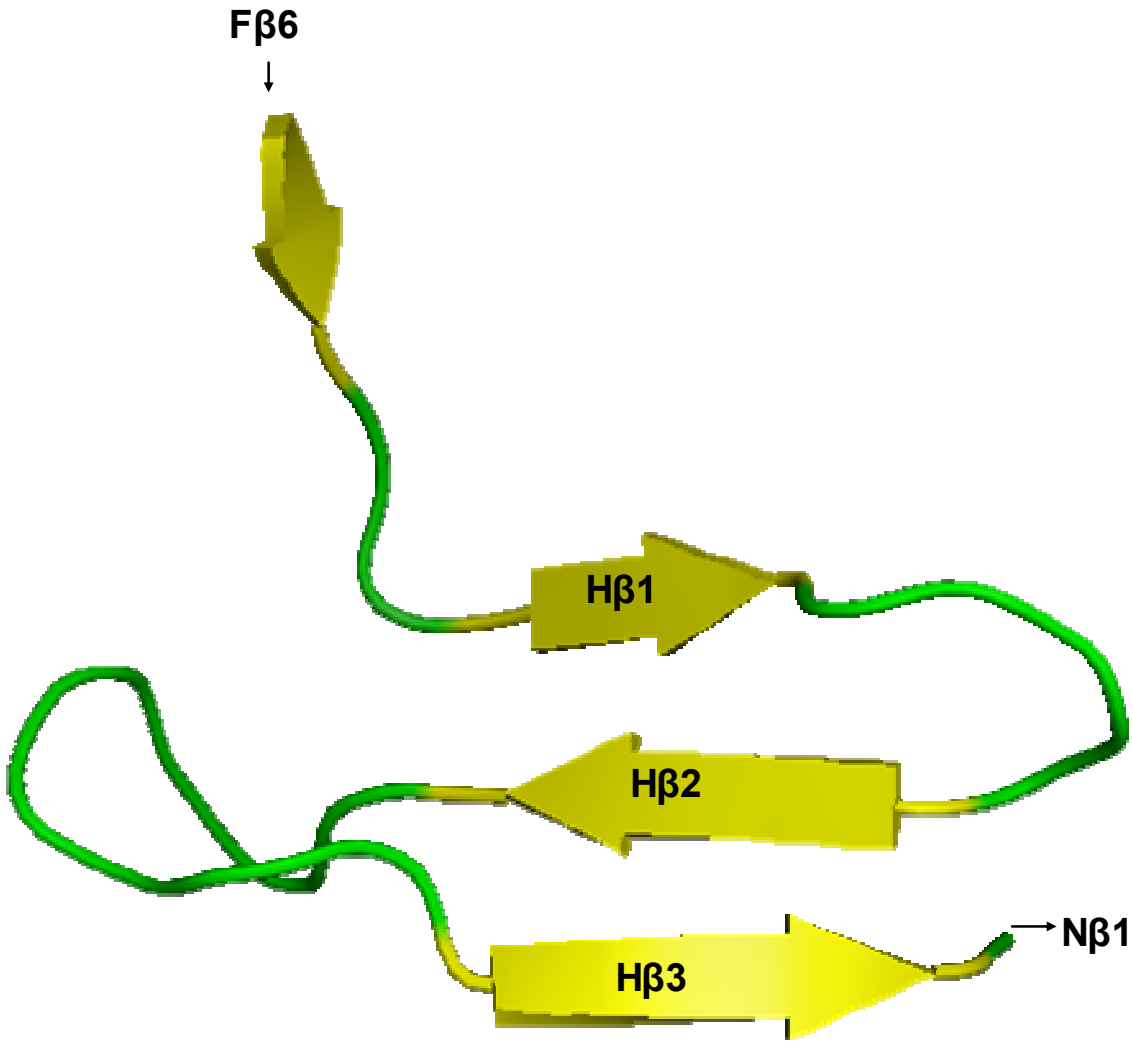

Figure 7. The Structure of the "Hinge" Region of Cytochrome b_5 Reductase. A view of the "hinge" region of rat cb5r (PDB 1IB0) [58] located between the FAD and NADH-binding domains. The polypeptide backbone is shown in green with the single α-helix in red and β-sheets colored yellow and are labeled accordingly.

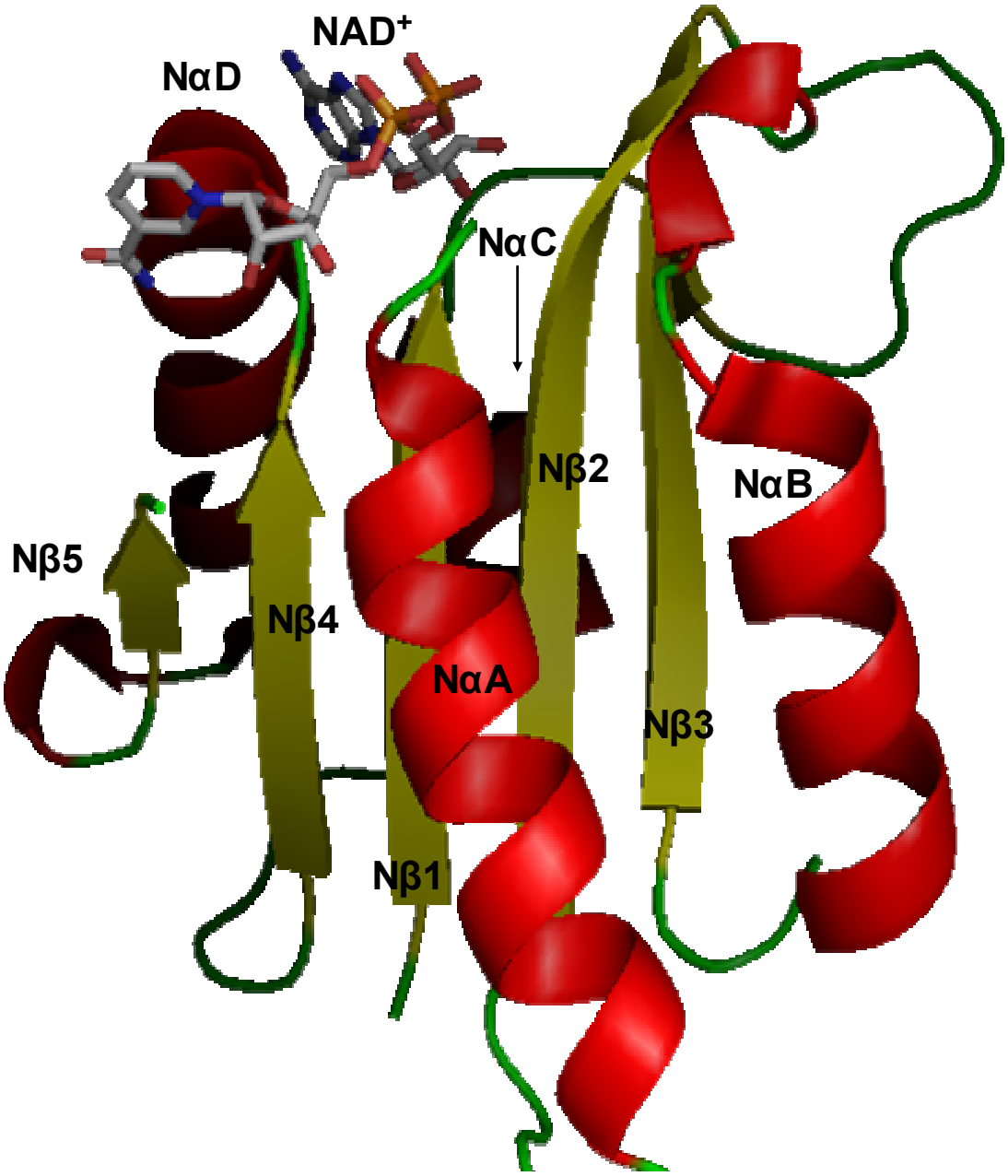

Figure 8. The Structure of the NADH-Binding Domain of Cytochrome b_5 Reductase. C-terminal NADH-binding domain of rat cb5r (PDB 1IB0) [58] with NAD^+ bound. NAD^+ is shown in stick configuration with standard CPK coloration. The polypeptide backbone is shown in green with the single α-helix in red and β-sheets colored yellow and are labeled accordingly.

either bovine or porcine liver [38, 47]. More recently, an array of recombinant expression systems have been developed for the production of several cb5r variants that include the soluble, diaphorase domains of the human [73], bovine [74], porcine [43] and rat [75] enzymes. The recombinant forms have been generated using an array of suitable expression vectors which resulted in various amino-terminal modifications, such as the addition of a poly-histidine tag [75] or glutathione *S*-transferase [76]. All the recombinant cb5r variants have been isolated as functional enzymes with a range of NADH:ferricyanide reductase specific activities (k_{cat}) that have varied from 368 s^{-1} for the human enzyme [76] to 1060 s^{-1} for the bovine variant [74]. Standardization of these kinetic parameters across the various commonly used animal systems, along with additional parameters such as thermal stability, redox potentials, and spectral properties, would be of benefit to universalize the information, thereby giving a rational foundation on which further investigations could be based.

Sequence Motifs in the FNR Family of Flavoprotein Oxidoreductases.

Through a sequence alignment utilizing the X-ray crystal structure of spinach ferredoxin-$NADP^+$ reductase [77], a family of flavin-dependent oxidoreductases have been identified which include: cytochrome b_5 reductase, cytochrome P-450 reductase, methionine synthase reductase, ferredoxin:$NADP^+$ reductase, as well as many others. Of significant interest was the pattern of conserved residues detected within the flavin- and nucleotide-binding domains characteristic of the FNR super-family (Figure 9). The structural motif of members of the FNR family is that of a two-domain module with one binding the flavin and the other binding the pyridine nucleotide. In regards to function,

the FNR family is typically classified by the two electron reduction of a flavin prosthetic group (FAD/FMN) by a pyridine dinucleotide coenzyme (NAD(P)H), followed by the sequential transfer of electrons in one electron reactions with carriers. An additional feature of the proteins found within the FNR super-family is the varying levels of complexity based on the structural domains and modulation of electron transfer. Cytochrome b_5 reductase and FNR are examples of the simplest members of the FNR family in that they each consist of only two domains and reduce molecules which are able to bind and then rapidly disassociate following electron transfer. In contrast, cytochrome P450 reductase, sulfite reductase-α, and PDR represent more complex enzymes. Although the structures also consist of two domains, the one-electron acceptor molecule is actually fused to the two-domain core by a linker region. Finally, the most complex members of the FNR family contain additional sequences and prosthetic groups indicative of more than three structural domains. These enzymes include: nitrate reductase and nitric oxide synthase.

The conservation of the "$RxY^{T}_{S}xx^{S}_{N}$", "$^{G}_{R}xx^{S}_{T}$", "GxGxxP", and "CGxxx-M" sequence motifs found within the members of the FNR flavoprotein family, clearly demonstrates the importance of these structural motifs towards the interactions of flavin-cofactor and pyridine nucleotide binding and utilization.

Research Aims and Approaches

The general goal of this research was to gain further insight into the roles of the conserved motifs found within cytochrome b_5 reductase that are involved in NADH-binding. To achieve this objective, analyses of the residues directly forming these motifs

Figure 9. Alignment of Conserved Flavin-Binding and NADH-Binding Motifs from Various Enzymes Belonging to the "FNR Family" of Flavoprotein Transhydrogenases. Each of the published amino acid sequences was obtained from the GenBank protein database [78] with the corresponding accession number and reference. The superscripted numbers indicate the amino acid positions of the first and last residue of each motif within the full-length sequence of each protein. Abbreviations are: CB5R , cytochrome b_5 reductase, NR, nitrate reductase, FNR, ferredoxin:NADP+ reductase, CPR, cytochrome P450 reductase, NOS, nitric oxide synthase, PDR, phthalate dioxygenase reductase, MSR, methionine synthase reductase, SR, sulfite reductase, FHG, flavohemoglobin, B5B5R, cytochrome b_5-cytochrome b_5 reductase fusion protein, ETP, electron transfer protein, NDR, naphthalene dioxygenase reductase, PH, phenol hydroxylase, NFR, NADPH:flavin reductase, CDPGR, CDP-glucose dehydratase reductase, CMR, p-cymene monooxygenase reductase, XMR, xylene monooxygenase reductase, NMR, nitrotoluene monooxygenase reductase, DQMR, dihydorquinoline monooxgenase reductase, MMOR, methane monooxygenase reductase, ADR, anthranilate dioxygenase reductase, TDR, toluate dioxygenase reductase, BDR, benzoate dioxygenase reductase, HBDR, hydroxybenzoate dioxygenase reductase, NQR1, Na^+ translocating NADH:quinone reductase 1, UNK1, unknown *M. loti* gene product, UNK2, unknown *Halobacterium sp. NRC-1* gene product, HYPR, hypothetical *Xanthobacter* reductase.

Enzyme	Motif 1	Motif 2	Motif 3	Motif 4	GenBank Accession/Ref
CB5R	^{91}RPYTPVS^{97}	^{125}GKMS^{128}	^{181}GTGIT-P^{186}	^{274}CGPPP-M^{279}	NP_620232 / [34]
NR	^{722}RAYTPPS^{728}	^{755}GVMS^{758}	^{805}GTGIT-P^{810}	^{898}CGPPP-M^{903}	P23312 / [79]
FNR	^{139}RLYSIAS^{145}	^{176}GVCS^{179}	^{217}GTGIA-P^{222}	^{318}CGLKG-M^{323}	P10933 / [80]
CPR	^{454}RYYSIAS^{460}	^{488}GVAT^{491}	^{534}GTGVA-P^{539}	^{629}CGDARNM^{635}	P16435 / [81]
NOS	^{1178}RYYSISS^{1184}	^{1214}GVCS^{1217}	^{1255}GTGIA-P^{1260}	^{1354}CGDVT-M^{1359}	P29475 / [82]
PDR	^{51}RNYSLSN^{57}	^{83}RGGS^{87}	^{123}GIGIT-P^{128}	^{202}CGPRPLM^{208}	Q05182 / [22]
MSR	^{478}RPYSCAS^{484}	^{514}GVCT^{517}	^{573}GTGIA-P^{578}	^{677}CGDKANM^{683}	Q9UBK8 / [83]
SR	^{386}RLYSIAS^{392}	^{420}GASS^{423}	^{461}GTGIA-P^{466}	^{552}CGDANRM^{558}	P38038 / [84]
FHG	^{204}RQYSLTR^{210}	^{227}GQVS^{230}	^{268}GVGQT-P^{273}	^{362}CGPVGFM^{368}	P24232 / [85]
B5B5R	^{289}KPYTPVS^{295}	^{323}GLFT^{326}	^{364}GTGFT-P^{369}	^{458}CGPTPFT^{464}	NP_596918 / [86]
ETP	^{56}RCYSITS^{62}	^{80}GRVS^{83}	^{120}GSGIA-P^{125}	^{203}CGPEPFM^{209}	BAA12809 / direct submission
NDR	^{142}RPYSMAG^{148}	^{165}GRVT^{168}	^{206}GTGLA-P^{211}	^{295}CGAPA-M^{300}	AAD02134 / [87]
PH	^{149}RAFSLAN^{155}	^{173}GAAT^{176}	^{214}GSGLSSP^{220}	^{306}CGPPP-M^{311}	AAA25944 / [88]
NFR	^{58}RPFSMAS^{64}	^{77}GASE^{80}	^{123}GTGFSYA^{129}	^{212}AGRFE-M^{217}	AAN83224 / [89]
CDPGR	^{141}RSYSIAN^{147}	^{164}GQMS^{167}	^{204}GTGFA-P^{209}	^{292}CGSPV-M^{297}	P26395 / [90]
CMR	^{159}RSYSFAN^{165}	^{185}GEFT^{188}	^{225}GSGLA-P^{230}	^{315}CGPPP-M^{320}	AAB62300 / [91]
XMR	^{160}RSYSFAT^{166}	^{184}GIFS^{187}	^{224}GTGLA-P^{229}	^{315}CGPPP-M^{320}	AAB70826 / direct submission
NMR	^{161}RSYSFSA^{167}	^{185}GVFS^{188}	^{225}GTGLA-P^{230}	^{316}CGPPP-M^{321}	AAC38360 / [92]
DQMR	^{155}RSYSPSS^{161}	^{179}GAMS^{182}	^{221}GTGLA-P^{226}	^{310}CGPQP-M^{315}	CAA73201 / [93]
MMOR	^{159}RSYSPAN^{165}	^{183}GRFS^{186}	^{224}GTGLA-P^{229}	^{314}CGPPG-M^{319}	P22868 / [94]
ADR	^{154}RSYSFAN^{160}	^{178}GVMS^{181}	^{218}GTGLS-A^{223}	^{307}CGPPP-M^{312}	AAC34815 / [95]
TDR	^{153}RAYSFSS^{159}	^{176}GLMS^{179}	^{216}GTGLA-P^{221}	^{304}CGPPP-M^{309}	AAD31449 / direct submission
BDR	^{166}RSYSFSS^{172}	^{189}GKMS^{192}	^{229}GTGIA-P^{234}	^{317}CGPVP-M^{322}	P07771 / [96]
HBDR	^{152}RAYSYSS^{158}	^{175}GKMS^{178}	^{215}GTGLA-P^{220}	^{305}CGPPP-M^{310}	Q51603 / [97]
NQR1	^{222}KAYSLAS^{228}	^{259}GVCS^{262}	^{298}GAGSSFG^{304}	^{401}CGPPLHN^{407}	Q9Z723 / [98]
UNK1	^{168}RLYLVST^{174}	^{201}GSSP^{204}	^{383}GIGIT-P^{388}	^{471}SGPQA-M^{476}	NP_107088 / [99]
UNK2	^{51}RYYTLSS^{57}	^{102}GEPS^{105}	^{112}GPGVG-P^{117}	^{188}CGAATDA^{194}	NP_279534 / [100]
HYPR	^{142}RAYSVAN^{148}	^{166}GAGT^{169}	^{207}GSGLA-P^{212}	^{297}AGPAP-M^{302}	CAA09916 / [101]
Consensus	RxY$^{T}_{S}$xx$^{S}_{N}$	Gxx$^{S}_{T}$ (FAD) Rxx$^{S}_{N}$ (FMN)	GxGxxP	CGxxx-M	

as well as naturally occurring methemoglobinemia variants which occur in proximity to these motifs were investigated. This was carried out by determining desired mutations of the residues under consideration. The desired variants were then generated utilizing site-directed mutagenesis of an affinity-tagged *R. norvegicus* cytochrome b_5 reductase construct [102]. Each cb5r variant generated was then subsequently characterized using biophysical, potentiometric, and enzymological techniques. Additional insight was obtained through comparison of enzymatic properties of the wild type isoform of *R. norvegicus* cytochrome b_5 reductase to that of *C. familiaris*.

The initial specific aim was to generate an expression construct of the canine variant of cytochrome b_5 reductase and compare the biophysical and enzymological properties of the resultant recombinant enzyme to those of the previously established rat isoform. Completion of a survey sequence of the canine (boxer) genome [103] resulted in the identification of two putative cb5r sequences based upon sequence conservation with the products of the human and mouse genomes. Analysis of the two sequences indicated the putative proteins had equivalent carboxyl-termini. However, the amino-terminal sequences exhibited marked heterogeneity to other mammalian cb5r sequences. The generation and expression of a full length canine cb5r cDNA containing the membrane associated amino acids was carried out to investigate the discrepancies in the sequence homology between the canine variants reported in GenBank (XM_531708, ENSCAFP000000000953) and that of the rodent and human sequences, thus confirming the primary sequence of the canine variant. Additionally, a viable protein containing only the 275 amino acid catalytic diaphorase domain of the canine isoform was generated and purified to homogeneity to investigate the structural and functional parameters of the

canine cb5r and compare the results to those of the rodent isoform.

The second specific aim was directed at the elucidation of the roles of two residues, tyrosine 112 (Y112) and glutamine 210 (Q210), in the correct binding and orientation of NADH to cb5r and thereby correct function of the enzyme. Through the analysis of the crystal structure of cytochrome b_5 reductase (PDB - 1IB0) it was shown that these two residues are found on opposite sides of the binding cleft for NADH and that each of these residues formed a hydrogen bond interaction with the pyrophosphate backbone of NAD^+. Because of this, it was hypothesized that the residues would act to properly orient and anchor the NADH into position for efficient electron transfer. Additionally, two naturally occurring type I RCM variants are found in proximity to these residues, with one variant located near each residue. The variants, T116S and E212K, have both been detected in patients with RCM. Upon inspection of the crystal structure of cb5r, each of these residues were found on the external surface of the protein and did not interact with either the flavin or NADH environments. Thus, we proposed that the effects of these mutations were likely to be moderate in nature and occur as a result of effects on nearby residues and structures. In order to better understand the causation of the pathology of these RCM variants, as well as the roles played by the nearby pyrophosphate associated residues, a series of variants were generated and analyzed for their effects on various functional parameters.

Specific aim three focused on the highly conserved NADH-binding motif ^{180}GxGxxP^{185}. Analysis of the crystal structure of cb5r allowed for visualization of the importance of this motif in the proper orientation of the NADH substrate. This motif is located at the N-terminus of the 16-residue helical segment Nα1. The leading three

residues, along with the preceding residue G179, form a compact segment that effectively reverses the direction of the polypeptide backbone, generating a "flattened" surface against which the NAD^+ can reside. The two conserved glycine residues, corresponding to G180 and G182, participate in hydrophobic contacts with the nicotinamide portion of the pyridine nucleotide substrate, while the intervening residue, T181, forms a hydrogen bond interaction with the nicotinamide ribose. T181, together with residue P185, also contributes to the hydrophobic interactions of the environment surrounding the isoalloxazine ring of the FAD cofactor, with which residue T184 forms two hydrogen bonds. The high level of interaction of the residues of this motif with both the cofactor and substrate suggest a pivotal role for this motif in the proper functioning of cb5r. Additionally, the preceding residue, G179, shows a high level of homogeneity amongst FNR family members, suggesting it too has a critical role in the association of NADH with cb5r. To further access the importance of this region of cb5r, the naturally occurring type I RCM mutants A178T and A178V were also characterized.

The fourth specific aim of this research involved the investigation of the conserved "^{273}CGxxxM^{278}" motif which is located within the NADH-binding domain of cb5r and is involved in the regulation of NADH-binding. While the residues comprising this motif do not form any direct electrostatic or hydrogen bond contacts with the bound NAD^+, the residues form a loop that provides an extensive framework of hydrophobic contacts that could orient the nicotinamide portion of the reduced pyridine nucleotide for subsequent efficient hydride transfer to the FAD prosthetic group. Residue C273 has been suggested to be important in facilitating electron transfer or in maintaining proper NADH-binding and orientation (104). The conserved glycine of the motif, corresponding

to G274, forms two critical hydrogen bonds with bound NAD^+. Previous studies have been conducted giving additional preliminary insight into the role this motif may play. Analysis of the type II RCM variant M272- demonstrated that the proper placement of this motif is vital to the proper functioning of the enzyme and the analysis of the type I RCM variant P275L suggested that, at least in part, this motif functions as a scaffold around which NADH lays for proper orientation [105]. These initial findings suggested that the ^{273}CGxxxM^{278} motif is essential in proper orientation of the NADH substrate to facilitate proper electron transfer. By analyzing additional variants of these residues, a clearer picture could be obtained as to the function that these residues contribute.

2. MATERIALS & METHODS

MATERIALS

Molecular Biology Reagents

Restriction enzymes were purchased from New England Biolabs (Beverly, MA). Plasmid preparation and agarose gel extraction kits were purchased from Qiagen Inc. (Valencia, CA). Oligonucleotide primers were obtained from Integrated DNA Technologies (Coralville, IA). Native *Pfu* and *Pfu*Turbo Polymerases and *Epicurian coli* BL21(DE3)-RIL cells were obtained from Stratagene (La Jolla, CA). The pET-23b vector was purchased from Novagen (Madison, WI). T4 DNA ligase was purchased from Promega (Madison, WI). Rapid DNA ligation kits were purchased from Roche Scientific (Palo Alto, CA). Triton X-100 and Hot Start Micro 50 PCR tubes were obtained from Molecular-Bio Products Inc. (San Diego, CA). DMSO and *p*CMB were obtained from Sigma Chemical Co. (St. Louis, MO). The Molecular Biology Core Facility at the H. Lee Moffitt Cancer Center and Research Institute performed nucleotide sequencing.

Microbiology and Protein Purification Reagents

Plastic and glassware were purchased from Fisher Scientific (Pittsburg, PA), VWR International (Suwannee, GA), and Midwest Scientific (St. Louis, MO). Tryptone

and yeast extract were obtained from EM Science (Gibbstown, NJ) and "Ultrol" grade MOPS buffer was purchased from Calbiochem (La Jolla, CA). IPTG and Ampicillin were obtained from Research Products International (Mt. Prospect, IL). Ni-NTA agarose was purchased from Qiagen Inc. (Valencia, CA). PMSF was purchased from Sigma Chemical Co. (St. Louis, MO).

Enzyme Assay and Spectroscopy Reagents

Chemicals including NADH, NAD^+, 5'-ADP-agarose, 2'5'-ADP, ADP-ribose, AMP, a-NAD^+, e-NAD^+, $APAD^+$, $APHD^+$, NADPH, NHD^+, nicotinamide; NMN^+, o-NAD^+, PCA, $PCAAD^+$, $PAAD^+$, PMSF, $TNAD^+$, $K_3Fe(CN)_6$, glucose, FAD, bovine serum albumin, potassium phosphate, riboflavin, ferric citrate, trifluoroacetic acid and Tris base were purchased from Sigma Chemical Co. (St. Louis, MO). Tetrahydronicotinamide adenine dinucleotides (H_4-NAD and H_4-NADP) were synthesized according to the protocol described by Mutaliev and Feyereisen [106] by bubbling molecular hydrogen through a stirred solution of 100 mM NAD^+ or $NADP^+$ contained in 50 mM Tris-HCl buffer, pH 8.0, in the presence of palladium catalyst (5 mg/mL). Sinapinic acid (3,5-dimethoxy-4-hydroxy cinnamic acid) was purchased from Aldrich Chemical Co. (Milwaukee, WI).

METHODS

Protein Expression and Purification

Expression of the wild-type and mutant cb_5r or NCR variants were accomplished using *E. coli* BL21(DE3)-RIL cells harboring either the pH4CB5R [102], or mutant constructs. Cells were grown aerobically in TB media supplemented with riboflavin (100 μM), ferric citrate (100 μM), and ampicillin (125 μM) overnight at 37°C, and recombinant protein expression was induced by addition of IPTG (0.4 mM) followed by an additional 6-8 h incubation at 25 °C. The cells were pelleted by centrifugation (5000xg, 10 min.), resuspended in lysis buffer (50 mM Tris-HCl, containing 300 mm NaCl and 5 mM imidazole, pH 8.0) and disrupted by sonication in the presence of PMSF (1.2 mg/ml). Lysates were clarified by centrifugation (30,000xg, 30 min.) at 4^{o}C followed by incubation with Ni-NTA agarose with gentle agitation (1 ml matrix/10 ml lysate) for up to 1h at 4°C. The His-tagged-(cb_5r or NCR)-Ni-NTA matrix suspension was collected by centrifugation (1000xg, 5 min.), washed twice with 25 mM phosphate buffer, containing 300 mM NaCl and 5 mM imidazole, pH 8.0 and transferred to a chromatography column (2.5 x 10 cm). Bound proteins were eluted with 25 mM phosphate buffer, containing 300 mM NaCl and 250 mM imidazole, pH 8.0. Fractions were pooled, assayed for NADH:FR activity and concentrated centrifugally using 10,000 MWCO concentrators (Fischer Scientific, Pittsburg, PA). Final purification was achieved by size-exclusion FPLC using either a Superdex 75 or Superdex 200 column (1 x 30 cm) equilibrated with 10 mM phosphate buffer, containing 0.1 mM EDTA, pH 7.0. Fractions exhibiting NADH:FR activity were pooled, concentrated, beaded and stored

under liquid N_2 until required. Wild-type NCR concentrations were estimated using ε_{413nm} = 130 cm^{-1} mM^{-1} and wild-type cb_5r concentrations were estimated using ε_{461nm} = 10.6 cm^{-1} mM^{-1}.

The recombinant soluble, heme domain of rat cytochrome b_5 was produced as described by Beck-von Bodman *et al*., [107] using an expression construct provided by Dr. Steven Sligar (University of Illinois, Urbana, IL). Briefly, *E. coli* BL21(DE3) cells harboring the pUC18 expression construct, which contained a codon-optimized gene encoding the soluble heme-containing domain of rat cb_5, were grown overnight at 37°C in TB medium supplemented with ferric citrate (100 μM) and ampicillin (125 μM). Protein expression was induced at 25°C by addition of IPTG (0.4 mM), and the cells were harvested 8 hours later by centrifugation, yielding pink pellets. Lysis of the cells was achieved as described for cb_5r. During fractionation of the cleared lysate, however, cb_5 was precipitated by 95% (w/v) $(NH_4)_2SO_4$. The pellet was resuspended in the minimum volume of low ionic strength phosphate buffer and dialyzed twice against a large volume of the same buffer before separation on DE52 anion exchange chromatographic media. Elution was achieved by a gradient of 0-1M NaCl before final purification by FPLC on a Superdex 75 10/30 HR column. Red fractions containing cb_5 protein were pooled, concentrated, beaded, and stored under liquid N_2.

SDS-polyacrylamide gel electrophoresis was performed as described by Laemmli [108] using 12.5% acrylamide/bis-acrylamide gels. 2-5 μg of protein was solubilzed in up to 30 μL of SDS loading buffer (10 mM Tris-HCl, pH 6.8, containing 1% SDS, 10% glycerol, 1 mM DTT, and 0.1% bromophenol blue) by boiling in water for 5 minutes before loading the gel. Gels were run at 150 volts in SDS running buffer (25 mM Tris-

HCl, pH 8.3, containing 192 mM glycine, 0.1% SDS) until the blue dye front traversed the gel. Gels were stained with Coomassie Brilliant Blue dye to visualize protein bands.

Site-directed Mutagenesis

The pH4CB5R [102] expression construct was specifically mutagenized using a modification of the Stratagene QuikChange™ (La Jolla, CA) protocol.

Mutagenic Oligonucleotide Primer Design

Complimentary oligonucleotide primers (30-40 mers) containing the desired codon change as well as a silent mutation (either inserting or deleting a restriction enzyme recognition sequence) were designed using the Primer Generator program (http://www.med.jhu.edu/medcenter/primer/primer.cgi) [109]. The sense strand annealing primers used in the construction of the various mutant proteins are listed in Appendices A, B and C.

Vector Polymerase Chain Reaction

Vector PCR was performed using *Pfu* Turbo polymerase (1.25 units) in the presence of cloned *Pfu* buffer (20 mM Tris-HCl, pH 8.8 containing 2 mM $MgSO_4$, 10 mM KCl, 10 mM $(NH_4)_2SO_4$, 0.1% Triton® X-100, and 0.1 mg/ml nuclease-free BSA) containing 10 ng vector DNA (pH4CB5R or pH6NCR), 125 ng of each synthetic primer, 5% DMSO, and 200 μM dNTP's with cycling parameters (20 cycles) of 1 min at 94 °C, 1 min at 55°C, 10 min at 68 °C. *DpnI* restriction enzyme was added directly to the cooled PCR reaction tube following the PCR cycling reaction to cleave only the methylated

template DNA. This step greatly reduced the percentage of wild-type background transformants. PCR products were subsequently purified using the Qiagen PCR Cleanup Kit. Products were eluted in 30μL of sterile elution buffer and stored at -20°C until ready for use.

Preparation of Competent Cells and Linear DNA Transformation

Competent *E. coli* DH5α cells were prepared according to the protocol by Yuckenberg et al. [110] for storage at -70°C. In brief, an overnight culture of bacteria, grown in LB, was used to inoculate a fresh 250 mL culture. The culture was incubated with shaking until an $O.D._{.600nm}$ of approximately 0.9 was reached. Cells were then harvested by centrifugation at 0°C and washed in a solution of ice-cold 100 mM $MgCl_2$. Cells were again harvested and resuspended in ice-cold 100 mM $CaCl_2$, where they were then incubated on ice for 90 minutes. Cells were finally harvested and resuspended in 85 mM $CaCl_2$ containing 15% glycerol before being snap frozen in liquid N_2 and stored at -80°C prior to use. This protocol was also used for the preparation of all other competent *E. coli* strains.

Competent *E. coli* DH5α cells were transformed with linear DNA constructs according to the protocol provided with the Quikchange™ Mutagenesis Kit (Stratagene) Frozen cells were thawed slowly on ice and 50 μL aliquots were transferred to sterile 15 mL polypropylene conical tubes maintained on ice. Up to 10 μL of the purified linear DNA construct was mixed carefully with the cells by swirling the pipette tip as the DNA was expelled. The mixture was then incubated on ice for 20 minutes before being heat-

shocked at 42°C for 45 seconds and then returned to ice for 2 more minutes. Finally, 1 mL of SOB media was added and the cells were allowed to recover for 1 hour at 37°C with gentle shaking before being plated on the appropriate selection media.

Mutagenic Screen by DNA Restriction Digest

Following overnight incubation at 37°C on ampicillin-containing SOB-agar plates, colonies were subcultured into 5 mL of liquid SOB media, containing ampicillin (125 μM). Clones were analyzed and screened for the silent mutations, introduced during mutagenesis, by restriction enzyme digestion using the appropriate enzymes listed in Table 3 and 4. Each digest was separated using polyacrylamide gel electrophoresis or agarose gel electrophoresis and the restriction pattern visualized by ethidum bromide staining of the gel. Figure 14 illustrates the result of a typical gel observed during screening of mutants. Mutant constructs exhibiting the predicted pattern that differentiated them from the wild-type construct were verified by nucleotide sequencing in both the forward and reverse directions. Positive constructs were subsequently used to transform competent *E. coli* BL21(DE3)-RIL cells to proliferate the generation of the mutant enzymes.

Homology modeling

The structure of the canine cb5r variant and point mutation variants of rat cb5r were generated using the automated comparative protein modeling server SWISS-MODEL [111] utilizing the ‘‘first approach mode’’ since the query sequence and the templates shared an average of 95.6% sequence identity. The X-ray coordinates of rat

cb5r (PDB ID: 1IP7; 90.7% identity) and rat cb5r complexed with NAD^+ (PDB ID: 1IB0) [58] together with those of the erythrocytic form of *H. sapiens* cb5r (PDB ID: 1UMK; 92.9% identity) [112] were used as templates. The modeling results were analyzed using the program ‘‘What If’’ to verify the fidelity of the calculated structure [113], and were visualized using the molecular modeling software Web Lab Viewer Pro [114].

Ultraviolet and Visible Absorbance Spectroscopy

Absorbance spectra in the far (190-250 nm) and near UV (250-350 nm), visible (360-750 nm), and near IR (750-1000 nm) wavelength range were obtained for wild type and mutant enzymes using a Hewlett Packard (Agilent Technologies, Palo Alto, CA) 8453 diode-array spectrophotometer utilizing micro-cuvettes of 200 μL capacity and with 1 cm path length.

Ultraviolet and Visible Circular Dichroism Spectroscopy

UV and visible CD spectra were obtained using a JASCO (Easton, MD) J710 spectropolarimeter calibrated for both signal intensity and wavelength maxima using an aqueous solution of *d*-10-camphosulfonic acid [115]. UV CD spectra were obtained in 10 mM phosphate buffer, containing 0.1 mM EDTA, pH 7.0 using a cylindrical quartz cell of 0.1 cm path length (300 μl total volume) while visible CD spectra were obtained in 10 mM MOPS buffer, containing 0.1 mM EDTA, pH 7.0 using a 1 cm path length cell (90 μl total volume). All spectra were corrected for the appropriate buffer contributions and are expressed in terms of molar ellipticities (M^{-1} cm^{-1}).

Fluorescence Spectroscopy

Fluorescence spectra were obtained using a Shimadzu Scientific Inst. Inc. RF-5301PC spectrofluorophotometer. Excitation and emission spectra were obtained using a slit width of 3 nm and emission and excitation wavelengths of 520 nm and 450 nm, respectively. Following acquisition of the wild type and mutant spectra, the enzymes samples were heated to 100^{o}C for 30 min, centrifuged to remove protein aggregates and the corresponding spectra for the liberated FAD were subsequently recorded. All spectra were corrected for the appropriate buffer contribution.

Steady-State Enzyme Activities

NADH:FR and NADH:CR activities were determined at 25°C under conditions of constant ionic strength and pH in 116 mM MOPS buffer (μ = 0.05), containing 0.1 mM EDTA, pH 7.0, while NADH:BR activities were determined at 25°C under conditions of constant ionic strength and pH in 10mM potassium phosphate buffer (μ = 0.01), containing 0.1mM EDTA, pH 7.0. NADH:FR activities were typically determined as the decrease in absorbance at 340 nm in the presence of NAD(P)H (250 μM) and ferricyanide (500 μM). NADH:BR activity was determined as the increase in absorbance at 423 nm in the presence of NADH (250 μM) and rat cb_5 (30 μM). All substrates were quantitated spectroscopically using the established calculated molar extinction coefficients for NADH, H_4NAD, NAD^+, cb_5, 2'-5', and ADP-ribose (Siegel 1959, Beck von Bodman 1986, The Merck Index 1989, Murataliev 2000). Activities are expressed as initial rates for the oxidation of NAD(P)H (μmol of NAD(P)H consumed/min/nmol FAD). Initial rate data at varying NAD(P)H, ferricyanide, or cb_5 concentrations were

analyzed using the software "ENZFIT" (Elsevier Biosoft, Ferguson, MO) to determine apparent k_{cat} and K_m values.

Spectral Binding Constant Determination by Differential Spectroscopy

Spectral binding constants, K_s, for various NADH analogs were determined by differential spectroscopic titrations as described by Sancho and Gomez-Moreno [116] and Barber *et al*. [117]. A Shimadzu UV2501-PC was used to measure the difference spectra of samples in matched split-cell quartz cuvettes with 0.439 cm pathlength and 2.5 ml capacity. Enzyme and NADH analogs were suspended in 10mM phosphate buffer, pH 7.0, containing 0.1mM EDTA for all spectral determinations. All analog concentrations were determined spectrophotometrically using previously published extinction coefficients.

The reference cuvette contained 50 μM enzyme (as determined by FAD concentration) in the front compartment and analog-titrated buffer in the rear compartment. The sample cuvette contained analog-titrated enzyme (50 μM) in the front compartment and buffer in the rear compartment. The appropriate buffer was added to the enzyme compartment of the reference cuvette to correct for the dilution caused by analog addition to the enzyme compartment of the sample cuvette. Following sample addition, each compartment was stirred briefly to insure thorough mixing. Spectra were then recorded over the wavelength range from 300-800 nm depending on the titration. The magnitude of the absorbance change was determined for each spectrum via peak to trough subtraction in order to compensate for any baseline drift between spectra.

Absorbance changes were plotted versus nucleotide concentration and the resulting plots were fit to the hyperbolic equation:

$$\Delta\text{Absorbance} = \Delta\text{Absorbance}_{max} * [\text{nucleotide}] / [K_s + (\text{nucleotide})]$$

in order to determine the spectral binding constant (K_s), which was defined as the concentration of analog at which half maximal spectral perturbation was observed.

Thermal Stability Measurements

Thermal stabilities of wild type and mutant enzymes were determined as described by Trimboli *et. al*. [93] by monitoring both the release of the FAD prosthetic group, as indicated by the change in flavin fluorescence, and the loss of NADH:FR activity over the temperature range from 0-100°C.

Determination of Flavin Midpoint Potential

Flavin oxidation-reduction midpoint potentials were determined by dye equilibration using the method of Massey [118]. Xanthine (30 μM) and xanthine oxidase (50 nM) were used to reduce a mixture of enzyme (40 μM FAD) and the indicator dye, phenosafranine (15 μM, $E^{0'}$ = -252mV) in 100 mM phosphate buffer containing 0.1 mM EDTA, first made anaerobic by repeated evacuation and flushing with oxygen-free argon. Benzyl viologen (6 μM) and methyl viologen (1 μM) were included to facilitate equilibration of the system. Visible absorbance spectra were collected over the course of each 3-hour equilibration. Flavin reduction was monitored at 410 nm while phenosafranine reduction was monitored at 530 nm. $E^{0'}$ values were calculated by

graphical analysis of the plot $[\log (ox)/(red)]_{phenosafranine}$ versus $[\log (ox)/(red)]_{FAD}$ using the published midpoint potential of phenosafranine of –252 mV [117].

3. RESULTS AND DISCUSSION

Expression and Characterization of a Functional Canine Variant of Cytochrome b_5 Reductase

Cytochrome b_5 reductase sequences have been identified within the genomes of a diverse array of eukaryotic organisms ranging from fungi and plants to insects and nematodes to several different vertebrates. Multiple sequence alignments demonstrated extensive primary structure conservation among these sequences. Of these various genomes, only a limited number have had the cb5r variant isolated. The human, bovine, porcine, and rat enzyme variants have been developed into recombinant expression systems, all of which have been isolated as functional enzymes with a range of NADH:ferricyanide reductase specific activities (k_{cat}) that have varied from 368 s^{-1} for the human enzyme [76] to 1060 s^{-1} for the bovine variant [74].

Within the pharmaceutical industry, dogs represent the most extensively utilized non-rodent species in preclinical xenobiotic safety studies. However, little information is generally available concerning either the specific metabolic roles of various enzymes within the species or evaluative studies that compare and contrast the specific activities of individual enzymes with their human or more frequently studied rodent orthologs.

Completion of a survey sequence of the canine (boxer) genome [118] has resulted in the identification of two putative cb5r sequences based upon sequence conservation

with the products of the human and mouse genomes. Automated computational analyses using GNOMON identified an ORF of 1441 bp on chromosome 10 encoding a 355 residue protein (GenBank XM_531708) while GeneWise identified an ORF of 906 bp coding for 301 amino acid residues (Ensemble ENSCAFP00000000953). While both sequences indicated the putative proteins retained equivalent carboxyl-terminal residues, the amino-terminal sequences exhibited marked heterogeneity with little similarity to other mammalian cb5r primary structures.

To confirm the primary structure of a canine variant of cb5r and to compare and contrast the functional properties of a recombinant form of the enzyme with those of the corresponding rat enzyme, we have cloned, expressed and characterized the soluble diaphorase domain of canine cb5r from beagle lung tissue.

Alignment of fifty, full-length translated amino acid sequences deposited in GenBank [119] that embrace known members of the cb5r flavoprotein family from a variety of diverse organisms indicated that seven sequences, corresponding to those from mammalian (human, monkey, steer, pig, rat and mouse) and avian (chicken) sources encompassed a group of conserved sequences that comprised 301 residues with amino- and carboxyl-terminal sequences of "MGAQLS" and "$^{R}_{M}{}^{C}_{R}F^{A}V_{T}F$", respectively. In contrast, predicted primary structures available for canine variants of cb5r suggested amino and carboxyl-terminal sequences of "MSLHLF" and "RCFAF" (XM_531708) and "MGLSLS" and "RCFAF" (ENSCAFP0000000000953), respectively. To accurately define the primary structure of canine cb5r, we constructed the oligonucleotide primers shown in Table 3, that corresponded to the various predicted amino-terminal sequences and the conserved carboxyl-terminal sequence. Extensive PCR analyses revealed that an

appropriately sized product of approximately 906 bp could only be obtained using Primer's 3 and 4, indicating "MGAQLS" and "RCFAF" to be the correct amino- and carboxyl-terminal sequences, respectively, of the microsomal variant of canine cb5r.

Table 3. Oligonucleotide primers used to amplify the full-length canine cb5r cDNA sequence.

Primer	Sequence[a]
1	5′- A CCC ATG TCC CTG CAC CTC TTC CAT CTC CAG -3′ N- Met Ser Leu His Leu Phe His Leu Gln
2	5′- CGC CAC ATG GGT CTG TCC TTG TCA TTT CAG -3′ N- Met Gly Leu Ser Leu Ser Phe Gln
3	5′- CAC ATG GGG GCC CAG CTG AGC ACG -3′ N- Met Gly Ala Gln Leu Ser Thr
4	5′- GC TTC GCC TTC TGA TGG CCA GGC GC -3′ N- Cys Phe Ala Phe ***

[a]Additional nucleotides were included in the primers as either 5' or 3' extensions for PCR purposes.

To confirm the full-length canine cb5r cDNA sequence, the ~906-bp PCR product was purified and sequenced in both the forward and reverse directions and yielded the nucleotide sequence shown in Figure 10. The translated amino acid sequence indicated a full-length protein comprising 301 residues that exhibited marked sequence similarity to the corresponding human (92.7% similarity) and rat (89.7% similarity) cb5r variants.

Following the successful cloning of the full-length canine cb5r cDNA, further rounds of PCR utilizing the primers described in "Methods" were used to construct an appropriate pET-based expression vector for the production of a six-histidine-tagged variant of the soluble, diaphorase domain of the enzyme using an identical strategy to that

Figure 10. Complete nucleotide sequence of canine cb5r. The cDNA sequence corresponding to the 903-bp full-length, membrane-associated form of canine cb5r (*Cf*) is shown together with the corresponding deduced amino acid sequence. Also shown are the corresponding human (*Hs*) and rat (*Rn*) cb5r primary sequences (GenBank accession number's P00387 and P20070). Amino acid residues that are not conserved between the three sequences are indicated in red. The amino-terminal myristylation signature sequence is shown in italics while the conserved flavoprotein transhydrogenase sequence motifs that are involved in either flavin-binding and selectivity or NADH binding, are shown underlined. Also shown underlined in bold italics is residue I33 which corresponds to the initial residue used for heterologous expression of the histidine-tagged soluble diaphorase domain in *E. coli*. For consistency, amino acid residues are numbered beginning with the amino-terminal residue of the mature protein (G1).

```
1    atgggggcccagctcagcacgctcggccacgtggtcctctccccagtctggttcctctat  60
 Cf    M  G  A  Q  L  S  T  L  G  H  V  V  L  S  P  V  W  F  L  Y   19
 Hs    M  G  A  Q  L  S  T  L  G  H  M  V  L  F  P  V  W  F  L  Y
 Rn    M  G  A  Q  L  S  T  L  S  R  V  V  L  S  P  V  W  F  V  Y
61   aacctgctcatgaagctgttccagcgctcgaccccggccatcacccttgagagcccggac 120
 Cf    N  L  L  M  K  L  F  Q  R  S  T  P  A  I  T  L  E  S  P  D   39
 Hs    S  L  L  M  K  L  F  Q  R  S  T  P  A  I  T  L  E  S  P  D
 Rn    S  L  F  M  K  L  F  Q  R  S  S  P  A  I  T  L  E  N  P  D
121  atcaagtacccactgcggctcatcgacaaggaggttatcaaccatgacacccggcggttc 180
 Cf    I  K  Y  P  L  R  L  I  D  K  E  V  I  N  H  D  T  R  R  F   59
 Hs    I  K  Y  P  L  R  L  I  D  R  E  I  I  S  H  D  T  R  R  F
 Rn    I  K  Y  P  L  R  L  I  D  K  E  I  I  S  H  D  T  R  R  F
181  cgcttcgctctgccgtcgccccagcacatcctgggcctcccagtcggccagcacatctac 240
 Cf    R  F  A  L  P  S  P  Q  H  I  L  G  L  P  V  G  Q  H  I  Y   79
 Hs    R  F  A  L  P  S  P  Q  H  I  L  G  L  P  V  G  Q  H  I  Y
 Rn    R  F  A  L  P  S  P  Q  H  I  L  G  L  P  I  G  Q  H  I  Y
241  ctctcagctcggatcgatggaaacctggtcattcggccctacacgcccgtctccagtgac 300
 Cf    L  S  A  R  I  D  G  N  L  V  I  R  P  Y  T  P  V  S  S  D   99
 Hs    L  S  A  R  I  D  G  N  L  V  V  R  P  Y  T  P  I  S  S  D
 Rn    L  S  T  R  I  D  G  N  L  V  I  R  P  Y  T  P  V  S  S  D
301  gatgacaaaggctttgtggacctggtcatcaaggtttacttcaaagacacccatcccaag 360
 Cf    D  D  K  G  F  V  D  L  V  I  K  V  Y  F  K  D  T  H  P  K  119
 Hs    D  D  K  G  F  V  D  L  V  I  K  V  Y  F  K  D  T  H  P  K
 Rn    D  D  K  G  F  V  D  L  V  V  K  V  Y  F  K  D  T  H  P  K
361  tttcctgctggagggaagatgtcccagtacctggaaagcatgaagattggagacaccatt 420
 Cf    F  P  A  G  G  K  M  S  Q  Y  L  E  S  M  K  I  G  D  T  I  139
 Hs    F  P  A  G  G  K  M  S  Q  Y  L  E  S  M  Q  I  G  D  T  I
 Rn    F  P  A  G  G  K  M  S  Q  Y  L  E  N  M  N  I  G  D  T  I
421  gagttccggggcccgaatggactgctggtctaccagggcaaaggaaagtttgccatccgt 480
 Cf    E  F  R  G  P  N  G  L  L  V  Y  Q  G  K  G  K  F  A  I  R  159
 Hs    E  F  R  G  P  S  G  L  L  V  Y  Q  G  K  G  K  F  A  I  R
 Rn    E  F  R  G  P  N  G  L  L  V  Y  Q  G  K  G  K  F  A  I  R
481  ccagacaagaagtccaaccccatcatcaagacggtgaagtctgtcggcatgatcgccgga 540
 Cf    P  D  K  K  S  N  P  I  I  K  T  V  K  S  V  G  M  I  A  G  179
 Hs    P  D  K  K  S  N  P  I  I  R  T  V  K  S  V  G  M  I  A  G
 Rn    A  D  K  K  S  N  P  V  V  R  T  V  K  S  V  G  M  I  A  G
541  ggaaccggcatcaccccgatgctgcaggtgatccgtgccatcatcaaagacccacacgac 600
 Cf    G  T  G  I  T  P  M  L  Q  V  I  R  A  I  I  K  D  P  H  D  199
 Hs    G  T  G  I  T  P  M  L  Q  V  I  R  A  I  M  K  D  P  D  D
 Rn    G  T  G  I  T  P  M  L  Q  V  I  R  A  V  L  K  D  P  N  D
601  cccaccgtgtgccacctactatttgccaaccagactgagaaggacatcctgctgcggccc 660
 Cf    P  T  V  C  H  L  L  F  A  N  Q  T  E  K  D  I  L  L  R  P  219
 Hs    H  T  V  C  H  L  L  F  A  N  Q  T  E  K  D  I  L  L  R  P
 Rn    H  T  V  C  Y  L  L  F  A  N  Q  S  E  K  D  I  L  L  R  P
661  gagctggaggaactgcggaatgaacattctgctcgcttcaagctctggtacacagtggac 721
 Cf    E  L  E  E  L  R  N  E  H  S  A  R  F  K  L  W  Y  T  V  D  239
 Hs    E  L  E  E  L  R  N  K  H  S  A  R  F  K  L  W  Y  T  L  D
 Rn    E  L  E  E  L  R  N  E  H  S  S  R  F  K  L  W  Y  T  V  D
721  aaagccccagaagcctgggactacagccagggcttcgtaaatgaagagatgatccgggac 780
 Cf    K  A  P  E  A  W  D  Y  S  Q  G  F  V  N  E  E  M  I  R  D  259
 Hs    R  A  P  E  A  W  D  Y  G  Q  G  F  V  N  E  E  M  I  R  D
 Rn    K  A  P  D  A  W  D  Y  S  Q  G  F  V  N  E  E  M  I  R  D
781  caccttccacctccagaggaggagccgctgatactgatgtgtggacccccgcccatgatc 840
 Cf    H  L  P  P  P  E  E  E  P  L  I  L  M  C  G  P  P  P  M  I  279
 Hs    H  L  P  P  P  E  E  E  P  L  V  L  M  C  G  P  P  P  M  I
 Rn    H  L  P  P  P  G  E  E  T  L  I  L  M  C  G  P  P  P  M  I
841  cagtatgcctgcctgcccaacctggaccgcgtgggccaccccaaggagcgctgcttcgcc 900
 Cf    Q  Y  A  C  L  P  N  L  D  R  V  G  H  P  K  E  R  C  F  A  299
 Hs    Q  Y  A  C  L  P  N  L  D  H  V  G  H  P  T  E  R  C  F  V
 Rn    Q  F  A  C  L  P  N  L  E  R  V  G  H  P  K  E  R  C  F  T
901  ttctga
 Cf    F  *  300
 Hs    F  *
 Rn    F  *
```

previously developed for production of the corresponding histidine-tagged rat cb5r diaphorase domain [102].

The Cfh_6cb5r plasmid encoding the soluble, diaphorase domain of canine cb5r, corresponding to residues I33 to F300, was used to transform E. coli BL21(DE3)-RIL cells The cells were disrupted by sonication and the canine cb5r purified to homogeneity by a combination of metal-affinity chromatography and gel filtration FPLC as previously described [102]. Evaluation of the expression yield of the diaphorase domain (Table 4) indicated that the protein was very efficiently expressed yielding approximately 32 mg of purified protein per L of bacterial culture, which represents the highest level of

Table 4. Purification of canine cb5r.

Fraction	**Total Protein** (mg)	**Volume** (mL)	**Activity NADH:FR** (units[a])	**Specific Activity** NADH:FR (units/mg)	**Yield** (%)
Lysate	260	21.5	615	6.2	100
Ni-NTA Agarose	63	5.5	501	8.0	82
Superdex 75	32	1.5	476	14.9	77

[a]units = μmoles NADH consumed/min.

expression of a cb5r variant to date. The application of the simple two-step purification protocol revealed the diaphorase domain was purified to apparent homogeneity as evident by the presence of a single protein band following SDS-PAGE analysis of the final FPLC fraction as shown in Figure 11, which indicated a molecular mass (M_r) of approx. 32 kDa, as anticipated from the deduced amino acid sequence. MALDI-TOF mass spectrometry (Figure 11) confirmed a molecular mass (m/z) of 31,364 for the purified

protein, in excellent agreement with the value of 31,391 calculated for the apoprotein from the deduced primary sequence.

The oxidized form of the purified *C. familiaris* cb5r diaphorase domain was yellow in color indicating the incorporation of a flavin prosthetic group which was subsequently confirmed by MALDI-TOF mass spectrometry by the presence of a peak in the low mass range at 798 (m/z) that identified FAD as the sole prosthetic group.

UV/visible absorbance spectra were obtained for oxidized samples of the purified canine enzyme and were compared with the spectra obtained for the corresponding rat domain in Figure 12A. The canine cb5r diaphorase domain exhibited spectra comparable to those that have been previously obtained for other cb5r variants, including the human and rat enzymes [71, 120] that are characterized by an absorption maximum detected at 273 nm in the UV region of the spectrum, and a peak at 461 nm with an associated pronounced shoulder in the range of 485-500 nm in the visible region of the spectrum, the latter peak attributable to protein-bound flavin. The $A_{273\ nm/462\ nm}$ absorbance ratio of the canine enzyme was within the range 5.5 ± 0.2 which was comparable to values previously obtained for rat cb5r (5.6 ± 0.2) [120], indicating a full complement of the FAD prosthetic group.

To assess the secondary structural content of the canine cb5r diaphorase domain, CD spectra were recorded in the UV wavelength range (190-300 nm). As shown in Fig. 12B, the canine protein exhibited positive CD from 190-210 nm and negative CD from 210-250 nm with the spectrum retaining both positive and negative intensities very similar to that of the rat domain. The absence of any significant differences between the spectra of the canine and rat proteins suggested conservation of the secondary structure

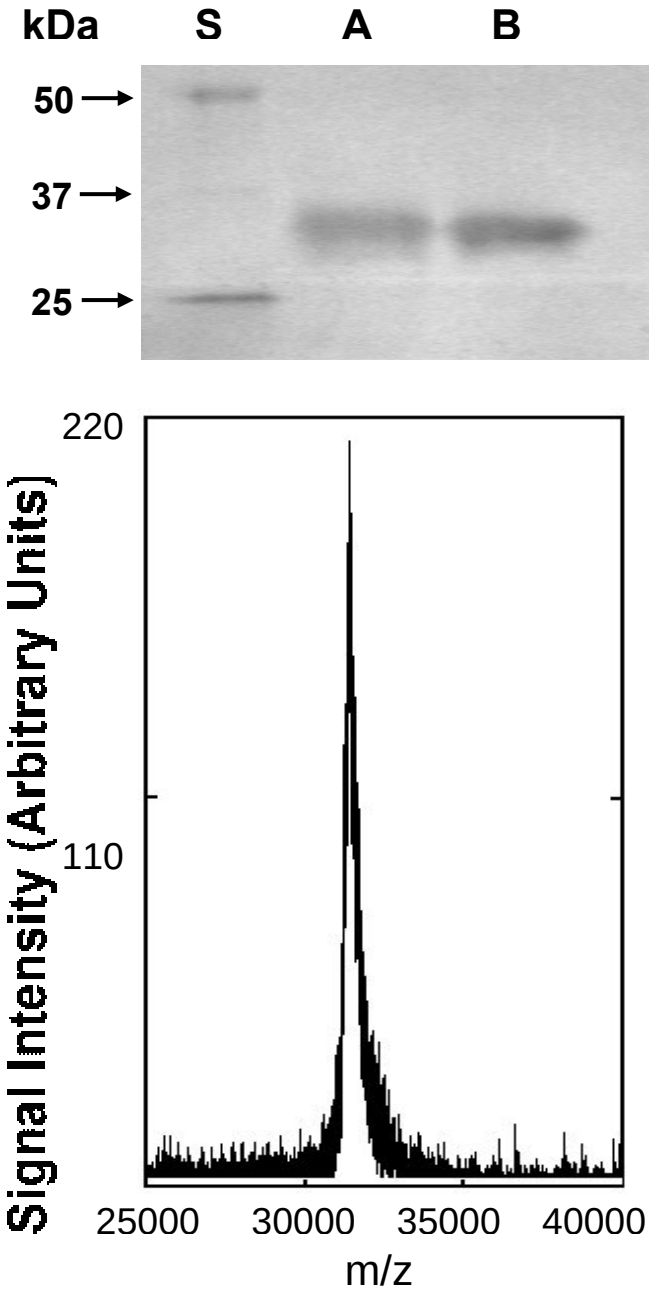

Figure 11. SDS-PAGE and MALDI-TOF mass spectrometric analyses of canine cb5r diaphorase domain expression. Upper panel: A sample (2 μg protein) obtained from the final FPLC gel filtration in the canine cb5r diaphorase domain isolation procedure analyzed using a 15% polyacrylamide gel as described in "Methods". Individual lanes correspond to: S, protein molecular weight standards with indicated molecular masses; A, purified recombinant canine cb5r. B, purified recombinant rat cb5r. Lower panel: MALDI-TOF mass spectrum obtained for a purified sample (10 pmole) of canine cb5r in the presence of sinapinic acid.

architecture and that none of the amino acid substitutions had any substantial effects on the folding of the protein.

Visible CD spectroscopy was utilized to examine the environment of the FAD prosthetic group. As shown in Figure 12C, the canine cb5r diaphorase domain exhibited a visible CD spectrum that was virtually indistinguishable from that of the corresponding rat domain and indicated that none of the amino acid substitutions had any significant effect on the conformation of the bound chromophore. Previous spectroscopic analyses of cb5r variants containing altered residues that are involved in FAD-binding, such as Y93 [121] and S127 [122], have revealed visible CD to be a sensitive indicator of flavin conformation changes.

The extent of quenching of the intrinsic fluorescence due to the FAD prosthetic group of cb5r has also proven to be a sensitive indicator of the retention of the native flavin environment. To probe the flavin fluorescence quenching of the canine cb5r variant, both excitation and emission fluorescence spectra were recorded prior to and following heat denaturation of the recombinant protein. Prior to denaturation, canine cb5r quenched the intrinsic flavin fluorescence by 96%, equivalent to that of the rat cb5r protein.

To examine the influence of the various amino acid substitutions on the stability of the resulting protein, thermal denaturation profiles were generated for the canine cb5r diaphorase by measuring both changes in the intrinsic flavin fluorescence emission intensity (λ_{ex}=450 nm, λ_{em}=523 nm) and retention of NADH:FR activity following incubation of the protein at temperatures ranging from 0–100 °C (Figure 13). Changes in the intrinsic fluorescence of the cofactor or the retention of NADH:FR activity following

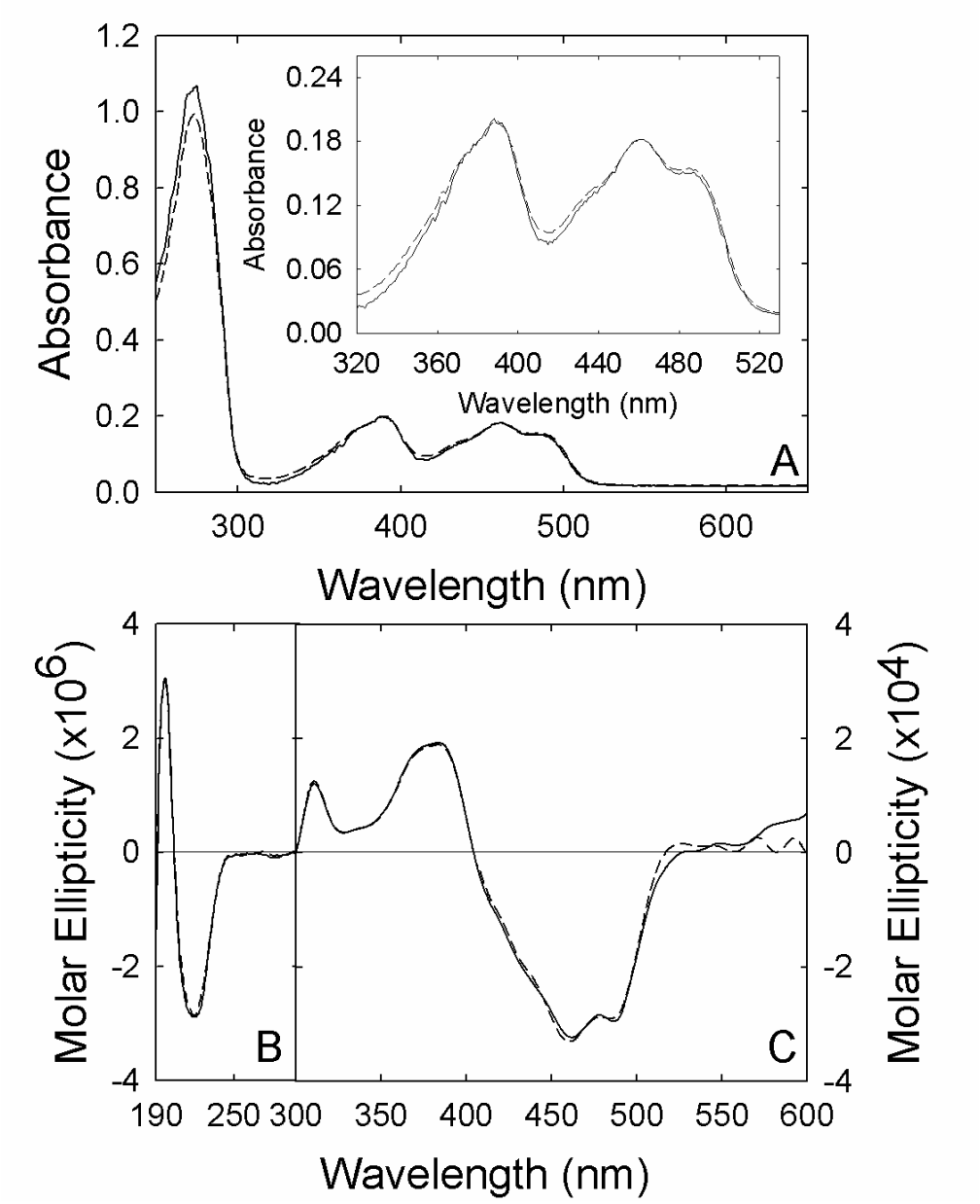

Figure 12. Ultra-Violet, Visible, and Circular Dichroism Spectra Obtained for the Canine cb5r Variant. (A) UV/visible absorption spectra were obtained for an oxidized sample of canine cb5r (1.7 μM FAD) in 10 mM phosphate buffer, containing 0.1 mM EDTA, pH 7.0. The inset shows an expanded region of the visible spectrum where the flavin prosthetic group makes a major contribution. Individual spectra correspond to canine (___) and rat (….) cb5r. (B) UV CD spectra were recorded using enzyme samples (7 μM FAD) in 10 mM phosphate buffer, containing 0.1 mM EDTA, pH 7.0. (C) Visible CD spectra were recorded using enzyme samples (50 μM FAD) in 10 mM phosphate buffer, containing 0.1 mM EDTA, pH 7.0. Line styles shown in "B" and "C" are the same as those depicted in "A".

thermal denaturation, was an effective indicator of the stability of the core structure of the protein. T_{50} values (the temperature at which 50% of maximum fluorescence or 50% retention of NADH:FR activity was detected) of 57 °C were observed which could be compared with the same values obtained for the corresponding rat domain, suggesting the canine and rat variants exhibited comparable protein folding and bound the flavin prosthetic group with similar affinities.

Initial-rate kinetic analyses were performed for the canine diaphorase cb5r domain to evaluate the effects of the various residue substitutions on both NAD(P)H and cytochrome b_5 (cb5) utilization. Values derived for the various kinetic constants for both the NAD(P)H:FR and NADH:BR activities are given in Tables 5A and 5C respectively. The canine enzyme exhibited k_{cat}'s of 767 and 600 s^{-1} for the NADH:FR and NADH:BR activities with K_m values of 7, 8 and 12 μM for NADH, ferricyanide and cb5 respectively.

As predicted by the conserved glycine, aspartate and phenylalanine residues at positions 179, 239 and 251 in the primary sequence, the canine diaphorase domain showed the same degree of specificity for NADH compared to NADPH, as previously described for the rat domain [123, 124]. The value for the NAD(P)H specificity constant (defined as ratio of $\{k_{cat}/K_m^{NADPH}\}/\{k_{cat}/K_m^{NADH}\}$) listed in Table 5C, which reflect the magnitudes of the individual k_{cat} and K_m values obtained for both NADH and NADPH, respectively, was observed to be comparable to that observed for rat cb5r, indicating the canine enzyme retained a similar preference for NADH as the physiological reductant.

To compare the interaction of the canine cb5r variant with various pyridine nucleotides and probe the effect of alterations and deletion of the nicotinamide moiety, differential spectroscopy was utilized to monitor complex formation. Examples of

alterations of the flavin visible absorbance difference spectrum are shown in Fig. 14. The formation of spectrally-detectable complexes were observed for the diaphorase domain during titrations with H_4NAD, NAD^+, ADP-ribose and a variety of NAD^+ analogs, including $APAD^+$, $PAAD^+$ and NHD^+.

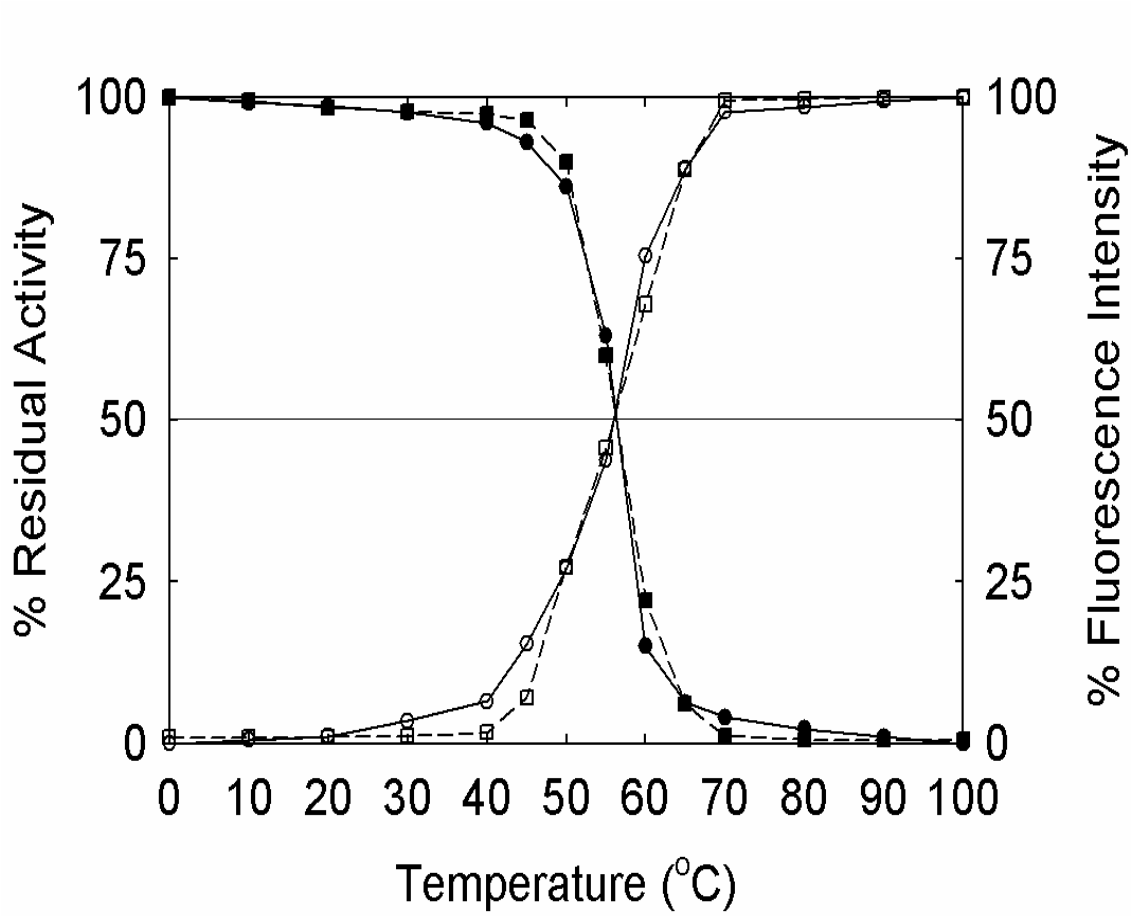

Figure 13. Thermal Stability Profile Obtained for the Canine cb5r Variant. Oxidized samples of canine cb5r and the human and rat variants (18-20 μM FAD) were incubated at the indicated temperatures and aliquots were withdrawn and assayed for both residual NADH:FR activity (open symbols) and intrinsic flavin fluorescence (closed symbols) in 10 mM phosphate buffer, containing 0.1 mM EDTA, pH 7.0, the latter using excitation and emission wavelengths of 450 nm and 523 nm, respectively. Excitation and emission spectra were scaled relative to that of a sample of free FAD at the equivalent concentration which was assigned a fluorescence intensity of 100%. The plots correspond to canine (○, ●) and rat (□, ■) cb5r, respectively. T_{50} values correspond to 57 °C for both canine and rat cb5r.

Table 5. NAD(P)H:FR and NADH:BR kinetic constants obtained for canine and rat cb5r.

A.

Variant	NADH:FR			
	k_{cat} (s^{-1})	K_m^{NADH} (μM)	k_{cat}/K_m^{NADH} (s^{-1} M^{-1})	$K_m^{Fe(CN)6}$ (μM)
Canine	767±10	7±1	1.1±0.2x10^8	8±1
Rat	800±17	6±1	1.4±0.3x10^8	8±1

B.

Variant	NADPH:FR			Nucleotide Specificity Constant
	k_{cat} (s^{-1})	K_m^{NADPH} (μM)	k_{cat}/K_m^{NADPH} (s^{-1} M^{-1})	Δ^a
Canine	50±3	1040±33	4.8±0.4x10^4	4.4x10^{-4}
Rat	33±5	924±15	3.6±0.3x10^4	2.6x10^{-4}

[a]The nucleotide specificity constant, Δ, is defined as the ratio $\{(k_{cat}/K_m^{NADPH})/(k_{cat}/K_m^{NADH})\}$.

C.

Variant	NADH:BR		
	k_{cat} (s^{-1})	$K_m^{cyt\ b_5}$ (μM)	$k_{cat}/K_m^{cyt\ b_5}$ (s^{-1} M^{-1})
Canine	600±20	12±3	5.4±1.5x10^7
Rat	600±17	12±2	5.2±1.0x10^7

For H_4NAD, the tetrahydronicotinamide derivative did not function as a hydride donor when substituted for NADH in either the NADH:FR or NADH:BR cb5r assays [111, 120] but provided a valuable tool for estimating the binding affinity for NADH. The H_4-nucleotide is a close isosteric analogue and is assumed to involve the same contacts at the active site as NADH, but lacks the positive charge on the nicotinamide ring that is present on NAD^+. The spectral changes observed following H_4NAD binding

were identical to those previously detected for the corresponding titrations of the rat enzyme and yielded positive absorbance changes with maxima at 421, 449 and 481 nm

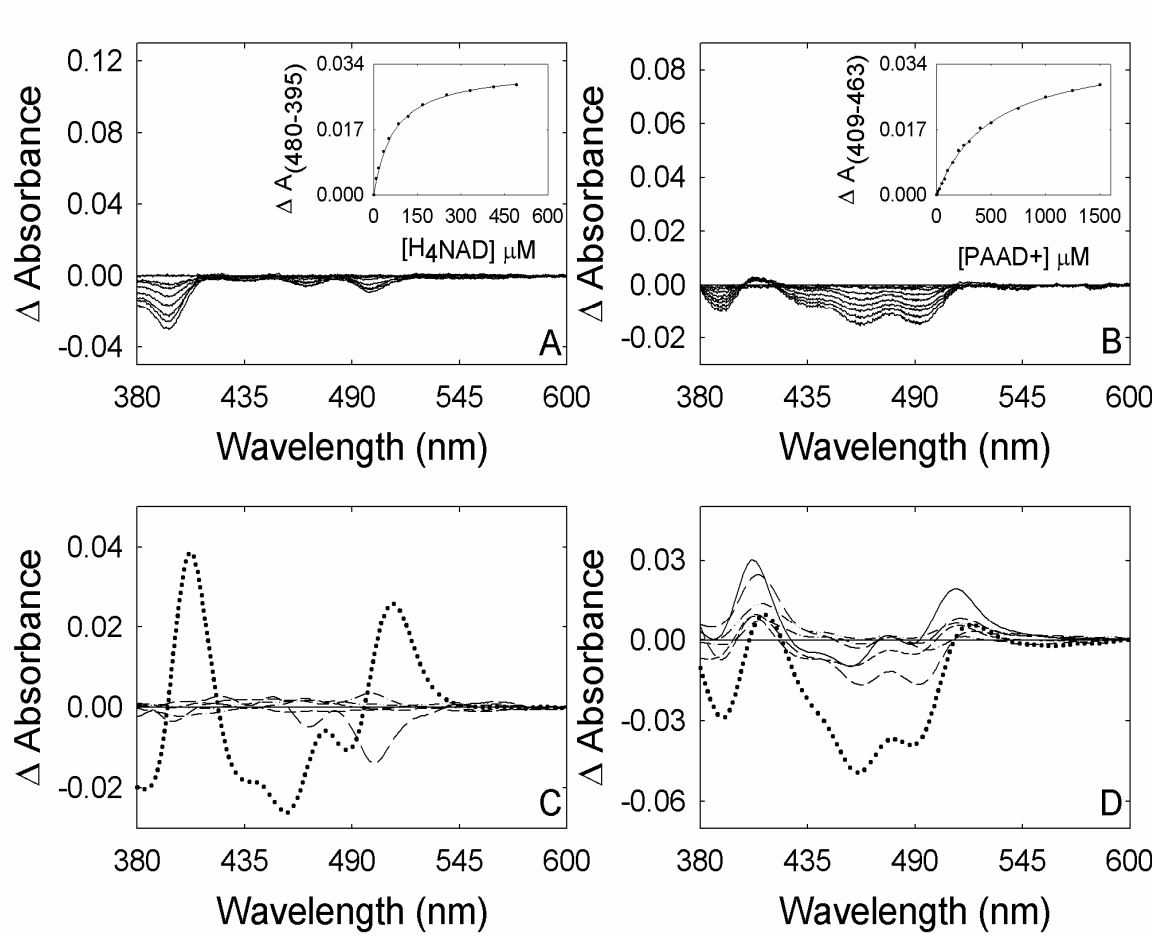

Figure 14. Differential Spectra Obtained Following Binding of Various Pyridine Nucleotides to the Canine cb5r Variant. Difference spectra were obtained for canine cb5r (50 μM FAD) in 20 mM MOPS buffer, containing 0.1 mM EDTA, pH 7.0 following titrations with either (A) H_4NAD or (B) $PAAD^+$ as described in "Methods". The insert panels correspond to plots of the magnitudes of the observed spectral perturbations (peak to trough measurements at the indicated wavelengths) versus ligand concentration. The corresponding K_s values are given in Table 4. (C) The final difference spectra obtained for NAD^+ (….), ADP-ribose (__ __), ADP (----), AMP (-.-.-) Nicotinamide (_ _ _) and NMN^+ (-..-..-) . (D) Final spectra obtained for the NAD^+-analogs α-NAD^+ (___), $TNAD^+$ (….), $PAAD^+$ (_ _ _), ε-NAD^+ (-.-.-), $APHD^+$ (-..-..-), NHD^+ (---) and $PCAAD^+$ (__ __).

and negative absorption changes at 396, 466 and 497 nm, respectively. The value obtained for the spectroscopic binding constant (K_s), shown in Table 6, was comparable to that obtained for rat cb5r.

For the binding of NAD^+ and the various NAD^+ analogs, differential flavin spectra were observed for 13 of the 15 analogs examined. NAD^+ binding yielded the largest spectral perturbation observed for any of the compounds tested, with positive absorbance maxima at 407 nm and 509 nm and negative absorbance maxima at 456 nm and 487 nm, respectively. The K_s value of 788 μM was identical to that obtained for the rat domain. Deletions of portions of the NAD^+ structure (Fig. 14) resulted in significant changes in both the lineshape and intensity of the resulting difference spectra. Removal of the nicotinamide ring effectively abolished the absorbance changes from 380 to 440 nm; however difference spectra were still observed for 5'-ADP-ribose, 5'-ADP and AMP, although the intensity of the difference spectra decreased as the NAD^+ molecular was truncated. Only minimal spectral changes were detected with NMN^+.

For the various NAD^+-analogs, the greatest spectral perturbations were observed for $TNAD^+$ with positive maxima at 405 and 485 nm and negative maxima at 389, 441 and 463 nm, respectively. $PAAD^+$ also effected significant spectral perturbations while α-NAD^+ had the least effect. The magnitude of the spectral changes was inversely proportional to the value of the spectroscopic binding constants (K_s). The analog binding studies also revealed the importance of the two amino substituents on either the adenine or nicotinamide moieties on influencing NAD^+ affinity. Substitution of the nicotinamide amino group by a methyl group ($APAD^+$), resulted in an 11-fold increase in analog affinity while removal of the group ($PAAD^+$) only increased affinity by 40%. In contrast,

substitution of the adenine amino moiety by a hydroxyl (NHD^+), decreased affinity by50%, reinforcing the important role of the adenine moiety in NAD^+ binding.

Table 6. Spectroscopic binding constants obtained for canine cb5r in the presence of various pyridine nucleotides.

Nucleotide	**Canine cb5r** K_s (μM)	**Rat cb5r**[a] K_s (μM)	***Chlorella*** K_i (μM)	**NR**[b] ΔG (kcal.Mol^{-1})
H_4NAD	67 ± 5	45 ± 10		5.688
$APAD^+$	71 ± 7		1390	5.653
ADP-ribose	77 ± 6	100 ± 20	750	5.605
ADP	165 ± 12		2040	5.154
ε-NAD	297 ± 11		6340	4.806
$PAAD^+$	540 ± 24		740	4.474
AMP	587 ± 29		5010	4.403
$TNAD^+$	590 ± 34		6490	4.400
NAD^+	549 ± 36	553 ± 30	2170	4.229
$APHD^+$	1007 ± 94		2300	4.084
PCAAD	1260 ± 31		4650	3.951
NHD^+	1350 ± 156		4480	3.910
α-NAD^+	2005 ± 250		1150	3.676
o-NAD^+	7898 ± 924		4660	2.865
PCA^+	>31000 ± 1000		4070	<2.056
NMN^+	ND*		11760	
Nicotinamide	ND*			

[a]Spectroscopic binding constants for rat cb5r were taken from *Marohnic et al.*[123].

[b]Inhibition constants for *Chlorella* nitrate reductase (NR) taken from *Trimboli and Barber* [125].

*ND indicates that the spectroscopic binding constant could not be determined, due to insufficient spectral change.

To examine whether the thermodynamic properties of the flavin prosthetic group were similar to those of the corresponding rat enzyme, potentiometric titrations were performed using the dye equilibration method for the canine cb5r diaphorase domain in the presence of phenosafranine ($E^{o'}$= -252 mV) as indicator. Flavin midpoint potentials ($E^{o'}$, n=2) were determined for the enzyme alone and in complex with NAD^+. Spectra obtained during representative titrations of canine cb5r in the absence and presence of NAD^+ are shown in Fig. 15A and B, respectively. Qualitative analysis of the individual spectra obtained from the various titrations indicated that the majority of the phenosafranine was reduced prior to FAD reduction in canine cb5r in the absence of any pyridine nucleotide, suggesting the flavin midpoint potential was more negative than that of phenosafranine. In contrast, analysis of the spectra obtained for the protein in the presence of NAD^+ revealed that the majority of the flavin was reduced prior to the dye, suggesting that complex formation significantly perturbed the flavin midpoint potentials to values more positive than that for phenosafranine. Spectra obtained from the redox titration of canine cb5r in the presence of NAD^+ also revealed the formation of the characteristic charge-transfer complex resulting in the increased absorbance in the 700-800 nm region of spectrum.

The flavin redox potentials (n=2) for canine cb5r alone or in the presence of NAD^+ were determined from the Nernst semi-log plots shown in Fig. 15C. The standard midpoint potentials obtained for the FAD/$FADH_2$ couple in both the native enzyme ($E^{o'}$= -273 mV) and in the enzyme-NAD^+ complex ($E^{o'}$= -190 mV) were significantly different, spanning a range of 83 mV.

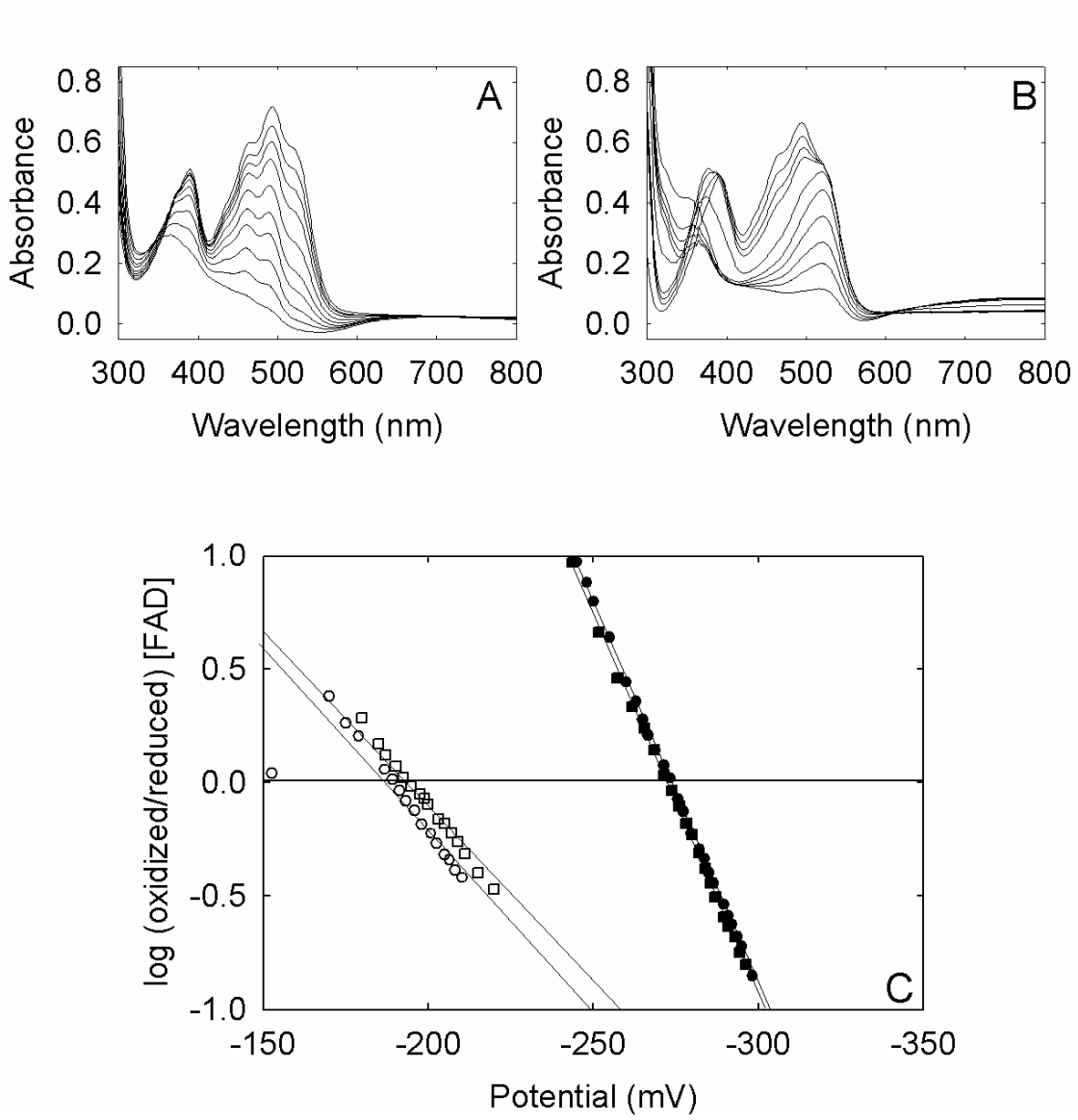

Figure 15. Oxidation-Reduction Midpoint Potentials Obtained for the FAD Prosthetic Group in the Canine cb5r Variant. Reductive dye-equilibration titrations of canine cb5r (40 μM FAD) were performed as described under "Methods" in 100 mM phosphate buffer, containing 0.1 mM EDTA, pH 7.0 in the presence of phenosafranine (15 μM, $E^{o'}$= -252 mV) as the indicator dye [117]. Individual spectra were collected at 30-90 sec intervals during the time course of the titrations. Upper Panels: representative spectra obtained during titrations of canine cb5r in the (A) absence and (B) presence of 2 mM NAD^+ are shown (a limited number of spectra are shown for clarity). (C) Nernst plots obtained for the FAD/$FADH_2$ couple (n=2) of the canine and rat cb5r variants. Canine cb5r in the absence (●, $E^{o'}$=-273±5 mV) and presence of NAD^+ (○; $E^{o'}$=-190±5 mV); rat cb5r in the absence (■, Eo'=-272±5 mV) and presence of NAD^+ (□; $E^{o'}$=-191±5 mV).

Summary of Expression and Characterization of a Functional Canine Variant of Cytochrome b_5 Reductase

These results provide the first documented insights into the structure and function of a catalytically-active canine variant of microsomal cb5r. Utilizing a consensus sequence developed from an alignment of several higher eukaryotic cb5r primary structures, we constructed PCR primers that could be used to amplify either the full-length, membrane-associated cb5r nucleotide sequence or that of a truncated, soluble form of the cb5r diaphorase domain comprising 258 residues (I33 to F300), equivalent to those previously used to develop a heterologous expression system for the rat variant [102]. The PCR results obtained using the primers designed to generate the full-length cDNA confirmed that the first six residues of the amino-terminal sequence of the membrane-associated canine cb5r corresponded to the residues "GAQLST" which were identical to the corresponding residues of both the human and rat enzymes. In addition, the first three residues, "GAQ", indicated the presence of a ProSite signature sequence [126], that suggested the mature, membrane-associated protein would be myristylated, as previously demonstrated for the steer protein [38].

The primary sequence of the full-length membrane-associated form of canine cb5r shared maximum similarity with the corresponding sequence of the human enzyme at 92.7% compared to 89.7% similarity to the corresponding rat sequence. Examination of the canine sequence revealed the presence of four conserved sequence motifs that are associated with flavin binding (^{91}RxY$^{T}_{S}$xx$^{S}_{N}{}^{97}$), FAD/FMN selectivity ($^{124G}_{R}$xx$^{S}_{T}{}^{127}$) and NADH-binding (^{180}GxGxxP^{185} and ^{273}CGxxxM^{278}) that have been identified as diagnostic for members of the FNR family of flavoprotein transhydrogenases [127].

Comparison of the results obtained from the spectroscopic, kinetic, thermodynamic and stability studies confirmed predictions generated from the pair-wise sequence alignments that the structural and functional properties of the recombinant canine cb5r diaphorase domain were directly comparable to those of the corresponding rat domain. The ability to generate both domains using identical expression systems and characterize their biophysical properties under equivalent conditions revealed that in addition to identical spectroscopic properties, the two cb5r variants exhibit identical kinetic properties including catalytic efficiency, affinities for both the reducing and oxidizing substrates and specificity for NAD(P)H. The equivalence in the kinetic properties is particularly significant and suggests that other cb5r variants exhibiting conserved sequences should retain comparable kinetic properties. Our preliminary results obtained using an identical *Danio* cb5r expression system, the *Danio* cb5r diaphorase domain shares 70.8% and 69.8% sequence similarity with the canine and rat domains, respectively, have confirmed this prediction. In addition to the conserved kinetic properties, the oxidation-reduction potentials of the FAD prosthetic groups were equivalent indicating a conserved flavin-binding environment.

The binding studies performed utilizing a variety of NADH- and NAD^+-analogs have provided further insight into the roles of the different portions of the pyridine nucleotide that are critical to regulating reducing substrate/product affinity as indicated by perturbation of the flavin prosthetic group's visible spectrum. The results obtained from the titrations using NAD^+ and various NAD^+-fragments confirm that the greatest spectral changes were produced by the binding of NAD^+ and that the positively-charged nicotinamide moiety was primarily responsible for the spectral perturbations, since ADP-

ribose and ADP were effective inhibitors but affected only modest spectral changes. In contrast, examination of the various NAD^+-analogs revealed a diverse array of spectral changes with $TNAD^+$ producing the most dramatic effects. There appeared to be a good correlation between the magnitude of the spectral changes and the affinity for the NAD^+-analog. The nicotinamide portion alone, in the form of NMN^+, also affected only modest spectral changes owing to its very low binding constant coupled with the requirement for the presence of the ADP moiety to firmly anchor the inhibitor in the correct orientation. These results were confirmed by comparison of the binding constants obtained for H_4NAD (K_s = 67 μM) and ADP-ribose (K_s = 77 μM) which indicated the presence of the nicotinamide moiety conferred only a modest increase in substrate affinity. In addition, loss of the ribose moiety resulted in a 2-fold decrease in affinity. In contrast to the binding constants obtained for the majority of the NAD^+-analogs, which were substantially greater than the values determined for ADP-ribose and ADP, the binding constant observed for $APAD^+$ was very similar in magnitude to that obtained for H_4NAD, despite the presence of the positively charged nicotinamide moiety, suggesting that this analog may bind in a different conformation than the remaining analogs. Similar results have been obtained from binding studies using a variety of $NADP^+$ analogs and the related flavoprotein, cytochrome P450 reductase [106] which shares substantial structural similarity in the FAD- and pyridine nucleotide-binding sites.

Combination of the results obtained with the canine enzyme and the various NAD^+-analogs with those obtained from mutagenesis studies of the corresponding rat cb5r diaphorase domain regarding residue side-chain substitutions and their effects of $NAD(P)^+$ specificity [123], provides important insights into structural features regulating

pyridine nucleotide binding.

The results of the binding studies indicated that the magnitudes of the spectral-binding constants obtained for the various NAD^+-analogs showed the same general transition as the results previously obtained for the closely related FAD-containing diaphorase domain of assimilatory NADH:nitrate reductase (NR) which were obtained using classical inhibitor-binding kinetic studies (Table 6) [125] reinforcing the striking structural similarity between the diaphorase domains of cb5r and NR that has been suggested by X-ray crystallographic studies.

To evaluate the structural organization of the canine cb5r soluble, diaphorase domain, comparative modeling was utilized to predict the tertiary structure of the recombinant protein. Homology modeling, utilizing the experimental structures determined for recombinant forms of the rat diaphorase domain in the absence (PDB = 1I7P) and in the presence (PDB = 1IB0) of NAD^+ [58] and the erythrocytic variant of human cb5r (PDB = 1UMK) [112] yielded a model that was nearly identical to that of the human domain and very similar to that of the rat domain, as revealed by the structural overlay shown in Figure 16. Comparison of the backbone structures indicated the canine model and the human and rat structures were nearly identical over the lengths of the entire polypeptide backbones with only minor differences among the three structures. The most notable difference was seen between the canine and human structures and the rat structure. This difference is confined to a small region of the sequence comprising residues P263 to L269. In the canine and human cb5r proteins, this region includes the sequence ‘‘^{263}PPEEEPL^{269}’’ while the rat sequence corresponds to ‘‘^{263}PPGEETL^{269}’’. The substitution of a glycine residue at position 265 in the rat protein introduces a

substantial deviation in the conformation of the backbone within this region, resulting in the disruption of the short α-helical region between P264 and E266 in the human and canine structures and the introduction of a β-bend between helix N α3 and β-strand N β5 in the rat NADH-binding lobe. However, this sequence region is not directly involved in any contacts with the FAD prosthetic group or either of the physiological substrates, NADH or cb5, and is unlikely to significantly affect the catalytic efficiency of the enzyme, in agreement with the results of the initial-rate kinetic studies.

A number of mutations of the human cb5r sequence have been reported that give rise to RCM [128]. Examination of the canine sequence indicated that all of the approximately 40 residues that have been identified so far as giving rise to either the type I or type II forms of RCM were conserved within the canine sequence with the exception of E227 which corresponds to K227 in the human variant. Thus, studies of the individual methemoglobinemia mutations in canine cb5r would be expected to be directly relevant to the human variant.

Comparative studies of the endogenous activity of cb5r have been applied as a predictor of an organism's capacity to convert methemoglobin to hemoglobin and have been used as an important component in evaluating the anti-cyanide effectiveness of various methemoglobin formers as potential prophylactics to minimize the effects of cyanide toxicity. Cytochrome b5 reductase is the rate-limiting enzyme controlling the toxicokinetics of methemoglobin reduction, effectively regulating the anti-cyanide efficacy of methemoglobin formers. While cb5r activity has been determined in humans and a diverse array of animal species including chimpanzee, baboon, horse, steer, sheep, goat, kangaroo, wallaby, dog, cat, rabbit, guinea pig, rat, mice, and platypus [129-131],

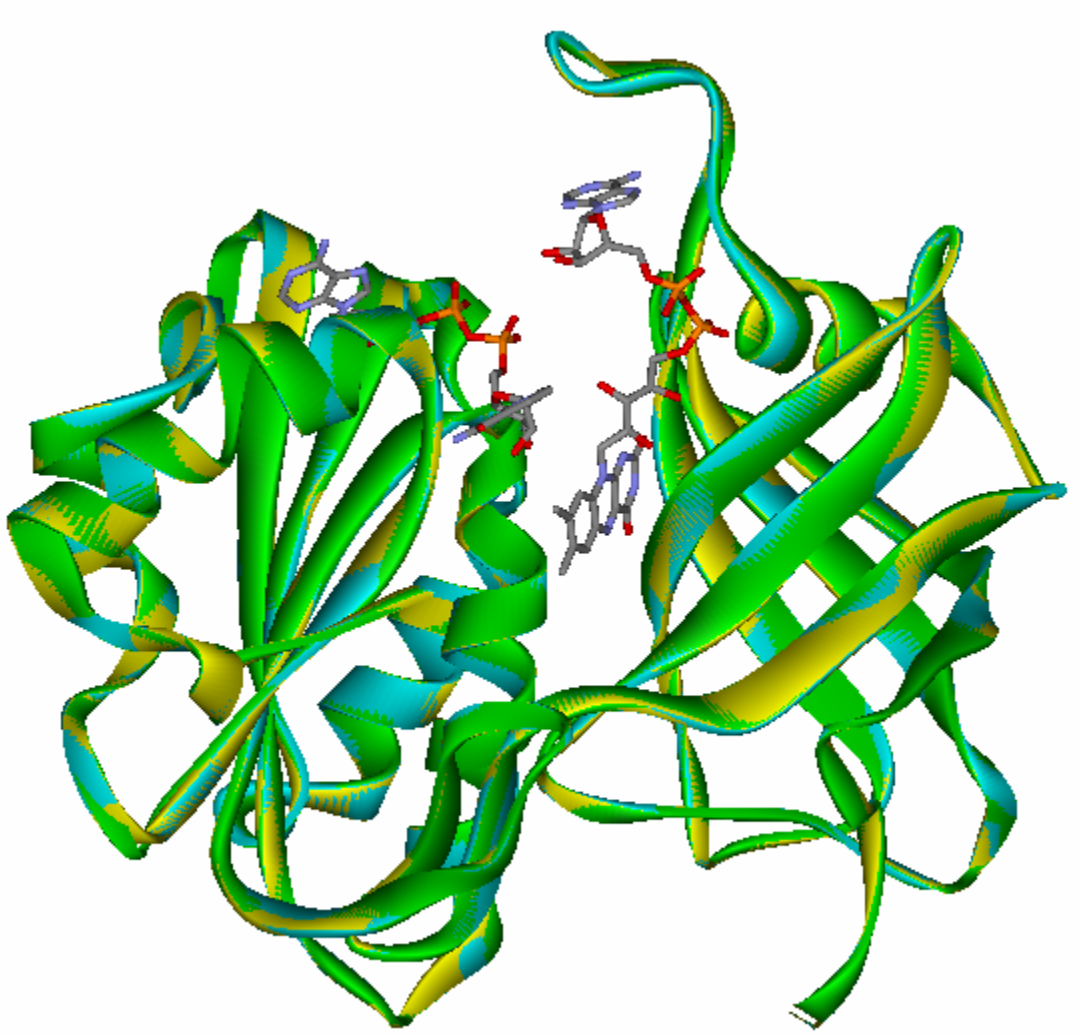

Figure 16. Comparison of the Predicted Structure of the Canine cb5r Diaphorase Domain with the Corresponding Human and Rat Diaphorase Domain Structures. The structure of the canine cb5r diaphorase domain, corresponding to residues T30 to F300, was predicted using SWISS-MODEL as described in "Methods". The diagram shows the canine structure model (cyan ribbon) as a ribbon representation superimposed on the corresponding structures of the human (yellow ribbon; PDB ID: 1UMK) and rat (green ribbon, PDB ID: 1IB0) proteins. Also shown are the FAD prosthetic group and the NAD^+ product in "stick" configuration using the CPK coloring scheme.

systematic evaluations of cb5r activity in different species have been primarily limited to non-human primates and have focused on determining hemolysate enzyme activities using the NADH:ferricyanide assay [132] in contrast to evaluating the specific activity of the enzyme using the physiological NADH:cytochrome b5 assay.

Limited *in vivo* comparative studies of cb5r functionality in hamsters, rodents and Beagles [50] has suggested that the erythrocytic concentrations of the enzyme are significantly lower in dogs than in the other mammals based upon conventional activity assays and PAGE studies and that the decreased concentrations of cb5r confer a high degree of susceptibility of Beagle erythrocytes to methemoglobin form. The results presented in this work confirm these initial results and indicate that it is changes in cb5r protein levels in dogs, rather than decreased specific activity that predisposes canines to cyanosis.

Analysis of residues, Y112 and Q210, involved in anchoring of the pyrophosphate backbone of NAD^+

Multiple sequence alignments of the cb5r sequences from a wide variety of species, ranging from "simple" single cellular organisms to more "complex" members of the avian and mammalian classes reveal a great number of highly conserved residues, indicating that these particular residues play a vital role in proper enzymatic function, thus were conserved through evolution. This, taken in combination with crystallography studies of the rat variant of cb5r [58] identifies two residues distinct from the highly conserved motif regions found in members of the flavoprotein transhydrogenases [127], that appear to play a role in the correct interaction of cb5r with its physiological substrate NADH. Based on X-ray crystallographic studies of rat cb5r in the presence of NAD^+ (PDB ID = 1IB0), residues Y112 and Q210 were shown to form hydrogen bond linkages with oxygens in the nicotinamide and adenine pyrophosphates of NAD^+ respectively as shown in Figure 17. These interactions appeared to serve to anchor the NAD^+ into position from the external side of the FAD- and NADH-binding pocket.

Residue Y112 is located in "lid" region of cb5r comprised of residues Y112-K125. The flavin ADP moiety made extensive interactions with residues in this lid forming a hydrophobic pocket that housed the adenine moiety, specifically between the planar rings of Y112 and F120. Additionally, the location of Y112 in the FAD binding domain of cb5r makes it unique in that it is the only residue of the FAD-binding domain to directly interact with $NADH/NAD^+$, forming a hydrogen bond interaction between NO2 of the nicotinamide pyrophosphate of NAD^+ and the hydroxyl group of the tyrosine side chain. It was previously determined that, in the type II RCM variant S127P, the Oç

Figure 17. Electrostatic Interaction of Amino Acid Residues Y112 and Q210 with NAD^+ Bound to Cytochrome b_5 Reductase. (A) Ligplot [99] of 1IB0. C, O, N, and P atoms are represented as white, blue, red, and violet spheres, respectively, while covalent bonds are violet sticks within NAD^+ and orange sticks within amino acid residues of the NADH-binding lobe. Hydrogen bonds are drawn as green dashed lines with distances between atoms labeled. Residues contributing to hydrophobic interactions are represented as arcs with rays and colored red. (B) Structural model of cb5r with NAD^+ and residues Y112 and Q210 shown in stick representation. (C) Enlarged view of the NADH binding pocket (atoms colored in CPK).

A

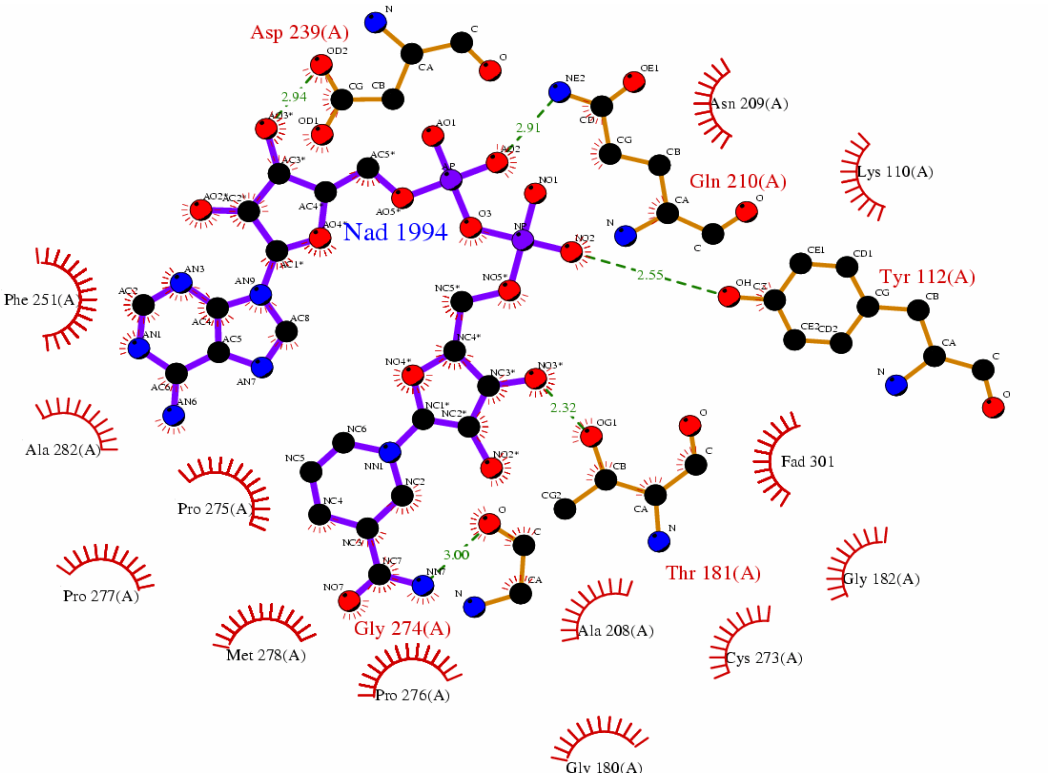
Asp 239(A)
Asn 209(A)
Lys 110(A)
Gln 210(A)
Nad 1994
Tyr 112(A)
Phe 251(A)
Ala 282(A)
Pro 275(A)
Fad 301
Thr 181(A)
Gly 182(A)
Pro 277(A)
Gly 274(A)
Ala 208(A)
Met 278(A)
Cys 273(A)
Pro 276(A)
Glv 180(A)
2.94
2.91
2.55
2.32
3.00

B

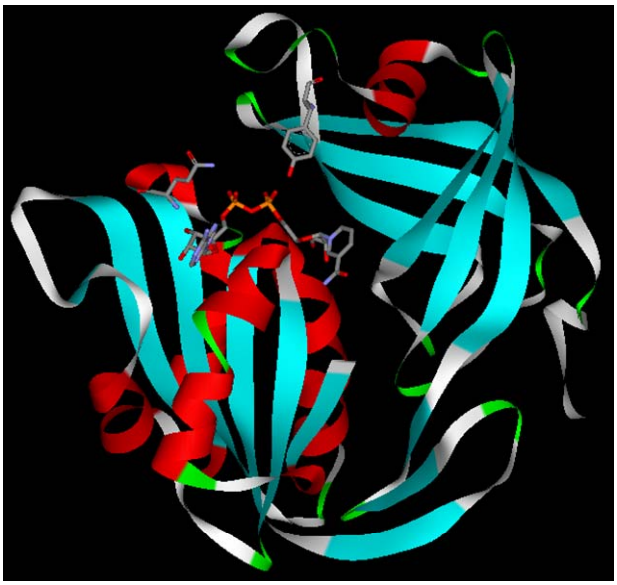

C

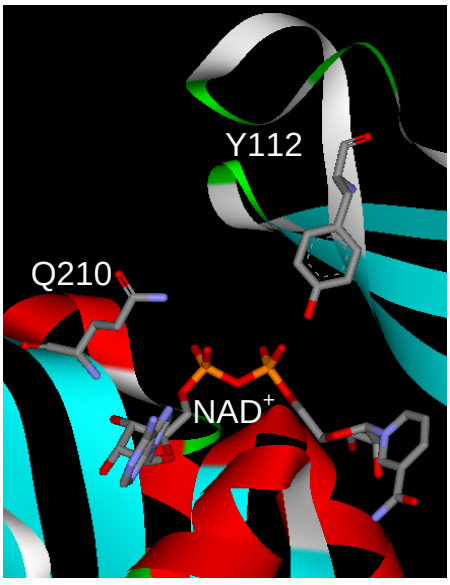
Y112
Q210
NAD+

atom of residue S127 was within hydrogen bonding distance of the amide nitrogen atom of Y112 and may assist in stabilizing this loop conformation. A major conformational change in the lid region noted in the X-ray crystal structure of S127P was proposed to be partially due to the removal of the interaction of the side chain of S127 with the amide nitrogen atom of Y112 [122].

In order to further probe the role of Y112, a series of variants were created as described in "Methods" utilizing the original four-histidine tagged cb5r expression construct and the corresponding oligonucleotide primers listed in Appendix A.

In multiple sequence alignments, Y112 is shown to be both ubiquitously conserved across species variants as well as highly conserved among members of the FNR family. Thus, the variants generated corresponded to a survey of alternate amino acid residues that cover the general properties of the side chains, allowing for investigation of polarity, charge, and steric interference on the overall structure and function of cb5r. The variants generated consisted of Y112A, Y112D, Y112F, Y112H, and Y112L.

Residue Q210 is located at the carboxy terminus of β-strand Nβ2. The NE2 of the glutamine side chain forms a hydrogen bond with AO2 of the adenosine pyrophosphate of NAD^+. Through multiple sequence alignments, Q210 has been shown to be highly conserved across FNR family members and among species variants. To further probe the role of Q210, a series of mutants were generated as described in "Methods and Materials," utilizing the original four-histidine tagged cb5r expression construct and the corresponding oligonucleotide primers listed in Appendix A. These mutants corresponded to alternate residues that occur in the same residue position within

additional GenBank sequences of other members of the FNR superfamily and cb5r variants. These variants consist of Q210A, Q210R, and Q210 V.

The fidelity of each variant was confirmed by nucleotide sequencing in both forward and reverse directions and the mutant proteins were then recombinantly expressed in BL21 (DE3)-RIL cells. Purification to homogeneity was carried out through the utilization of a combination of Ni-NTA affinity and gel filtration chromatography for the mutant proteins, all being expressed at levels comparable to that of the WT domain as observed by the appearance of single protein bands following SDS-PAGE analysis.

UV/visible absorption spectra were obtained for oxidized samples of each of the purified variants together with WT cb5 and are presented in Figure 18A (Y112 series) and Figure 19A (Q210 series). Both series of mutants displayed spectra comparable to that of the WT domain, attributable to protein-bound flavin with an aromatic absorption maxima detected at 272 nm in the UV region of the spectrum and a peak at 461 nm with a pronounced shoulder within the range of 485-500 nm in the visible region of the spectrum. The absorption ratios (A_{276}/A_{461}) for each viable mutant were within a range of 5.5 to 5.9 which indicated a full flavin complement.

To examine the effects of each mutation upon the secondary structure of the protein, UV circular dichroism spectra were determined in the UV wavelength range (190 – 300 nm). As shown in Figures 18B and 19B, all of the generated mutants displayed line shapes comparable to WT cytochrome b_5 reductase with positive CD from 190-210 nm and negative spectra from 210-250 nm, with minor alterations in the intensity of the negative deflections of the spectra. Alterations may indicate an adverse structural change within the overall α-helical or β-sheet components of the two variants. However, due to

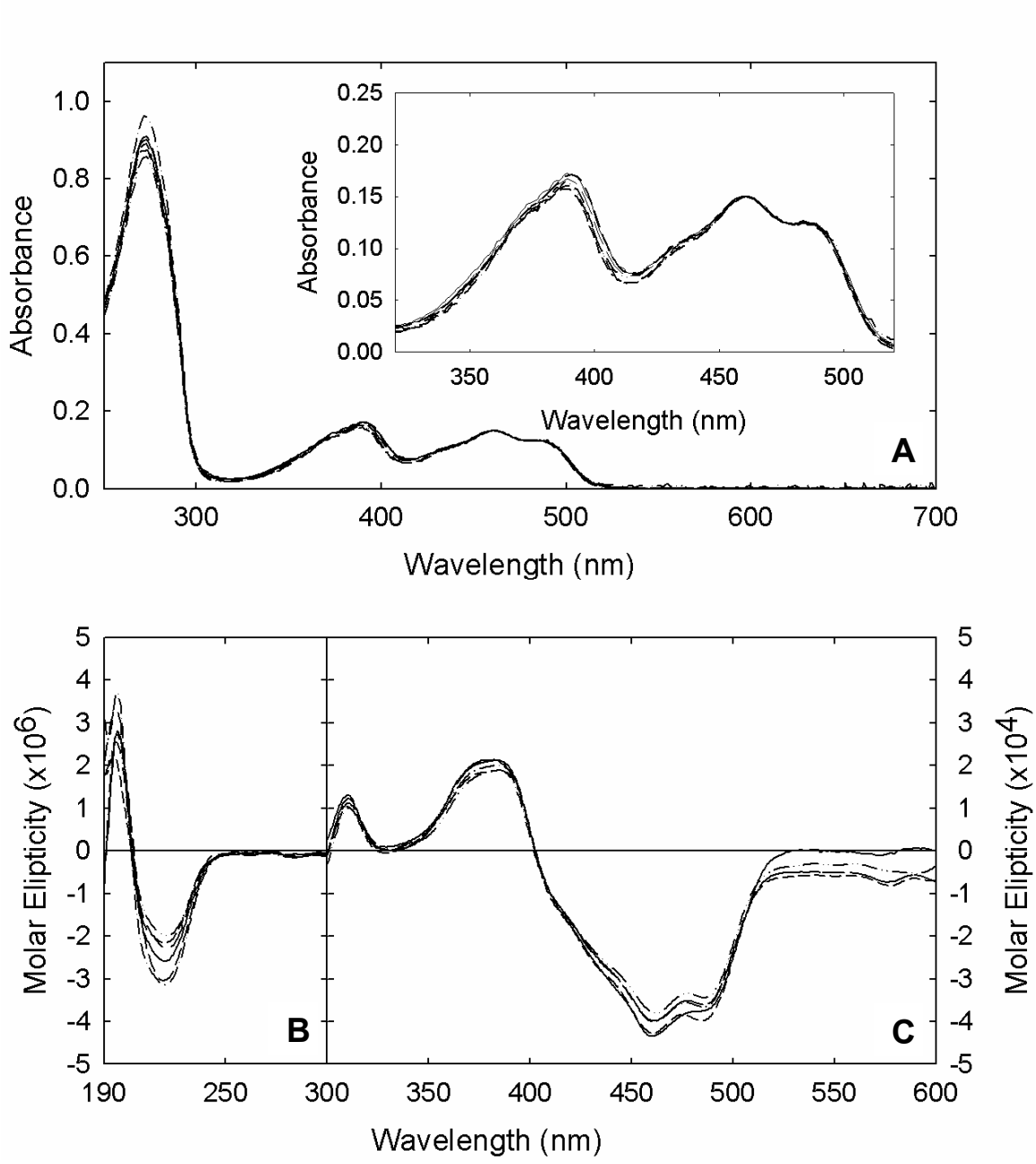

Figure 18. Ultra-Violet, Visible, and Circular Dichroism Spectra Obtained for the Y112 Series of cb5r Variants. (A) Oxidized samples of WT and mutant cb5rs (20μM), (B) 7μM, and (C) 60μM FAD in 10mM phosphate with 0.1mM EDTA, pH 7.0 buffer. The inset shows an expanded region of the visible spectrum where the flavin cofactor makes a major contribution. Individual spectra correspond to (——) H_4cb5r; (— —) Y112A; (— — —) Y112D; (- - - -) Y112F; (— · —) Y112H and (— · · —) Y112L.

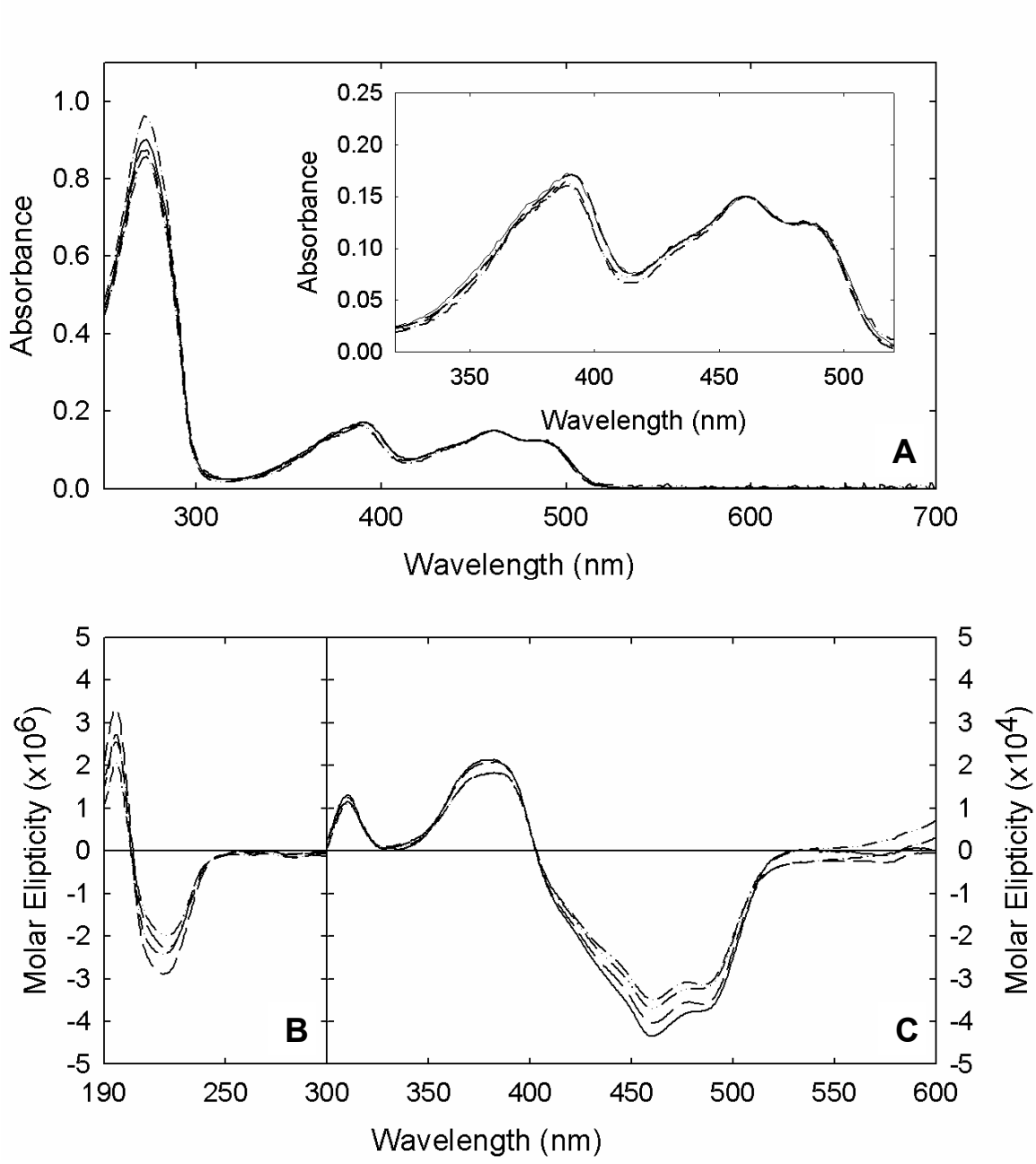

Figure 19. Ultra-Violet, Visible, and Circular Dichroism Spectra Obtained for the Q210 Series of cb5r Variants. (A) Oxidized samples of WT and mutant cb5rs (20μM), (B) 7μM, and (C) 60μM FAD in 10mM phosphate with 0.1mM EDTA, pH 7.0 buffer. The inset shows an expanded region of the visible spectrum where the flavin cofactor makes a major contribution. Individual spectra correspond to (——) H_4cb5r; (— —) Q210A; (—·—) Q210R; (—··—) and Q210V.

the minimal nature of these alterations, it is more likely a result of the noise reduction process involved with analysis of the data. In order to examine the flavin environment of each variant, visible CD spectra were obtained as shown in Figure 18C and 19C. Representative spectra demonstrated that each variant retained a similar line shape to that of WT cb5r, processing positive maxima at 310 and 390 nm and negative maxima at 460 and 485 nm. Again, minor alterations were observed in the intensity of both the positive and negative deflections, mostly attributable to noise reduction.

To establish effects of the alterations of the side chains on the catalytic function of the enzyme, initial-rate kinetic parameters for NADH:FR assays were determined for the WT cb5r and for each purified variant. The values obtained for the NADH:FR assays for the Y112 and Q210 series of variants are presented in Tables 7 and 8, respectively. For the Y112 series, the NADH catalytic efficiencies (k_{cat}/K_m^{NADH}) were at least moderately decreased for all variants, having values that ranged between 2 and 27% compared to WT cb5r, with Y112D yielding the lowest catalytic efficiency (Table 7). The observed decrease on overall catalytic efficiency was attributable to both a decreased k_{cat} for each of the variants (>50% in all cases) as well as a decrease in substrate affinity, with observed K_m^{NADH} of each mutant being 2-2.5 times greater than that of WT cb5r. Most notable of the results was Y112D, which had the most profound effect on catalytic efficiency, reducing it to 2% of WT activity.

For the Q210 series, the NADH catalytic efficiencies (k_{cat}/K_m^{NADH}) for all variants were decreased with values that ranged between 21 and 47% compared to WT cb5r, with Q210A yielding the lowest catalytic efficiency (Table 8). The decrease in efficiency was again due equally to decreased affinity for substrate and decreased rate of turn-over.

Table 7. NADH:FR Kinetic Constants and Thermal Stability (T_{50}) Values for the Y112 Series of cb5r Variants.

	NADH:FR				
cb5r Variant	k_{cat} (s^{-1})	K_m^{NADH} (μM)	K_m^{FeCN6} (μM)	k_{cat}/K_m^{NADH} (s^{-1} M^{-1})	T_{50} (°C)
WT H4cb5r	800 ± 21	6 ± 1	8 ± 1	1.4 ± 0.3 x 108	56.1
Y112A	325 ± 5	12 ± 0.3	7 ± 1	2.8 ± 0.1 x 107	51.4
Y112D	45 ± 2	15 ± 2.6	8 ± 1	3.1 ± 0.7 x 106	51.2
Y112F	400 ± 17	11 ± 0.9	8 ± 1	3.7 ± 0.5 x 107	54.3
Y112H	333 ± 28	10 ± 1.1	7 ± 1	3.4 ± 0.7 x 107	56.3
Y112L	397 ± 20	11 ± 1.2	8 ± 1	3.8 ± 0.6 x 107	57.2

Protein stability was evaluated by monitoring the thermal NADH:FR inactivation profile coupled with the increase in intrinsic flavin fluorescence and emission intensity of each of the variants which was compared to values obtained for WT cytochrome b_5 reductase. The results obtained for the thermal denaturation profiles and changes in intrinsic flavin fluorescence are shown in Figure 20. For the Y112 variants, T_{50} values (the temperature at which 50% of maximum fluorescence and 50% retention of NADH:FR activity was detected) indicated a slightly decreased protein thermal stability for Y112A, D, and F as compared to the T_{50} value of 56 °C for WT cb5r, whereas the values for both the Y112H and Y112L variants were comparable to WT (Table 7). Similar results occurred for the Q210 variants, with all three having slightly decreased values compared to WT (Table 8). Overall, these results indicated alteration to either of these residue results in a decreased stability of the protein.

Table 8. NADH:FR Kinetic Constants and Thermal Stability (T_{50}) Values for the Q210 Series of cb5r Variants.

	NADH:FR				
cb5r Variant	k_{cat} (s^{-1})	K_m^{NADH} (μM)	K_m^{FeCN6} (μM)	k_{cat}/K_m^{NADH} (s^{-1} M^{-1})	T_{50} (°C)
WT H_4cb5r	800 ± 21	6 ± 1	8 ± 1	1.4 ± 0.3 x 10^8	56.1
Q210A	437 ± 42	15 ± 1.5	8 ± 1	2.9 ± 0.6 x 10^7	52.7
Q210R	510 ± 5	8 ± 0.3	7 ± 1	6.6 ± 0.3 x 10^7	52.9
Q210V	565 ± 17	13 ± 1.8	8 ± 1	4.3 ± 0.7 x 10^7	52.3

From the kinetic data obtained it was demonstrated that each of the variants generated displayed an elevated K_m^{NADH} for both the Y112 and Q210 variants, on the order of 2 fold as compared to WT cb5r for most variants. To further establish the binding affinity of the substrate NADH and the product NAD^+, spectroscopic binding constants were determined utilizing differential spectroscopy.

As stated in "Methods" the isosteric analog 1,4,5,6-tetrahydro-NAD (H_4NAD) was utilized as an alternative substrate analog to evaluate the affinity for the physiological substrate NADH [106]. Differential spectroscopy was used to monitor complex formation during titrations with either H_4NAD or the physiological product NAD^+. The results are shown in Figures 21 and 22 for Y112 and in Figure 23 for the Q210 variants. In the case of Y112, spectra obtained for each of the titrations carried out in the presence of H_4NAD displayed a line shape comparable to WT cb5r with varying intensities of the negative maxima at 395nm. Values observed for the spectroscopic binding constant (K_s) for the H_4NAD titrations, shown in Table 9, demonstrated that the binding affinity for each of the variants was not significantly altered, with the exception of Y112D, which had a value approximately 9 times greater than that of WT cb5r.

Figure 20. Thermal Stability Profiles of the Y112 and Q210 Series of Variants. Oxidized samples of cb5r variants and WT H_4cb5r (5 μM FAD) were incubated at the indicated temperatures, and aliquots were withdrawn and assayed for both residual NADH:FR activity (closed symbols) and intrinsic flavin fluorescence (open symbols) in 10 mM phosphate buffer, containing 0.1 mM EDTA, pH 7.0 using excitation and emission wavelengths of 450 nm and 523 nm, respectively. (A) Points correspond to: (●,○) H_4cb5r; (■, □) Y112A; (▲, Δ) Y112D; (▼,▽) Y112F; (♦, ◊) Y112H; and (x) Y112L. (B) Points correspond to: (●,○) H_4cb5r; (■, □) Q210A; (▲, Δ) Q210R; and (▼,▽) Q210V

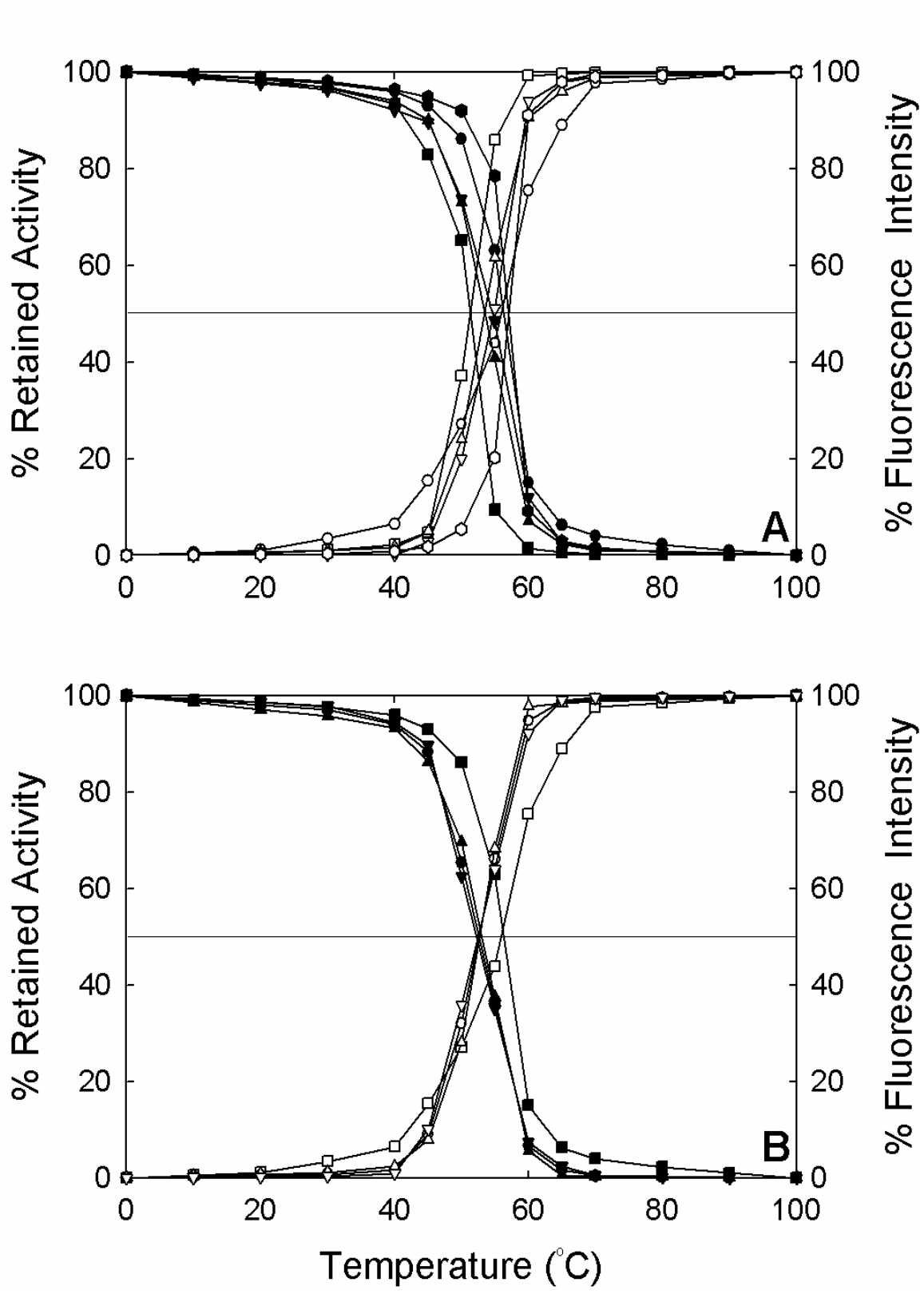
% Retained Activity
% Fluorescence Intensity
A
B
0
20
40
60
80
100
Temperature (°C)

While little alteration for the affinity for the substrate analog H_4NAD was observed for the Y112 series of variants, the spectra obtained in the NAD^+ titrations demonstrate a high level of alteration in both degree of affinity and in conformation of binding. As seen in Figure 21, all variants, with the exception of Y112H, demonstrated an altered line shape in the titration spectra. Moreover, the spectra for Y112A, D, F, and L were more reminiscent of the spectra obtained for WT enzyme in the presence of H_4NAD. Additionally, the intensities of the differential spectra were greatly diminished in comparison to WT enzyme. The K_s values were markedly altered for all variants, displaying an moderately enhanced binding affinity for the NAD^+ product in the case of Y112A and Y112L, while the Y112F, Y112H, and most notable the Y1112D variants demonstrated dramatically increased values as compared to WT cb5r (Table 9). These results are in good agreement with the kinetic values obtained in that the substrate H_4NAD is still able to bind efficiently, but at a decreased affinity. In respect to affinity for the product NAD^+, the altered conformation indicated by the differing line shape of the spectra indicates improper orientation leading to decreased turnover as evidenced by the decreased k_{cat} values for the NADH:FR assays.

For the Q210 series of variants, titrations carried out in the presence of H_4NAD yield spectra retaining the line shape shown in titrations of WT enzyme. Values obtained for the K_s for H_4NAD were comparable to that of WT (Table 10), with Q210R showing an increased affinity for substrate. Results obtained for titrations in the presence of NAD^+, showed that all variants maintained the same line shape as that for WT. Q210A showed a K_s value on par with WT, whereas values for Q210R and Q210V indicated and increased affinity for substrate (Table 10).

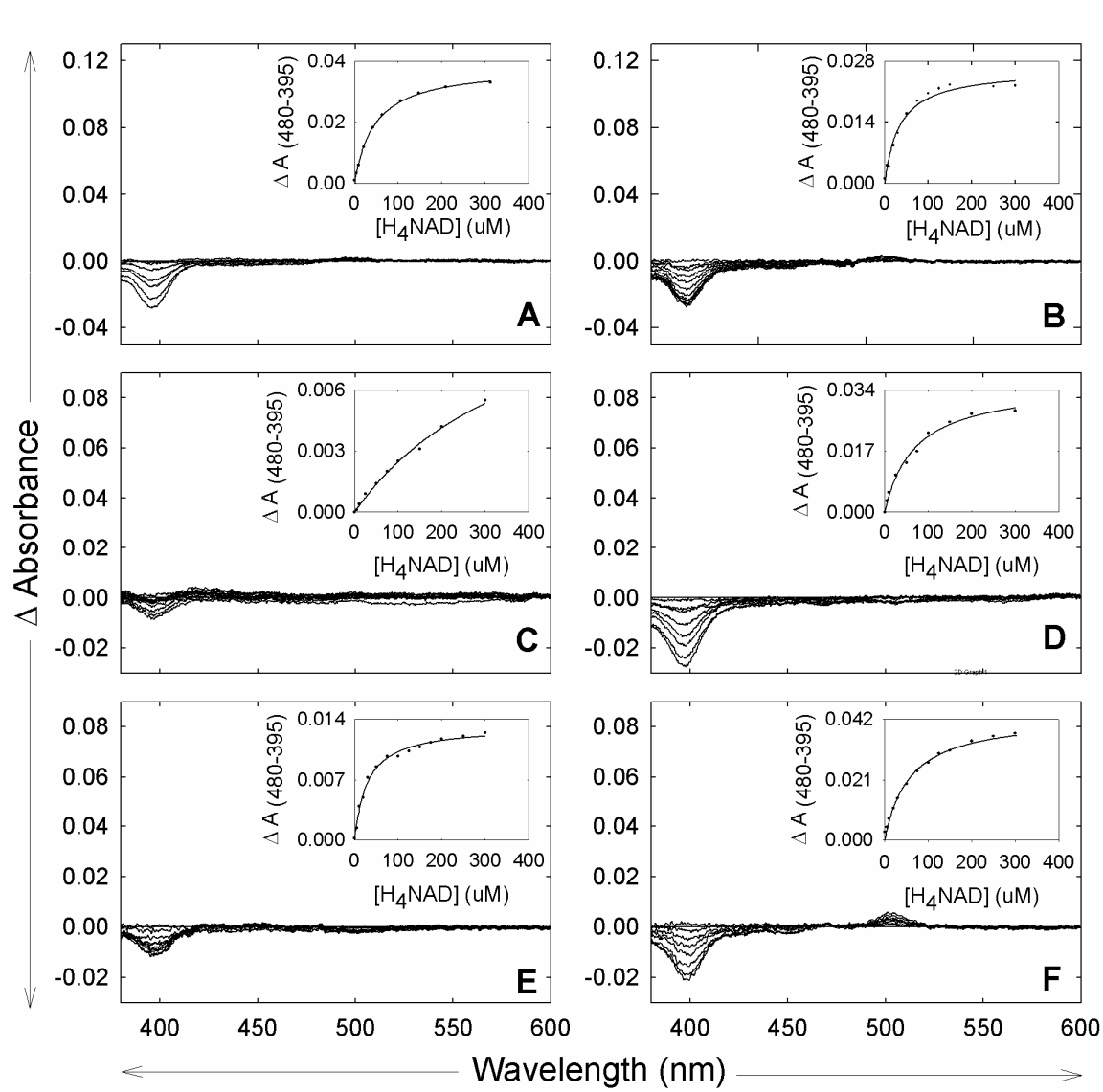

Figure 21. Spectroscopic Titrations of WT cb5r and the Y112 Series of Variants in the Presence of H_4NAD. Titrations of all mutants (50μM) were performed in split cell optical cuvettes in 10mM phosphate buffer containing 0.1mM EDTA, pH 7.0 at 23 °C. Difference spectra were recorded following the addition of solution containing H_4NAD (5mM). The inset panel corresponds to a plot of the magnitude of the spectral perturbations at the indicated wavelengths versus pyridine nucleotide concentration where a difference spectrum was observed. Plots of the relative absorbance changes observed are as follows: (A) H_4cb5r; (B) Y112A; (C) Y112D; (D) Y112F; (E) Y112H; and (F) Y112L.

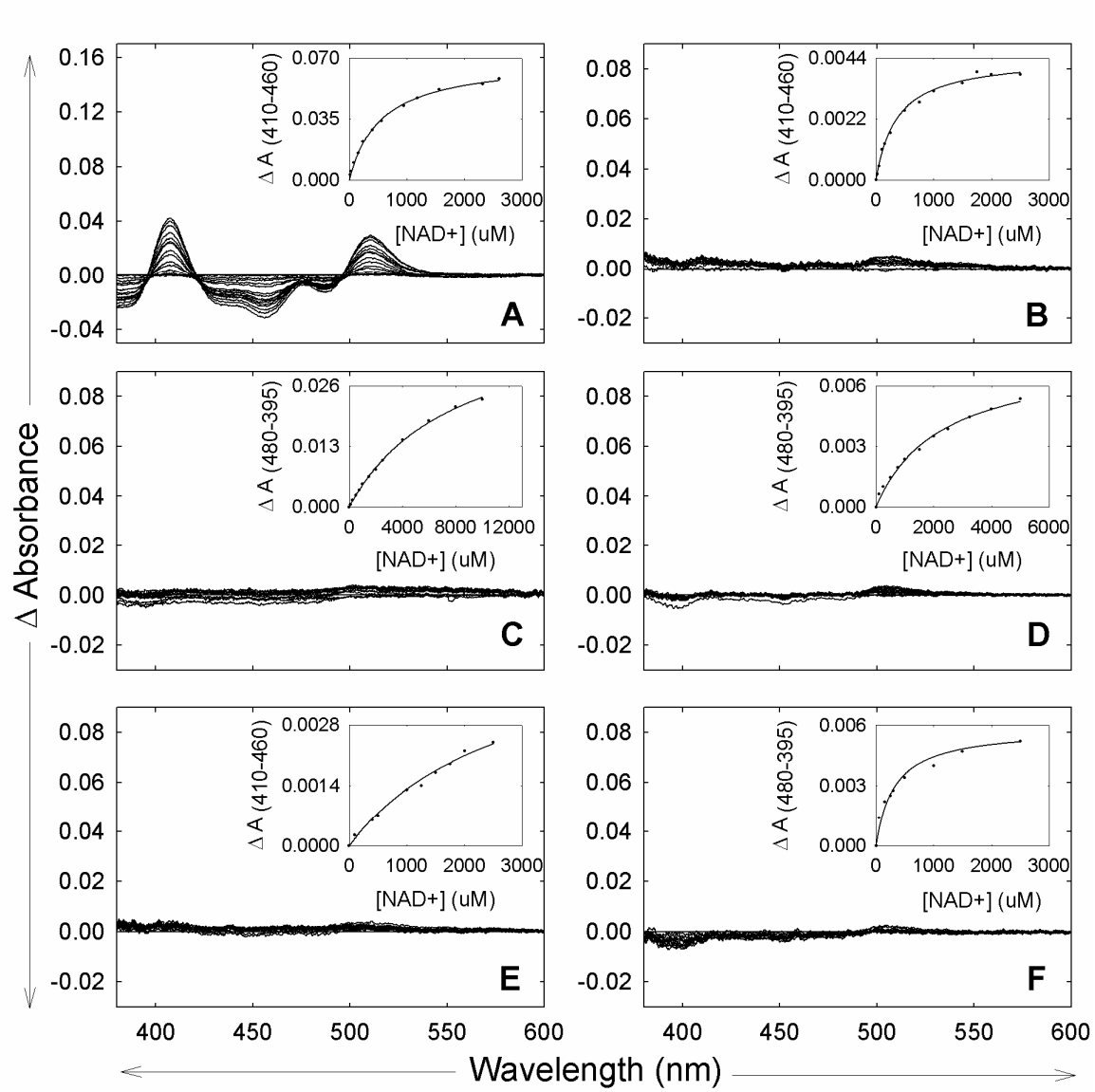

Figure 22. Spectroscopic Titrations of WT cb5r and the Y112 Series of Variants in the Presence of NAD^+. Titrations of all mutants (50μM) were performed in split cell optical cuvettes in 10mM phosphate buffer containing 0.1mM EDTA, pH 7.0 at 23 °C. Difference spectra were recorded following the addition of solution containing NAD^+ (30mM). The inset panel corresponds to a plot of the magnitude of the spectral perturbations at the indicated wavelengths versus pyridine nucleotide concentration where a difference spectrum was observed. Plots of the relative absorbance changes observed are as follows: (A) H_4cb5r; (B) Y112A; (C) Y112D; (D) Y112F; (E) Y112H; and (F) Y112L.

Figure 23. Spectroscopic Titrations of WT cb5r and the Q210 Series of Variants in the Presence of H_4NAD and NAD^+. Titrations of all mutants (50μM) were performed in split cell optical cuvettes in 10mM phosphate buffer containing 0.1mM EDTA, pH 7.0 at 23 °C. Difference spectra were recorded following the addition of solution containing H_4NAD (5mM) (A, C, E, G) NAD^+ (30mM) (B, D, F, H). The inset panel corresponds to a plot of the magnitude of the spectral perturbations at the indicated wavelengths versus pyridine nucleotide concentration where a difference spectrum was observed. Plots of the relative absorbance changes observed are as follows: (A, B) H_4cb5r; (C, D) Q210A; (E, F) Q210R; and (G, H) Q210V.

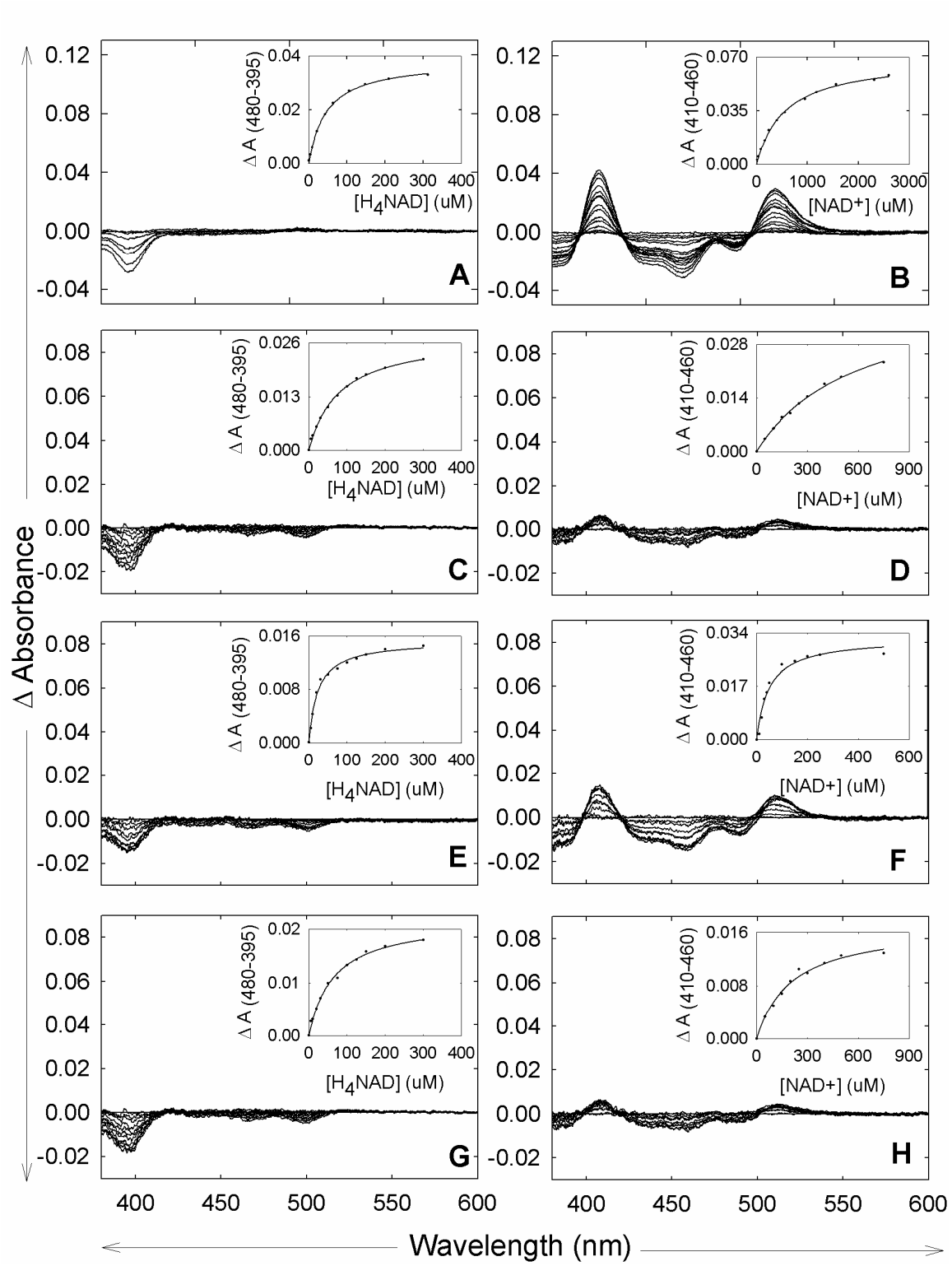
Δ Absorbance
Wavelength (nm)
A
B
C
D
E
F
G
H
Δ A (480-395)
Δ A (410-460)
[H4NAD] (uM)
[NAD+] (uM)

Table 9. Spectral Binding Constants (K_s) and Standard Midpoint Potentials ($E^{o\prime}$) Obtained for the Y112 Series Variants.

cb5r Variant	$K_s^{H_4NAD}$ (μM)	K_s^{NAD+} (μM)	$E^{\circ\prime}_{FAD/FADH_2}$ (mV)	
			-NAD$^+$	*+NAD*$^+$
WT H_4cb5r	45 ± 10	553 ± 30	-271	-190
Y112A	37 ± 4	359 ± 62	-271	-219
Y112D	414 ± 47	7958 ± 410	-261	-201
Y112F	69 ± 9	2234 ± 242	-269	-193
Y112H	28 ± 3	2808 ± 267	-266	-217
Y112L	56 ± 4	313 ± 50	-271	-197

Effects of potential structural changes on the properties of the flavin prosthetic group were examined by determining oxidation-reduction potentials for the FAD cofactor utilizing dye-equilibration titrations in the presence of phenosafranine ($E^{\circ\prime}$ = -252 mV) as described in Methods [117]. Flavin midpoint potentials ($E^{\circ\prime}$, n = 2) for the FAD/$FADH_2$ couple were determined for the variants alone and in the presence of NAD^+. The flavin redox potentials (n = 2) for the WT cytochrome b_5 reductase and generated variants for the FAD/$FADH_2$ couple were determined from the Nernst semi-log plots of the log $([oxidized]/[reduced])_{FAD}$ versus potential (mV) and are shown in Figures 24 and 25 for the Y112 and Q210 series respectively, with the standard midpoint potential values obtained for each shown in Tables 9 and 10, respectively. For the standard flavin midpoint potentials of the Y112 variants in the absence of NAD^+, all potentials were nearly identical to that of the WT domain, indicating that the introduction of structural alterations of these variants did not have a dramatic effect on the environment of the FAD as inferred from flavin midpoint potential. In the presence of NAD^+ however, the resulting midpoint potentials of the variants, with the exception of Y112A, were more

negative than that of the WT domain (-191mV), having a value more comparable to the value obtained for the midpoint potential of free flavin (-220 mV) [133]. Similar results were noted for the Q210 series, with values in the absence of NAD^+ being similar to that of WT and values in the presence of NAD^+ being midway between the expected value for WT and that of free flavin.

Table 10. Spectral Binding Constants (K_s) and Standard Midpoint Potentials ($E^{o\prime}$) Obtained for the Q210 Series Variants.

cb5r Variant	$K_s^{H_4NAD}$ (μM)	K_s^{NAD+} (μM)	$E^{o\prime}_{FAD/FADH_2}$ (mV)	
			$-NAD^+$	$+NAD^+$
WT H_4cb5r	45 ± 10	553 ± 30	-271	-191
Q210A	78 ± 5	578 ± 42	-277	-210
Q210R	22 ± 3	48 ± 8	-271	-204
Q210V	64 ± 8	205 ± 29	-271	-206

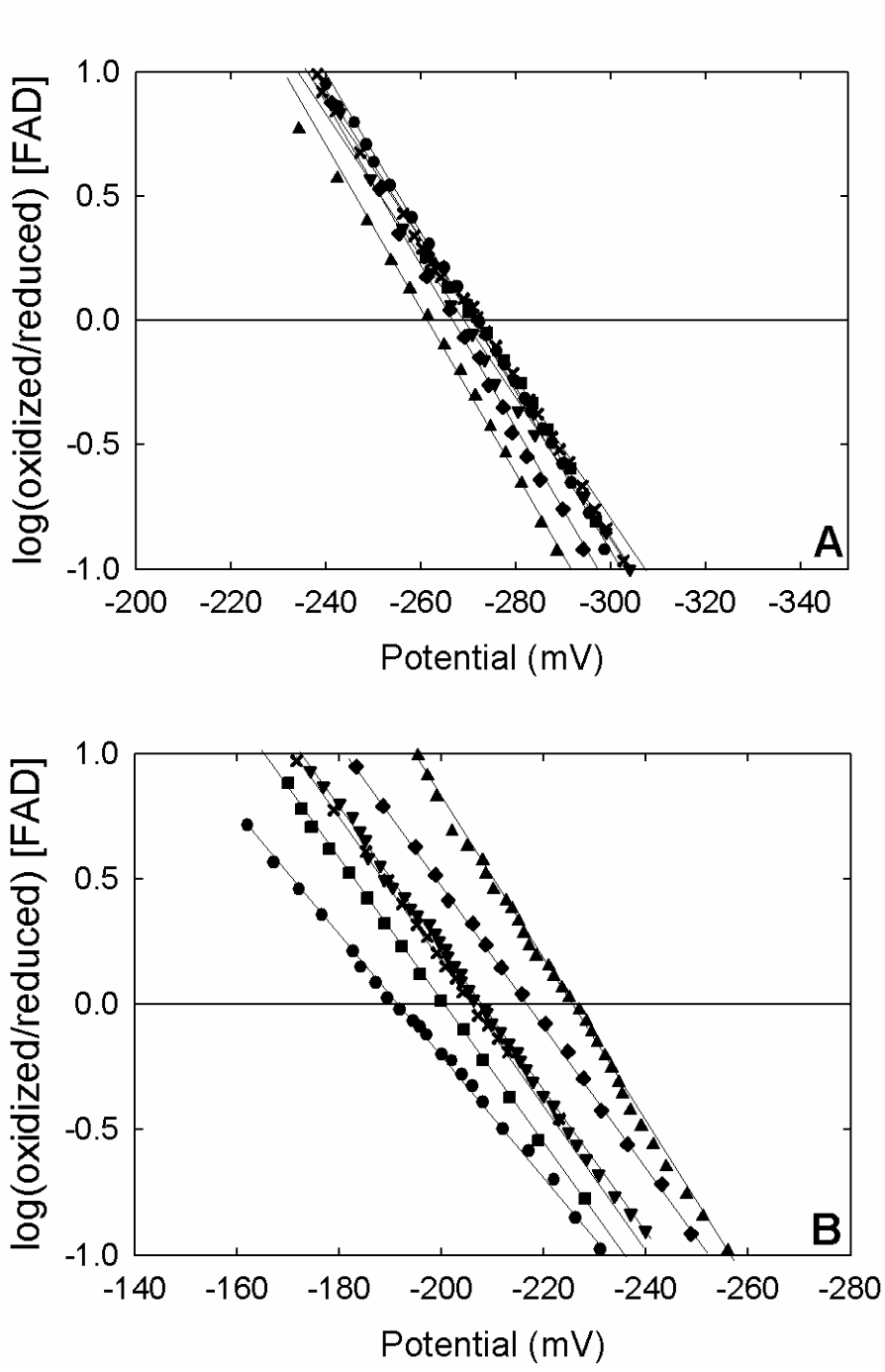

Figure 24. Oxidation-Reduction Midpoint Potentials for the FAD Prosthetic Group in the WT cb5r and Y112 cb5r Variants. Reductive dye titrations were performed at 25 °C as described in "Materials and Methods" using phenosafranine as the indicator dye in 100 mM phosphate buffer containing 0.1 mM EDTA, pH 7.0. Nernst plots in the absence (A) and presence (B) of 2 mM NAD^+. Plots correspond to (●) H_4cb5r; (■) Y112A; (▲) Y112D; (▼) Y112F; (♦)Y112H; and (x) Y112L.

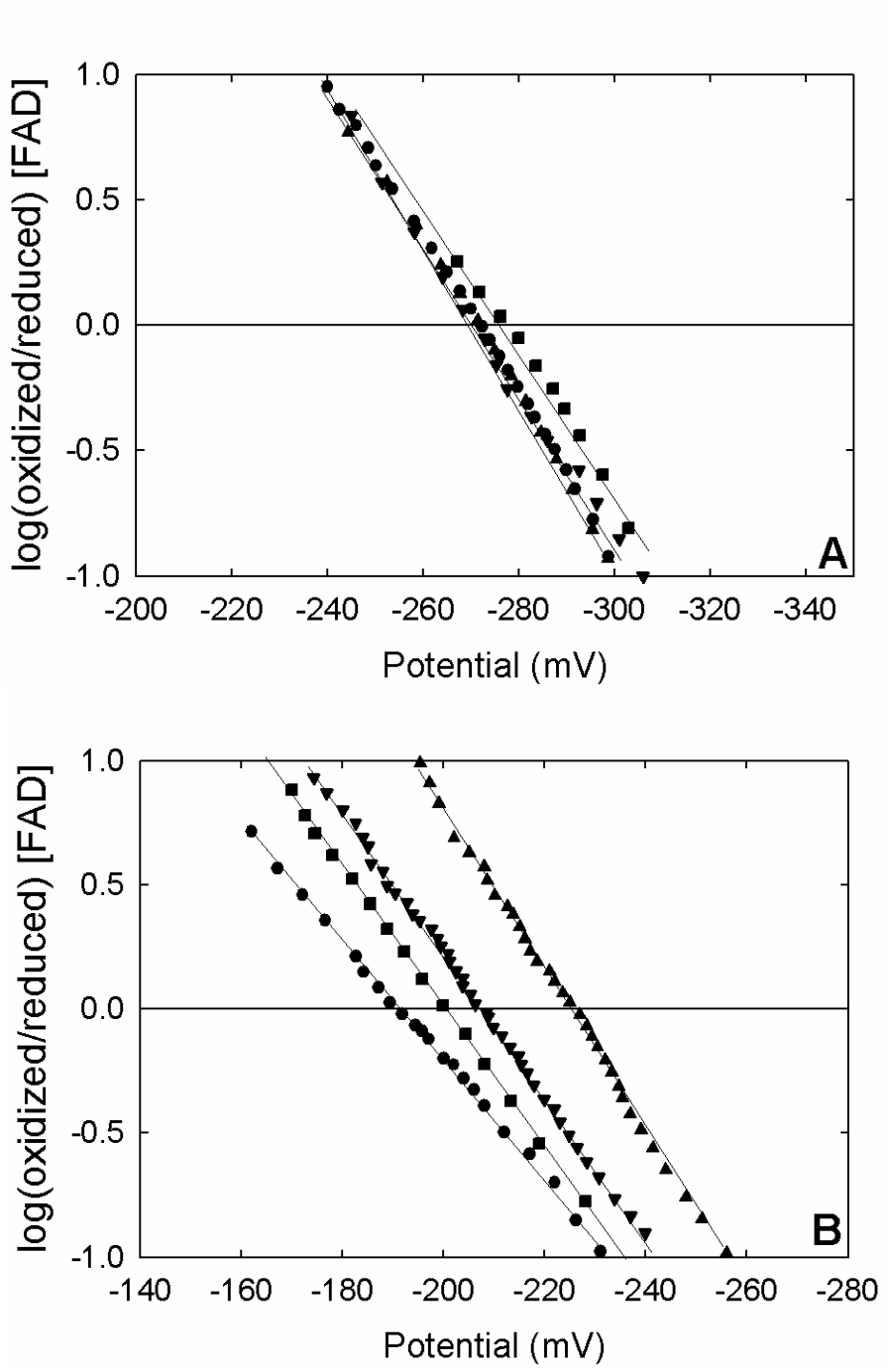

Figure 25. Oxidation-Reduction Midpoint Potentials for the FAD Prosthetic Group in the WT cb5r and Q210 cb5r Variants. Reductive dye titrations were performed at 25 °C as described in "Materials and Methods" using phenosafranine as the indicator dye in 100 mM phosphate buffer containing 0.1 mM EDTA, pH 7.0. Nernst plots in the absence (A) and presence (B) of 2 mM NAD^+. Plots correspond to (●) H_4cb5r; (■) Q210A; (▲) Q210R; and (▼) Q210V.

Summary of Analysis of residues, Y112 and Q210, involved in anchoring of the pyrophosphate backbone of NAD^+

Multiple sequence alignments have demonstrated that residues Y112 and Q210 have a high level of conservation, occurring with only a few exceptions across cb5r proteins from divergent species as well as amongst the members of the FNR family of transhydrogenases. This fact, coupled with the implication of both residues in interactions with the pyrophosphate backbone of bound NAD^+ as demonstrated by X-ray crystallographic studies of the rat variant of cb5r in the presence of the substrate, indicate that these two residues potentially play a vital role in proper structure-function interactions yielding proper enzymatic activity of cb5r. The location of Y112 in the vital FAD associated "lid" region further suggests that this residue in particular may function in some way to ensure proper orientation of both the cofactor and the coenzyme.

In order to fully elucidate the role of each residue, a series of variants were generated corresponding to naturally occurring substitutions observed within the FNR superfamily or in variants of cb5r from divergent species. These included Y112A, D, F, H, and L and Q210A, R, and V. The data presented here provides further insight into the role of these two residues towards correct orientation and binding of the NADH substrate. While both series of variants generated impaired functionality of cb5r to some level, the Y112 variants appeared to demonstrate a greater impact than the Q210 variants. Additionally, among the Y112 variants, the greatest impact was noted in the substitution of the native residue with residues carrying a charge, either positive (H) or negative (D).

Substitution of residue Y112 with any of the chosen residue alterations resulted in some degree of impaired function, regardless of side chain characteristics. In general an

approximate 2 fold decrease in substrate affinity coupled with an approximate 2 fold decrease in rate of turnover was observed for all substitutions in regards to NADH:FR activity. A notable exception to this was the Y112D variant which had a much more profound impact on the turnover rate. These data indicate that changing the side chain at position 112 causes a mild impairment in the binding of NADH, via disruption of the anchoring effect of the hydroxyl group found on the tyrosine side chain. The introduction of a negative charge into this position greatly affected the ability of the protein to not only properly associate with NADH; it directly impacted the ability of the protein to properly function. This is due to disruption of the electrostatic environment near the FAD.

While absorbance spectra and circular dichroism analyses indicate that the flavin environment was not affected, the introduction of the negative charge would impact the ability of FAD to properly accept electrons from the NADH. Analysis of an *in silico* model of Y112 in relation to FAD compared to that of Y112D, suggested that the adenine moiety of FAD in situated close to and associates with Y112. In the WT protein, analysis indicated a moderate positive charge toward the backbone portion of Y112 with the end of the side chain having a mildly negative charge. This polarity compliments the charge dispersal on the adenine moiety of FAD. The proposed model of D112 in association with FAD indicates a highly negative region being introduced into a pocket of positive charges found in the FAD. The introduction of this level of strong negative charge into a region normally occupied by a mild electronegative charge would be sufficient to disrupt the electron transfer properties of FAD, rendering it unable to efficiently accept electrons from NADH. This would support the drastic effects observed

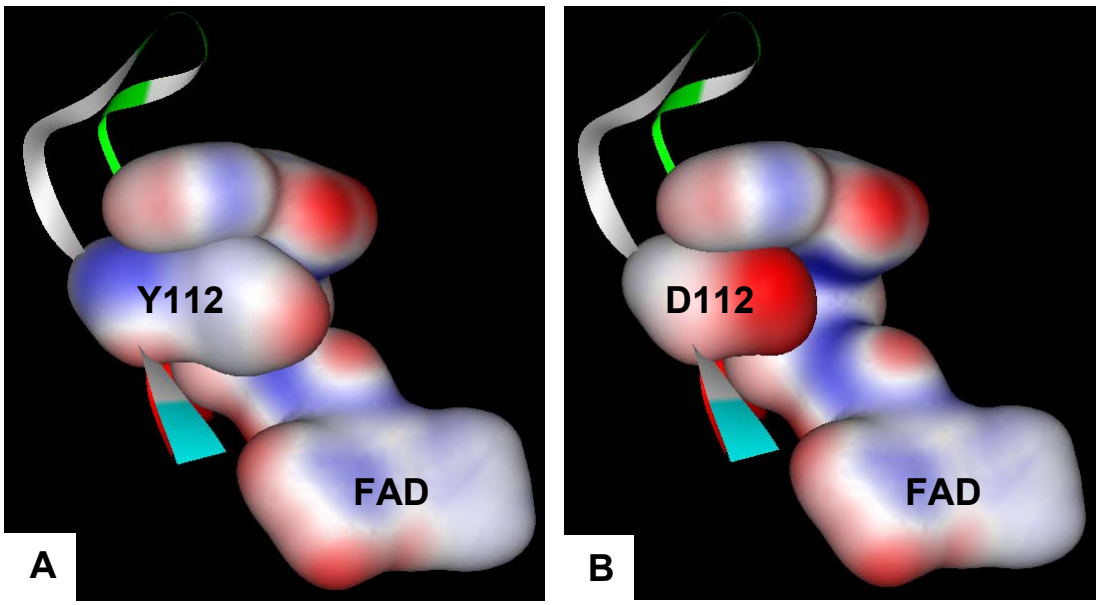

Figure 26. Structures of WT cb5r and the Y112D Variant with FAD Generated *in silica*. The molecular model of cb5r displaying the charged surfaces of (A) residue Y112 and (B) cb5r variant Y112D in association with FAD generated utilizing the automated comparative protein modeling server SWISS-MODEL [111] and analyzed using the molecular modeling software Web Lab Viewer Pro [134]. This model represents a surface representation of cb5r in complex with FAD (1IB0) where the acidic residues are red, basic residues are blue, and neutral residues are displayed as white clouds.

seen on the k_{cat} value for Y112D, being one-twentieth that of WT and the midpoint potential in the presence of NAD^+ being comparable to that of free flavin. These effects may also be indirect, with alterations of the Y112 residue affecting nearby residues in the "lid" region responsible for proper FAD incorporation. Additionally, the presence of the negative charge from the carboxylic acid side chain would prevent the NADH from associating correctly. This latter fact is made more evident by the 10-fold+ greater spectral binding constants for H_4NAD and NAD^+.

Of notable importance is the fact that all substitutions at residue Y112 resulted in altered and/or diminished differential spectra when titrated with NAD^+. This indicates

that the hydroxyl group of Y112 is important to properly orient the product. In its absence, the NAD^+ adopts an altered conformation for binding. Despite this fact, the differential spectra for the variants in the presence of H_4NAD retained similar line shape to WT, with only diminished intensities. This indicates that the isosteric analog was bound similar in the variant.

Unlike Y112, residue Q210 demonstrated a moderately higher level of tolerance to substitutions made to the side chain. In the case of all variants, catalytic efficiency was decreased, but not to the magnitude observed in Y112. Interestingly, affinity for binding of substrate, as indicated by both the K_m value from NADH:FR assays and the K_s values in the presence of H_4NAD and NAD^+, was increased in the case of Q210R. From *in silica* modeling of the cb5r structure with the Q210R mutation we observed that the positive charge on the WT residue centered in the area between the pyrophosphate and adenine moieties of NAD^+ would be diminished in the Q210R variant. This change might result in a decrease in the attraction in this area, but would not eliminate it entirely, thus not decreasing the binding constants associated with it. Furthermore, the distal end of the side chain in Q210R redirects away from the NAD^+ as compared to the WT. This would decrease any physical/steric obstruction that would exist in the native structure, thereby allowing for easier access of NAD^+ to the environment, explaining the increased affinity observed for Q210R. Q210V also showed an increased affinity for NAD^+, as determined by differential spectroscopy, which was also likely due to the decreased steric hindrance from the shortened side chain. Due to the greater affinity shown for NAD^+ in both Q210R and V, we conducted inhibition assays in the presence of NAD^+. The resulting K_i values (data not shown) for the Q210R and Q210V variants (639 μM and 677

μM respectively) were not significantly different than the value for WT cb5r (675 μM), indicating that the decreased catalytic efficiency was not due to product inhibition, and instead likely results from misalignment between the cofactor and substrate.

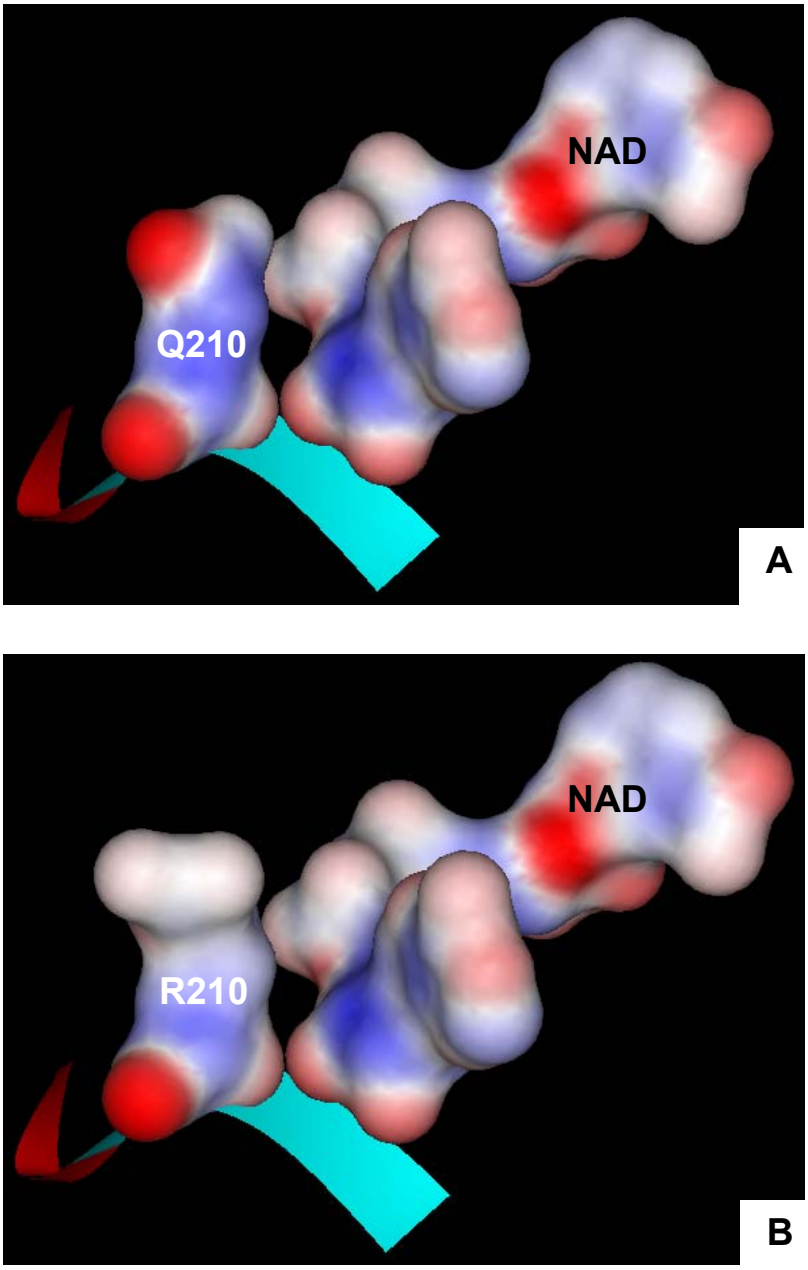

Figure 27. Structures of WT cb5r and the Q210R Variant with FAD Generated *in silica*. The molecular model of cb5r displaying the charged surfaces of (A) residue Q210 and (B) cb5r variant Q210R in association with FAD generated utilizing the automated comparative protein modeling server SWISS-MODEL [111] and analyzed using the molecular modeling software Web Lab Viewer Pro [134]. This model represents a surface representation of cb5r in complex with FAD (1IB0) where the acidic residues are red, basic residues are blue, and neutral residues are displayed as white clouds.

Characterization of the Type I Recessive Congenital Methemoglobinemia Mutants T116S and E212K

In proximity to the two highly conserved NAD^+ phosphate backbone binding residues, Y112 and Q210, are two additional residues of which naturally occurring mutants have been identified that result in a diagnosis with type I Recessive Congenital Methemoglobinemia. These naturally occurring mutations are T116S and E212K, both originally discovered in patients of African American decent.

Previous studies first identified a transversion of C-to-G at codon 116 in exon 5 of cb5r, resulting in a T116S mutant, which was found in two unrelated African American methemoglobinemic patients. Further analysis demonstrated that not only did both patients have the variant, their asymptomatic relatives as well as unselected healthy African-American controls with normal enzymatic function were also either heterozygous or homozygous for this substitution, with an allelic frequency of 0.23 [135]. The T116S mutation was not, however, found in Caucasian, Asian, Indo-Aryan, of Arabic subjects tested, thus suggesting that this was a high frequency polymorphism unique to African American populations. To date, however, no selective advantage has been linked to the presence of this polymorphism [135].

Further studies were carried out on one of the patients having the T116S mutation. The patient was found to also be homozygous for a G to A transition in exon 8 at codon 212 resulting in the amino acid substitution E212K. The patient's mother was also shown to be heterozygous for this mutation, and displayed decreased enzymatic activity. Unlike the T116S mutation, analysis indicated that among 62 African-American and 54 unselected white individuals, the E212K mutation occurred only in the propositus and her

mother, indicating that E212K is not a polymorphism. The combination of a polymorphism and a single pathogenic mutation has been shown to result in disease phenotypes in the case of fatal familial insomnia, Creutzfeld-Jacob disease, and primary hyperoxaluria type I. Thus it is possible that the E212K mutation is alone causative of RCM type I in the patient, or it may interact with the T116S, and this combination leads to the disease phenotype [135].

To further elucidate the effects of the naturally occurring T116S polymorphism and the E212K mutation on the functioning of cb5r, a series of variants were generated including T116S, E212K and a double mutant T116s/E212K as described in "Methods and Materials," utilizing the original four-histidine tagged cb5r expression construct and the corresponding oligonucleotide primers listed in Appendix A. These variants were characterized on the basis of kinetic, spectral, and thermal stability parameters.

UV/visible absorbance spectra were obtained for oxidized samples of the purified RCM variants T116S, E212K, and T116S/E212K and were compared with the spectra obtained for the corresponding WT domain in (Figure 28A). All three variants exhibited spectra identical to that of the WT domain, characterized by absorption maximum detected at 273 nm in the UV range of the spectrum, and a peak at 461 nm with an associated pronounced shoulder in the range of 485-500 nm in the visible region of the spectrum, the latter peak attributable to protein- bound flavin. The $A_{273\ nm}/A_{461\ nm}$ absorbance ratios of the variants were within the range of 5.9 ± 0.2, comparable to values previously obtained for WT rat cb5r of 5.7 ± 0.2 [121], indicating a full complement of the FAD prosthetic group.

To assess any alterations in the secondary structural content of the different type I

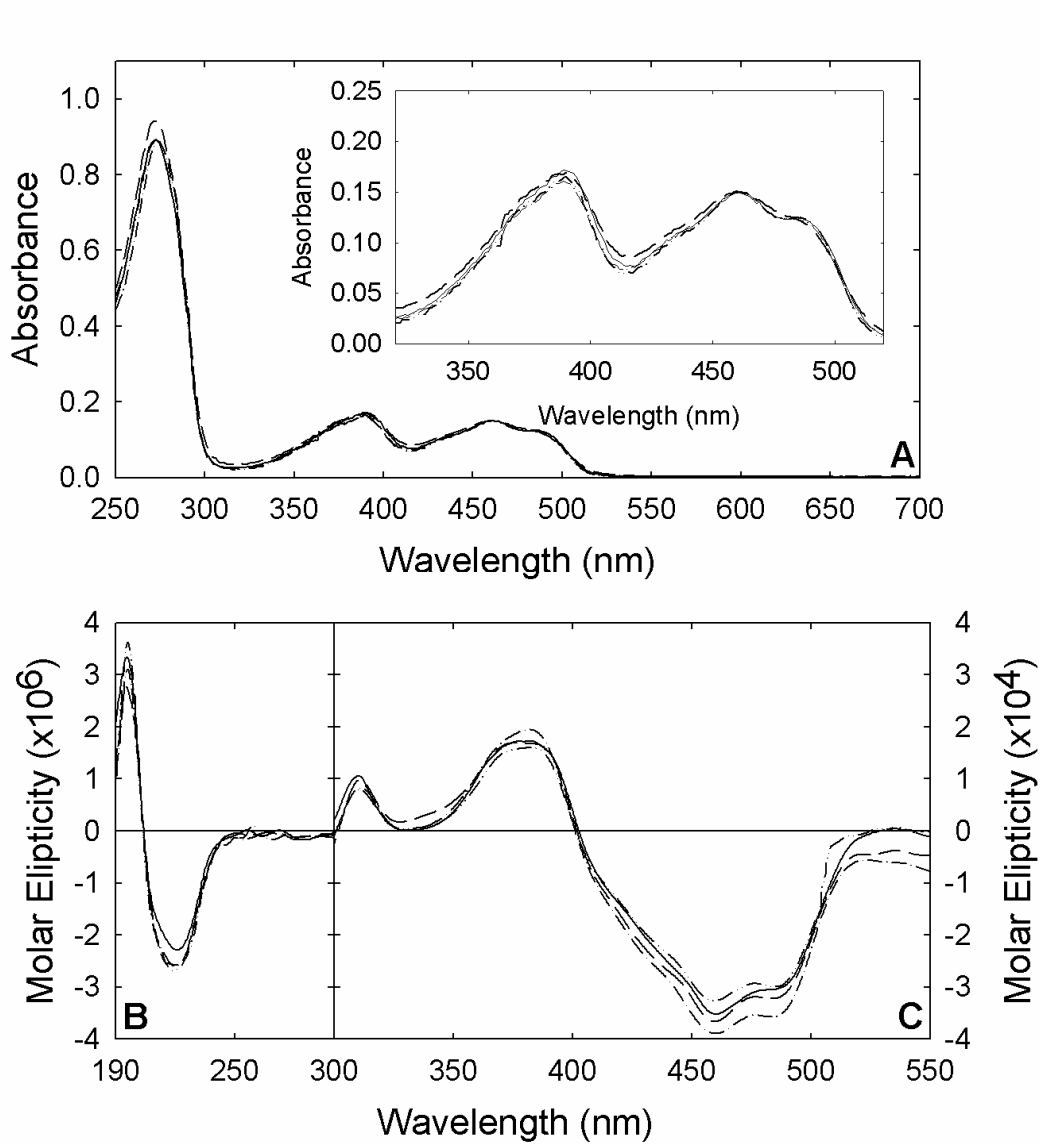

Figure 28. Ultra-Violet, Visible, and Circular Dichroism Spectra Obtained for the RCM Type I Associated Mutants T116S, E212K and T116S/E212K (A) UV/visible absorption spectra were obtained for oxidized samples of cb5r and the T116S, E212K and T116S/E212K mutants at equivalent flavin concentrations (1.7 μM FAD) in 10 mM phosphate buffer, containing 0.1 mM EDTA, pH 7.0. The inset shows an expanded region of the visible spectrum where the flavin prosthetic group makes a major contribution. Individual spectra correspond to WT cb5r (—); T116S (--- ---); E212K (-.-.-); and T116S/E212K (-..-..-); (B) UV CD spectra were recorded using enzyme samples (7 μM FAD) in 10 mM phosphate buffer, containing 0.1 mM EDTA, pH 7.0. (C) Visible CD spectra were recorded using enzyme samples (50 μM FAD) in 10 mM phosphate buffer, containing 0.1 mM EDTA, pH 7.0. Line styles shown in "B" and "C" are the same as those depicted in "A".

RCM cb5r variants, circular dichroism spectra were recorded in the UV wavelength range (190-300 nm). As shown in Figure 28B, all three variants exhibited positive CD spectra from 190-210 nm and negative CD spectra from 210-250 nm with the spectra retaining both positive and negative intensities very similar to that of the WT domain. The absence of any significant differences between the spectra of the various mutants and the WT domain suggested conservation of the secondary structure architecture and that none of the amino acid substitutions or deletions had any substantial effects on the folding of the protein. Visible CD spectroscopy was utilized to examine the environment of the FAD prosthetic group. As shown in Figure 28C, all three variants generated exhibited visible CD spectra that were virtually indistinguishable from that of WT cb5r, indicating that none of the amino acid substitutions had any significant effect on the conformation of the bound FAD prosthetic group.

To assess the effect of the mutations on the catalytic function of the enzyme, initial rate kinetic parameters for NADH:FR assays were determined for the WT cb5r and for each purified variant. The values obtained for the NADH:FR assays are presented in Table 11. Of the three mutations, the double mutant T116S/E212K demonstrated the greatest decrease in both k_{cat} and K_m^{NADH}, retaining approximately 31% of WT catalytic efficiency (k_{cat}/K_m^{NADH}) with the individual mutations T116S and E212K retaining 45% and 37% of WT efficiency respectively. The observed decrease on overall catalytic efficiency was attributable to both moderate decreases of the k_{cat} as well as a decrease in substrate affinity, with observed K_m^{NADH} of each mutant being 1-1.5 times greater than that of WT enzyme.

To examine the influence of the various amino acid substitutions on protein

stability, the thermal NADH:FR inactivation profile coupled with the increase in intrinsic flavin fluorescence and emission intensity of each of the variants was monitored and was compared to values obtained for WT enzyme. The results obtained for the thermal denaturation profiles and changes in intrinsic flavin fluorescence are shown in Figure 29. Changes in the intrinsic fluorescence of the cofactor or the retention of NADH:FR activity following thermal denaturation was an effective indicator of the stability of the core structure of the protein. T_{50} values (the temperature at which 50% of maximum fluorescence and 50% retention of NADH:FR activity was detected) are reported in Table 11 and ranged from of 49.6 °C for the T116S/E212K mutant to a high of 55.5 °C for the T116S variant as compared to a T_{50} of 56 °C obtained for WT cb5r.

Table 11. NADH:FR Kinetic Constants and Thermal Stability (T_{50}) Values for the Type I RCM Associated Mutants T116S, E212K, and T116S/E212K

cb5r Variant	NADH:FR				
	k_{cat} (s^{-1})	K_m^{NADH} (μM)	K_m^{FeCN6} (μM)	k_{cat}/K_m^{NADH} (s^{-1} M^{-1})	T_{50} (°C)
WT H_4cb5r	800 ± 17	6.0 ± 1	8 ± 1	1.4 ± 0.3 x 10^8	56.1
T116S	676 ± 11	10.8 ± 0.8	8 ± 1	6.4 ± 0.6 x 10^7	55.5
E212K	546 ± 10	10.5 ± 0.9	7 ± 1	5.2 ± 0.5 x 10^7	51.2
T1116S/E212K	498 ± 23	11.4 ± 0.9	8 ± 1	4.4 ± 0.6 x 10^7	49.6

Differential spectroscopy was used to evaluate the effect of the RCM mutations on the binding affinity for both the isosteric NADH analog H_4NAD and NAD^+. As shown in Figure 30, both of the individual mutations resulted in similar line shapes for the spectra in both titrations, and exhibited moderately increased affinity, as indicated by decreased K_s values, for both titrated compounds (Table 12). The T116S/E212K double

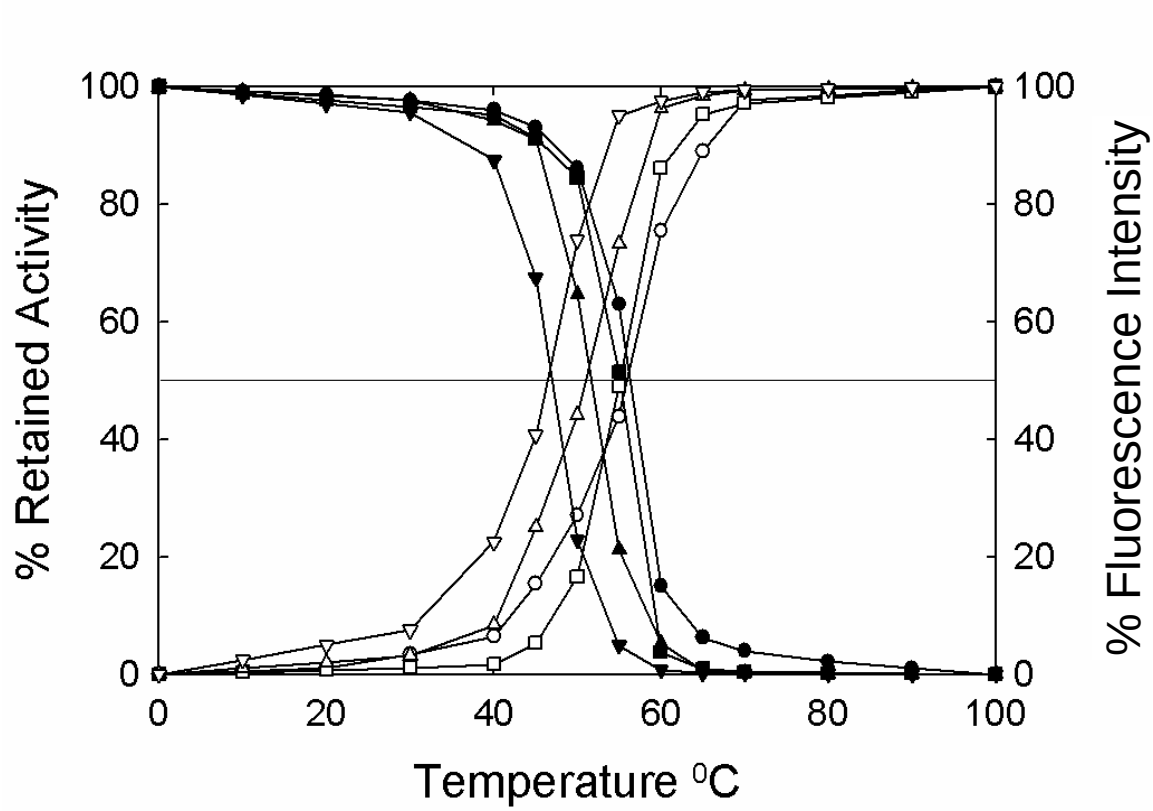

Figure 29. Temperature Stability Profiles Obtained for the Type I RCM Associated Mutants T116S, E212K, and T116S/E212K. Oxidized samples of WT H_4cb5r (5 μM FAD) and cb5r RCM variants were incubated at the indicated temperatures, and aliquots were withdrawn and assayed for both residual NADH:FR activity (closed symbols) and intrinsic flavin fluorescence (open symbols) in 10 mM phosphate buffer, containing 0.1 mM EDTA, pH 7.0 using excitation and emission wavelengths of 450 nm and 523 nm, respectively. Points correspond to (●,○) H_4cb5r; (■, □) T116S; (▲, Δ) E212K; and (▼,▽) T116S/E212K

mutant showed lineshape and K_s value comparable to that of WT for the H_4NAD titration.

In titrations with NAD^+, however, a diminished intensity was noted in the titrated spectra, while maintaining similar line shape. The binding constant again, was significantly decreased (187μM compared to 553μM for WT) indicating increased

affinity for the product.

Effects of potential structural changes on the properties of the flavin prosthetic group were examined by determining the oxidation-reduction potentials for the FAD cofactor as described in the "Methods" section. Flavin midpoint potentials (E°′, n = 2) for the FAD/$FADH_2$ couple were determined for the variants alone and in the presence of NAD^+. Spectra obtained during a representative titration of the WT cb5r protein are shown in Figure 31. With out the addition of NAD^+ to the titration, each of the mutations demonstrated midpoint potentials equivalent to that of WT, ranging from -272mV to -266mV. In the presence of NAD^+ however, all the mutations had midpoint values that ranged from -208mV to -200 mV, showing a positive shift, as was observed for WT cb5r. Values for midpoints at reported in Table 12.

Table 12. Spectral Binding Constants (K_s) and Standard Midpoint Potentials ($E^{o\prime}$) Obtained for the Type I RCM mutants T116S, E212K and T116S/E212K

cb5r Variant	$K_s^{H_4NAD}$ (μM)	K_s^{NAD+} (μM)	$E^{\circ\prime}_{FAD/FADH_2}$ (mV)	
			$-NAD^+$	$+NAD^+$
WT H_4cb5r	45 ± 10	553 ± 30	-271	-191
T116S	37 ± 12	261 ± 23	-269	-200
E212K	20 ± 2	88 ± 6	-266	-205
T116S/E212K	56 ± 3	187 ± 13	-272	-208

Figure 30. Spectroscopic Titrations of WT cb5r and the Type I RCM Mutants T116S, E212K, and T116S/E212K in the presence of H_4NAD and NAD^+. Titrations of all mutants (50μM) were performed in split cell optical cuvettes in 10mM phosphate buffer containing 0.1mM EDTA, pH 7.0 at 23 °C. Difference spectra were recorded following the addition of solution containing H_4NAD (5mM) (A, C, E, G) NAD^+ (30mM) (B, D, F, H). The inset panel corresponds to a plot of the magnitude of the spectral perturbations at the indicated wavelengths versus pyridine nucleotide concentration where a difference spectrum was observed. Plots of the relative absorbance changes observed are as follows: (A, B) WT cb5r; (C, D) T116S; (E, F) E212K; and (G, H) T116S/E212K.

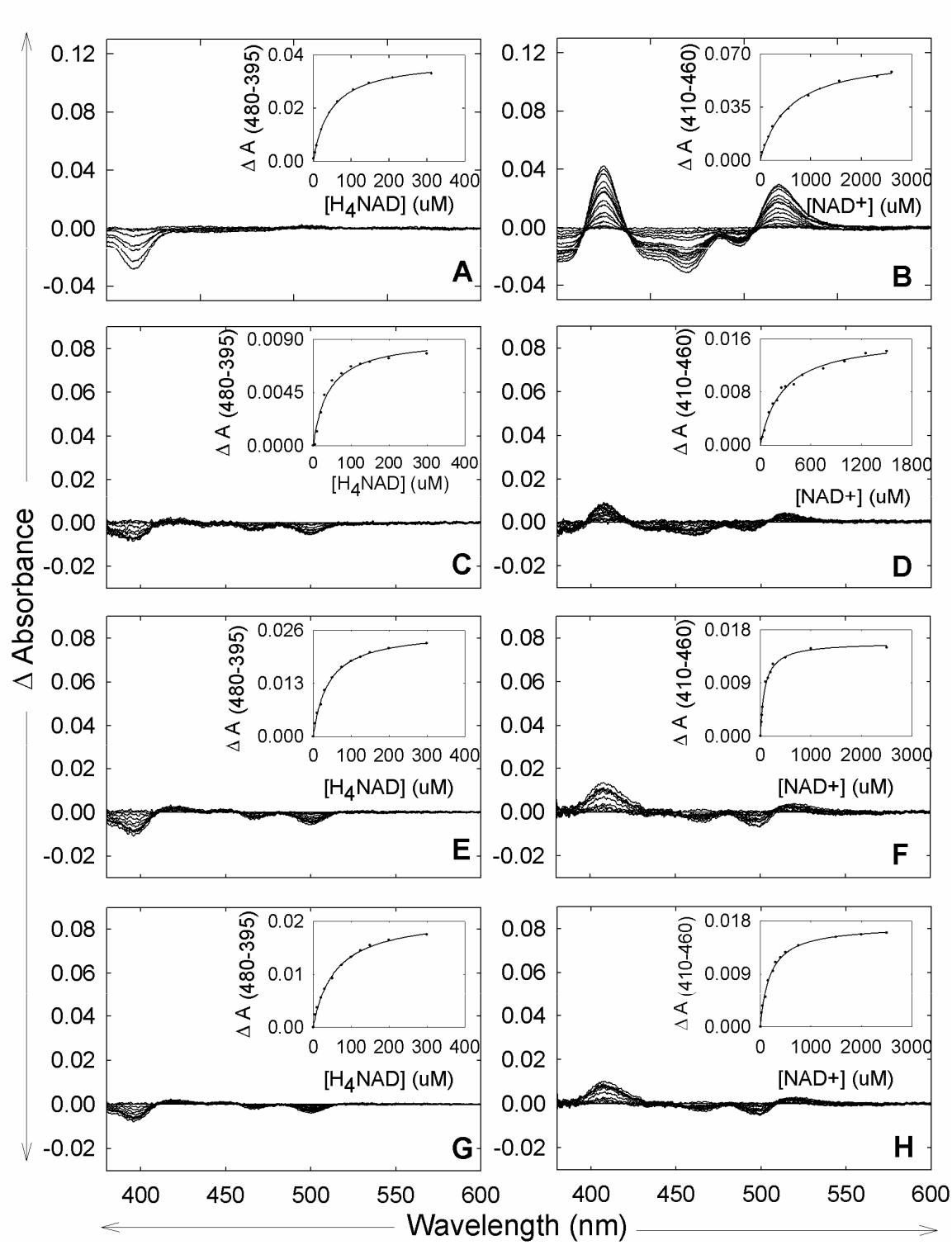
Δ Absorbance
Wavelength (nm)
A
B
C
D
E
F
G
H
Δ A (480-395)
Δ A (410-460)
[H4NAD] (uM)
[NAD+] (uM)

Summary of the Characterization of the Type I Recessive Congenital Methemoglobinemia Mutants T116S and E212K

Previous investigations by Prchal et. al. [135] identified two unique point mutations in the *DIA*1 gene of individuals of African American decent displaying disease phenotype for Type I RCM. The two mutations correspond to two distinct amino acid substitutions in the cb5r protein, T116S and E212K, with one individual being homozygous for both mutations. After further investigation including samples from a large pool of unselected individuals of diverse ethnic backgrounds, it was concluded that, while the E212K mutation was unique to individuals expressing a disease phenotype, the T116S mutation was a polymorphism, occurring in approximately 20% of healthy African American subjects, but not found in subjects of different ethnic backgrounds [135]. Thus, it is likely that the E212K mutation is the causative agent in the presentation of RCM in the patient. The data here further investigated the properties of E212K, as well as T116S and a double mutant T1116S/E212K, in order to determine the nature of these variants and how their contribution to the presentation of the disease.

Both residues are located on the external surface of the cb5r protein as shown in Figure 32. Neither residue is involved in any contacts between the protein and its co-factor or substrate. Thus, any effect on the catalytic function of the enzyme would likely be the result of alterations to interactions between residues, protein structure, or stability.

Analysis of the structure of the mutants through the use of UV/Visible absorbance and circular dichroism spectroscopy indicated that the mutants did not differ significantly in overall secondary structure from the WT protein, and incorporated the FAD cofactor in a similar manner. Initial-rate kinetic studies indicated that the mutants maintained greater

than 50% of the rate of turn-over exhibited by the WT enzyme, and did not significantly differ in the binding affinity for substrate as indicated by similar K_m values. In addition, differential spectroscopy indicated that each of the three mutants bound H_4NAD, a non-reactive analog of NADH, in a manner similar to WT and with equal or greater affinity.

The mutants did, however, differ from WT in two significant properties. First, thermal stability studies, monitoring decrease of activity and increase of intrinsic fluorescence as a function of increasing temperature, showed that each of the mutations, not just E212K or the double mutant, resulted in decreased stability, with T_{50} values significantly lower than that of WT, particularly in the case of the double mutation. This would indicate a potential causation for the disease phenotype. Since circulating erythrocytes do not generate additional copies of proteins during their lifespan, proteins with a decreased stability would degrade over time and thus not be able to properly and efficiently carry out their functions. This is a common cause for type I RCM, which is limited to dysfunction in the soluble cb5r found in circulating erythrocytes.

The second notable difference found in all the mutants as compared to WT, was an increased affinity for NAD^+ as shown in differential spectroscopy. While the line shapes for the spectra resulting from titration with increasing amounts of NAD^+ were similar to that of WT, each of the three mutant proteins exhibited lower K_s values, suggesting that they were able to bind NAD^+ more efficiently than WT. This suggests the possibility of competitive inhibition of catalytic function

The premise that E212K is itself sufficient to elicit the disease phenotype observed in a homozygous individual having the mutation is plausible. The mutation clearly does decrease the catalytic properties of the protein, albeit only moderately, which

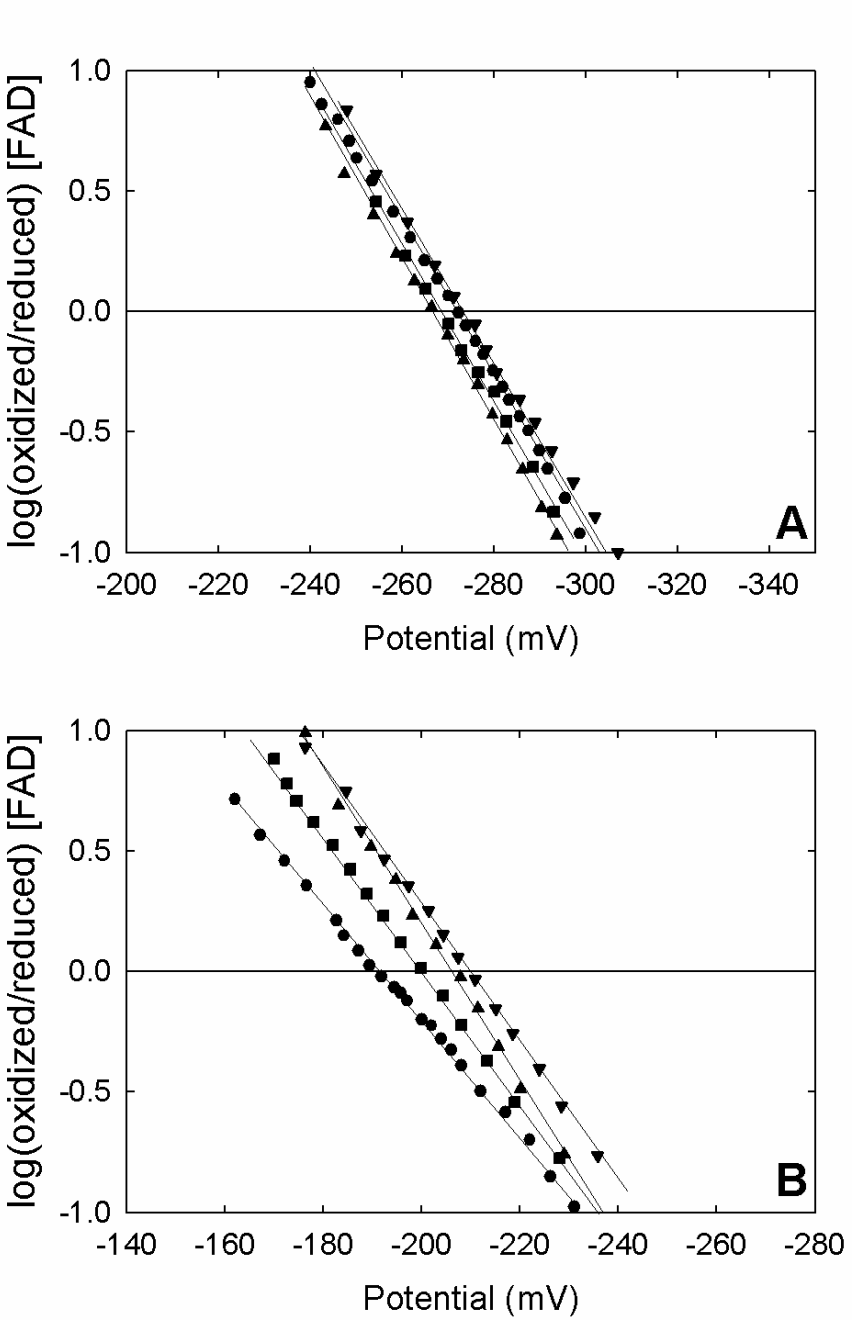

Figure 31. Oxidation-Reduction Midpoint Potentials for the FAD Prosthetic Group in the WT cb5r and the Type I RCM Associated Mutants T116S, E212K, and T116S/E212K. Reductive dye titrations were performed at 25 °C as described in "Materials and Methods" using phenosafranine as the indicator dye in 100 mM phosphate buffer containing 0.1 mM EDTA, pH 7.0. Nernst plots in the absence (A) and presence (B) of 2 mM NAD^+. Plots correspond to (●) H_4cb5r; (■) T116S; (▲) E212K; and (▼) T116S/E212K

would likely invoke the minor phenotypic presentation of symptoms seen in the patient; the patient had slightly elevated methemoglobin levels and exhibited enzyme activity close to that of a heterozygous individual. Additionally, the decreased stability generated by the E212K mutation likely adds to the presentation, limiting the amount of partially functional protein available to reduce methemoglobin. The stability issue is potentially due to the introduction of a lysine which can become involved in cross linkages in the protein, destabilizing interactions among residues leading to a less thermally stable protein overall. This alteration to structure is likely only minor, as no significant changes in CD spectra were noted, but enough to cause the decrease in stability.

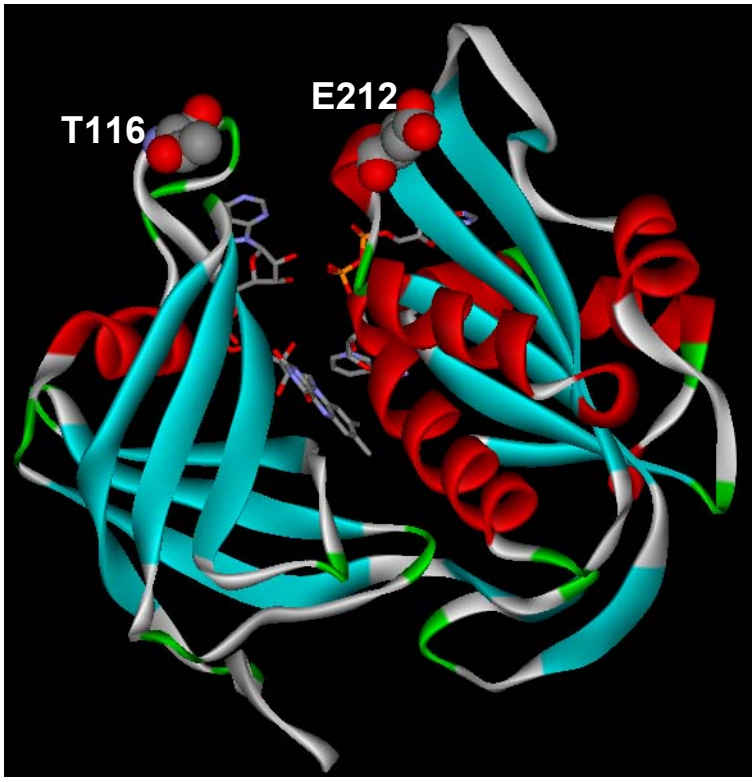

Figure 32. Structural Model of cb5r Showing Position of Residues T116 and E212. Ribbon depiction of the tertiary structure of WT cb5r. Residues T116 and E212 are presented in CPK form. Residues are located on the external surface of the protein outside the FAD and NADH- binding pocket.

Most interesting of the results, however, is the fact that the T116S substitution, reported as a polymorphism that occurs in 20% of the African American population, was also responsible for causing decreased functionality of the protein. The results for T116S were along the same degree of severity as the E212K mutation. The main difference appeared in the stability of the variant, with T116S demonstrating a thermal stability equivalent to that of WT. Since the T116S variant is not unstable, it would not degrade in the circulating erythrocytes, and thus not generate the same level of presentation as the E212K mutation. This could explain why individuals with the polymorphism appear healthy and without signs of methemoglobinemia. The combination of the T116S substitution with E212K does however increase the detrimental effects of both mutations.

The proposition that the presence of the polymorphism T116S in conjunction with the mutation E212K may potentially increase the effect of the mutation was analyzed by characterization of a double mutant containing both substitutions. Similar results were observed for the double mutant as were observed in the E212K variant, with the detrimental effects to catalytic efficiency and stability presenting to an even greater degree than with the E212K substitution alone. Again, it would seem that the greatest impact of the mutations is in decreasing the stability of the protein, decreasing the life span of the protein in the erythrocytes.

Mutagenesis of conserved residue G179: Role in Pyridine Nucleotide Specificity

Within the cb5r primary structure, four sequence motifs have been identified that are involved in either flavin binding ("$RxY^{T}_{S}xx^{S}_{N}$") and FAD/FMN selectivity ("Gxx^{S}_{T}"), or reduced pyridine nucleotide binding ("GxGxxP" and "CGxxxxM") [22, 136] together with several residues that have been shown to regulate NADH/NADPH sepcificity [123]. One of the conserved motifs involved in pyridine nucleotide binding corresponds to the six amino acid residue motif, "GxGxxP", that comprises residues G180 to P185 in the carboxyl-terminal lobe of rat cb5r (Figure 33). However, structural studies have identified a number of additional residues that also surround this motif in the primary sequence and which are potentially involved in regulating nucleotide binding, including G179, which is obligatorily conserved in all cb5r primary structures identified to date with the exception of the outer mitochondrial membrane form of *S. cerevisiae* cb5r [137].

Within the X-ray structure of the rat cb5r diaphorase domain (PDB=1I7P), G179 has been shown to be located at the terminus of the strand Nβ1, which is part of a six-stranded parallel β-sheet motif, and just prior to the start of the helix NαA, which comprises residues G180 to K195, both of which comprise part of the pyridine nucleotide-binding lobe [58]. Residues G179 to G182 form a compact four residue segment of the sequence that effectively reverses the direction of the polypeptide backbone and initiates the start of the α-helical segment. In addition, analysis of the diaphorase domain structure obtained in complex with NAD^{+} (PDB=1IB0) has revealed that while G179 provides no direct electrostatic or hydrogen bond contacts with either the nicotinamide or ribose moieties of the bound NAD^{+}, the two conserved glycine residues

in the adjacent "GxGxxP" motif, corresponding to G180 and G182, do participate in

Species	Sequence	Accession #
H. sapiens	^{173}SVGMIA**G**GTGITPMLQVIRAI^{193}	NP_000389
B. taurus	^{173}SVGMIA**G**GTGITPMLQVIRAI^{193}	P07514
S. scrofa	^{145}SVGMIA**G**GTGITPMLQVIRAI^{163}	1NDH
R. norvegicus	^{173}SVGMIA**G**GTGITPMLQVIRAV^{193}	P20070
M. musculus	^{176}KLGMIA**G**GTGITPMLQLIRAI^{197}	NP_084063
G. gallus	^{127}HLGMIA**G**GTGITPMLQLIRHI^{147}	XP_416445
D. rerio	^{176}SLGLIA**G**GTGITPMLQLIRDI^{196}	AAH45880
I. furcatus	^{173}HLGMIA**G**GTGITPMLQIIRGI^{193}	CK408748
X. laevis	^{173}HLGMIA**G**GTGITPMLQLIRAI^{193}	BC045265
D. melanogaster	^{184}RVNMIA**G**GTGITPMLQLAREV^{204}	NM_168479
A. gambiae	^{229}QVGLIA**G**GTGITPMLQLIREV^{249}	XM_309347
C. elegans	^{182}HLSMIA**G**GTGITPMLQVIAAI^{202}	NP_504638
S. japonicum	^{177}RVNMIC**G**GSGITPMFQLLSYI^{197}	AAP05890
A. thaliana	^{155}AFGMLA**G**GSGITPMFQVARAI^{175}	T52470
C. maxima	^{189}HIGMIA**G**GTGITPMLQVIDAI^{209}	AAK69398
Z. mays	^{153}AFGMLA**G**GSGITPMFQVARAI^{173}	AAD17694
O. sativa	^{179}QIGMIA**G**GTGITPMLQVVRAI^{199}	AK071324
M. acuminata	^{38}DIGMIA**G**GTGITPMLQVIKAI^{58}	AAR88781
S. pombe	^{168}HFGMIA**G**GTGITPMLQIIRAV^{188}	NP_587852
N. crassa	^{175}HFGMVA**G**GTGITPMLQVIRAI^{195}	XP_322302
M. alpina	^{165}AIGMIA**G**GTGLTPMLQIIRAI^{185}	AB020034
L. major	^{167}AYAAIA**G**GTGITPILQIIHAI^{187}	CAB92390
G. zeae	^{142}KIGLIA**G**GTGITPMFQVIRAV^{162}	BAC66099
D. disciodeum	^{161}SIGMLA**G**GTGITPMLQVIKAI^{181}	EAL64774
P. falciparum	^{220}HIVMIA**G**GTGMTPFFRLINHL^{240}	CAD52795
S. cerevisiae	^{186}HLGMIA**G**GTGIAPMYQIMKAI^{206}	CAA86908
S. cerevisiaeOM	^{161}SITLLG**A**GTGINPLYQLAHHI^{181}	P36060
	:: :*:*::*: ::	

Figure 33. Multiple sequence alignment of cb5r primary structures. Various eukaryotic cb5r amino acid sequences deposited in GenBank were retrieved, aligned using the CLUSTAL X algorithm and the alignment optimized for maximum sequence conservation. Only the portions of the sequences surrounding the conserved pyridine nucleotide-binding "GxGxxP" motif are shown for clarity. Beginning and ending residue numbers within the translated GenBank sequences are indicated by superscripts while the conserved glycine residue corresponding to G179 in *R. norvegicus* cb5r is shown in bold face and underlined. The consensus sequence is also shown below with identical residues indicated by "*****" and similar residues indicated by "**:**". *S. cerevisciae*OM corresponds to the sequence of the outer mitochondrial form of *S. cerevisciae* cb5r.

hydrophobic contacts with the nicotinamide portion of the pyridine nucleotide substrate (Figure 34).

The "GxGxxP" pyridine nucleotide-binding motif is conserved in all other members of the ferredoxin:$NADP^+$ reductase superfamily of flavoprotein transhydrogenases, including the prototypical member, FNR [22]. However, the nature of the residue preceding the motif exhibits some heterogeneity, although amino acids with primarily hydrophobic side chains appear to comprise the most frequently utilized residues. Further, studies of the determinants of coenzyme specificity in *Anabaena* PCC7119 FNR have indicated that amino acid residues that are not directly situated in the 2'-phosphate $NADP^+$ interacting region, such as T155 (which is equivalent to G179 in cb5r), may influence $NADP^+/NAD^+$ selectivity [138].

To probe the role of G179 in cb5r structure and function, mutant constructs encoding for the variants G179A, P, T, and V were generated through site-directed mutagenesis as described in "Methods" utilizing the original four-histidine tagged cb5r expression construct and the corresponding oligonucleotide primers listed in Appendix B. The selected amino acid residues (A, P, T and V) have been shown to commonly occur at the equivalent positions within other members of the FNR superfamily. The goal of these mutations was to examine the effects of these substitutions on the spectroscopic and thermodynamic properties of the FAD prosthetic group and interactions with the physiological reducing substrate, NADH.

Mutant constructs encoding the four different cb5r variants, G179A, P, T and V, which corresponded to the most frequently encountered amino acid residues occurring at positions corresponding to G179 in the FNR superfamily of pyridine nucleotide-

dependent flavoprotein transhydrogenases, were generated through directed mutagenesis of the original four-histidine tagged cb5r construct. Nucleotide sequencing confirmed the

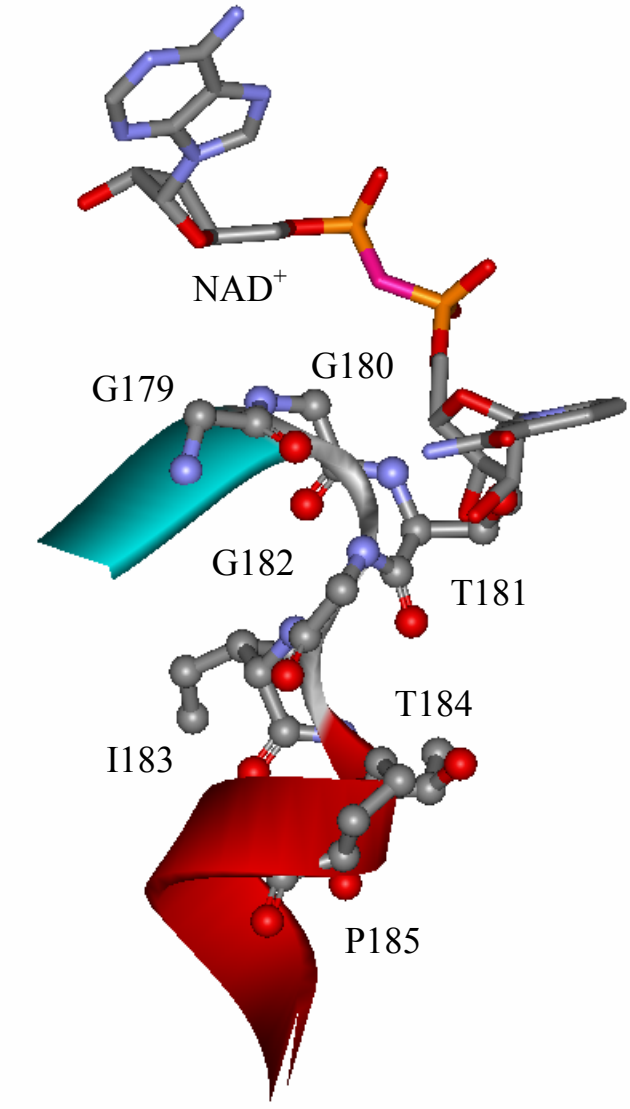

Figure 34. Structural Model of G179 and the "GxGxxP" Motif. Schematic diagram of a portion of the *R. norvegicus* cb5r X-ray crystal structure (PDB = 1IB0) showing the arrangements of the amino acids that comprise the conserved "GxGxxP" motif and residue G179 that precedes the motif. Amino acid residues are shown in "ball and stick" representation using the CPK color scheme while the appropriate portion of the peptide backbone is displayed as a ribbon diagram. The location of the complexed NAD^+ is shown in "stick" representation using the CPK color scheme.

fidelity of each construct and each of the mutant proteins was subsequently expressed in the *E. coli* strain BL21(DE3)-RIL and purified to homogeneity by Ni-chelate chromatography and gel filtration FPLC. Evaluation of the expression yields of the various mutants indicated that all four G179 variants were expressed at levels comparable to that of the WT domain. All four mutants were purified to apparent homogeneity as evident by the presence of single protein bands following SDS-PAGE analysis of the various mutants, which also indicated molecular masses comparable to that of the native enzyme (M_r approx. 32 kDa).

The oxidized forms of all four purified G179 variants were yellow in color indicating the incorporation of a flavin prosthetic group and confirming that G179 did not provide backbone or side-chain contacts that were essential for the stable incorporation of the flavin prosthetic group into any of the cb5r variants.

UV/visible absorbance spectra were obtained for oxidized samples of each mutant and WT cb5r and are compared in Figure 35A. The G179A, G179P, G179T and G179V variants each exhibited spectra comparable to that of the WT enzyme with an aromatic absorption maximum detected at 270 nm in the UV region of the spectrum, and a peak at 461 nm with an associated pronounced shoulder in the range of 485-500 nm in the visible region of the spectrum, attributable to protein-bound flavin. None of the mutant visible spectra were blue-shifted with respect that of the WT protein, as has been previously demonstrated for mutations of other residues, such as R91P [102] and Y93H [1221], suggesting that none of the G179 substitutions had any significant influence on the spectroscopic properties of the FAD. Blue shifts in the visible absorbance spectra of flavoproteins have previously been attributed to changes in the hydrophilicity of the

flavin environment near the N(5) locus of the isoalloxazine ring

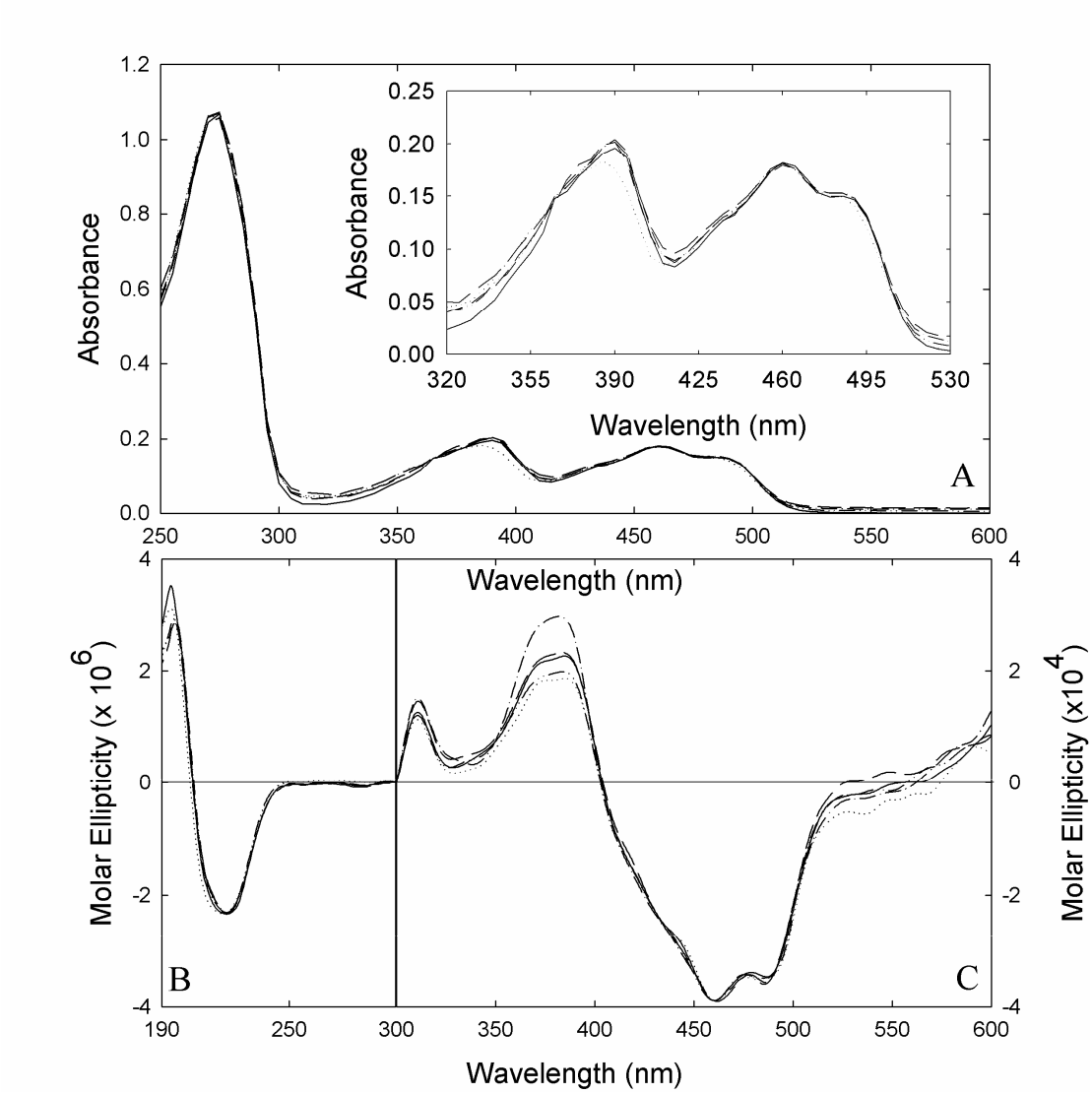

Figure 35. Ultra-Violet, Visible, and Circular Dichroism Spectra Obtained for the G179 Series of cb5r Variants. (A) UV/visible absorption spectra were obtained for oxidized samples of cb5r and the various G179 mutants at equivalent flavin concentrations (1.7 μM FAD) in 10 mM phosphate buffer, containing 0.1 mM EDTA, pH 7.0. The inset shows an expanded region of the visible spectrum where the flavin prosthetic group makes a major contribution. Individual spectra correspond to WT cb5r (____); G179A (-----); G179P (…..); G179T (-.-.-) and G179V (-..-..-). (B) UV CD spectra were recorded using enzyme samples (7 μM FAD) in 10 mM phosphate buffer, containing 0.1 mM EDTA, pH 7.0. (C) Visible CD spectra were recorded using enzyme samples (50 μM FAD) in 10 mM phosphate buffer, containing 0.1 mM EDTA, pH 7.0. Line styles shown in "B" and "C" are the same as those depicted in "A".

[139, 140]. Absorbance ratios ($A_{280\ nm/461\ nm}$) were within the range 6.1±0.2 for all four mutants and were comparable to that obtained for WT cb5r indicating a full complement of the FAD prosthetic group.

To assess the secondary structural content of each of the mutant enzymes, CD spectra were recorded in the UV wavelength range (190-300 nm). As shown in Figure 35B, all of the cb5r variants exhibited positive CD from 190-210 nm and negative CD from 210-250 nm with all the spectra retaining both positive and negative intensities very similar to that of the WT domain. The absence of any significant differences between the spectra of the WT and mutant proteins suggested conservation of the secondary structure architecture and that none of the G179 residue substitutions had any deleterious effects on the folding of the diaphorase domain.

Visible CD spectroscopy was utilized to examine the environment of the FAD prosthetic group. As shown in Figure 35C, all four mutants exhibited visible CD spectra that were virtually indistinguishable from that of the WT domain and indicated that none of the amino acid substitutions had any significant effect on the conformation of the bound chromophore. Previous spectroscopic analyses of cb5r mutants containing altered residues that are involved in FAD-binding, such as S127 [122], have revealed visible CD to be a sensitive indicator of flavin conformation changes.

The extent of quenching of the intrinsic fluorescence due to the FAD prosthetic group of cb5r has also proven to be a sensitive indicator of the retention of the native flavin environment. To probe the flavin fluorescence quenching of the various G179 mutants, both excitation and emission fluorescence spectra were recorded prior to and following heat denaturation of the various mutants. Prior to denaturation, WT cb5r and

the G179 variants quenched the flavin fluorescence to varying degrees ranging from 95% for the WT enzyme to only 60% for the G179V variant, with the G179A, P, and T variants being quenched 89%, 81%,and 68% respectively.

To examine the influence of the various G179 residue substitutions on the stabilities of the resulting proteins, thermal denaturation profiles were generated for WT cb5r and each of the mutant proteins by measuring both changes in the intrinsic flavin fluorescence emission intensity (λ_{em}=523 nm) and retention of NADH:FR activity following incubation of the proteins at temperatures ranging from 0–100 °C. Changes in the intrinsic fluorescence of the cofactor or the retention of NADH:FR activity following thermal denaturation was an effective indicator of the stability of the core structure of the protein. T_{50} values (the temperature at which 50% of maximum fluorescence or 50% retention of NADH:FR activity was detected) increased in the order G179A < G179P < G179T < WT < G179V with all variants exhibiting T_{50} values in the range between 52 and 57°C, which suggested that none of the substitutions had a dramatic effect on the thermal stability of flavin binding. The G179T variant exhibited a T_{50} value of approximately 54°C, in good agreement with the value of 55°C obtained for WT cb5r. The A and P variants exhibited slightly lowered T_{50} values at 53°C and 52°C respectively, while the V mutation caused an increase in the value to 57^{o}C, suggesting a potential small increase in stability. These results suggested that substitution of G179 with alanine, proline, threonine or valine residues had only modest effects on the thermal stability of the different cb5r variants.

Initial-rate kinetic analyses were performed on all four cb5r G179 mutants to evaluate the effects of the various residue substitutions on NAD(P)H utilization. Values

derived for k_{cat} and K_m for both NADH:FR and NADPH:FR activities of the various mutants are given in Table 13A and 13B respectively together with the corresponding values obtained for WT cb5r.

With the exception of the G179A variant which retained 70% of WT activity with a corresponding four-fold decrease in affinity for NADH, the remaining three variants exhibited both substantially decreased NADH:FR activities and NADH affinities with the G179V variant showing the most dramatic changes. NADH catalytic efficiencies, as indicated by k_{cat}/K_m^{NADH}, were observed to decrease in the order WT > G179A > G179P > G179T > G179V with the G179V variant retaining only 0.01 % of the NADH:FR efficiency of the WT protein. In contrast, NADPH:FR efficiencies, as indicated by the values of k_{cat}/K_m^{NADPH}, were only modestly altered and increased in the order G179P < G179V < G179T < WT < G179A with the G179A mutant exhibiting the smallest increase in NADPH:FR efficiency, corresponding to approximately 8%, when compared to the WT protein. It should be noted that while none of the G179 variants displayed the desired properties of rapid turnover of NADPH together with a high Michaelis constant for NADH, the G179V variant exhibited both significantly decreased activity with NADH coupled with a substantial decrease in NADH affinity combined with an increased affinity for NADPH.

However, the values for the NAD(P)H specificity constant (defined as the ratio of $\{k_{cat}/K_m^{NADPH}\}/\{k_{cat}/K_m^{NADH}\}$) listed in Table 15, and which reflect the magnitudes of the individual k_{cat} and K_m values obtained for both NADH and NADPH, were observed to increase in the order WT < G179A < G179P < G179T < G179V. As anticipated, the relatively conservative substitution of G179 with alanine had the lowest impact on

Table 13. NAD(P)H:FR and NADH:BR kinetic constants obtained for G179 mutants.

A.

cb5r Variant	NADH:FR			
	k_{cat} (s^{-1})	K_m^{NADH} (μM)	k_{cat}/K_m^{NADH} (s^{-1} M^{-1})	$K_m^{Fe(CN)6}$ (μM)
WT H_4cb5r	800±17	6±1	1.4±0.3x10^8	8±1
G179A	595 ± 18	25 ± 2	2.3±0.2x10^7	8 ± 1
G179P	42 ± 2	595 ± 40	7.1±0.8x10^4	7 ± 1
G179T	33 ± 2	662 ± 37	5.1±0.5x10^4	8 ± 1
G179V	12 ± 1	1077 ± 78	1.1±0.2x10^4	7 ± 1

B.

cb5r Variant	NADPH:FR			Nucleotide Specificity Constant
	k_{cat} (s^{-1})	K_m^{NADPH} (μM)	k_{cat}/K_m^{NADPH} (s^{-1} M^{-1})	Δ[a]
WT H_4cb5r	33±5	924±15	3.6±0.3x10^4	2.6x10^{-4}
G179A	48 ± 8	1360 ± 322	3.9 ± 0.2x10^4	1.7x10^{-3}
G179P	17 ± 3	2317 ± 702	8.4 ± 0.4x10^3	1.2x10^{-1}
G179T	12 ± 2	507 ± 145	2.6 ± 0.1x10^4	5.1x10^{-1}
G179V	8 ± 1	375 ± 25	2.2 ± 0.1x10^4	1.9x10^0

[a]The nucleotide specificity constant, Δ, is defined as the ratio $\{(k_{cat}/K_m^{NADPH})/(k_{cat}/K_m^{NADH})\}$.

C.

Variant	NADH:BR	
	k_{cat} (s^{-1})	$K_m^{cyt\ b_5}$ (μM)
WT H_4cb5r	600 ± 17	12 ± 2
G179A	245 ± 17	8 ± 1
G179P	10 ± 1	1 ± 0.1
G179T	18 ± 2	43 ± 2
G179V	17 ± 2	107 ± 8

altering the degree of NAD(P)H selectivity, corresponding to only an approximately 7-fold increase in NADPH selectivity. This can be contrasted with increases of 304-fold

and 462-fold for the G179P and G179T variants, respectively, whereas the greatest increase in NADPH selectivity, corresponding to 7,692-fold enhancement, was observed for the G179V mutant.

To compare the interactions of the various G179 variants and WT cb5r with various pyridine nucleotides, differential spectroscopy was utilized to monitor complex formation. Alterations of the flavin visible absorbance spectrum, shown in Figure 36, were detected for the WT enzyme during titrations with H_4NAD and NAD^+, but not with H_4NADP or $NADP^+$. These tetrahydronicotinamide derivatives do not function as hydride donors when substituted for NADH in either the NADH:FR or NADH:BR cb5r assays but are valuable tools for examining the binding affinity for NADH and NADPH, respectively. Both H_4-nucleotides are close isosteric analogues and are assumed to involve the same contacts at the active site as NADH or NADPH, but lack the positive charge on the nicotinamide ring that is present on NAD^+ and $NADP^+$, respectively. In contrast, for the G179 mutants, spectral differences indicating detectable complexes were only observed for the G179A variant with H_4NAD, yielding a K_s of 238 μM, which may be compared with the corresponding value of 85 μM obtained for WT cb5r. Values for the K_s determinations are given in Table 14.

These results suggested that pyridine nucleotides containing a 2'-phosporyl groups were most readily accommodated by the G179V variant. That the WT cb5r showed no detectable complex formation with any of the 2'-phosphorylated nucleotides suggests a significant role for G179 in discriminating between NADH and NADPH.

To examine whether substitution of G179 influenced NAD(P)H utilization through modulation of the flavin oxidation-reduction midpoint potential, potentiometric

titrations were performed using the dye equilibration method for WT cb5r and the different G179 variants in the presence of phenosafranine ($E^{o'}$= -252 mV) as indicator. Flavin midpoint potentials ($E^{o'}$, n=2) were determined for the enzymes alone and in

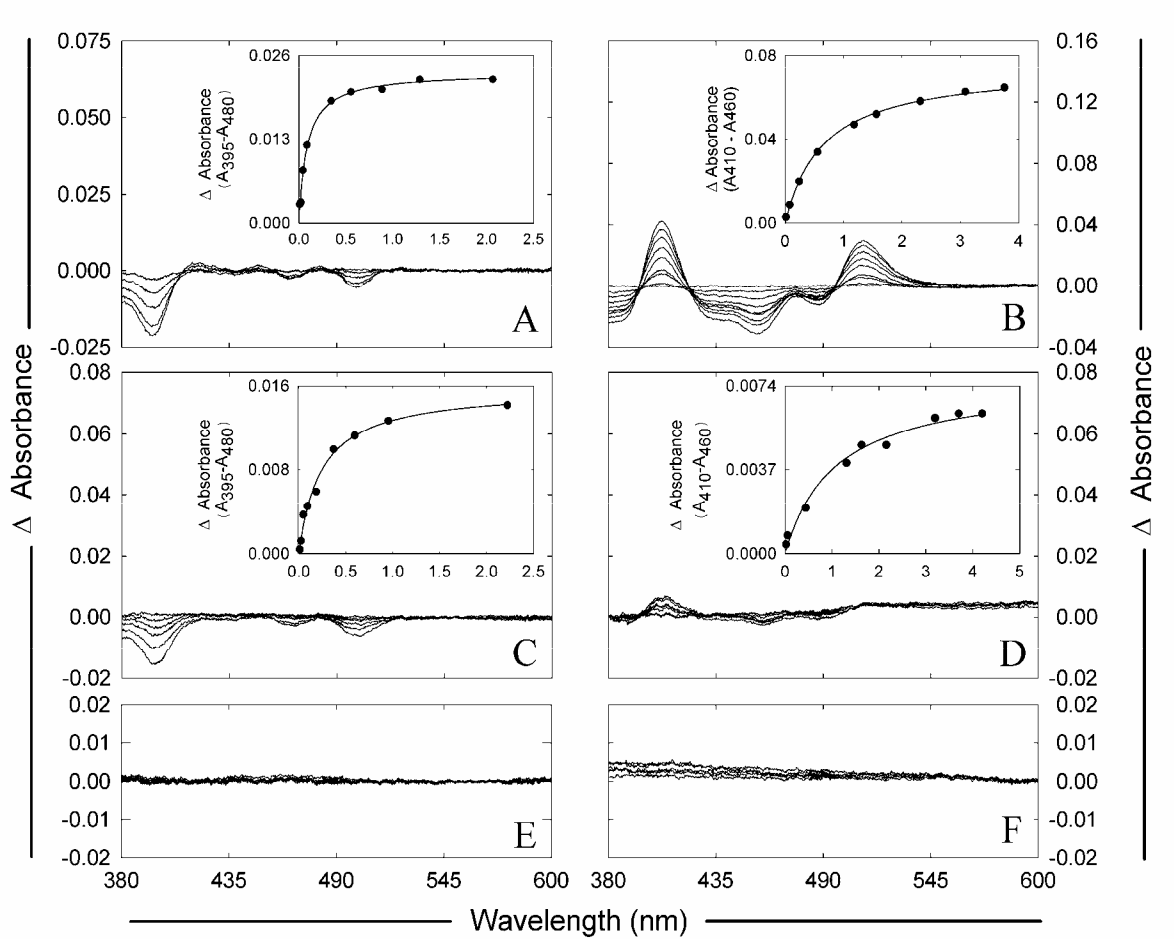

Figure 36. Spectroscopic Titrations Obtained for the G179 Series of Variants in the Presence of H_4NAD and NAD^+. Difference spectra were obtained for both WT cb5r and the selected G179 mutants at equivalent flavin concentrations (50 μM FAD) in 20 mM MOPS buffer, containing 0.1 mM EDTA, pH 7.0 following titrations with either H_4NAD (left panels) or NAD^+ (right panels) as described in "Methods". (A and B) WT cb5r; (C and D) G179A; (E and F) G179T. G179P and G179V gave spectra identical to G179T. The insert panels correspond to plots of the magnitudes of the observed spectral perturbations (peak to trough measurements at the indicated wavelengths) versus ligand concentration. The corresponding K_s values are given in Table 16.

complex with NAD^+. Qualitative analysis of the individual spectra obtained from the various titrations indicated that the majority of the phenosafranine was reduced prior to FAD reduction for all four G179 variants and WT cb5r in the absence of any pyridine nucleotide, suggesting the flavin midpoint potentials were more negative than that of phenosafranine, for all the cb5r variants examined. Analysis of the spectra obtained for the G179A and G179P variants and WT cb5r in the presence of NAD^+ revealed that the majority of the flavin was reduced prior to the dye, suggesting that complex formation significantly perturbed the flavin midpoint potentials to values more positive than that for phenosafranine for these three proteins. In contrast, the presence of NAD^+ had less effect on the titration behavior of the G179T and G179V variants, suggesting little perturbation or modulation of the FAD redox potential.

Table 14. Spectral Binding Constants (K_s) and Standard Midpoint Potentials ($E^{o\prime}$) Obtained for the G179 Series Variants

cb5r Variant	K_s ^{H_4NAD} (μM)	K_s $^{NAD+}$ (μM)	$E^{\circ\prime}$ $_{FAD/FADH_2}$ (mV)	
			-NAD$^+$	*+NAD*$^+$
WT H_4cb5r	45 ± 10	553 ± 30	-271	-191
G179A	238 ± 33	1083 ± 260	-272	-208
G179P	ND[a]	ND[a]	-270	-224
G179T	ND[a]	ND[a]	-271	-254
G179V	ND[a]	ND[a]	-274	-262

[a]ND indicates that the spectroscopic binding constant could not be determined, due to insufficient spectral change.

The flavin redox potentials (n=2) for the different G179 variants and WT cb5r alone or as the enzyme-nucleotide complex were determined from the Nernst semi-log

plots shown in Figure 37B and C. The standard midpoint potentials obtained for the FAD/$FADH_2$ couple in both the WT enzyme ($E^{o'}$= -272 mV) and the different G179 variants ($E^{o'}$= -270 mV to -274 mV) were approximately equivalent for all five proteins in the absence of any pyridine nucleotide, the values spanning a range of only 4 mV. In contrast, significant differences in flavin midpoint potential were observed for the WT cb5r and the G179 variants in the presence of NAD^+. In the presence of NAD^+, the redox potential of the FAD/$FADH_2$ couple in the WT enzyme was positively-shifted by 78 mV ($E^{o'}$= -193 mV) which may be compared to the values of -207 mV for the G179A variant, -225 mV for G179P, -254 mV for G179T and -263 mV for G179V, respectively, illustrating that the progressively decreased affinity for NAD^+ observed in the G179 variants was reflected in progressively smaller perturbations of the flavin redox potential. Values obtained for the midpoint potentials both in the absence and presence of NAD^+ are given in Table 14.

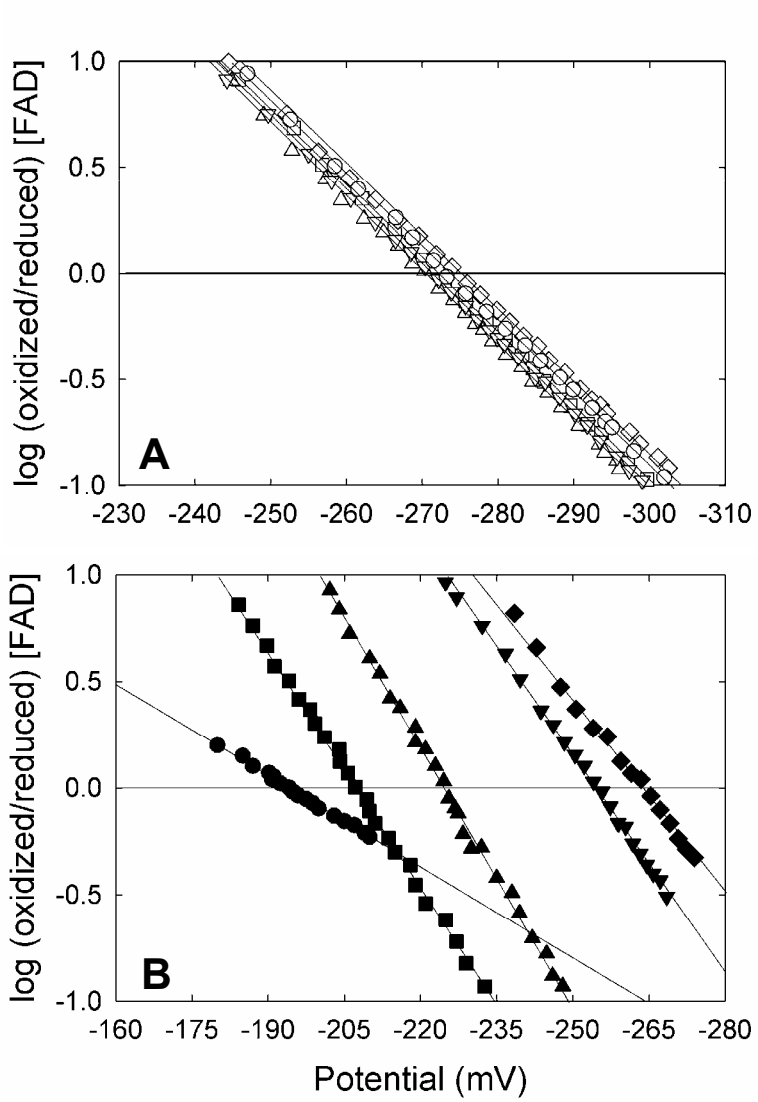

Figure 37. Oxidation-Reduction Midpoint Potentials for the FAD Prosthetic Group in the G179 Series of cb5r Variants. Reductive dye-equilibration titrations of WT and the different G179 variants of cb5r (40 μM FAD) were performed as described under "Methods". Individual spectra were collected at 2-3 min intervals during the time course of the titrations. (B) Nernst plots obtained for the FAD/$FADH_2$ couple (n=2) are shown for the titrations of the various G179 mutants and correspond to WT cb5r (○), G179A (□), G179P (△), G179T (▽) and G179V (◇). (C) Nernst plots obtained for the FAD/$FADH_2$ couple (n=2) in the presence of NAD^+ (2 mM) are shown for the titrations of the various G179 mutants and correspond to WT cb5r (●), G179A (■), G179P (▲), G179T (▼) and G179V (◆)

Summary of Mutagenesis of conserved residue G179: Role in Pyridine Nucleotide Specificity

The preceding results provide the first documented insights into the role of G179 in maintaining both the structure and function of cb5r and contribute additional evidence to support a role for this residue (or its equivalent) in modulating the pyridine nucleotide selectivity within the flavoprotein transhydrogenase superfamily of enzymes.

A multiple alignment of the 50 currently known cb5r primary structures deposited in GenBank revealed that of the approximately 275 residues that comprise the flavin- and NADH-binding domains together with the intervening "hinge" region, G179 represents one of only thirteen conserved residues within the cb5r sequences, suggesting a potentially important role in functionality. Of the thirteen residues, four (Y93, T94, P95 and G124) and seven (G179, G180, G182, P185, N209, I215 and G274) are distributed throughout the FAD- and NADH-binding lobes, respectively, while two (G143 and P144) are present in the connecting "hinge" region. Several of these conserved residues are components of the four sequence motifs that are characteristic of the flavoprotein transhydrogenase family and have been the subject of previous studies that have contributed to our understanding of the roles of individual residues such as Y93 [121], T94 [43] and P144 [120].

To probe the role of G179 in substrate binding, hydride transfer, and NADH/NADPH discrimination, we have substituted the glycine residue with alternate amino acids that are primarily found at the equivalent position in other members of the FNR superfamily. Analysis of 1293 sequences that contain the "NAD binding 1" domain, identified within the Pfam database (PF00175) [141] and that contain the conserved

"GxGxxP" nucleotide-binding motif, revealed that only a limited number of different residues were observed at the position preceding this motif, which corresponded to G179 in cb5r. Proteins containing the "NAD binding 1" domain exhibited a marked preference for residues that were either proline, threonine or alanine, in addition to the dominant residue, glycine.

The results of our mutagenesis studies revealed that substitution of G179 primarily affected the kinetic properties of the enzyme with no significant adverse effects on the properties of the FAD chromophore. Absorption and CD spectra and FAD/$FADH_2$ redox potentials in the absence of NAD^+ for all four G179 variants were comparable to those of WT cb5r, as would be anticipated for mutations limited to the NADH-binding lobe. In contrast, the four amino acid substitutions, A, P, T and V, were observed to adversely impact NADH utilization, both in terms of decreasing k_{cat} and increasing K_m, with the magnitude of the perturbations greatest for the P,T and V substitutions. The changes in NADH affinity were also reflected in the absence of spectral changes observed during the H_4NAD and NAD^+ titrations and the more modest shifts in the flavin redox potential in the presence of NAD^+.

The crystal structure of the cb5r-NAD^+ complex [58], has revealed that G179 is situated approximately 4-5 Å distant from the nucleotide opposite the pyrophosphate moiety and in a cleft formed by the ribityl and ribose moieties of NAD^+. G179 is not involved in any direct contacts with the pyridine nucleotide, suggesting that side chain substitutions should not adversely impact substrate utilization. However, G179 and G180 comprise part of a tight 180^o turn within the polypeptide backbone that is situated at the apex of strand Nβ1 within the NADH-binding lobe and which precedes helix Nα1 which

forms part of the "GxGxxP" motif. Strand Nβ1 also makes extensive contacts with strand Nβ5, which comprises part of the second conserved pyridine nucleotide-binding motif corresponding to residues C273 to M278 ("CGxxxM"). This motif contains the active-site cysteine residue considered to be critical for accurately positioning the nicotinamide moiety prior to efficient hydride transfer [104]. Analysis of the crystal structure indicates that the close packing of side chains in this region effectively precludes accommodation of side chains other than that of glycine, and to a limited extent that of alanine, and that substitution by more bulky groups, such as those of P, T or V, would potentially result in distortion of the backbone configuration in the region of this turn that would be accompanied by displacement of the side chain of C273 with concomitant decreases in both activity and substrate affinity.

While the results of our mutational studies could be adequately described in terms of potential alterations in the positioning of residues comprising the two conserved pyridine nucleotide-binding motifs, the observed changes in NADH/NADPH discrimination were less obvious. Our prior studies of NADH/NADPH discrimination have been limited to evaluating the contributions of D239 and F251 [123] towards regulating pyridine nucleotide specificity. Analyses of a series of both single and double mutants revealed that while F251 contributed modestly to specificity, construction of a D239T variant resulted in an approximately 40,000-fold increase in the efficiency of NADPH versus NADH utilization. In contrast, the results generated by our G179 mutants revealed the greatest increase in NADPH/NADH discrimination, corresponding to an approximately 8,000-fold increase, was achieved for the G179V variant.

Both sequence and structural analyses have indicated that several residues participate in NAD(H)/NADP(H) discrimination within the FNR superfamily. Changes in NAD(P)(H) specificity have been described for other constituents including FNR [142], cytochrome P450 reductase [143] and assimilatory nitrate reductase [144, 145], with the latter the only example of pyridine nucleotide coenzyme studies that examined both NADH- and NADPH-specific isoforms of the enzyme. For nitrate reductase, mutagenesis of two residues, S920 and R932 in the NADPH-specific isoform, resulted in a $7.3x10^4$-fold change in nucleotide specificity whereas substitutions of the same residues in the NADH-specific isoform resulted in only a $6.2x10^3$–fold alteration in selectivity. However, these studies of FNR family members have primarily focused on residues that specifically interact with the 2'-phosphoryl group while additional amino acid residues clearly participate in regulating pyridine nucleotide selectivity.

Sequence alignments of FNR family members indicate that most of the constituents that favor NADP(H) as a substrate primarily contain the sequence "$^{T}P_{V}$GxGxxP" whereas those that utilize NAD(H) retain a glycine prior to the motif. Mutational studies of the residue prior to the "GxGxxP" motif, corresponding to G179 within cb5r, have previously been limited to analyses of T155 in *Anabaena* PCC7119 ferredoxin:$NADP^+$ reductase [138]. In FNR, the hydroxyl group of T155 has been suggested to function in $NADP^+/NAD^+$ selectivity by participating in a H-bond network that is involved in maintaining the correct backbone architecture of a loop comprising residues 261-268 (CGLRGMEE) within the nucleotide-binding lobe that is required for correctly orienting the bound $NADP^+$ for hydride transfer. Generation of the T155G variant revealed displacement of this loop together with an increased affinity for NAD^+

and decreased affinity for $NADP^+$. Within cb5r and other NAD(H)-utilizing FNR variants, an alternate arrangement of the H-bond network is observed, together with a hairpin-like loop structure, corresponding to residues 272 to 280 (CGPPPMIQ), rich in proline residues. The organization of this proline-rich region would be disrupted by T, P or V substitutions at G179, resulting in NADH binding in an altered conformation that both decreased NADH activity and affinity whereas the catalytic efficiency with NADPH would potentially remain unchanged. The current work complements the studies of *Anabaena* FNR and illustrates that mutating the residue preceding the "GxGxxP" motif can alter pyridine nucleotide specificity in favor of either NAD(H) or NADP(H) with varying degrees of efficiency.

Finally, it should be noted that the efforts to alter the NADH/NADPH specificity of cb5r have not generated changes of the magnitude produced for some other dehydrogenases, such as *S. cerevisiae* format dehydrogenase, where construction of the D196A/Y197R double mutant resulted in a 2,500,000-fold change in $NAD^+/NADP^+$ specificity [146]. However, it is clear that for cb5r, residues positioned both at the pyridine nucleotide-binding site, such as D239 [123] and some distance away, including G179, can each have a profound impact on NAD(P)H selectivity, suggesting that multiple mutations may be required to effectively reverse the enzyme's pyridine nucleotide selectivity.

Systematic analysis of the conserved NADH binding motif "^{180}GxGxxP^{185}"

In all members of the FNR family, a highly conserved motif of three residues, corresponding to "GxGxxP", can be identified, and has been shown to be involved in the binding and association of the enzyme with NAD(P)H. Analysis of the crystal structure of cb5r allows for visualization of the importance of this motif in the proper orientation of the NADH substrate. Located at the amino-terminus of the 16-residue helical segment Nα1, this motif plays a vital role in correctly aligning and positioning the NADH for efficient electron transfer. The leading three residues, along with the preceding residue G179, form a compact segment that effectively reverses the direction of the polypeptide backbone, generating a "flattened" surface against which the NAD^+ can position. The three ubiquitously conserved residues of this motif each participate in hydrophobic interactions with the nicotinamide portion of the pyridine nucleotide substrate, in the case of G180 and G182 (Figure 38), or, in the case of P185, the isoalloxazine ring of the FAD cofactor (Figure 39). These interactions in conjunction with the tendency for glycine and proline residues, in general, to play roles in organizing and directing the backbone structure of polypeptides, suggest that the major part that the GxGxxP motif plays in cb5r function is as a scaffolding around which the NADH substrate is able to orient in order to result in efficient electron transfer.

In addition to the three ubiquitously conserved residues of this motif, the three intervening residues, T181, I183, and T184, each show a high level of conservation, with only a minor few substitutions seen in the sequences of other cb5r variants or in other members of the FNR family. X-ray crystallographic studies of cb5r in the presence of NAD^+ have indicated that both T181 and T184 form potentially crucial hydrogen bonds

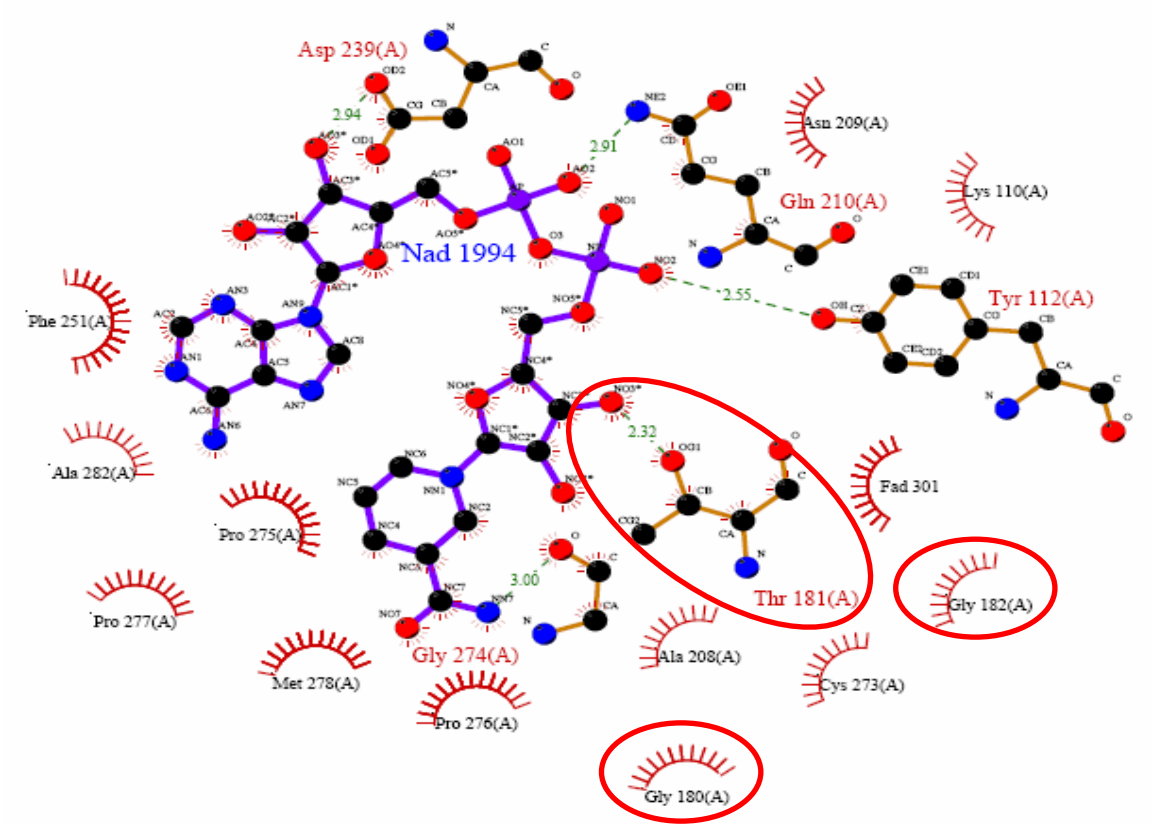

Figure 38. Electrostatic Interaction of Amino Acid Residues G180, T181, and G182 with NAD^+ Bound to Cytochrome b_5 Reductase. Ligplot [99] of 1IB0. C, O, N, and P atoms are represented as white, blue, red, and violet spheres, respectively, while covalent bonds are violet sticks within NAD^+ and orange sticks within amino acid residues of the NADH-binding lobe. Hydrogen bonds are drawn as green dashed lines with distances between atoms labeled. Residues contributing to hydrophobic interactions are represented as arcs with rays and colored red. Referenced residues highlighted with red circle.

with the substrate and cofactor respectively. The side chain of T181 forms a hydrogen bond interaction with nicotinamide ribose of NAD^+ (Figure 38), while T184 forms two side chain hydrogen bonds with the O4 and N5 atoms of the isoalloxazine ring of FAD (Figure 39). Additionally, the T94 equivalent in porcine cb5r (T66) has previously been shown to be involved in the stabilization of semiquinone intermediates within the

reaction mechanism of cb5r [43]. This residue lies within 4.02Å of residue T184, and also forms a backbone hydrogen bond to N5 of the isoalloxazine ring of FAD. Additional mutagenesis studies of T94 demonstrated that substitution of this residue hinders the release of a proton from the N5 position necessary for efficient electron transfer and proper cb5r function. The similar natures of the residues suggest that T184 may play role similar to T94 in the actions of cb5r [105].

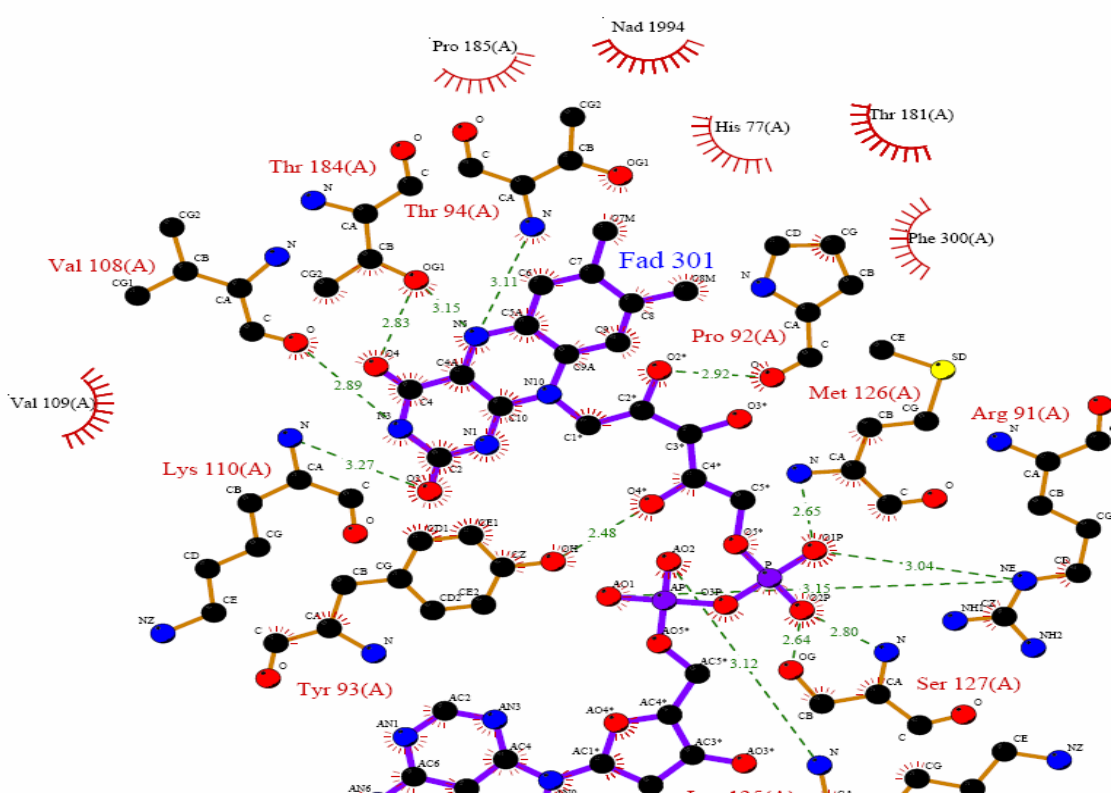

Figure 39. Electrostatic Interaction of Amino Acid Residues T184 and P185 with FAD Bound to Cytochrome b_5 Reductase Ligplot [99] of 1IB0. C, O, N, and P atoms are represented as white, blue, red, and violet spheres, respectively, while covalent bonds are violet sticks within NAD^+ and orange sticks within amino acid residues of the NADH-binding lobe. Hydrogen bonds are drawn as green dashed lines with distances between atoms labeled. Residues contributing to hydrophobic interactions are represented as arcs with rays and colored red. Referenced residues highlighted with red circle.

Finally, residue I183 does not form any interactions with either the FAD cofactor or the NAD^+ as shown by x-ray crystallography. While this could indicate a limited, if any, role for the residue, its high level of conservation and tendency to be substituted by residues of similar structure and side chain characteristics (valine and leucine) would suggest that the presence of non-polar residue at this position is necessary for proper activity of cb5r, potential through affects, or lack there of, on neighboring residues in the tertiary structure.

Overall, the high level of interaction of the residues of this motif with both the cofactor and substrate suggest a pivotal role for this motif in the proper functioning of cb5r. To probe the characteristics of the individual residues of this motif and the role they play in the function of cb5r, a series of substitution mutants were generated for each residue. Initial studies centered on an alanine scanning of the motif, in which each residue was individually substituted with alanine, generating six variants for characterization. Following the alanine scan, additional variants were generated based on one of two criteria. For the ubiquitously conserved residues, the substitutions were based upon the characteristic nature of the side chains and the proposed structural role of the residues. For the intervening residues, variants were based upon naturally alternate residues that occur naturally in equivalent positions in other cb5r variants or in members of the FNR family. The mutants generated and characterized for this aim were G180A, G180P, T181A, T181I, T181S, G182A, G182P, I183A, I183F, I183l, I183M, T184A, T184H, T184S, T184V, P185A, and P185G.

Characterization of Alanine Substitution Mutants of ^{180}GtGitP^{185}

Mutant constructs encoding for the variants G180A, T181A, G182A, I183A, T184A and P185A were generated through site-directed mutagenesis as described in "Methods" utilizing the original four-histidine tagged cb5r expression construct and the corresponding oligonucleotide primers listed in Appendix B. Nucleotide sequencing in both directions confirmed the correct sequence and proper introduction of each mutation, and each variant was further expressed in the *E. coli* strain BL21 (DE3)-RIL and purified to homogeneity via Ni-NTA agarose chromatography and size exclusion FPLC. Expression yields for each of the variants were comparable to that of WT cb5r. Purification to homogeneity was further confirmed by SDS-PAGE analysis as demonstrated by the appearance of single protein bands, which displayed molecular masses comparable to that of WT cb5r (M_r = 31 kDa).

UV/visible absorption spectra were obtained for oxidized samples of WT cb5r and each of the variants generated and are shown in Figure 40A. With the exception of T184A, each of the variants displayed absorption spectra comparable to that of the WT domain characterized by an aromatic absorption maxima at 272 nm in the UV region and peaks in the visible region at 386, 460, and a pronounced shoulder at 485 nm, all characteristic of simple flavoproteins, suggesting that none of the variants generated had any significant effects on the spectroscopic properties of the flavin prosthetic group. T184A, however, demonstrated an altered spectrum, with a blue-shifted λ_{max} of 457 nm compared to that of the WT cb5r visible λ_{max} of 461 nm. Shifts within the visible absorption spectra of flavoproteins have previously been attributed to changes in the hydrophilicity of the flavin environment near the N(5) locus of the isoalloxazine ring

[102]. The absorption ratios (A_{276}/A_{461}) for each viable mutant were within a range of 5.5 to 5.9 which indicated a full flavin complement.

To establish the effects of each mutation upon the secondary structure of the oxidized protein, far UV CD spectra were recorded in the range of 190–300 nm for each variant and WT cb5r. As shown in Figure 40B, spectra of all of the mutants correlated well to the WT domain by displaying positive CD maxima at 196 nm and negative maxima at 222 nm, indicating that the mutations introduced had no effect on the secondary structure characteristics of the folded protein. The visible CD spectra of all the variants, with the exception of T184A, again displayed spectra comparable to that of WT cb5r, indicating that these mutations did not generate alterations in the environment of the FAD-cofactor. As shown in Figure 40C, representative spectra demonstrated that each variant retained a similar line shape as that of WT cb5r with positive maxima at 310 and 390 nm and negative maxima at 460 and 485 nm. The spectrum for T184A demonstrated a similar line shape to WT, with the negative maxima shifting similarly to the shift seen in the UV-Visible Absorbance spectra.

In order to determine how the *GtGitP* alanine variants affected the overall catalytic efficiency, initial-rate kinetic analyses were performed as described in "Methods." Kinetic values obtained from these assays are reported in Table 15. As expected, all of the generated variants resulted in a decreased specific activity when compared to WT cb5r, though over a wide range. For the NADH:FR assays the catalytic efficiencies, k_{cat}/K_m^{NADH}, for the variants were determined to range from 1.9 to 45.7% that of the catalytic efficiency of the WT domain. The large range of effects resulted in most cases from a combination of decreased turnover and decreased affinity.

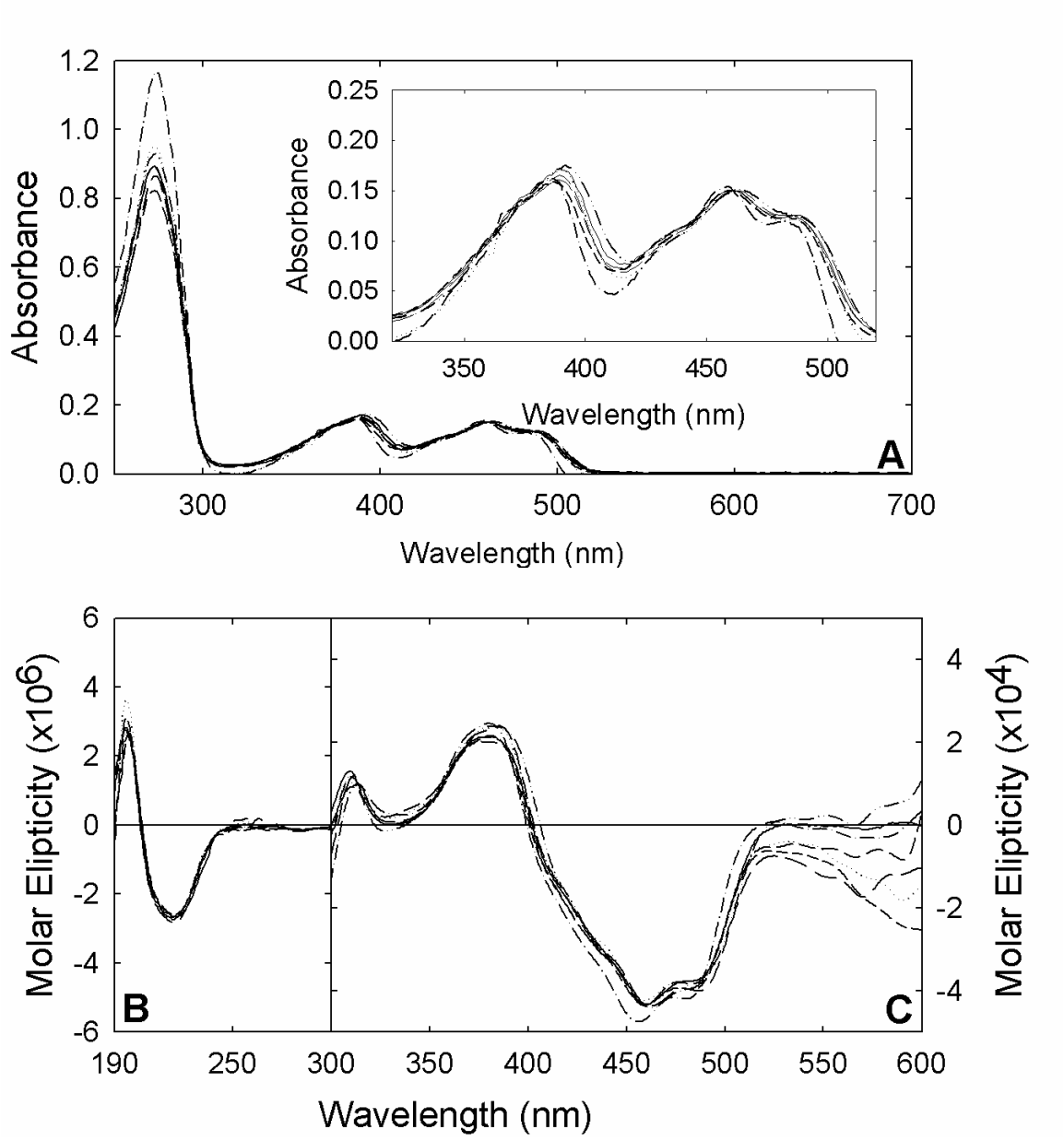

Figure 40. Ultra-Violet, Visible, and Circular Dichroism Spectra Obtained for the WT cb5r and the "GtGitP" Alanine Variants. (A) Oxidized samples of WT and mutant cb5rs (10 μM), (B) (7 μM), and (C) (60 μM) FAD in 10 mM phosphate with 0.1 mM EDTA, pH 7.0 buffer. The inset shows and expanded region of the visible spectrum where the flavin cofactor makes a significant contribution. Individual spectra correspond to (——) H_4cb5r; (— — —) G180A; (— — —) T181A; (- - - -) G182A; (· · · · ·) I183A; (—·—·—) T184A; and (—··—··—) P185A.

G182A, notably, increased the affinity for substrate, having a K_m equal to two-thrids that of WT cb5r. There was a definite trend showing that the ubiquitously conserved residues had a great impact on the rate of turnover than the intervening residues. This trend did not necessarily apply to the affects on K_m, however, as negative impact was seen in all mutants with the exception of G182.

Table 15. NADH:FR Kinetic Constants and Thermal Stability (T_{50}) Values for the "GtGitP" Alanine Variants.

cb5r Variant	NADH:FR				T_{50}
	k_{cat} (s^{-1})	K_m^{NADH} (μM)	K_m^{FeCN6} (μM)	k_{cat}/K_m^{NADH} (s^{-1} M^{-1})	(°C)
WT H_4cb5r	800 ± 17	6 ± 1	8 ± 1	1.4 ± 0.3 x 10^8	56
G180A	178 ± 15	68 ± 4.3	7 ± 1	2.6 ± 0.4 x 10^6	52.5
T181A	487 ± 8	20 ± 1.1	7 ± 1	2.4 ± 0.2 x 10^7	53.8
G182A	288 ± 7	4.5 ± 0.3	7 ± 1	6.4 ± 0.6 x 10^7	52.2
I183A	640 ± 7	12.7 ± 0.9	7 ± 1	5.1 ± 0.4 x 10^7	51.6
T184A	341 ± 12	7.8 ± 0.1	7 ± 1	4.4 ± 0.2 x 10^7	53.5
P185A	47 ± 2	15.6 ± 1.2	8 ± 1	3.0 ± 0.3 x 10^6	51.7

To analyze the overall protein stability of each of the variants, thermal denaturation profiles were generated utilizing thermal NADH:FR profiling in tandem with the loss of intrinsic flavin fluorescence emission quenching, following incubation of the proteins at temperatures ranging from 0-100 ºC. Changes in the intrinsic fluorescence of the FAD prosthetic group monitored together with the retention of NADH:FR activity following thermal denaturation yielded a T_{50} value, the temperature at which there is 50% of maximum fluorescence or 50% retention of NADH:FR activity. The resulting graphs are presented in Figure 41. All variants demonstrated slightly decreased T_{50} values ranging from 51.6 to 53.8ºC for the I183A and T181A mutants respectively (Table 15).

Though decreased, these values are still comparable to WT cb5r T_{50} of 55ºC, only suggesting slight decrease in stability.

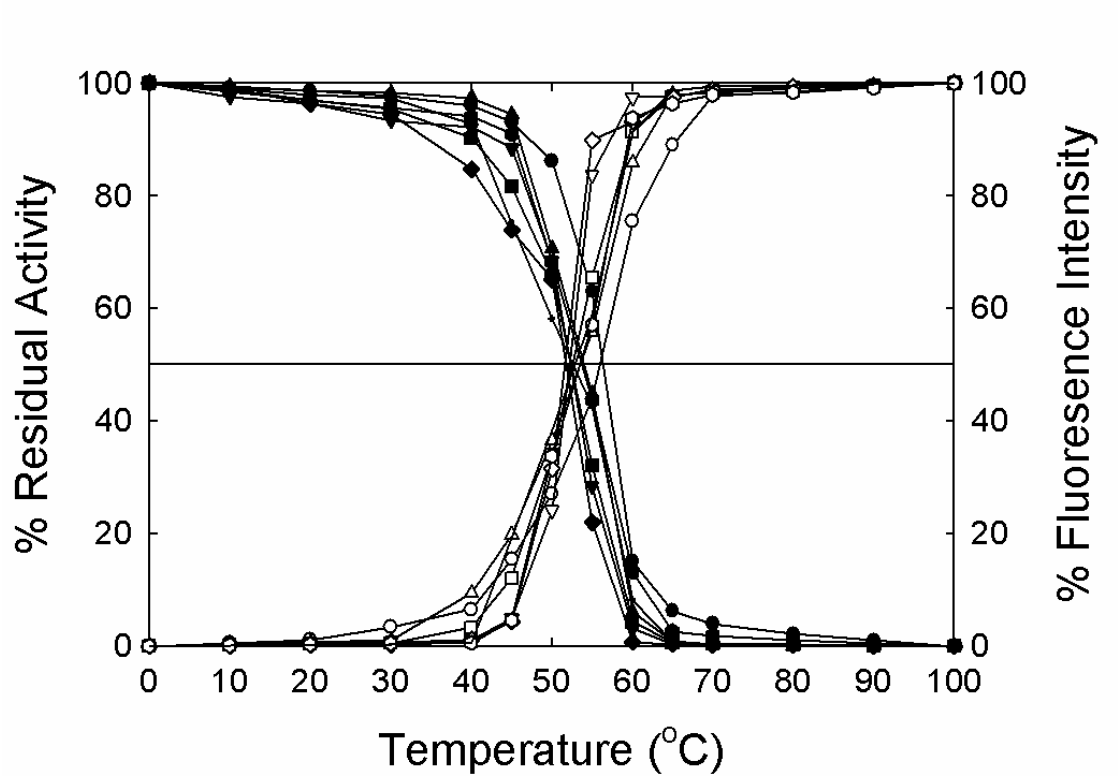

Figure 41. Thermal Stability Profiles Obtained for the WT cb5r and the "GtGitP" Alanine Mutants. Oxidized samples of G180A, T181A, G182A, I183A, T184A, and P185A and WT H_4cb5r (5 μM FAD) were incubated at the indicated temperatures, and aliquots were withdrawn and assayed for both residual NADH:FR activity (closed symbols) and intrinsic flavin fluorescence (open symbols) in 10 mM phosphate buffer, containing 0.1 mM EDTA, pH 7.0 using excitation and emission wavelengths of 450 nm and 523 nm, respectively. Points correspond to: (●,○) H_4cb5r; (■, □) G180A; (▲, Δ) T181A; (▼,▽) G182A; (♦, ◊) I183A; (hexagon) T184A; and (+) P185A.

As demonstrated through the kinetic analyses, each of variants displayed an affect on the affinity of the enzyme for the NADH substrate. Thus, spectral binding constants were determined for each of the mutants utilizing differential spectroscopy in order to compare the affinities for both the substrate NADH and product NAD^+. As described in

"Methods", the NADH isosteric analog H_4NAD was utilized to monitor complex formation and establish a spectral binding constant [106]. Differential spectroscopy was utilized to monitor complex formation during titrations with either H_4NAD or NAD^+. The results are illustrated in Figures 42 and Figure 43. For each of the variants, the titrations performed in the presence of H_4NAD yielded spectra with altered line shape compared to that of WT cb5r (Figure 41). The alterations ranged in magnitude, with G180A, G182A, and T184A showing the most drastic alterations, adopting line shapes characteristic of ADP-Ribose, $APAD^+$, and NAD^+ respectively. Less drastic alterations were noticed in T181A, I182A, and P185A, each having spectra reminiscent of WT in the presence of $H_4$4NAD, with alterations confined to the 450 to 500nm region. These alterations presented shifted positive maxima at ~415nm (T181A) or ~450nm (I1183A and P185A) compared to the WT spectra possessing positive maxima spectra at ~480nm. The line shapes appeared to be hybrids of H_4NAD with other NAD^+ analogs, including $PAAD^+$ (T181A) and ADP-ribose (I183A).

Titrations performed with the variants in the presence of the product NAD^+ again produced spectra with line shapes differing from that of WT (Figure 42). In the cases of G182A I183A T184A and P185A, the major difference was not as much in the line shape as it was in the magnitude between spectra of increasing concentration of titrant. G182A and T184A retained spectra most similar to that of WT, while I183 and P185A showed a significant decrease in the magnitude of the deflections. In addition to the decreased magnitude, the spectra of P185A were also some what similar to that of WT in the presence of $APHD^+$. Spectra for G180A and T181A were drastically different than that of WT, having spectra more comparable to WT titrations with 5'-ADP (G180A) or only

Figure 42. Spectroscopic Titrations Obtained for the WT cb5r and the "GtGitP" Alanine Variants in the Presence of H_4NAD. Titrations of all mutants (50μM) were carried out as previously described in 10mM phosphate buffer containing 0.1mM EDTA, pH 7.0 at 23 °C. Difference spectra were recorded following the addition of solution containing H_4NAD (5mM). The inset panel corresponds to a plot of the magnitude of the spectral perturbations at the indicated wavelengths versus pyridine nucleotide concentration where a difference spectrum was observed. Plots of the relative absorbance changes observed are as follows: (A) WT H_4cb5r; (B) G180A; (C) T181A; (D) G182A; (E) I183A; (F) T184A; and (G)P185A

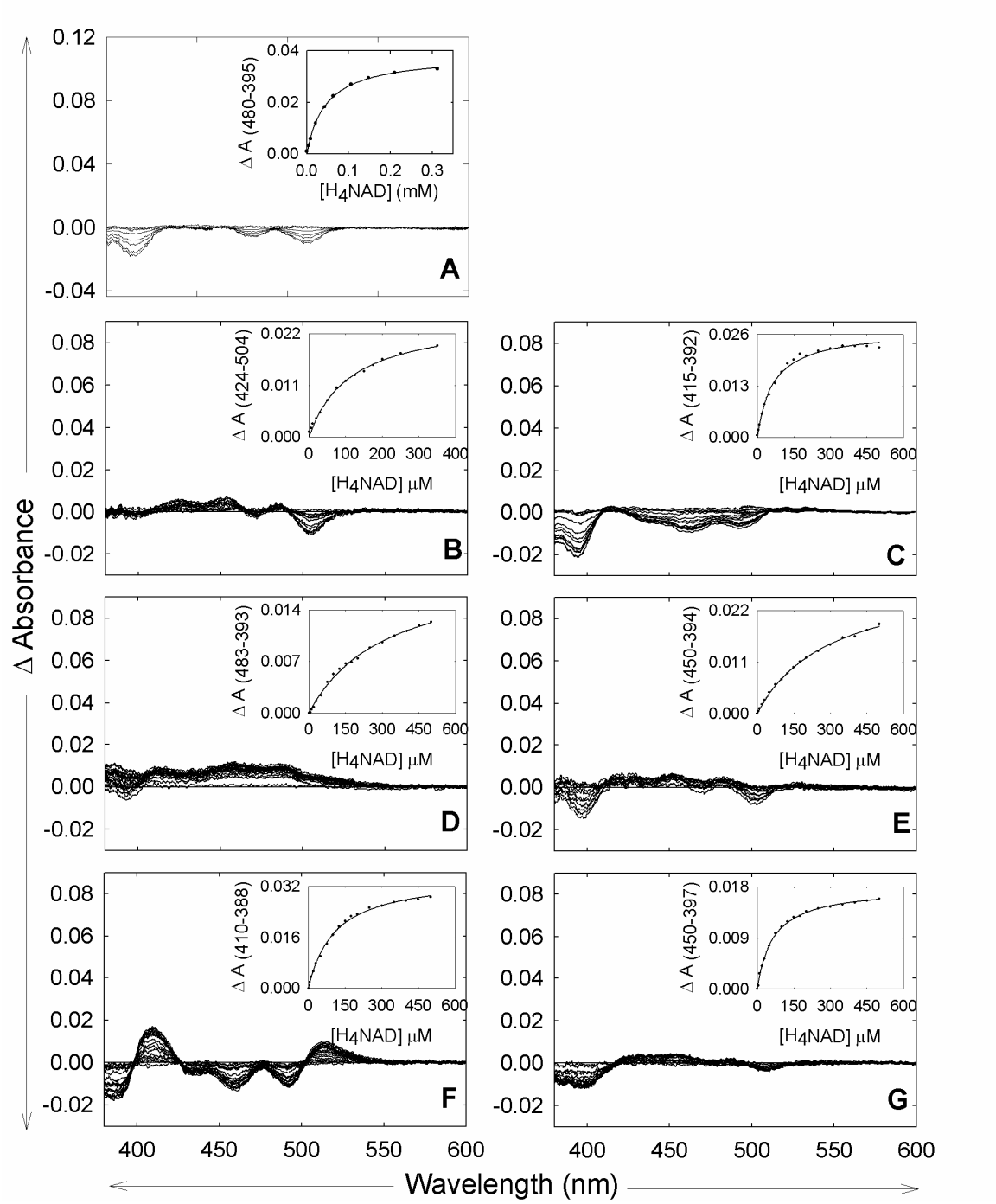
Δ Absorbance
Wavelength (nm)
A
B
C
D
E
F
G
Δ A (480-395)
[H4NAD] (mM)
Δ A (424-504)
Δ A (415-392)
Δ A (483-393)
Δ A (450-394)
Δ A (410-388)
Δ A (450-397)
[H4NAD] μM

marginally similar to titration with $PAAD^+$ (T181A). The values obtained for the respective binding constants (K_s) for all variants are given in Table 16. Interestingly, the K_s values obtained for the variants in the presence of H_4NAD were 1-2 times greater than that of the WT cb5r value of 45μM, indicating an affinity and mode of binding similar to the WT domain. Additionally, P185A demonstrated increased affinity, with a K_s value less than that of WT. A greater effect was observed in the titrations performed in the presence of NAD^+ with the variants, excluding T184A, yielding K_s values of >3-fold higher than WT.

Table 16. Spectral Binding Constants (K_s) and Standard Midpoint Potentials ($E^{o\prime}$) Obtained for the "GtGitP" Alanine Variants.

cb5r Variant	K_s		$E^{\circ\prime}_{FAD/FADH_2}$ (mV)	
	$K_s^{H_4NAD}$ (μM)	K_s^{NAD+} (μM)	$-NAD^+$	$+NAD^+$
WT H_4 cb5r	45±10	533±30	-271	-191
G180A	80.3±7	1974±121	-265	-220
T181A	62.5±3.9	1760±155	-270	-202
G182A	74.1±4.4	802±73	-265	-233
I183A	114±12	1817±198	-265	-214
T184A	106±9.8	400±21	-265	-217
P185A	34±1.4	800±27	-270	-214

To examine the effects of the structural changes on the flavin prosthetic group of each variant, oxidation-reduction potentials for the FAD cofactor were determined utilizing the dye-equilibration potentiometric titration method for WT cb5r and the "GtGitP" mutants in the presence of phenosafranine ($E^{\circ\prime}$= -252 mV). Flavin midpoint

Figure 43. Spectroscopic Titrations Obtained for the WT cb5r and the "GtGitP" Alanine Variants in the Presence of NAD^+. Titrations of all mutants (50μM) were carried out as previously described in 10mM phosphate buffer containing 0.1mM EDTA, pH 7.0 at 23 °C. Difference spectra were recorded following the addition of solution containing NAD^+ (30mM). The inset panel corresponds to a plot of the magnitude of the spectral perturbations at the indicated wavelengths versus pyridine nucleotide concentration where a difference spectrum was observed. Plots of the relative absorbance changes observed are as follows: (A) WT H_4cb5r; (B) G180A; (C) T181A; (D) G182A; (E) I183A; (F) T184A; and (G)P185A

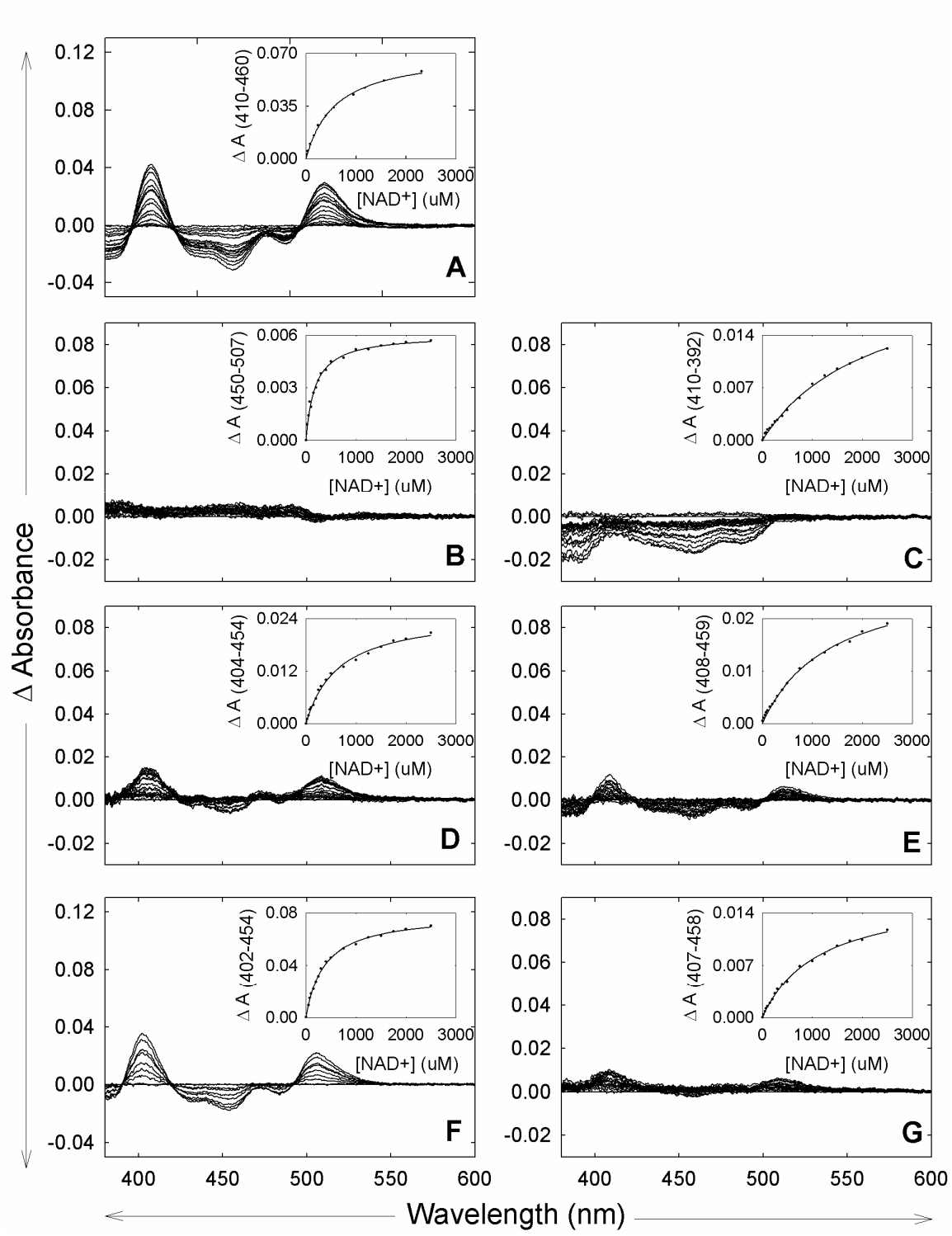
Δ Absorbance
Wavelength (nm)
A
B
C
D
E
F
G
Δ A (410-460)
[NAD+] (uM)
Δ A (450-507)
Δ A (410-392)
Δ A (404-454)
Δ A (408-459)
Δ A (402-454)
Δ A (407-458)

potentials ($E^{o\prime}$, n=2) for the FAD/$FADH_2$ couple were determined both in the absence and presence of NAD^+ from the linear Nernst plots of the log [FAD_{ox}/FAD_{red}] versus the potential (mV) and are shown in Figure 44. Values established for all redox potentials are shown in Table 16. Analysis of the midpoint potentials of the alanine variants in the absence of any pyridine nucleotide indicated that FAD reduction occurred after the reduction of phenosafranine, resulting in values comparable to that of WT cb5r, within the $\pm$ 5mV standard error. Midpoint titrations carried out in the presence of NAD^+ all displayed a more negative shift in the redox behavior for all of the variants yielding values ranging from -220 for G180A to -202 for T181A. These values are similar to the reported value of -220 mV for that of free flavin [133].

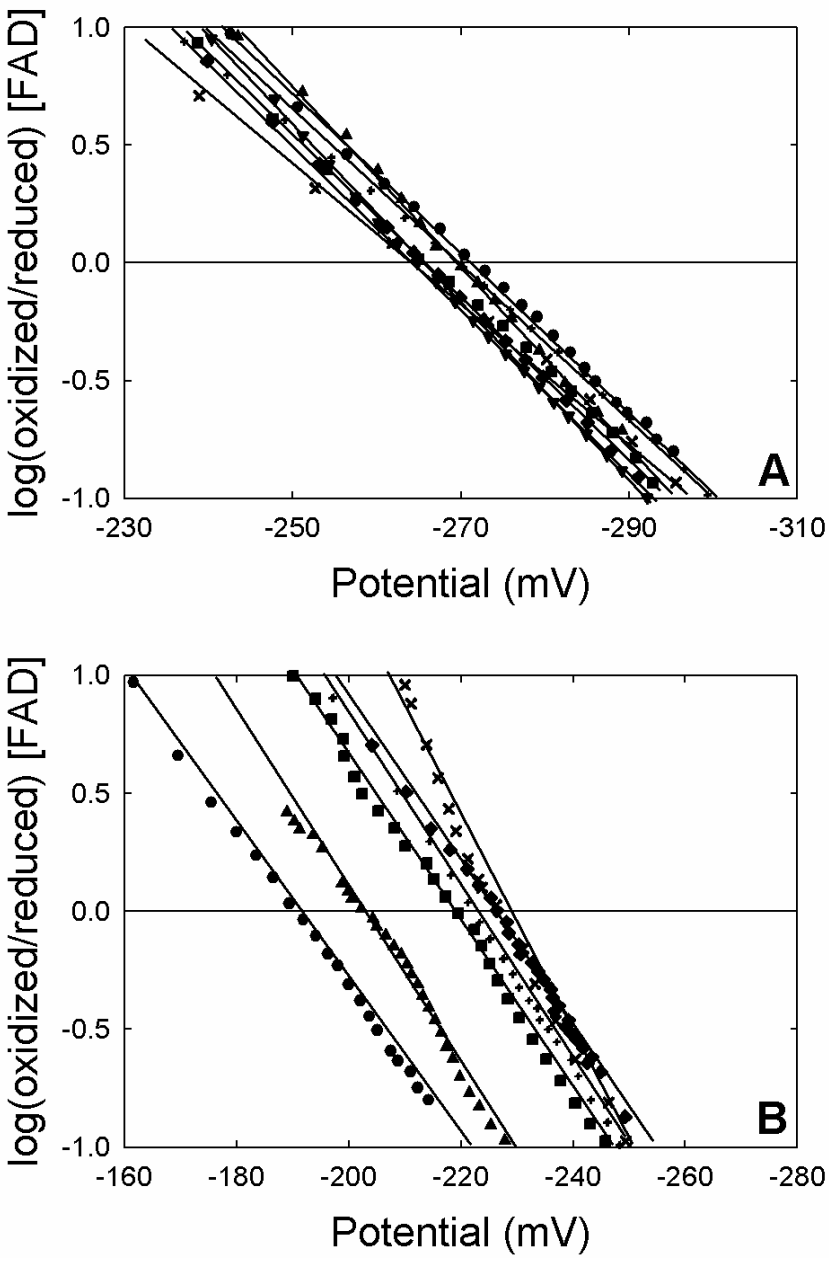

Figure 44. Oxidation-Reduction Midpoint Potentials for the FAD Prosthetic Group in the "GtGitP" Alanine Variants. Reductive dye titrations were performed at 25 °C as described in "Materials and Methods" using phenosafranine as the indicator dye in 100 mM phosphate buffer containing 0.1 mM EDTA, pH 7.0. Nernst plots in the absence (A) and presence (B) of 2 mM NAD^+. Plots correspond to (●) H_4cb5r; (■) G180A; (▲) T181A; (▼) G182A; (♦) I183A; (**x**) T184A; and (+) P185A.

Characterization of additional structural variants of the "GtGitP" NADH-binding motif of cb5r

As stated above, various substitutions of the residues of the "GtGitP" motif were generated in order to further define the roles that the individual residues as well as the collective motif play in the functioning of cb5r. Following the alanine screening study described above, additional mutations were created based upon the structural quality of the naturally occurring residue (in the case of G180, G182, and P185) or based upon alternative naturally occurring residues in FNR family members or in species variants of cb5r based on multiple sequence alignments (in the case of T181, I183 and T184). In the interest of clarity, only data from the residues that generated a significant effect on cb5r structure or function as compared to WT or that are representative of multiple results have been reported in the following figures. The values of the spectral, kinetic, thermal stability and electrochemistry parameters for all generated variants are reported in the respective tables and in the text.

Mutant constructs encoding the variants G180P, T181I, T181S, G182P, I183F, I183L, I183M, T184H, T184S, T184V, and P185G were generated through site-directed mutagenesis as described in "Methods" utilizing the original four-histidine tagged cb5r expression construct and the corresponding oligonucleotide primers listed in Appendix B. Nucleotide sequencing in both directions confirmed the correct sequence and proper introduction of each mutation, and each variant was further expressed in the *E. coli* strain BL21 (DE3)-RIL and purified to homogeneity via Ni-NTA agarose chromatography and size exclusion FPLC. Expression yields for each of the variants were comparable to that of WT cb5r. Purification to homogeneity was further confirmed by SDS-PAGE analysis

as demonstrated by the appearance of single protein bands, which displayed molecular masses comparable to that of WT cb5r (M_r = 31 kDa).

UV/visible absorption spectra were obtained for oxidized samples of WT cb5r and each of the variants. Selected spectra are shown in Figure 45A. With the exception of T184H and V, each of the variants displayed absorption spectra comparable to that of the WT domain by an aromatic absorption maxima at 272 nm in the UV region and peaks in the visible region at 386, 460, and a pronounced shoulder at 485 nm, all characteristic of simple flavoproteins, suggesting that none of the variants generated had any significant effects on the spectroscopic properties of the flavin prosthetic group. The T184 variants, however, demonstrated an altered spectrum, with shifted λ_{max} of 463 and 459 nm for the T184H and T184 V variants, respectively, as compared to that of the WT cb5r visible λ_{max} of 461 nm. These shifts were similar to that seen in the T184A mutant, as well as that seen in T94H [105], and again reflect previously reported results attributable to changes in the hydrophilicity of the flavin environment near the N(5) locus of the isoalloxazine ring [102]. The absorption ratios (A_{276}/A_{461}) for each viable mutant were within a range of 5.5 to 5.9 which indicated a full flavin complement.

In order to establish the effects of each mutation upon the secondary structure of the oxidized protein, far UV CD spectra were recorded in the range of 190–300 nm for each variant and WT cb5r. Spectra of all of the mutants correlated well to the WT domain by displaying positive CD maxima at 196 nm and negative maxima at 222 nm, indicating that the mutations introduced had no effect on the secondary structure characteristics of the folded protein. As with the T184A mutant, the T184H variant was the only variant that demonstrated visible CD spectra significantly different than

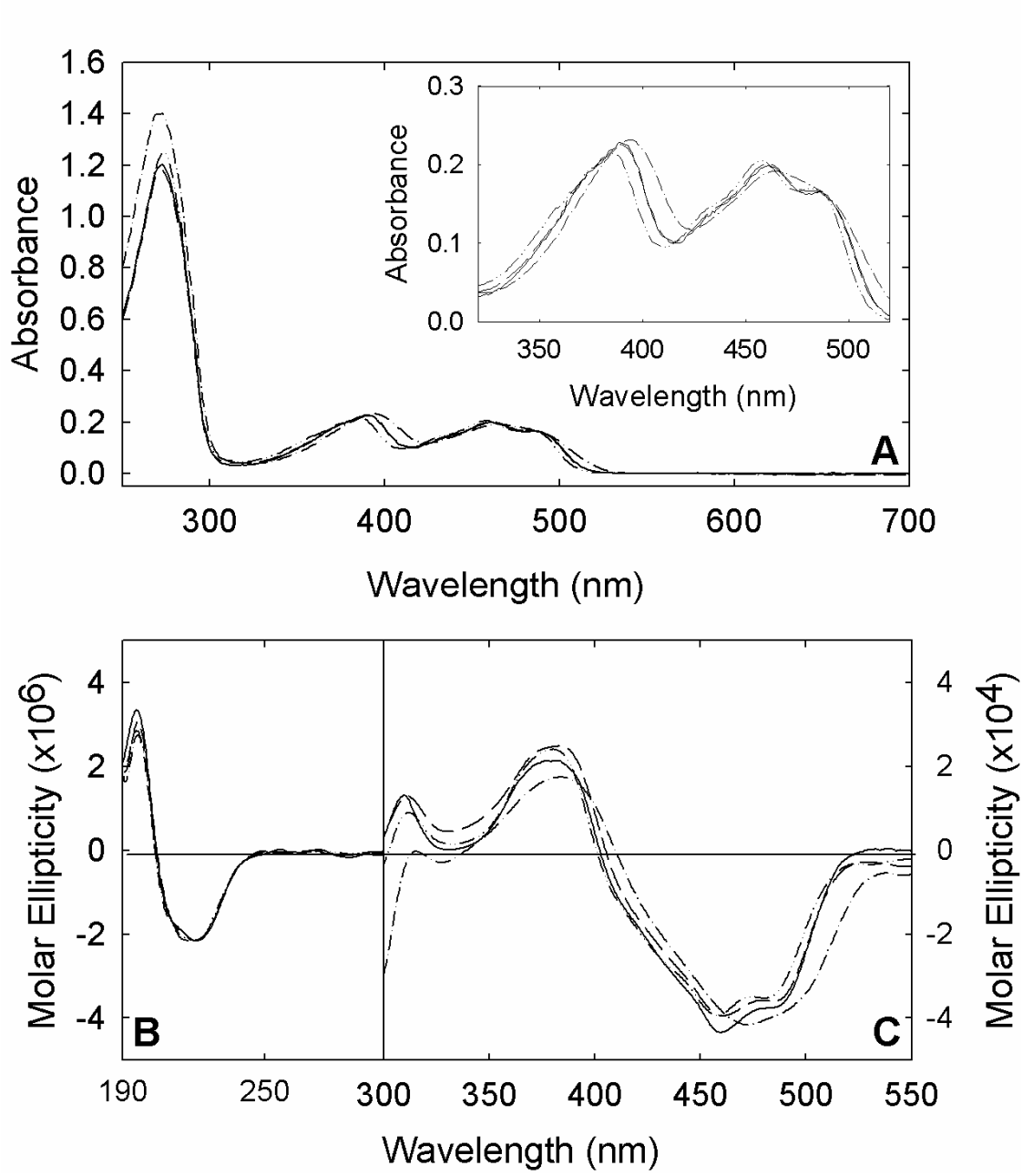

Figure 45. Ultra-Violet, Visible, and Circular Dichroism Spectra Obtained for the Wild-Type and the T184H, T184S, and T184V cb5r Variants. (A) Oxidized samples of WT and mutant cb5rs (10 μM), (B) (7 μM), and (C) (60 μM) FAD in 10 mM phosphate with 0.1 mM EDTA, pH 7.0 buffer. The inset shows and expanded region of the visible spectrum where the flavin cofactor makes a significant contribution. Individual spectra correspond to (——) H_4cb5r; (— · — · —) T184H; (— —) T184S; and (— · · — · · —) T184V. T184S spectra are representative of the spectra of variants not shown.

that of WT cb5r, having an altered line shape as well has shifted negative maxima in the 450-470nm range, indicating that this mutation generated alterations in the environment of the FAD-cofactor. Additionally, T184H showed an effective removal of the positive maxima at 310nm, further indicating perturbations to the FAD binding region. Figure 45B and C depicts selected spectra to highlight the effects on the above described characteristics. In each panel, the spectrum for T184S variant represents the spectra of the additional mutants investigated, each being comparable to WT cb5r. Also included are the T184H and T184V variants which showed altered spectra. Representative spectra of the additional mutants demonstrated that each variant retained a similar line shape to that of WT cb5r with positive maxima at 310 and 390 nm and negative maxima at 460 and 485 nm. In some cases the magnitude of the positive of negative deflections were mildly altered, but not to a significant extent.

In order to determine how the *GtGitP* alanine variants affected the overall catalytic efficiency, initial-rate kinetic analyses were performed as described in "Methods." Kinetic values obtained from these assays are reported in Table 17. As expected, all of the generated variants resulted in a decreased specific activity when compared to WT cb5r, though over a wide range. For the NADH:FR assays the catalytic efficiencies, k_{cat}/K_m^{NADH}, for the variants were determined to range from <.1% to 47.9% of the catalytic efficiency of the WT domain. The large range of effects resulted in most cases from a combination of decreased turnover and decreased affinity. The introduction of a proline residue at G180 or G182 had drastic effects and the rate of turnover of substrate, though only mild effects on binding of substrate. I183M and T184H both caused a significant decrease in affinity for substrate, with K_m values 6 times that of WT

cb5r. In both cases, this was accompanied by a decrease in the rate of activity, especially in the case of T184H. T184V also showed a significant decrease in k_{cat} as compared to WT.

Table 17. NADH:FR Kinetic Constants and Thermal Stability (T_{50}) Values Obtained for the G180P, T181I/S, G182P, I183F/L/M, T184H/S/V, and P185G Variants.

cb5r Variant	NADH:FR				T_{50}
	k_{cat} (s^{-1})	K_m^{NADH} (μM)	K_m^{FeCN6} (μM)	k_{cat}/K_m^{NADH} (s^{-1} M^{-1})	(°C)
WT H_4cb5r	800 ± 17	6 ± 1	8 ± 1	1.4 ± 0.3 x 10^8	56.0
G180P	0.28 ± 0.03	17 ± 4.3	8 ± 1	1.7 ± 0.4 x 10^4	52.1
T181I	310 ± 8.3	22 ± 1.1	7 ± 1	1.4 ± 0.1 x 10^7	53.2
T181S	655 ± 18.3	13.6 ± 0.3	7 ± 1	4.8 ± 0.3 x 10^7	50.8
G182P	0.07 ± .01	7.9± 0.9	7 ± 1	8.6 ± 0.2 x 10^3	51.5
I183F	2 30 ± 11.7	10 ± 0.1	8 ± 1	2.3 ± 0.1 x 10^7	45.1
I183L	617 ± 20.0	11.8 ± 1.2	8 ± 1	5.3 ± 0.8 x 10^7	48.4
I183M	608 ± 28.3	37.2 ± 0.3	7 ± 1	1.6 ± 0.2 x 10^7	44.5
T184H	24.2 ± 2.3	31.9± 0.9	7 ± 1	7.7 ± 0.1 x 10^5	53.2
T184S	785 ± 23.3	14.4± 0.1	8 ± 1	5.5 ± 0.6 x 10^7	52.1
T184V	52.3 ± 3.83	5.1± 1.2	8 ± 1	1.0 ± 0.1 x 10^7	56.2
P185G	208 ± 5.0	3.1 ± 1.2	7 ± 1	6.7 ± 0.9 x 10^7	49.9

To analyze the overall protein stability of each of the variants, thermal denaturation profiles were generated utilizing thermal NADH:FR profiling in tandem with the loss of intrinsic flavin fluorescence emission quenching, following incubation of the proteins at temperatures ranging from 0-100 ºC. Changes in the intrinsic fluorescence of the FAD prosthetic group monitored together with the retention of NADH:FR activity following thermal denaturation yielded a T_{50} value, the temperature at which there is 50% of maximum fluorescence or 50% retention of NADH:FR activity. All variants

demonstrated varied levels of decreased temperature stabilities with T_{50} values ranging from 44.5.6 to 56.2ºC for the I183M and T184V mutants respectively (Table 17). The I183 variants seemed to elicit the greatest effect on the thermal stability, with all substitutions causing a 5 to 12ºC decrease in T_{50} value. The graphs of the T_{50} data for the I183 series of variants are shown in Figure 46. Additionally, the graphs of T181S and T184H are shown to illustrate the range obtained for the remaining variants.

As demonstrated through the kinetic analyses, several variants displayed altered affinities for substrate. To further investigate this alterations, spectral binding constants were determined for each of the mutants utilizing differential spectroscopy in order to compare the affinities for both the substrate NADH and product NAD^+. As described in "Methods", the NADH isosteric analog H_4NAD was utilized to monitor complex formation and establish a spectral binding constant [106]. Differential spectroscopy was utilized to monitor complex formation during titrations with either H_4NAD or NAD^+. The results are illustrated in Figures 47 and Figure 48 respectively.

Titrations performed in the presence of H_4NAD yielded spectra with a line shape similar to that of WT cb5r for the majority of the variants. The T181S, T184H/S/V, and P185G variants each showed spectra very similar to that of WT, with magnitude differences being the main disparity among the spectra. The I183 series of variants demonstrated an altered line shape that had qualities similar to that of WT in the presence of H_4NAD. I183L and I183M generated spectra that were similar to H_4NAD between 380 and 420nm, but was more similar to WT in the presence of NAD^+ in the region of 420 to 480nm. This hybrid quality to the spectra indicated an altered mode of binding. I183F generated spectra similar to that of WT titrated with NHD^+. G180P, G182P and

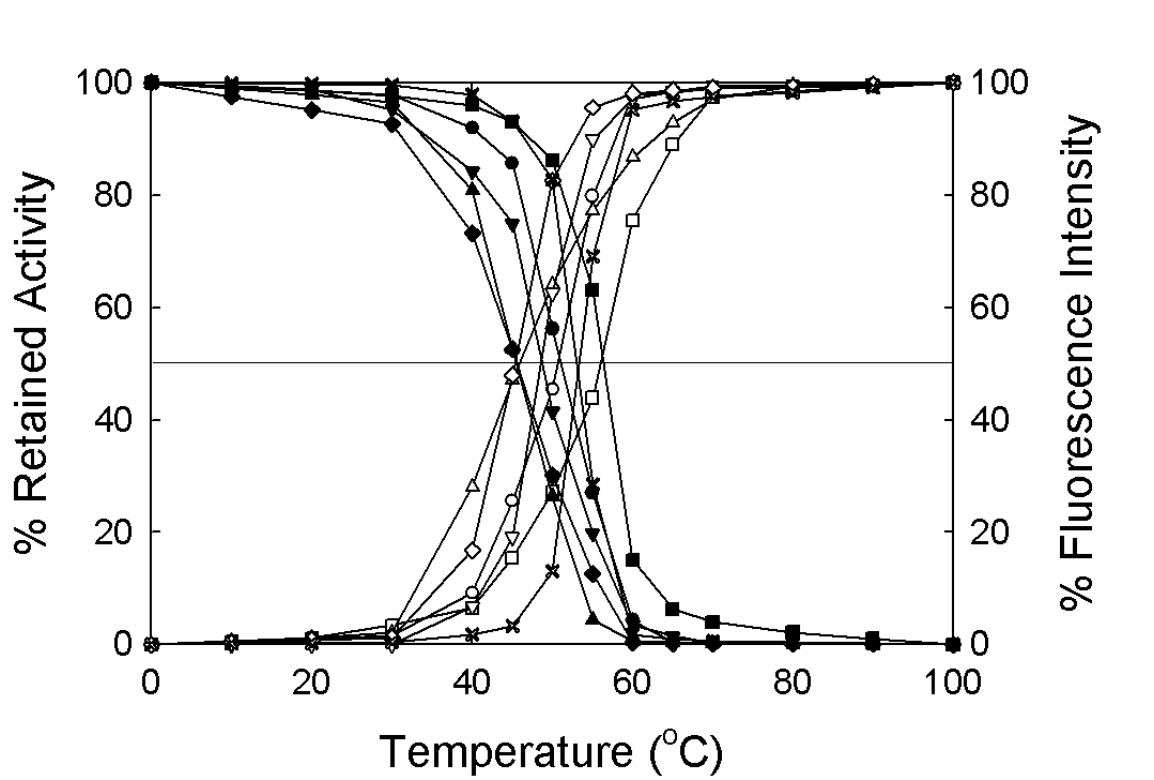

Figure 46. Thermal Stability Profiles of Wild-Type cb5r and Selected Variants of the "CGpppM" Motif. Oxidized samples of each variant and WT H_4cb5r (5μM FAD) were incubated at the indicated temperatures, and aliquots were withdrawn and assayed for both residual NADH:FR activity (closed symbols) and intrinsic flavin fluorescence (open symbols) in 10 mM phosphate buffer, containing 0.1 mM EDTA, pH 7.0 using excitation and emission wavelengths of 450 nm and 523 nm, respectively. Selected variants shown for clarity. The graphs of T181S and T184 represent the boundaries of the range within which the remaining variants fit. The I183 variants demonstrated the most significant impact on thermal stability. Points correspond to: (●,○) H_4cb5r; (■, □) T181SA; (▲, Δ) I183F; (▼,▽) I183L; (♦, ◊) I183M; and (**x**) T184H.

T181I each generated spectra that were significantly different that that of WT titrated with H_4NAD. The spectra of T181P was nearly identical to that of T181A in the presence of H_4NAD, differing only in magnitude. G180P and G182P each generated spectra unlike any other previously analyzed NAD^+ analog, suggesting a drastic alteration

to the binding environment for NADH. The values obtained for the respective binding constants (K_s) for all variants are given in Table 18.

Titrations performed for the variants in the presence of the product NAD^+ again produced diverse spectra with lines shapes both similar to and differing from that of WT. Residues T181S, I183F/L/M, T184S, and P185G each generated spectra that mirrored that of WT cb5r titrated with NAD^+, differing mainly in magnitude of positive and negative deflections only, with minor alterations in the overall line shape of the spectra. T184H generated spectra similar to that expected for H_4NAD, only differing in the absence of the negative maxima at 395nm. The remaining variants each generated unique spectra significantly different from WT, with the exception of G180P, which failed to generate a spectroscopically-active species during the titration within detectable concentrations. T181I again generated spectra similar to that obtained from T181A. The spectra generated for G182P in the presence of NAD^+ showed a high level of similarity to the spectra it generated in the presence of H_4NAD. T184V generated spectra appearing as hybrids of the spectra obtained for WT in the presence of NAD^+ with spectra from titrations with $PAAD^+$. The values obtained for the respective binding constants (K_s) for all variants are given in Table 18.

To examine the effects of the structural changes on the flavin prosthetic group of each variant, oxidation-reduction potentials for the FAD cofactor were determined utilizing the dye-equilibration potentiometric titration method for WT cb5r and the "GtGitP" mutants in the presence of phenosafranine ($E°' = -252$ mV). Flavin midpoint potentials ($E^{o\prime}$, n=2) for the $FAD/FADH_2$ couple were determined both in the absence and presence of NAD^+ from the linear Nernst plots of the log $[FAD_{ox}/FAD_{red}]$ versus the

Figure 47. Spectroscopic Titrations Obtained for the WT cb5r and Selected Variants of the "GtGitP" Motif in the Presence of H_4NAD. Titrations of all mutants (50μM) were carried out as previously described in 10mM phosphate buffer containing 0.1mM EDTA, pH 7.0 at 23 °C. Difference spectra were recorded following the addition of solution containing H_4NAD (5mM). The inset panel corresponds to a plot of the magnitude of the spectral perturbations at the indicated wavelengths versus pyridine nucleotide concentration where a difference spectrum was observed. Plots of the relative absorbance changes observed are as follows: (A) WT H_4cb5r; (B) G180P; (C) T181I; (D) G182P; (E) I183F; (F) I183L; and (G) T184S (representative of spectra of variants not shown)

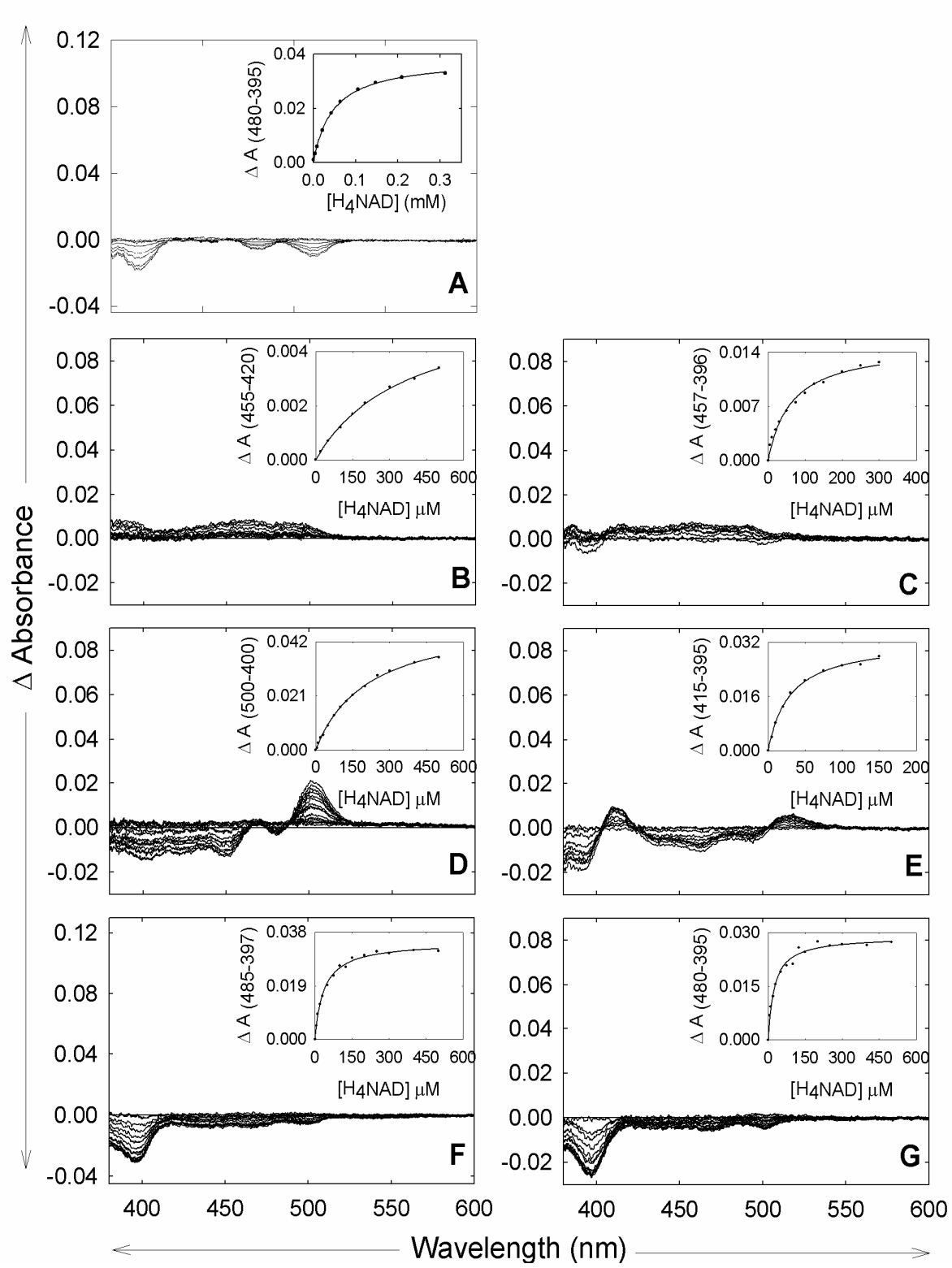
Δ Absorbance
Wavelength (nm)
A
B
C
D
E
F
G
Δ A (480-395)
[H4NAD] (mM)
Δ A (455-420)
[H4NAD] μM
Δ A (457-396)
[H4NAD] μM
Δ A (500-400)
[H4NAD] μM
Δ A (415-395)
[H4NAD] μM
Δ A (485-397)
[H4NAD] μM
Δ A (480-395)
[H4NAD] μM

Figure 48. Spectroscopic Titrations Obtained for the WT cb5r and Selected Variants of the "GtGitP" Motif in the Presence of NAD^+. Titrations of all mutants (50μM) were carried out as previously described in 10mM phosphate buffer containing 0.1mM EDTA, pH 7.0 at 23 °C. Difference spectra were recorded following the addition of solution containing NAD^+ (30mM). The inset panel corresponds to a plot of the magnitude of the spectral perturbations at the indicated wavelengths versus pyridine nucleotide concentration where a difference spectrum was observed. Plots of the relative absorbance changes observed are as follows: (A) WT H_4cb5r; (B) G180P; (C) T181I; (D) G182P; (E) T184H; (F) T184V; and (G) T181S (representative of spectra of variants not shown)

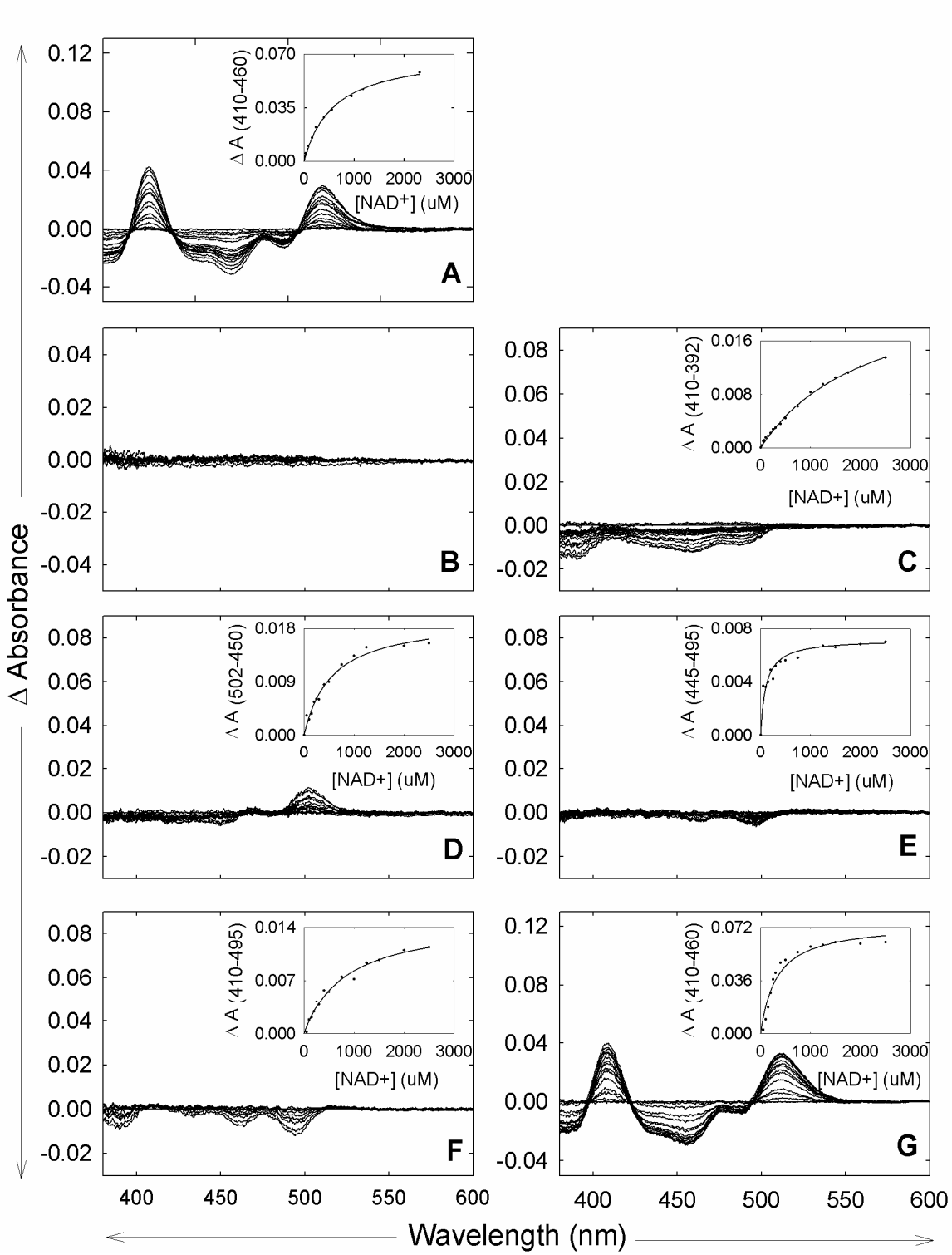
Δ Absorbance
Wavelength (nm)
A
B
C
D
E
F
G
Δ A (410-460)
[NAD+] (uM)
Δ A (410-392)
Δ A (502-450)
Δ A (445-495)
Δ A (410-495)

potential (mV). Variants yielding significant alterations to the midpoints are shown in Figure 49. Graphs of the midpoint determination for P185G are representative of the majority of the variants. Values established for all redox potentials are shown in Table 18. Analysis of the midpoint potentials of the variants in the absence of NAD^+ indicated that FAD reduction occurred after the reduction of phenosafranine, resulting in values comparable to that of WT cb5r, within the $\pm$ 5mV standard error. Midpoint titrations carried out in the presence of NAD^+ resulted in values that were more negative, as compared to WT, for the majority of the variants, with values ranging from -228 for G180P to -196 for T181S.

Table 18. Spectral Binding Constants (K_s) and Standard Midpoint Potentials (E°′) Obtained for the G180P, T181I/S, G182P, I183F/L/M, T184H/S/V, and P185G cb5r Variants.

cb5r Variant	K_s		$E°'_{FAD/FADH_2}$ (mV)	
	$K_s^{H_4NAD}$ (μM)	K_s^{NAD+} (μM)	$-NAD^+$	$+NAD^+$
WT H_4 cb5r	45 ± 10	533 ± 30	-271	-191
G180P	370 ± 16.7	ND[a]	-275	-227
T181I	72.5 ± 7.9	1387 ± 124	-271	-203
T181S	63.3 ± 3.4	308 ± 5.1	-272	-196
G182P	211 ± 12	544 ± 89	-275	-210
I183F	29.7 ± 3.2	29 ± 1.5	-276	-209
I183L	35.7 ± 1.9	154 ± 19	-276	-206
I183M	36.3 ± 2.1	113 ± 14	-275	-201
T184H	35.1 ± 2.2	103 ± 4.9	-276	-228
T184S	24.8 ± 1.9	233 ± 17	-276	-198
T184V	62.6 ± 5.1	810 ± 23	-275	-217
P185G	22.6 ± 3.1	55 ± 1.6	-271	-209

[a]ND indicates that the spectroscopic binding constant could not be determined, due to insufficient spectral change.

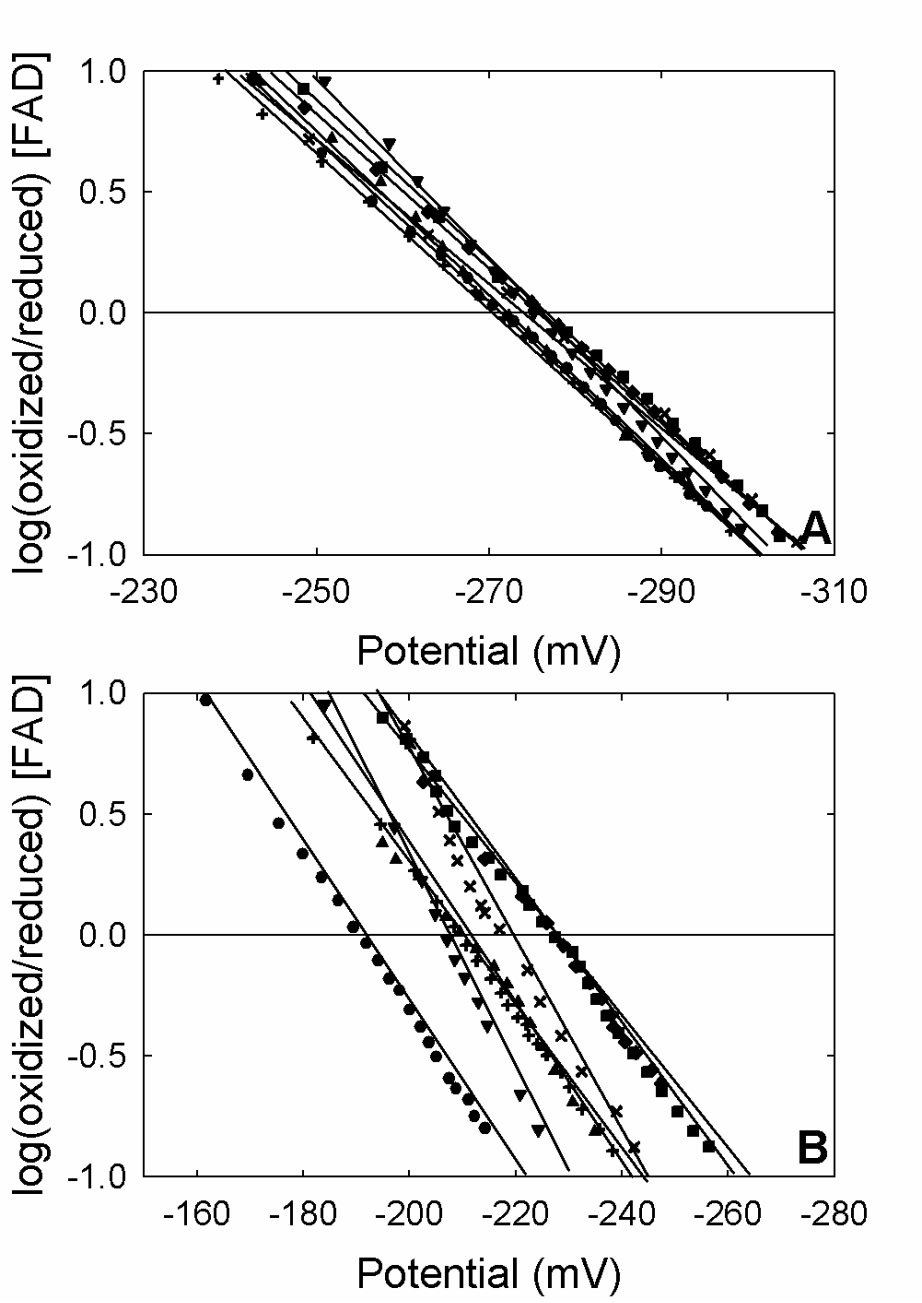

Figure 49. Oxidation-Reduction Midpoint Potentials for the FAD Prosthetic Group in the Wild-Type cb5r and Selected Variants of the "GtGitP" Motif. Reductive dye titrations were performed at 25 °C as described in "Methods" using phenosafranine as the indicator dye in 100 mM phosphate buffer containing 0.1 mM EDTA, pH 7.0. Nernst plots in the absence (A) and presence (B) of 2 mM NAD^+. Plots correspond to (A) (●) H_4cb5r; (■) G180P; (▲) G182P; (▼) I183L; (♦) T184H; (**x**) T184V; and (+) P185G. (B) (●) H_4cb5r; (■) G180P; (▲) T181S; (▼) G182P; (♦) I183F; (**x**) T184H; and (+) P185G.

Summary of Systematic analysis of the conserved NADH binding motif "^{180}GxGxxP^{185}"

Glycine and proline residues each confer structural qualities to the backbone of polypeptides. Glycine, lacking a side chain, allows for a high level of rotational freedom in the backbone, allowing a polypeptide more rotational freedom and conferring a "plastic" like quality to the protein. Additionally, the lack of side chain eliminates steric problems, and allow for "openness" in a protein useful, for example, in allowing substrate to contact and bind appropriately to a protein. Proline residues, being secondary amines, possess a distinctive cyclical structure to the side chain which confers a exceptional level of conformational rigidity to a protein. Therefore, the presence of the residues in a highly conserved protein domain indicates that the structural characteristics imbued by the residues are essential for proper function. Using cb5r as a model, we can see that, in part, the function of the GxGxxP motif in cb5r and other FNR family members would be to create a "perch" onto which the NADH can sit to be positioned for efficient electron transfer with the flavin cofactor. Homology modeling of the mutants of G180 (Figure 50) and G182 (Figure 51) further demonstrates how the distinct individual characteristics of glycine residues confer the necessary structural features for the proper association of NADH. From these models, it is evident that the slightest alterations to the side chain at position 180 or 182, as demonstrated by alanine substitutions of these residue (Figures 50B and 51B), cause electrostatic interference with the proper fitting of the NAD^+ molecule into the binding site. This effect is intensified in the proline substitutions (Figures 50C and 51C), where actual physical steric hindrances can be noted. In the case of G180, the effect appears mostly directed toward the pyrophosphate moiety of NAD^+, potentially repositioning the nicotinamide and/or adenine moieties, whereas

Figure 50. Structures of WT cb5r and G180A and G180P Variants with NAD^+ Generated *in silica*. The molecular model of cb5r displaying the charged surfaces of (A) residue G180 (blue stick) (B) cb5r variant G180A (green stick) and (C) cb5r variant G180P (magenta stick) in association with NAD^+ generated utilizing the automated comparative protein modeling server SWISS-MODEL [111] and analyzed using the molecular modeling software Web Lab Viewer Pro [134]. Model depicts surface representation of the residue in transparent wire mesh display style and NAD^+ in transparent display style. Models generated from cb5r in complex with FAD and NAD^+ (1IB0) where the acidic residues are red, basic residues are blue, and neutral residues are white.

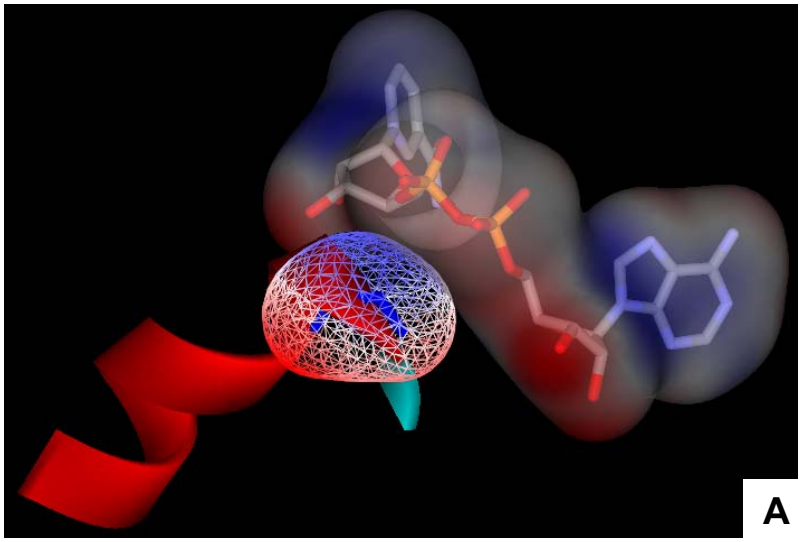
A

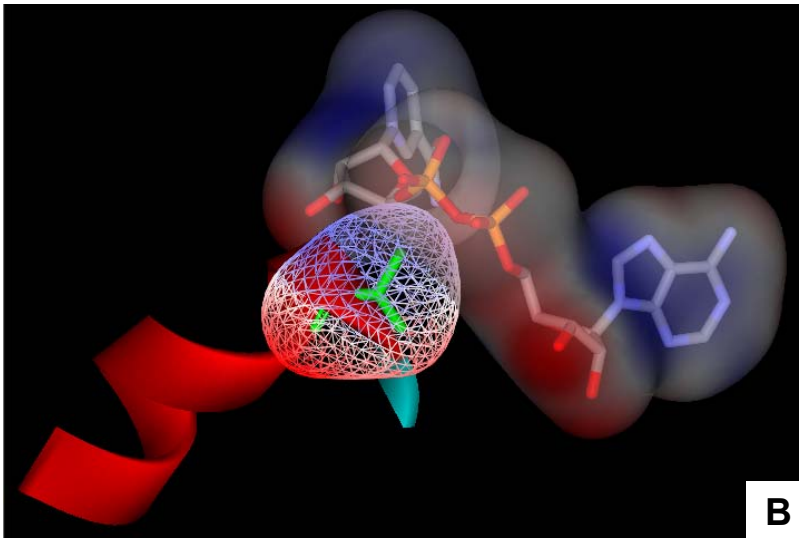
B

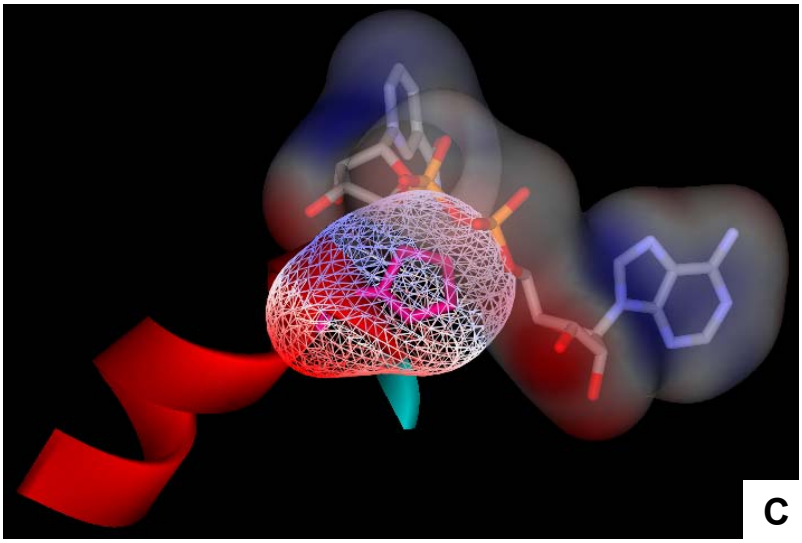
C

alterations of G182 appear to affect the nicotinamide moiety directly. This observation is further supported by the differential spectroscopy results. For G180A, spectra obtained from titrations with NAD^+ were similar to those of WT cb5r titrated with 5'-ADP. Since 5'-ADP is a structural analog of NAD^+ lacking the ribose of the adenine moiety and the nicotinamide ring, a variant demonstrating spectra similar in appearance to it indicates that the variant is affecting the proper orientation of the NAD^+, preventing either of those groups from properly fitting. The lack of detectable spectral difference for G180P again further indicates that placement of any obstruction in the 180 position prevents the substrate from being able to properly bind. The G182 variants again showed a correlation between the molecular modeling and the differential spectroscopy in that the spectra obtained for both G182A and G182P titrated with NAD^+ were mirror images of the spectra of WT with ADP-ribose. This similarity indicates that the substitutions at position 182 do indeed affect the proper association of NAD^+ by affecting the aligning of the nicotinamide moiety. As this is the portion of the molecule involved in the electron transfer reaction with FAD, incorrect orientation of the nicotinamide ring would drastically decrease the catalytic efficiency of the enzyme. This was evidenced in the NADH:FR assays for these residues, yielding catalytic efficiencies less than 1% that of WT. From this we can conclude that the two glycine residues of "GxGxxP" motif are vital to the proper placement of the NADH to ensure correct interaction of the nicotinamide moiety with the isoalloxazine ring of FAD.

The other conserved residue in the GxGxxP motif, P185, appears to be important in maintaining the structural integrity of the secondary structure of cb5r in the proximity of the pyridine nucleotide binding pocket. Substitutions of this residue did not show any

Figure 51. Structures of WT cb5r and G182A and G182P Variants with NAD^+ Generated *in silica*. The molecular model of cb5r displaying the charged surfaces of (A) residue G182 (blue stick) (B) cb5r variant G182A (green stick) and (C) cb5r variant G182P (magenta stick) in association with NAD^+ generated utilizing the automated comparative protein modeling server SWISS-MODEL [111] and analyzed using the molecular modeling software Web Lab Viewer Pro [134]. Model depicts surface representation of the residue in transparent wire mesh display style and NAD^+ in transparent display style. Models generated from cb5r in complex with FAD and NAD^+ (1IB0) where the acidic residues are red, basic residues are blue, and neutral residues are white.

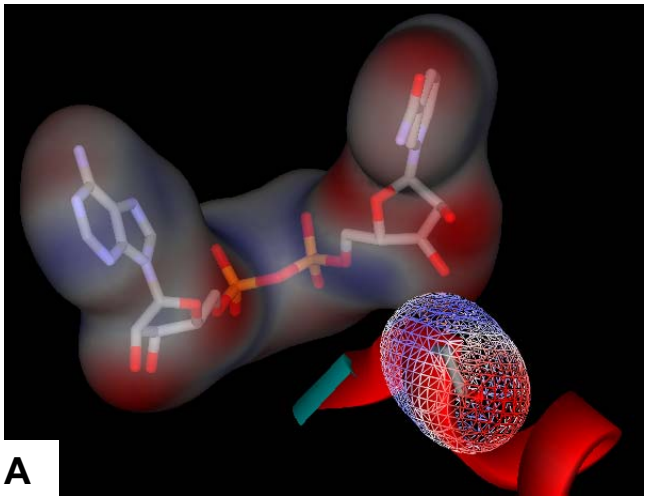

A

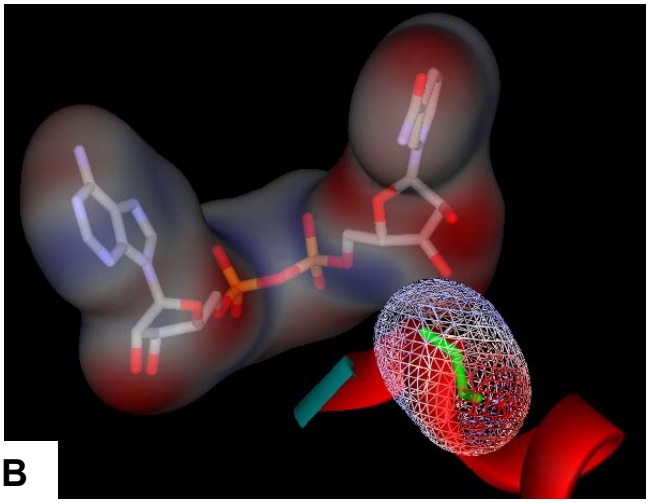

B

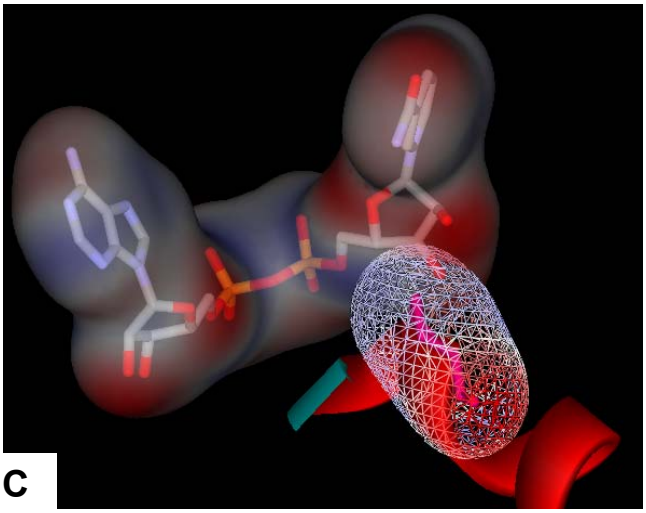

C

negative impact on the ability to associate and bind to NADH. In fact, substitution of this position with glycine resulted in enhanced binding affinity as shown by a 2-fold increase in K_m^{NADH} in the NADH:FR assay and increased K_s values in the titration with H_4NAD, indicating that the relaxing affects of glycine residue on the rigidity of the backbone structure allowed for the NADH to associate better. This, however, was actually a negative consequence overall, as it prevented the proper alignment of the NADH and FAD resulting in highly diminished catalytic activity. A structural model of P185 and its position in relation to NAD^+ and FAD is shown in Figure 52. The isoalloxazine ring is in proximity of the proline residue. Substituting the proline with a glycine would remove the electrostatic interactions allowing more "openness"' to the binding pocket of NADH and FAD. This would explain the ability of the mutants to bind NADH with higher affinity. Further evidence of the structural importance of P185 is shown in the decreased stability observed in thermal denaturation studies. The relaxing of the backbone resulting from substitution of the proline caused the FAD cofactor to become more "open" to the environment, and as a result more easily removed, as demonstrated by an average T_{50} value 5 °C lower than WT.

The effects of substitutions of residue I183 on the function of cb5r also result from structural perturbations, however with a decreased magnitude as compared to substitution of P185. Except in the case of I183F, the substitutions examined demonstrated a mild decrease in rate of turnover NADH. Additionally, with the exception of I183M, the substitutions only mildly decreased substrate affinity. Both of these substitutions represent non-conserved mutations in respect to side chain characteristics. Introduction of an aromatic ring (I183F) or a polar sulfur group (I183M),

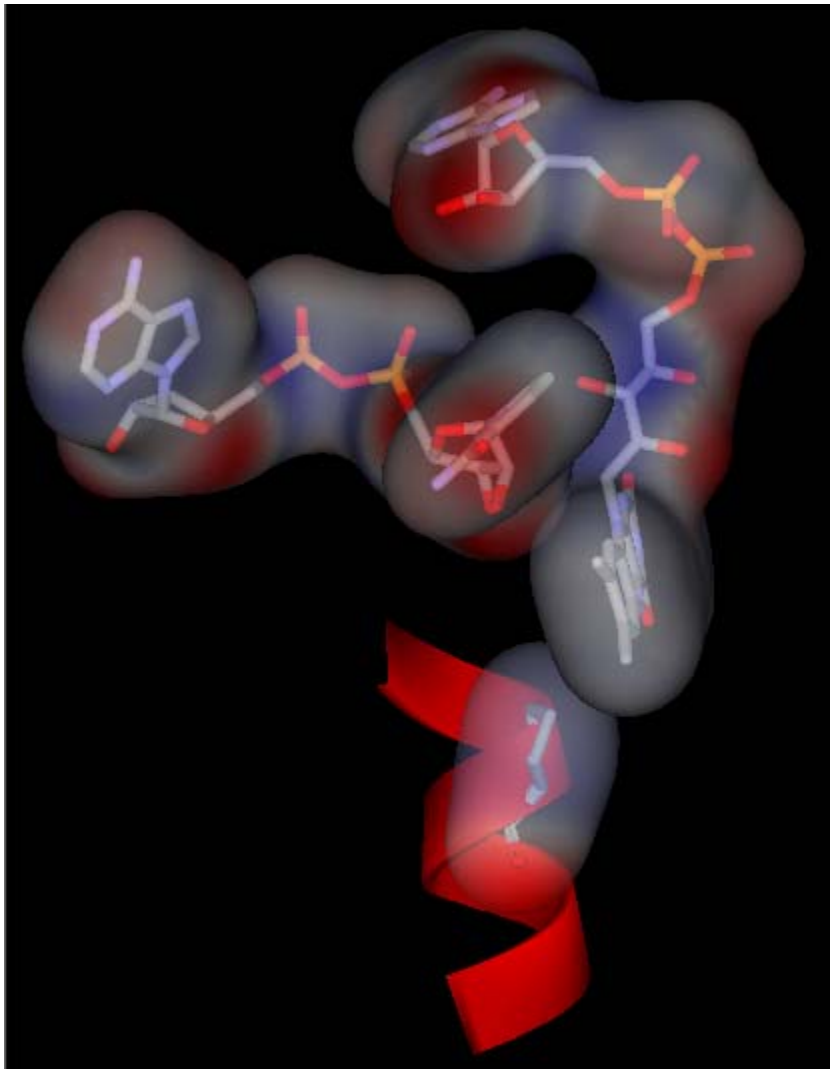

Figure 52. Structure of WT cb5r residue P185 in Association with NAD^+ and FAD Generated *in silica*. The molecular model of cb5r displaying the charged surfaces of P185 in association with NAD^+ and FAD generated utilizing the automated comparative protein modeling server SWISS-MODEL [111] and analyzed using the molecular modeling software Web Lab Viewer Pro [134]. Model depicts surface representation of the residue in transparent wire mesh display style and NAD^+ and FAD in transparent display style. Models generated from cb5r in complex with FAD and NAD^+ (1IB0) where the acidic residues are red, basic residues are blue, and neutral residues are white.

produced a more severe impact on catalytic activity than the smaller non-polar substitutions (I183A/L). This indicated that the effect of these mutations resulted from the physical structure of the side chain. The side chain of I183 extends toward neighboring residues A178 and F207. Introduction of a large aromatic ring in this location would result in steric conflicts among these residues, causing an alteration in the local tertiary structure, sufficient to affect the functioning of the protein. Additionally, the substitution with methionine at this position introduces a sulfur group near residue T184, disrupting its association with FAD. The main impact of the substitution of I183 occurs as a result of decreased stability as shown by the thermal denaturation results. All substitutions lead to a decrease in T_{50} values ranging from 6-12^{o}C. While not directly involved with catalytic function or substrate binding, the presence of a small non-polar residue at position 183 is clearly required to assure folding into the proper tertiary structure allowing for efficient activity of cb5r.

The potential importance of residues T181 and T184 are self-evident from studies of the X-ray crystal structure of cb5r. Since the residues are involved in hydrogen bond formation with the substrate and cofactor, respectively, T181 and T184 should be vital in maintaining proper catalytic activity of the enzyme. The results of the characterization support such a hypothesis. In the case of T181, it is evident that the polarity of the residue is vital to correct function. Substitution with serine yielded only mild impairments across all spectral and catalytic parameters. Because the hydroxyl group of serine would face in the opposite direction of that of threonine, the distance from the N3 oxygen of the nicotinamide ribose is increased by 1.07Å, and bond formation is impaired

Figure 53. Replacement of non polar residue complete eliminates the ability of bond

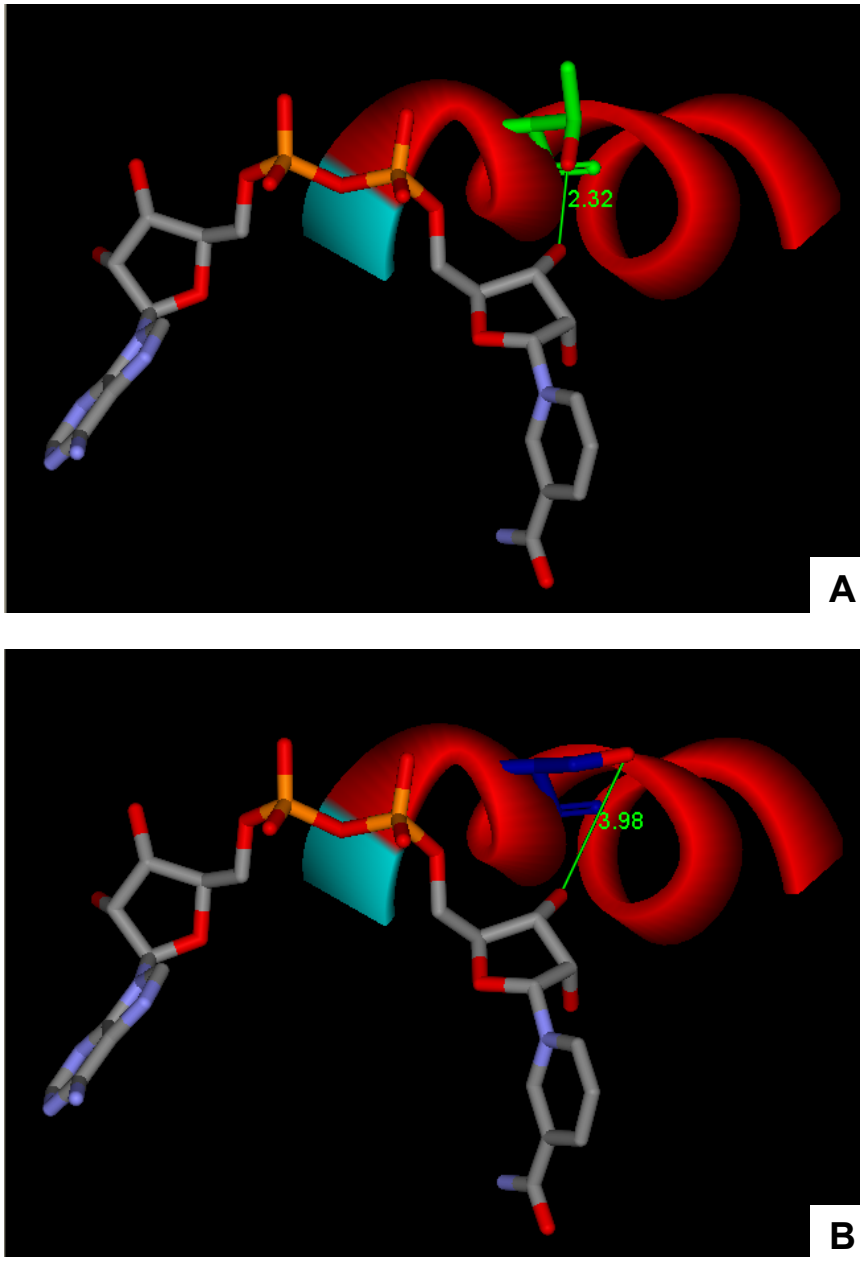

Figure 53. Structures of WT cb5r residue T181 and Variant T181S in Association with NAD^+ Generated *in silica*. The molecular model of cb5r displaying (A) residue T181 (green stick representation and (B) Variant T181S (blue stick representation) in association with NAD^+ generated utilizing the automated comparative protein modeling server SWISS-MODEL [111] and analyzed using the molecular modeling software Web Lab Viewer Pro [134]. Model indicates distance of the side chain oxygen (red stick) of each residue to the N3 oxygen of NAD^+ ribose. NAD^+ depicted in stick formation with CPK coloring. Models generated from cb5r in complex with FAD and NAD^+ (1IB0).

formation, resulting in more drastic impairments. In the case of both T181A and T181I, the affinity for substrate was decreased, with K_m values 3 times greater than that of WT. Additionally, both bound H_4NAD in altered conformations indicating that the presence of a threonine residue and its hydroxyl group are necessary for aligning NADH properly into the binding site. The similarity of the resulting differential spectra for both variants in to the spectra obtained for WT titrated with $PAAD^+$, which lacks the N7 nitrogen of NAD^+, points to the possibility that the substitutions cause the NADH to adopt an orientation causing this nitrogen to be out of position. As this nitrogen is involved in the electron transfer process between NADH and FAD, alteration of its position would lead to inefficient transfer.

We proposed that substation of residue T184 would have a significant effect on the environment of the FAD cofactor of cb5r, and this was clearly demonstrated in the spectral shifts observed in both UV/Visible absorbance and circular dichroism spectroscopy studies. In addition, substitution of T184 resulted in drastically decreased rates of turnover. The reason for these observation is the removal of two hydrogen bonds to the isoalloxazine ring of FAD. T184 forms bond with O4 and N5 of the FAD ring system, the latter of which is the location to which one hydrogen is added in the electron transfer process. Removal of this interaction, demonstrate through the T184A variant, results in a moderately decreased catalytic efficiency, likely due to destabilization of the NAD^+-FAD^- semiquinone intermediate in a manner similar to that of T94 [43]. T184H yielded more drastic effects on the rate of turnover, decreasing it by 35-fold as compared to WT. The introduction of a large positive residue in this location would more severely alter the electron transfer process than merely removing the bond normally present. The

alteration in the FAD environment was further confirmed by the results of the oxidation/reduction potential of the FAD/$FADH_2$ couple which yielded a midpoint potential comparable to that of free flavin (-220 mV) in the absence and presence of NAD^+, indicating an unfavorable electron transfer environment. Little effect was seen on the ability to associate with NADH or H_4NAD, indicating that the decrease in catalytic efficiency and electron transfer is mainly due to the missing stabilizing presence of the threonine side chain.

Properties of the Type I recessive congenital methemoglobinemia mutants A178T and A178V.

Preceding the highly conserved ^{180}GxGxxP^{185} NADH-binding motif is an equally highly conserved residue of which two mutations have been identified which lead to clinical presentation of Type I RCM in two patients. The first of these mutations arises from a G535A mutation in exon 6 of the *DIA1* gene. The mutation has been found in two unrelated individuals. The first patient was a newborn girl of North African origin who presented with severe cyanosis, having low methemoglobin (metHb) reductase levels and 31% metHb in her circulating erythrocytes. The mutation predicts an A178T substitution. This substitution occurs in the Nβ2 sheet immediately preceding the NADH specificity/binding motif. The patient was found to be homozygous for the mutation, with both parents being heterozygous and presenting with normal metHb levels but decreased enzyme activity. No neurological abnormalities were noted by age of 9 months, leading to diagnosis as Type I RCM [147]. The second patient was a male newborn of Turkish decent. He was cyanotic within one hour of birth, and had a metHb concentration of 25%. The patient responded well to treatment with methylene blue (0.5 mg/kg), reducing metHb levels to 2%. A second rise in metHb levels was successful treated with ascorbic acid (20mg/kg/day), bringing the levels back down to 5-10%. No neurologic impairment was noted by age of 8 months, the age at the time of study [148]. In both cases, DNA samples from a pool of unrelated individuals were analyzed for the presence of the mutation. The mutation was not found in any of the additional subjects, and thus was determined to not be a polymorphism.

In another patient, a C to T substitution was discovered at the second position of codon 178 in exon 6 leading to a replacement of A178 by valine. The patient, 29 years old at time of study, was of Thai origin and was first diagnosed at age 4. Born to a healthy mother, the patient was born full term and had been cyanotic since birth. Her only elder brother is healthy without cyanosis. Preliminary investigations indicated that the mutant retained near WT activity and substrate affinity, noting little difference between the two. Thermal stability studies indicated that the mutant was less stable than the WT enzyme, and thus was concluded to be the causative agent for the cyanosis. As with the A178T mutation, the A178V mutation was looked for in additional individuals and ruled out as being a polymorphism [149]. The identification of the A178V mutation along with the finding of the A179T mutation, together with the reported mutations at codon 204 [150, 151], make codons 179 and 204 the only ones within the cb5r gene where more than one mutation has been identified.

To further elucidate the effects of the naturally occurring A178T and A178V mutations on the functioning of cb5r, variants of each mutation were generated as described in "Methods," utilizing the original four-histidine tagged cb5r expression construct and the corresponding oligonucleotide primers listed in Appendix B. These variants were characterized on the basis of kinetic, spectral, and thermal stability parameters.

UV/visible absorbance spectra were obtained for oxidized samples of the purified RCM variants A178T and A178V and were compared with the spectra obtained for the corresponding WT domain (Figure 54A). All three variants exhibited spectra identical to that of the WT domain, characterized by absorption maximum detected at 273 nm in the

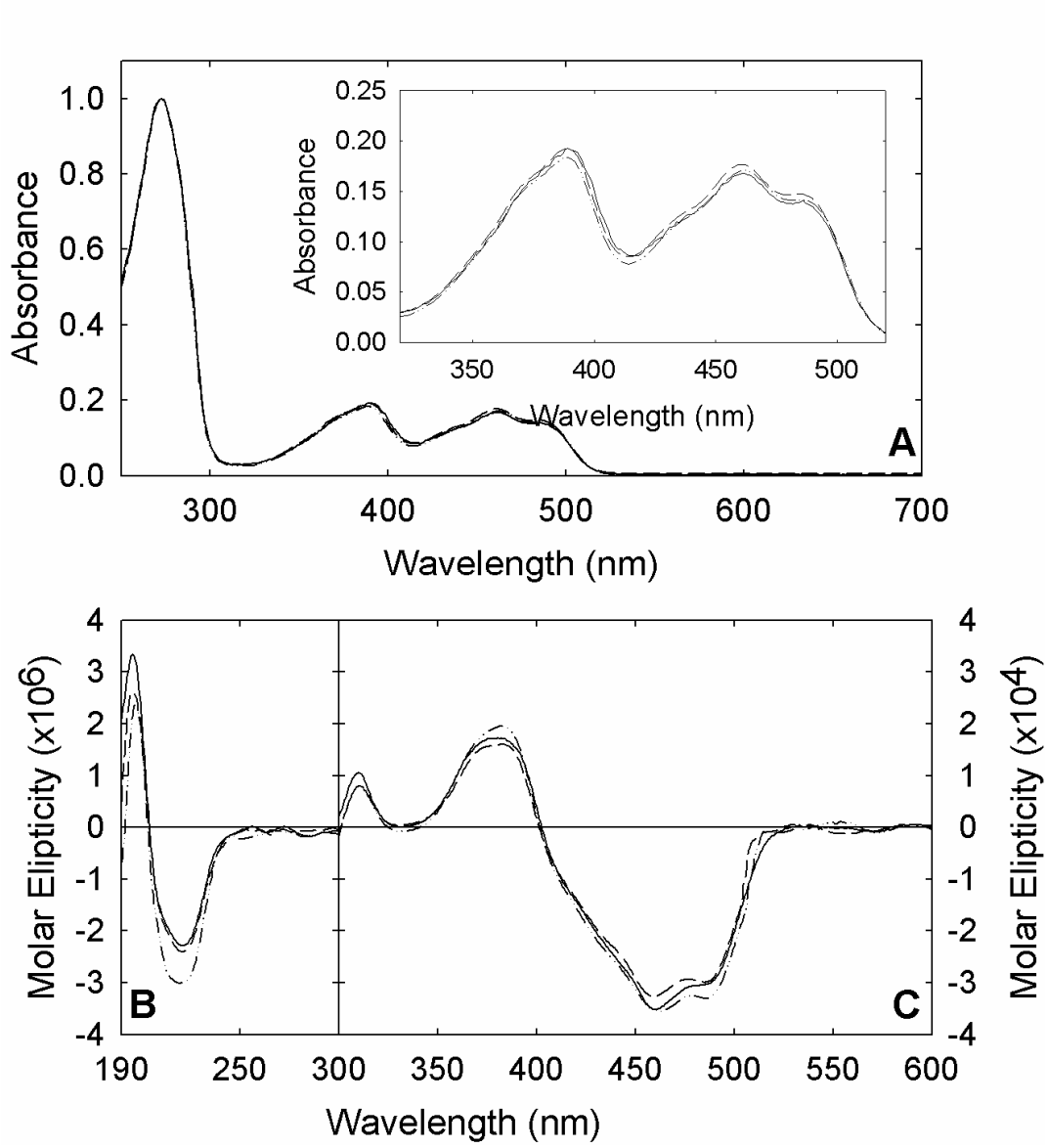

Figure 54. Ultra-Violet, Visible, and Circular Dichroism Spectra Obtained for the Wild-Type and the RCM Type I Associated Variants A178T and A178V. (A) UV/visible absorption spectra were obtained for oxidized samples of cb5r and the A178T and A178V mutants at equivalent flavin concentrations (1.7 μM FAD) in 10 mM phosphate buffer, containing 0.1 mM EDTA, pH 7.0. The inset shows an expanded region of the visible spectrum where the flavin prosthetic group makes a major contribution. Individual spectra correspond to WT cb5r (—); A178T (-- --); and A178V (- .. - .. -); (B) UV CD spectra were recorded using enzyme samples (7 μM FAD) in 10 mM phosphate buffer, containing 0.1 mM EDTA, pH 7.0. (C) Visible CD spectra were recorded using enzyme samples (50 μM FAD) in 10 mM phosphate buffer, containing 0.1 mM EDTA, pH 7.0. Line styles shown in "B" and "C" are the same as those depicted in "A".

UV range of the spectrum, and a peak at 461 nm with an associated pronounced shoulder in the range of 485-500 nm in the visible region of the spectrum, the latter peak attributable to protein- bound flavin. The $A_{273\ nm}/A_{461\ nm}$ absorbance ratios of the variants were within the range of 5.9 ± 0.2, comparable to values previously obtained for WT rat cb5r of 5.7 ± 0.2 [121], indicating a full complement of the FAD prosthetic group.

To assess any alterations in the secondary structural content of the different type I RCM cb5r variants, circular dichroism spectra were recorded in the UV wavelength range (190-300 nm). As shown in Figure 54B, all three variants exhibited positive CD spectra from 190-210 nm and negative CD spectra from 210-250 nm with the spectra retaining both positive and negative intensities very similar to that of the WT domain. The A178T variant produced a spectrum with increased magnitude of the negative CD component. The absence of any significant differences between the spectra of various mutants and the WT domain suggested conservation of the secondary structure architecture and that none of the amino acid substitutions or deletions had any substantial effects on the folding of the protein. Visible CD spectroscopy was utilized to examine the environment of the FAD prosthetic group. As shown in Figure 54C, all three variants generated exhibited visible CD spectra that were virtually indistinguishable from that of WT cb5r, indicating that none of the amino acid substitutions had any significant effect on the conformation of the bound FAD prosthetic group.

To assess the effect of the mutations on the catalytic function of the enzyme, initial-rate kinetic constants for the NADH:FR activity were determined for the WT cb5r and for each purified variant. The values obtained for the NADH:FR activities are presented in Table 19. Of the two mutations, the A178T variant demonstrated the

greatest decrease in both k_{cat} and K_m^{NADH}, retaining approximately 34% of WT catalytic efficiency (k_{cat}/K_m^{NADH}). Decreased functionality was observed for both the rate of turn over and the affinity for substrate, having both parameters decreased by approximately 60% when compared to WT. The impact of the A178V variant was less severe in nature, retaining 64% of WT efficiency, and a near equivalent rate of turnover to that of the WT enzyme.

Table 19. NADH:FR Kinetic Constants and Thermal Stability (T_{50}) Values of the Type I RCM Associated Mutants A178T and A178V

cb5r Variant	NADH:FR				T_{50}
	k_{cat} (s^{-1})	K_m^{NADH} (μM)	K_m^{FeCN6} (μM)	k_{cat}/K_m^{NADH} (s^{-1} M^{-1})	(°C)
WT H_4cb5r	800 ± 17	6.0 ± 1	8 ± 1	1.4 ± 0.3 x 10^8	56.1
A178T	493 ± 8.3	10.4 ± 0.8	7 ± 1	4.8 ± 0.4 x 10^7	55.0
A178V	763 ± 3.3	8.6 ± 0.9	7 ± 1	8.9 ± 0.3 x 10^7	49.2

To examine the influence of the various amino acid substitutions on protein stability, the thermal NADH:FR inactivation profile coupled with the increase in intrinsic flavin fluorescence and emission intensity of each of the variants was monitored and was compared to values obtained for the WT enzyme. The results obtained for the thermal denaturation profiles and changes in intrinsic flavin fluorescence are shown in Figure 55. Changes in the intrinsic fluorescence of the cofactor or the retention of NADH:FR activity following thermal denaturation was an effective indicator of the stability of the core structure of the protein. T_{50} values (the temperature at which 50% of maximum fluorescence and 50% retention of NADH:FR activity was detected) are reported in Table

19. A178T demonstrated equivalent stability as compared to WT while A178V proved to be less stable, having a T_{50} value 7 °C lower than that of WT.

Differential spectroscopy was used to evaluate the effect of the RCM mutations on the binding affinity for both the isosteric NADH analog H_4NAD and NAD^+. As shown in Figure 56, both of the mutations resulted in similar line shapes for the spectra obtained from the titrations with H_4NAD, with minor alterations detected in the 415-

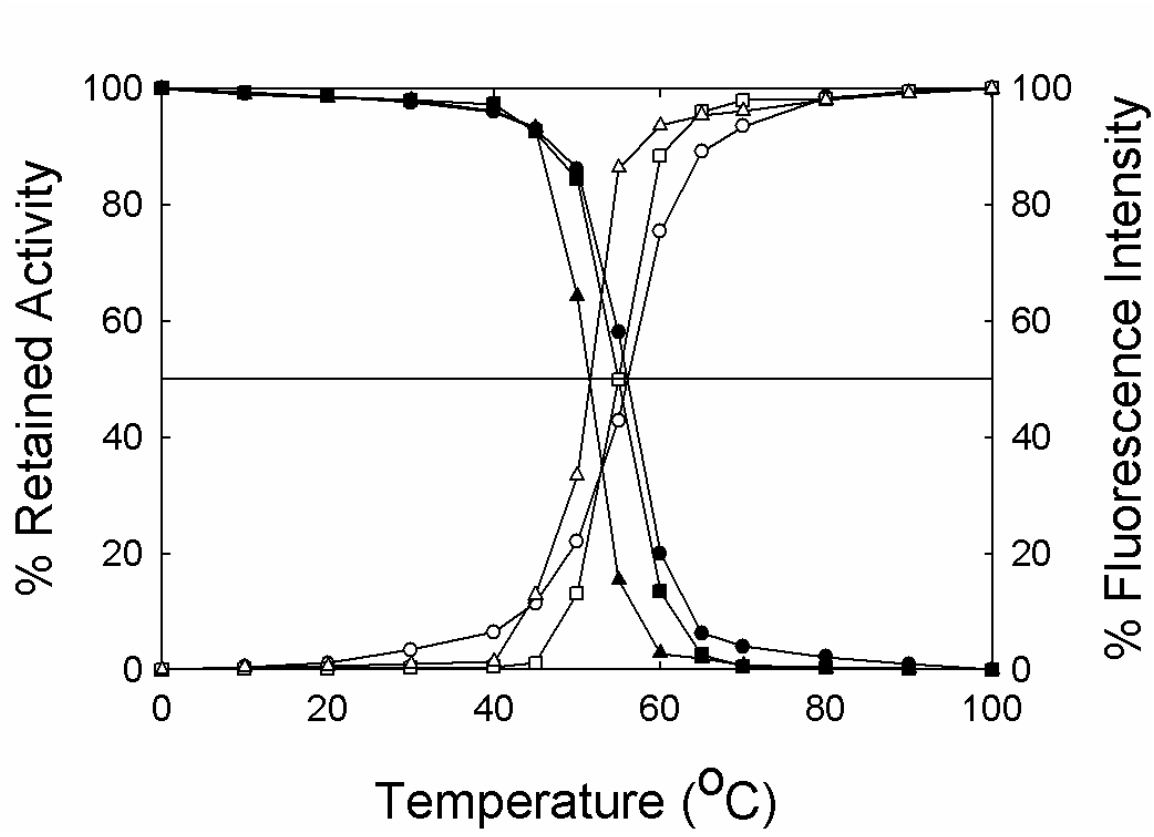

Figure 55. T Thermal Stability Profiles of the Type I RCM Associated Variants A178T and A178V. Oxidized samples of WT H_4cb5r (5 μM FAD) and cb5r RCM variants were incubated at the indicated temperatures, and aliquots were withdrawn and assayed for both residual NADH:FR activity (closed symbols) and intrinsic flavin fluorescence (open symbols) in 10 mM phosphate buffer, containing 0.1 mM EDTA, pH 7.0 using excitation and emission wavelengths of 450 nm and 523 nm, respectively. Points correspond to (●,○) H_4cb5r; (■, □) A178T; and (▲, Δ) A178V

490nm region. Both mutants exhibited an increased K_s value, with A178V being only slightly elevated and A178T being 2 fold higher when compared to WT cb5r (Table 20).

In the case of titration with NAD^+, both mutations maintained a similar line shape to that of WT, however, at rather diminished intensities. The resulting spectral binding constants followed the same pattern seen in the H_4NAD titrations, with A178V having a value equivalent to WT and A1178T having a value 3 times that of WT (Table 20)

Potential effects of structural changes on the properties of the flavin prosthetic group were examined by determining the oxidation-reduction potentials for the FAD cofactor as described in the "Methods" section. Flavin midpoint potentials (E°′, n = 2) for the FAD/$FADH_2$ couple were determined for the variants alone and in the presence of NAD^+. Spectra obtained during a representative titration of the WT cb5r protein are shown in Figure 57. In the absence of NAD^+, each of the mutations exhibited midpoint potentials equivalent to that of WT, with values of -275 and -276mV for the A178T and A178V mutants respectively. In the presence of NAD^+ however, both mutations demonstrated a positive shift in the midpoint potential, but not to the same extent seen in the WT domain in the presence of NAD^+, with values of -212mV and -201 mV for the A178T and A178V mutants respectively. Midpoint values are reported in Table 20.

Summary of Properties of the Type I recessive congenital methemoglobinemia mutants A178T and A178V.

Previous investigations [147-149] identified two unique point mutations in the *DIA*1 gene of individuals of North African and Turkish decent (A178T) and from Thai decent (A178V) displaying disease phenotype for Type I RCM. The two mutations resulted from single point mutations in the *DIA1* gene coding for cb5r protein, and were found to be unique to the patients, and not polymorphisms in the respective populations.

Analysis of the structure of the mutants through the use of UV/Visible absorbance and circular dichroism spectroscopy indicated that the mutants did not differ significantly in overall secondary structure from the WT protein, and incorporated the FAD co-factor in a similar conformation. Initial-rate kinetic studies indicated that the mutants retained greater than 50% of the rate of turn-over exhibited by the WT enzyme, and did not significantly differ in the binding affinity for the reducing substrate as indicated by similar K_m^{NADH} values. Differential spectroscopy indicated that the A178V mutant bound

Table 20. Spectral Binding Constants (K_S) and Standard Midpoint Obtained for the Type I RCM Associated Mutants A178T and A178V.

cb5r Variant	**K_S (μM)**		**$E^{\circ\prime}_{FAD/FADH_2}$ (mV)**	
	$K_S^{H_4NAD}$	**K_S^{NAD+}**	**$-NAD^+$**	**$+NAD^+$**
WT H_4cb5r	45 ± 10	553 ± 30	-271	-191
A178T	55 ± 5	1530 ± 37	-275	-212
A178V	49 ± 5	545 ± 1	-276	-201

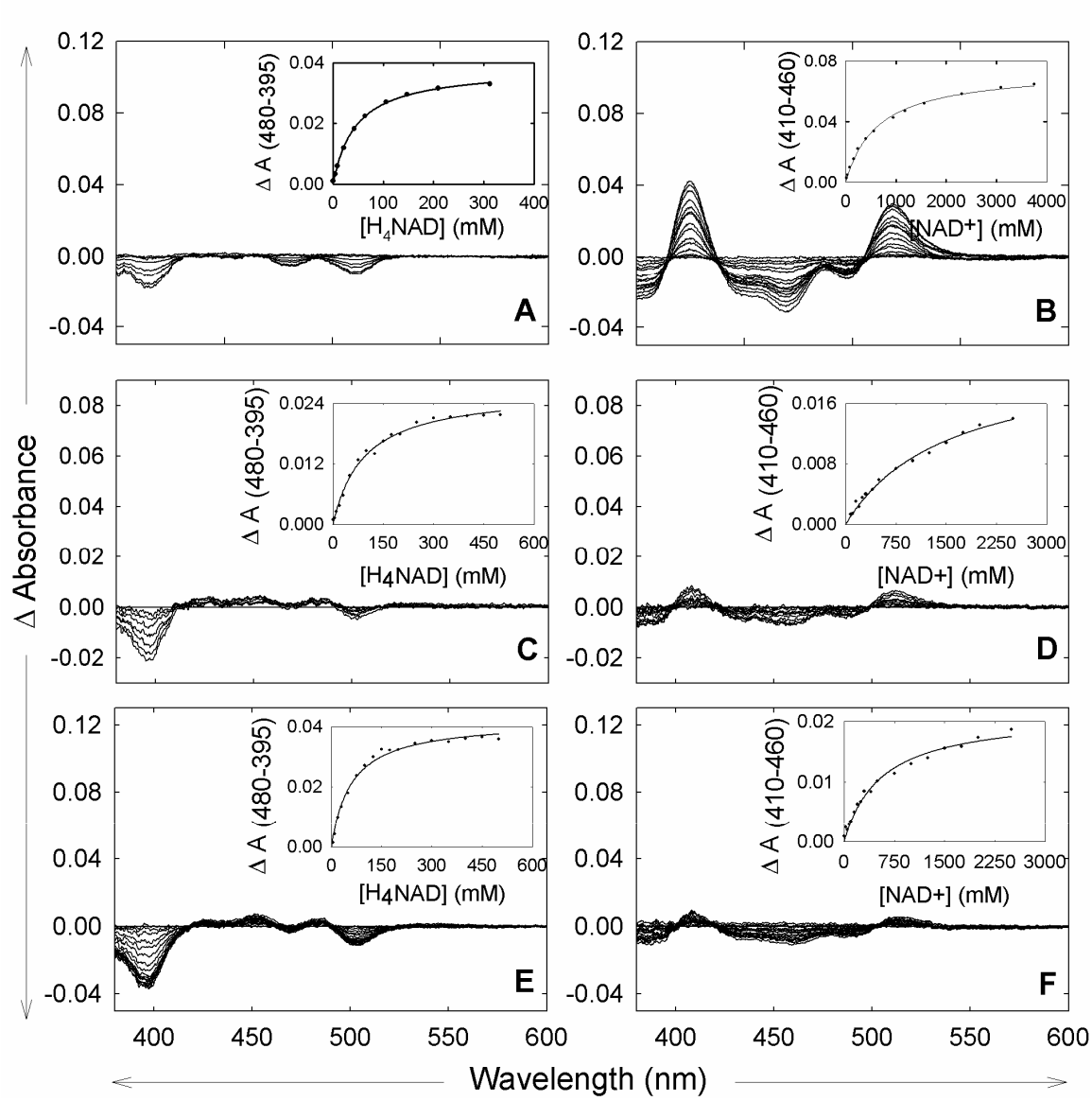

Figure 56. Spectroscopic Titrations Obtained for the WT cb5r and the Type I RCM Associated Variants A178T and A178V in the Presence of H_4NAD and NAD^+. Titrations of all mutants (50μM) were performed in split cell optical cuvettes in 10mM phosphate buffer containing 0.1mM EDTA, pH 7.0 at 23 °C. Difference spectra were recorded following the addition of a solution of H_4NAD (5mM) (A, C, E) or NAD^+ (30mM) (B, D, F). The inset panel corresponds to a plot of the magnitude of the spectral perturbations at the indicated wavelengths versus pyridine nucleotide concentration where a difference spectrum was observed. Plots of the relative absorbance changes observed are as follows: (A, B) WT cb5r; (C, D) A178T; and (E, F) A178V.

H_4NAD in a conformation similar to WT and with equal or affinity. However, the A178T mutant, while binding the analog in a similar conformation, did so with a decreased affinity. In titrations with NAD^+, the results indicated high level of similarity between the A178V mutant and WT enzyme, with the A178T mutant again showing a decreased affinity for the product. Midpoint potential determinations further highlighted the similarity between A178V and WT and the difference between A178T and WT. The potential in the presence of NAD^+ for A178T was closer to that of free flavin than to WT, suggesting inefficiency in the ability to transfer electrons in the mutant. A178V also showed a more negative potential in the presence of NAD^+ as compared to WT, but to a lesser degree, a fact mirrored in its retention of catalytic efficiency similar to that of WT as shown by the NADH:FR assays. From this data, it can be concluded that it is the presence of the polar hydroxyl group on the side chain of A178T that resulted in the decrease in activity. From homology modeling studies, we generated structures of each mutant to compare to WT to illustrate what potential effects would occur, as shown in Figure 58. The introduction of the threonine side chain caused an electrostatic interference with the backbone of I183 (Figure 58B). The introduction of a negative charge in this region would cause an alteration in the helical structure, as evidenced by the increased negative maxima seen in the circular dichroism spectra in the far UV region. While not a major alteration, it is strong enough to cause a displacement in the nearby "GxGxxP" motif preventing the substrate from binding in the appropriate orientation. While differential spectroscopy indicated that A178T bound H_4NAD similarly to WT, the slight alterations seen in the 415-490nm area indicate a minor alteration in the conformation of the complex. Thus, we proposed that the causative

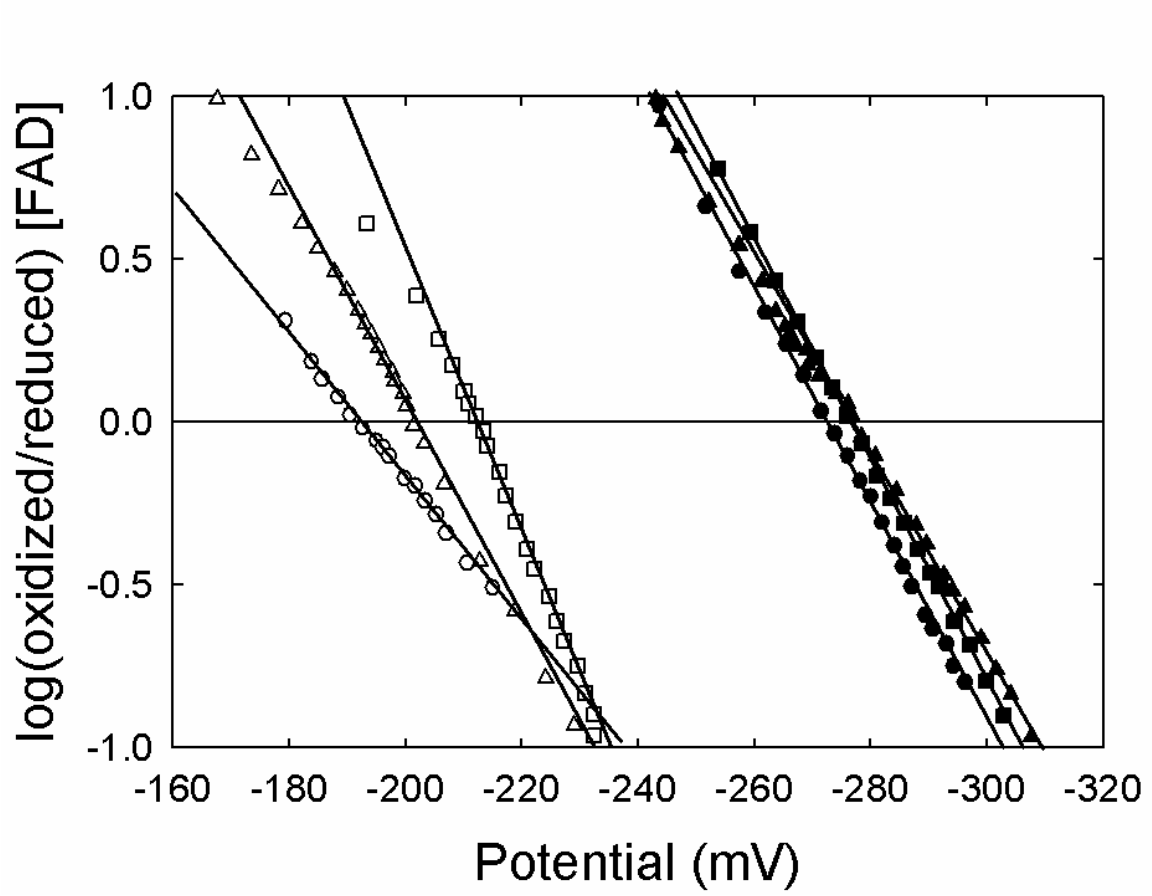

Figure 57. Oxidation-Reduction Midpoint Potentials for the FAD Prosthetic Group in the WT cb5r and the Type I RCM Associated Variants A178T and A178V. Reductive dye titrations were performed at 25 °C as described in "Materials and Methods" using phenosafranine as the indicator dye in 100 mM phosphate buffer containing 0.1 mM EDTA, pH 7.0. Nernst plots in the absence (closed symbols) and presence (open symbols) of 2 mM NAD^+. Plots correspond to (●,○) H_4cb5r; (■, □) A178T; and (▲, Δ) A178V.

agent of RCM in the case of the A178T mutation is a result of a minor displacement of the correct orientation of the NADH binding motif "GxGxxP," leading to inefficient electron transfer from the bound NADH. Since this is a minor alteration, the overall effect results in a type I RCM.

Correlating with previous studies [149], the A178V mutant retained the catalytic properties of the WT protein, with only slightly decreased efficiency. The main

difference observed in the A178V mutant was in its thermal stability. The mutation proved to be less stable than WT as determined by thermal denaturation. Having a T_{50} value 7 °C lower than WT, the mutant protein would not be able to remain efficient in circulating erythrocytes, thus leading to a mild cyanotic phenotype in patients. In other cells of the body, degraded protein would be able to be cleared and newly translated protein, with efficiency similar to that of the WT, would be able to compensate. Thus, as concluded by Higasa et. al. [149], the A178V results in type I RCM simply due to destabilization effects. However, homology modeling did not yield any indication as to where this destabilizing effect would occur. The most likely cause is again an affect on I183. As shown in Figure 58C, the presence of the branched side chain of valine could sterically hinder the neighboring I183 residue, alterations of which have been demonstrated to lead to decreased thermal stability. To more accurately determine the cause of the destabilization, a crystal structure of the mutant enzyme would facilitate comparison of the A178V and WT structures.

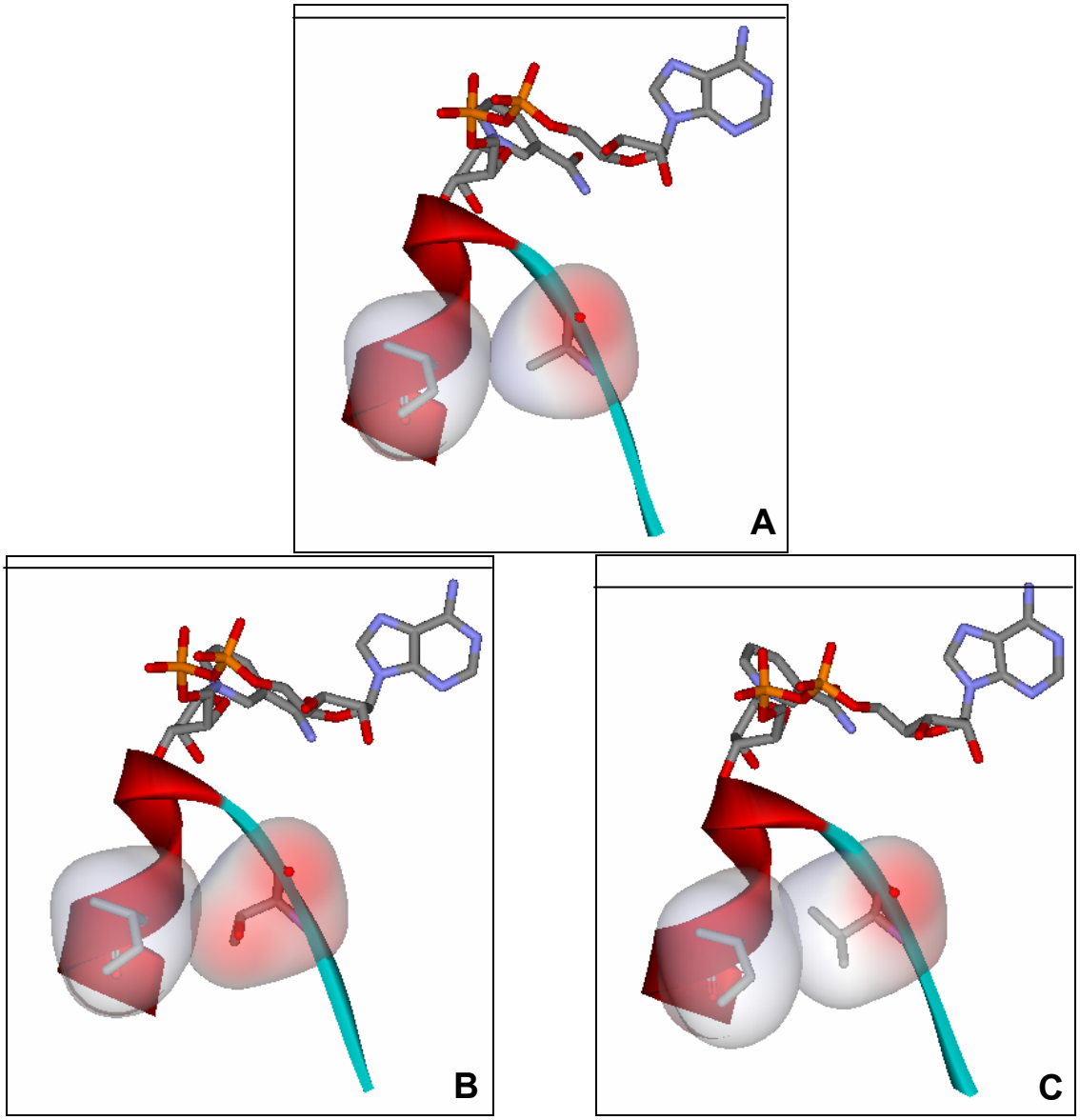

Figure 58. Structures of WT cb5r Residue A178 and RCM Variants A178T and A178V Generated *in silica*. The molecular model of cb5r displaying (A) residue A178 (B) Variant A178T and (C) Variant A178V in association with NAD^+ generated utilizing the automated comparative protein modeling server SWISS-MODEL [111] and analyzed using the molecular modeling software Web Lab Viewer Pro [134]. The model indicates electrostatic surfaces of the residues in relation to residue I183. Residues and NAD^+ depicted in stick formation with CPK coloring. Models generated from cb5r in complex with FAD and NAD^+ (1IB0).

The role of the NADH binding motif ^{273}CGxxxM^{278}

Within the cb5r primary structure, several sequence motifs have been identified that are involved in either flavin binding ("^{91}RxY$^{T}_{S}$xx$^{S}_{N}$^{97}") or FAD/FMN specificity ("$^{124G}_{R}$XX$^{S}_{T}$^{127}") or function in modulating reduced pyridine nucleotide binding ("^{180}GxGxxP^{185}" and "^{273}CGxxxM^{278}"). The second of these conserved motifs that are involved in regulating pyridine nucleotide affinity, corresponds to a six amino acid "^{273}CGpppM^{278}" residue motif that comprises the residues C273 to M278 in the carboxyl-terminal lobe of rat cb5r (Figure 59).

Analysis of the structure of the diaphorase domain complexed with NAD^+ (PDB ID=1IB0) has revealed that the majority of the residues comprising the conserved "CGxxxM" motif do not provide any direct electrostatic or hydrogen bond contacts with either the nicotinamide or ribose moieties of the bound NAD^+, with the notable exception of G274. However, the residues do form a loop connecting Nβ4 with the final α helical 'return' in the NADH binding domain. This loop is generated by three sequential proline residues which effectively induce a kink into the backbone of the protein, causing an immediate redirection and initiating the following helical structure (Figure 59B). Additionally, the residues in this motif provide an extensive framework of hydrophobic contacts that are involved in binding the reducing substrate, NADH, specifically orienting the nicotinamide portion of the reduced pyridine nucleotide for subsequent efficient hydride transfer to the FAD prosthetic group (Figure 59A). Within the "CGxxxM" motif, the conserved glycine, corresponding to G274, forms two critical hydrogen bonds with bound NAD^+, its backbone oxygen binding with the N7 nitrogen of the nicotinamide moiety. Also, C273 has been suggested to be important in maintaining equilibrium

Figure 59. Electrostatic Interaction of the "CGpppM" Motif with NAD^+. (A) Ligplot [99] of 1IB0. C, O, N, and P atoms are represented as white, blue, red, and violet spheres, respectively, while covalent bonds are violet sticks within NAD^+ and orange sticks within amino acid residues of the NADH-binding lobe. Hydrogen bonds are drawn as green dashed lines with distances between atoms labeled. Residues contributing to hydrophobic interactions are represented as arcs with rays and colored red. Residues of the motif are circled in red. (B) Schematic diagram of a portion of the *R. norvegicus* cb5r X-ray crystal structure (PDB code IIB0) showing the arrangements of the amino acids that comprise the conserved "CGPxxxM" motif . Amino acids and the complexed NAD^+ are shown in "stick" representation using the CPK color scheme. Hydrogen bonds are drawn as dashed green lines. Secondary structure of the protein is shown using line ribbon scheme, colored according to secondary structure with helices colored red, sheets colored blue, and turns colored white.

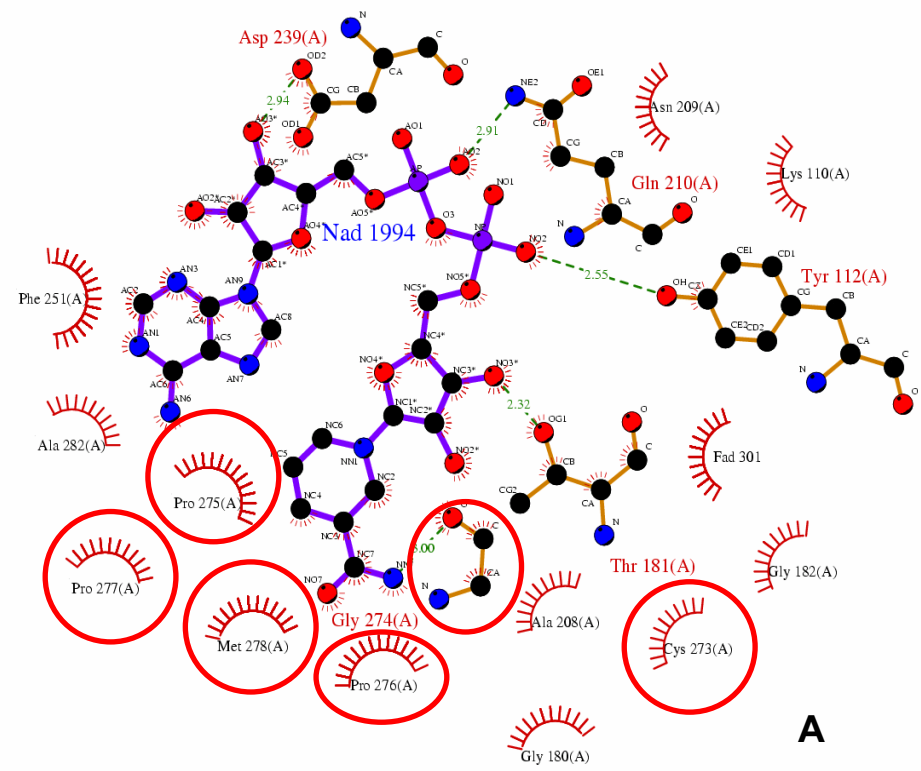
Asp 239(A)
Asn 209(A)
Gln 210(A)
Lys 110(A)
Nad 1994
Tyr 112(A)
Phe 251(A
Ala 282(A)
Pro 275(A)
Fad 301
Pro 277(A)
Thr 181(A)
Gly 182(A)
Met 278(A)
Gly 274(A)
Ala 208(A)
Cys 273(A)
Pro 276(A)
Gly 180(A)
A

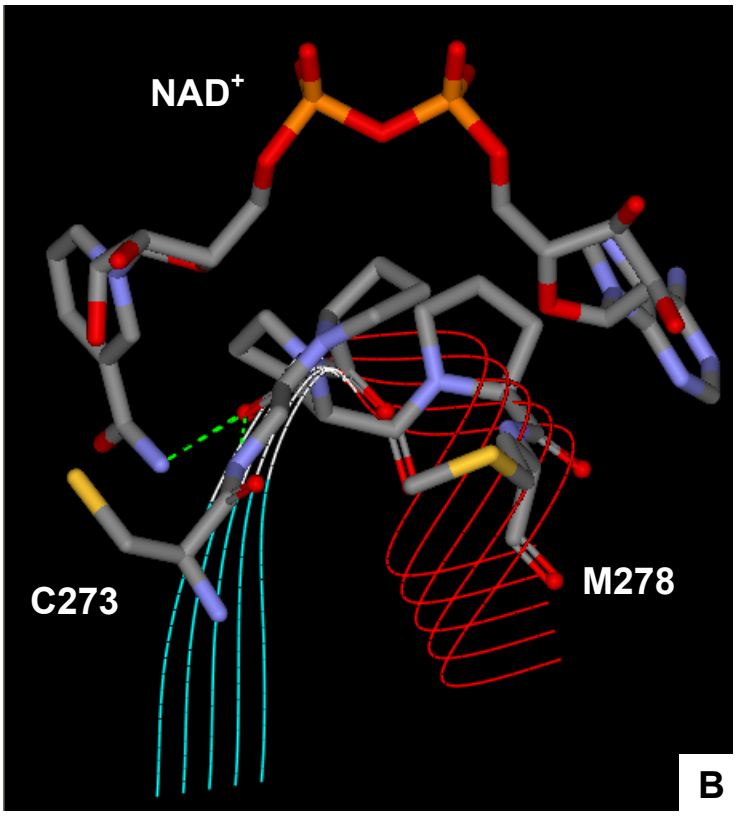
NAD+
C273
M278
B

between the unstacked configuration of bound NADH and the charge transfer complex [104].

To probe the role of this conserved motif in cb5r structure and function and to examine the effects of substituting these residues on the enzyme's function, we have applied site-directed mutagenesis of the H_4cb5r construct using the corresponding oligonucleotide primers listed in Appendix C as described in "Methods" as a tool to replace or alter the properties of each residue. This was done in two stages. First, the individual residues were each replaced with alanine (alanine-scanning mutagenesis). The resulting mutants were examined on the basis of the effects of these substitutions on the spectroscopic properties of the FAD prosthetic group and the interactions of cb5r with the physiological substrate, NADH. Based on the results of the alanine-scanning, additional mutants were constructed and again analyzed using the same parameters to give further insight into the function of the individual residues as well as the motif in its entirety. These additional variants consisted of the four substitution mutations C273M, C273S, G274P, and G274S and two insertion mutations in which an alanine or glycine was inserted between residues P277 and M278. These single residue insertion mutants were generated as a result of other members of the FNR superfamily, such as cytochrome P450 reductase and methionine synthase reductase, exhibiting a motif with the structural "CGxxx**x**M" configuration.

Characterization of Alanine Substitution Mutants of the ^{273}CGpppM^{278}motif

Mutant constructs encoding the C273A, G274A, P275A, P276A, P277A, and M278A, cb5r variants, corresponding to the residues in the conserved "CGPPPM" sequence motif, were generated using site-directed mutagenesis of the original four-histidine tagged cb5r construct. Dideoxy sequencing confirmed the fidelity of the constructs. The mutant proteins were subsequently expressed in the *E. coli* strain BL21(DE3)-RIL and purified by metal–chelate affinity chromatography and gel filtration FPLC. Evaluation of the expression yield of the variants indicated an expression efficiency comparable to that of the WT cb5r domain, indicating production of stable protein products which could be purified to apparent homogeneity as indicated by the presence of single protein bands following SDS–PAGE analysis (results not shown).

UV/visible absorbance spectra were obtained for both the oxidized samples of the alanine variants and WT cb5r as a control and are presented in Fig 60A. All of the variants exhibited spectra comparable to that of the WT enzyme with aromatic absorption maximum observed at 273 nm in the UV region of the spectrum, and peaks at 461 nm with an associated pronounced shoulder in the range of 485–500 nm in the visible region of the spectrum, attributable to protein-bound flavin.

To compare the secondary structural characteristics of the alanine variants with that of the WT protein, circular dichroism (CD) spectra were recorded in the UV wavelength range (190–300 nm). As shown in Fig. 60B, the alanine variants exhibited positive CD from 190 to 210 nm and negative CD from 210 to 250 nm with the spectra retaining both positive and negative intensities very similar to those of the WT domain. The absence of any significant differences between the spectra of the WT and mutant

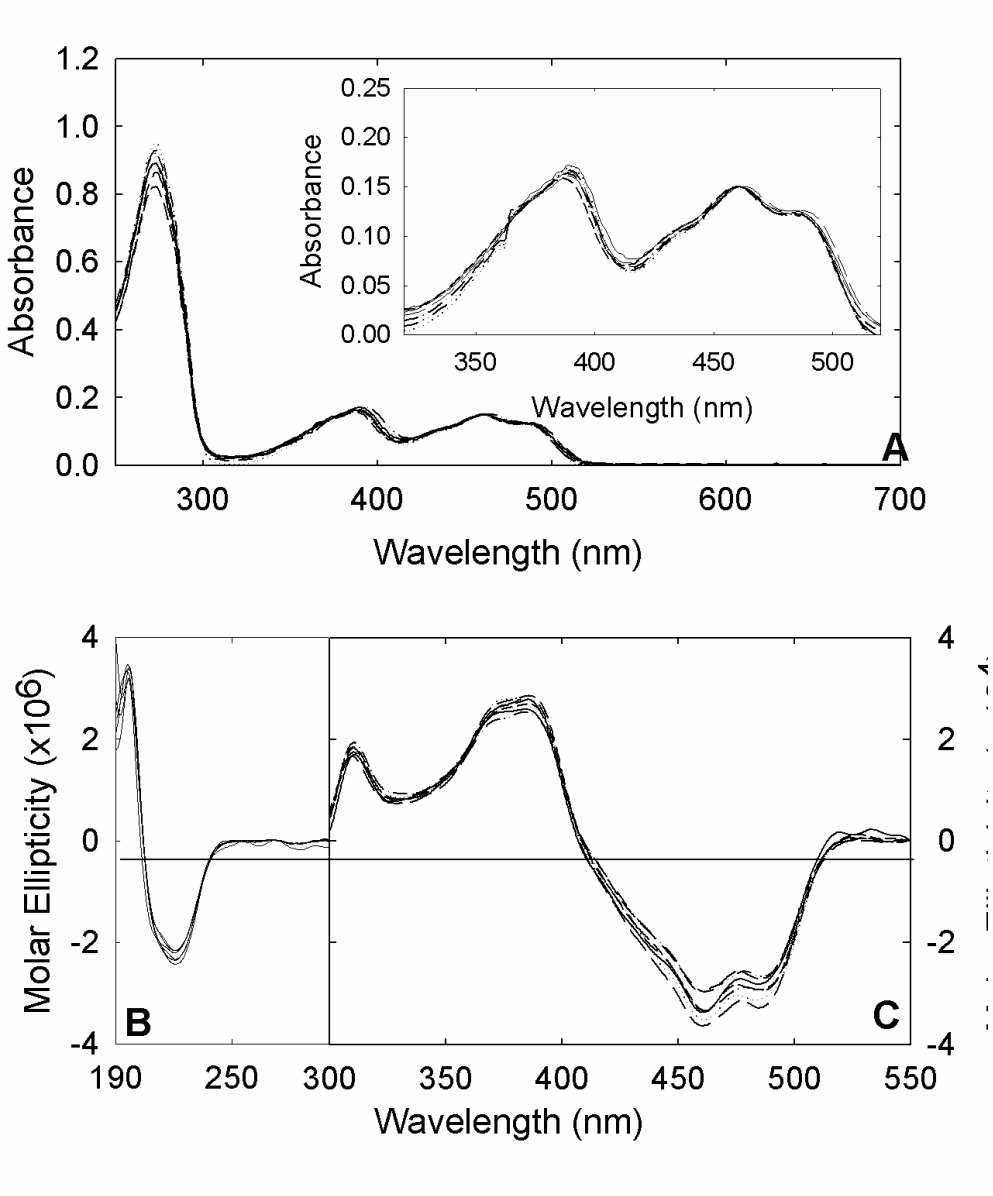

Figure 60. UV/Visible Absorption and CD Spectra of WT cb5r and the Alanine Mutants of the CGpppM Motif. (A) UV/vis absorption spectra were obtained for oxidized samples of cb5r and the various mutants at equivalent flavin concentrations (1.7 μM FAD) in 10 mM phosphate buffer, containing 0.1 mM EDTA at pH 7.0. The inset shows an expanded region of the visible spectrum where the flavin prosthetic group makes a major contribution. Individual spectra correspond to WT cb5r (—), C273A (— — —), G274A (– – – –), P275A (------), P276A (·····), P277A (– · – · –), M278A (-·-·-·-.) (B) UV CD spectra were recorded using enzyme samples (7 μM FAD) in 10 mM phosphate buffer, containing 0.1 mM EDTA at pH 7.0. (C) Visible CD spectra were recorded using enzyme samples (50 μM FAD) in 10 mM phosphate buffer, containing 0.1 mM EDTA at pH 7.0. Line styles shown in B and C are the same as those depicted in A.

proteins suggested the conservation of secondary structure and that the alanine residue substitutions had no deleterious effects on the folding of the diaphorase domain. Similar results were observed for the corresponding visible CD spectra. Circular dichroism measurements were performed in the near-UV/visible range (300–600 nm) in order to probe possible effects of the mutations on both flavin conformation and polarity of the prosthetic group microenvironment. As shown in Fig. 60C, the spectra of the mutants were unperturbed when compared to that of WT cb5r, exhibiting positive maxima at 310 and 390 nm and negative maxima at approximately 460 and 485 nm,. suggesting no significant change in either the polarity of the flavin environment or the conformation of the bound prosthetic group.

To examine the influence of the residue substitutions on the stability of the resulting proteins, thermal denaturation profiles were generated for the alanine variants and WT cb5r by measuring changes in both intrinsic flavin fluorescence emission (Figure 61A) and retention of NADH:ferricyanide reductase activity (Figure 61B) following incubation of the proteins at temperatures ranging from 0 to 100 °C. The temperature (T_{50}) at which 50% of maximum fluorescence was detected or 50% of the protein's NADH:FR activity was retained, were effective indicators of the stability of the core structure of the protein. Each of the variants displayed a reduced thermal stability related to that of the WT (Table 21) with G274A maintaining a T_{50} value of 53 °C, comparable to that of WT cb5r, followed by the variants C273A, P276A, and P277A variants which were approximately 4 °C lower than that of WT cb5r suggesting that these residue substitutions had a moderate effect on the thermal stability. The most severally affected variants of the NADH-binding motif were P275A and M278A, with T_{50} values

of 49 °C and 46 °C, respectively. These more significant decreases suggest that the alanine substitutions at amino acid residues P275 and M278 severely affected the overall stability of the protein.

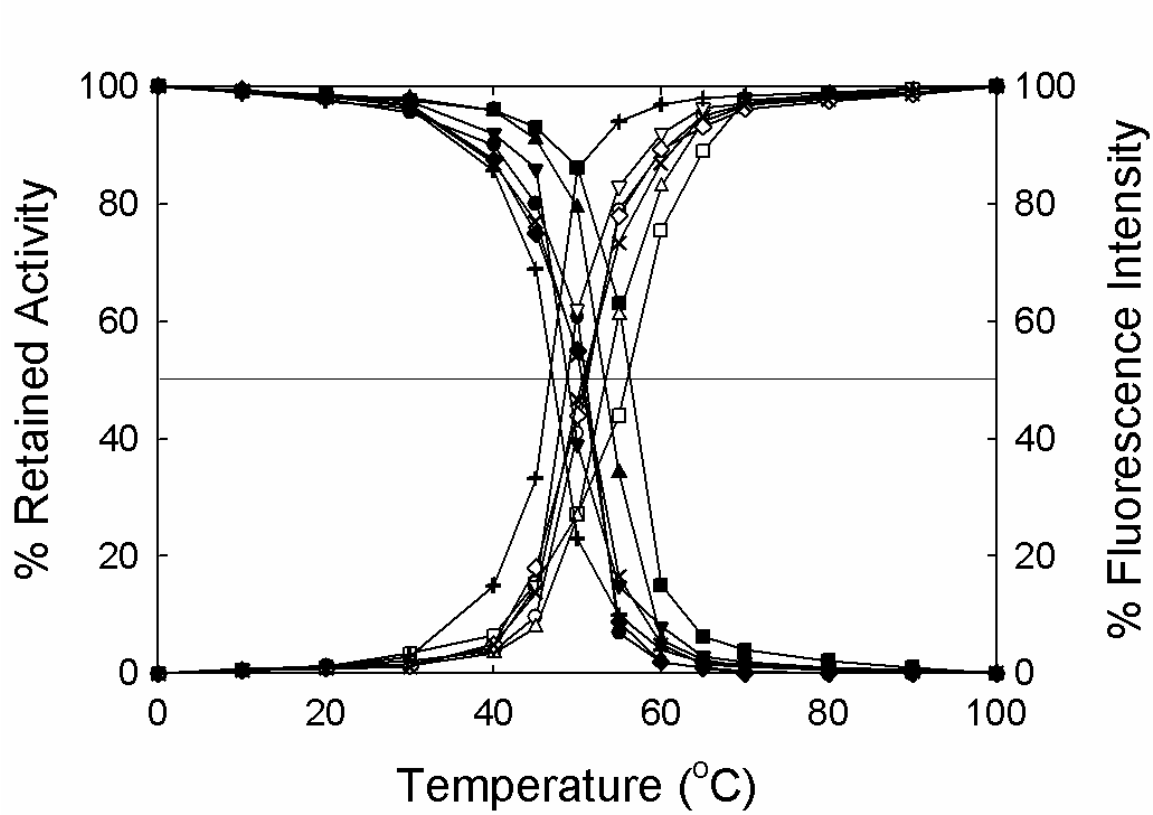

Figure 61. Thermal Stability Profiles Obtained for the WT cb5r and the Alanine Variants of the "CGpppM" Motif. Oxidized samples of C273A, G274A, P275A, P276A, P277A, M278A, and WT H_4cb5r (5μM FAD) were incubated at the indicated temperatures, and aliquots were withdrawn and assayed for both residual NADH:FR activity and intrinsic flavin fluorescence in 10 mM phosphate buffer, containing 0.1 mM EDTA, pH 7.0 using excitation and emission wavelengths of 450 nm and 523 nm, respectively. Points correspond to: (●) H_4cb5r; (■) C273A; (▲) G274A; (▼) P275A; (♦) P276A; (x) P277A; (+) M278A.

As a measure of catalytic efficiency, NADH:FR activities were determined for the WT cb5r and alanine variants. Kinetic constants derived from these assays are reported in

Table 21. All variants exhibited a decreased NADH:FR turn-over rate when compared to that of WT cb5r, with C273A and G274A being the most severely affected. The substitution of an alanine for a cysteine at residue 273 had the most deleterious affect on the enzymes catalytic activity, showing a 38-fold decrease as compared to WT enzyme. P275A resulted in the most moderate affects on catalytic activity, having maintianed a k_{cat} comparable to that of WT, indicating turnover was not significantly inhibited in the variant.

Table 21. NADH:FR Kinetic Constants and Thermal Stability (T_{50}) Values Obtained for the Alanine Variants of the "CGpppM" Motif.

cb5r Variant	NADH:FR				T_{50}
	k_{cat} (s^{-1})	K_m^{NADH} (μM)	K_m^{FeCN6} (μM)	k_{cat}/K_m^{NADH} (s^{-1} M^{-1})	(°C)
WT H_4cb5r	800 ± 17	6.0 ± 1	8 ± 1	1.4 ± 0.3 x 10^8	56.1
C273A	20 ± 1.0	9.4 ± 0.8	8 ± 1	2.3 ± 0.4 x 10^6	51.0
G274A	88 ± 2.1	65 ± 2.1	8 ± 1	1.4 ± 0.3 x 10^6	53.2
P275A	750 ± 50	22 ± 0.8	8 ± 1	3.5 ± 0.5 x 10^7	49.1
P276A	650 ± 22	14 ± 1.1	8 ± 1	4.8 ± 0.8 x 10^7	50.9
P277A	617 ± 9.4	34 ± 1.1	8 ± 1	1.8 ± 0.1 x 10^7	50.7
M278A	202 ± 10	24 ± 1.0	8 ± 1	8.4 ± 0.8 x 10^6	46.3

Binding efficiency, as determined by examining the Michaelis constants (K_m), demonstrated a decreased affinity for NADH for all variants. G274A demonstrated the most significant impact, having a K_m value 10-fold greater than that of WT protein, indicating a significant decrease in the affinity for the reducing substrate. The additional variants exhibited K_m's as shown in Table 21. The C273A demonstrated a K_m near that of WT cb5r, suggesting substrate affinity was not significantly affected. In contrast, the

Michaelis constant for the artificial electron acceptor, ferricyanide, was similar to that of WT cb5r, suggesting that the mutation did not affect the binding of the oxidizing substrate.

Catalytic efficiency, reflected in the k_{cat}/K_m^{NADH} value, was decreased in all variants as compared to WT cb5r. The effect of the G274A substitution was most notable, the variant retaining only 0.3% of WT cb5r NADH:FR catalytic efficiency. These results suggested that the lower catalytic efficiency observed for the mutants was the result of both the decreased affinity for, and decreased utilization of NADH.

To confirm the effects of the alanine substitutions on the affinities for either NADH or NAD^+, spectral binding constants (K_s) were determined using differential spectroscopy. Representative spectra obtained from the titrations of the alanine variants and the WT enzyme with either H_4NAD or NAD^+ are shown in Figures 62 and 63 respectively. With the exception of G274A, all the variants demonstrated some degree of spectral change following the addition of H_4NAD (Figure. 63). C273A exhibited a spectrum similar to the titration with NAD^+. P275A, P276A, P277A, and M278 all demonstrated line shape similar to that of WT, with diminished intensities. G274A had insufficient changes for analysis. The binding constants for H_4NAD suggested that C273A and P277A bound the substrate more efficiently than WT, with K_s values of 40 μM and 35 μM H_4NAD respectively.

Titrations of the C273A, P276A, and P277A variants with NAD^+ generated line-shape similar to WT cb5r, but with decreased positive and negative intensities. P275A exhibited spectral changes of greatly diminished intensity. Variants G274A and M278 exhibited insufficient spectral change to determine the spectroscopic binding constants

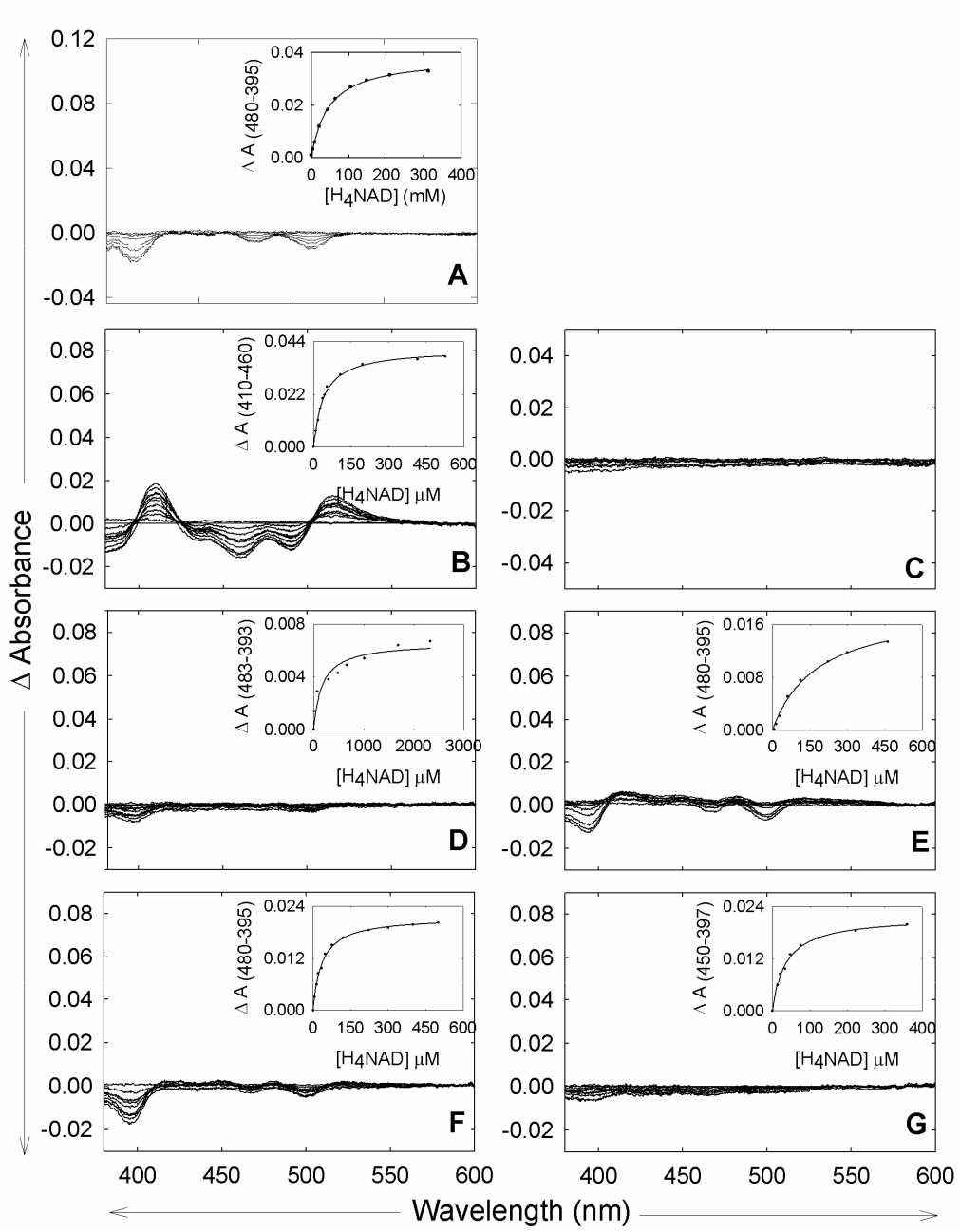

Figure 62. Spectroscopic Titrations Obtained for the WT cb5r and the Alanine Variants of the "CGpppM" Motif in the presence of H_4NAD. Difference spectra were obtained for the C273A, G274A, P275A, P276A, P277A, and M278A cb5r mutants at equivalent flavin concentrations of (50 μM FAD) in 20 mM MOPS buffer, containing 0.1 mM EDTA, pH 7.0 following titrations with H_4NAD as described in "Methods". The insert panels correspond to plots of the magnitudes of the observed spectral perturbations (peak to trough measurements at the indicated wavelengths) versus ligand concentration. The corresponding *K*s values are given in Table 22.

for NAD^+. The binding constants (Table 22) for NAD^+ suggest all variants that exhibited spectral changes bind product better than WT, with the exception of P275A which had a K_s of 1,048 μM.

Table 22. Spectral Binding Constants (K_s) and Standard Midpoint Potentials (E°′) Obtained for Alanine Variants of the "CGpppM" Motif.

cb5r Variant	K_s (μM)		$E°'_{FAD/FADH_2}$ (mV)	
	$K_s^{H_4NAD}$	K_s^{NAD+}	$-NAD^+$	$+NAD^+$
WT H_4cb5r	45 ± 10	553 ± 30	-271	-191
C273A	40 ± 3	131 ± 9	-268	-225
G274A	ND*	ND*	-271	-221
P275A	165 ± 36	1048 ± 441	-268	-193
P276A	152 ± 14	247 ± 25	-271	-200
P277A	35 ± 3	213 ± 11	-277	-201
M278A	65 ± 2	314 ± 21	-273	-223

*ND indicates that the spectroscopic binding constant could not be determined, due to insufficient spectral change.

Potential effects of structural changes on the properties of the flavin prosthetic group were examined by determining the oxidation-reduction potentials for the FAD cofactor as described in the "Methods" section. Flavin midpoint potentials (E°′, n = 2) for the $FAD/FADH_2$ couple were determined for the variants alone and in the presence of NAD^+. The flavin redox potentials (n = 2) for the WT cb5r and the variants for the $FAD/FADH_2$ couple were determined from the Nernst semi-log plots of the log $([oxidized]/[reduced])_{FAD}$ versus potential (mV) and are shown in Figure 64. Without the addition of NAD^+ to the titration, all variants demonstrated midpoint potentials equivalent to that of WT, with values of ranging form -277 and -268 mV. In the presence of NAD^+ however, the C273A, G274A and M278A mutations demonstrated only a slight

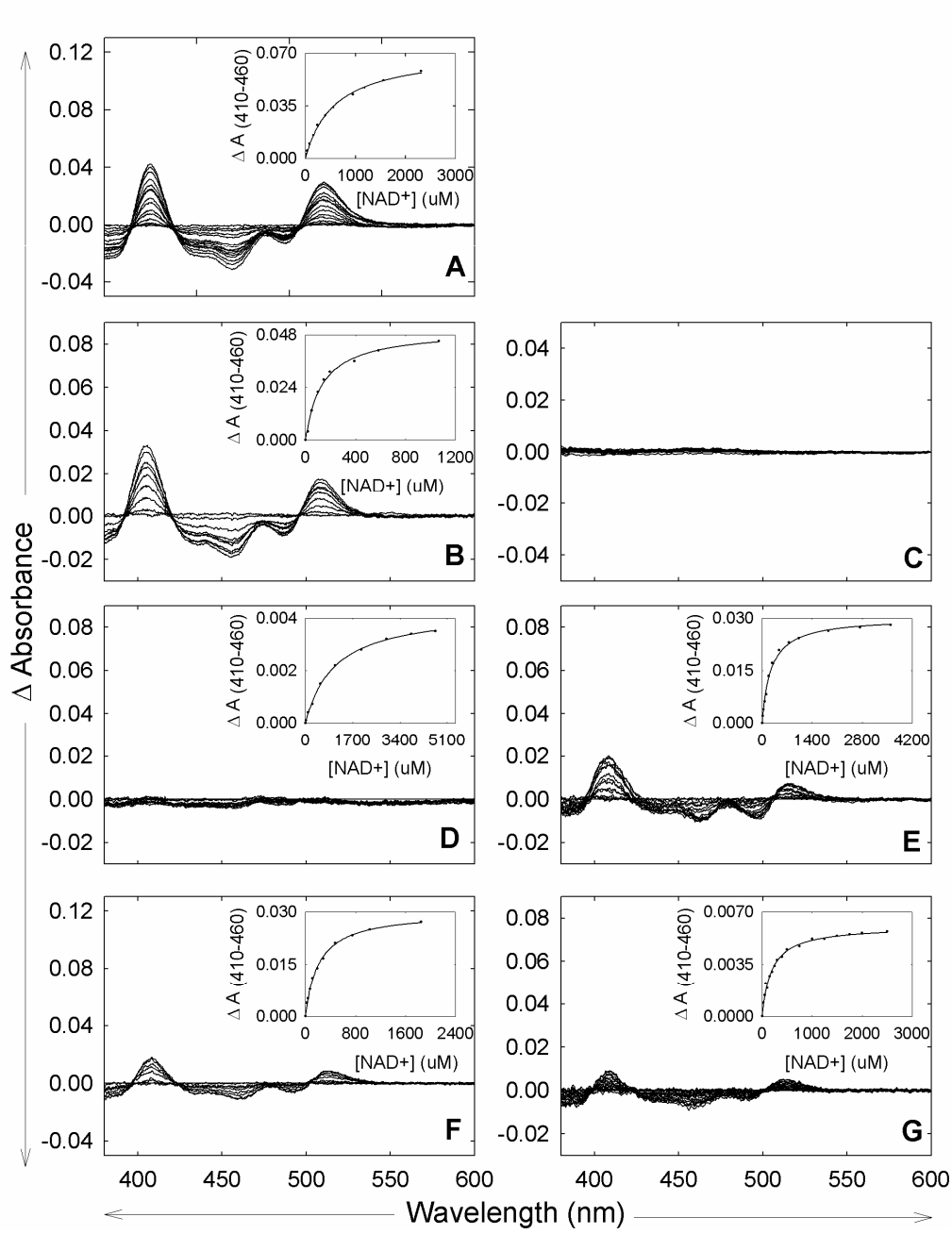

Figure 63. Spectroscopic Titrations Obtained for the WT cb5r and the Alanine Variants of the "CGpppM" Motif in the presence of NAD^+. Difference spectra were obtained for the C273A, G274A, P275A, P276A, P277A, and M278A cb5r mutants at equivalent flavin concentrations of (50 μM FAD) in 20 mM MOPS buffer, containing 0.1 mM EDTA, pH 7.0 following titrations with NAD^+ as described in "Methods". The insert panels correspond to plots of the magnitudes of the observed spectral perturbations (peak to trough measurements at the indicated wavelengths) versus ligand concentration. The corresponding K_s values are given in Table 22.

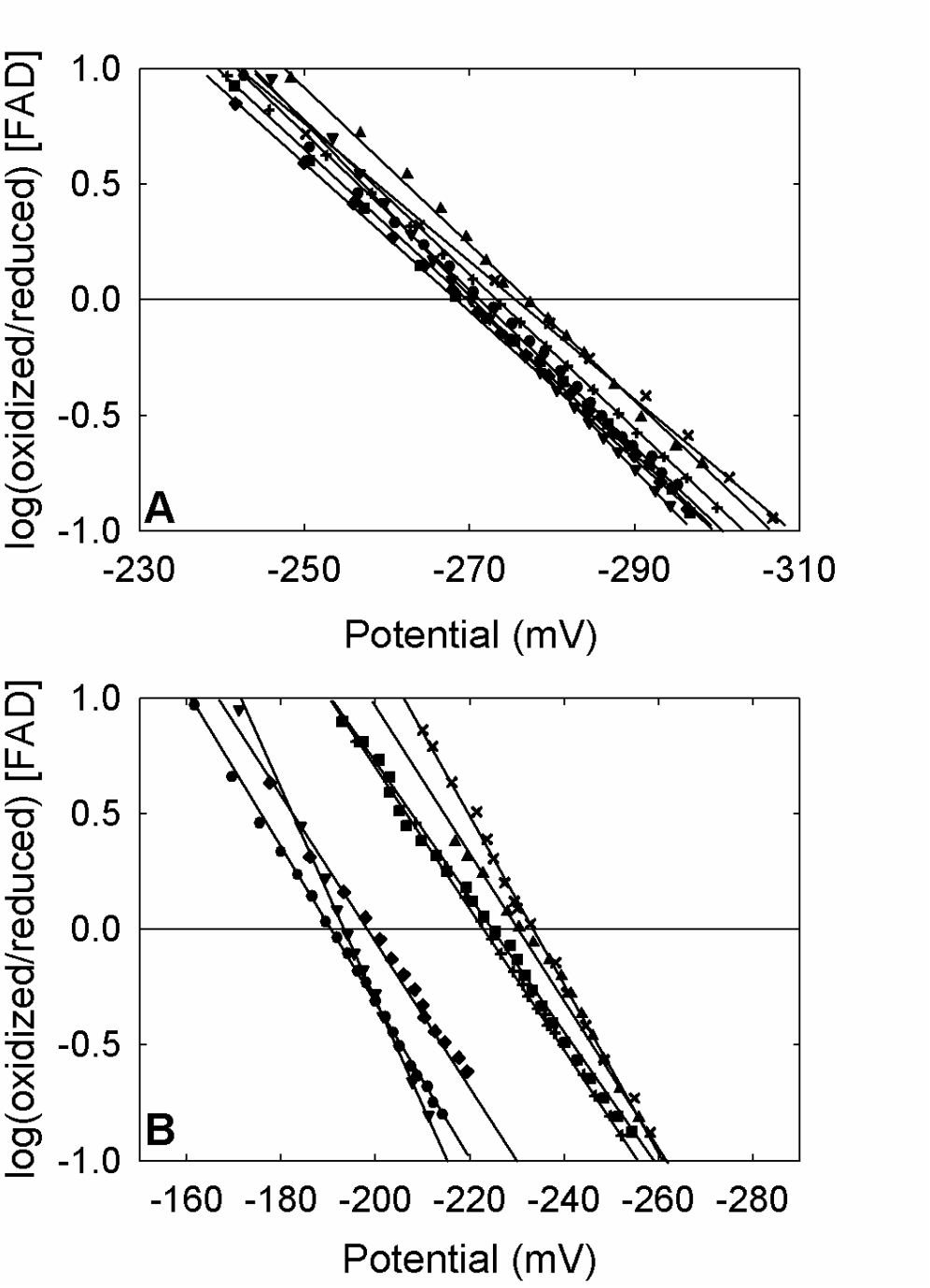

Figure 64. Oxidation-Reduction Midpoint Potentials for the FAD Prosthetic Group in the WT cb5r and the "CGpppM" Alanine Variants. Reductive dye titrations were performed at 25 °C as described in "Materials and Methods" using phenosafranine as the indicator dye in 100 mM phosphate buffer containing 0.1 mM EDTA, pH 7.0. Nernst plots in the absence (A) and presence (B) of 2 mM NAD^+. Plots correspond to (●) H_4cb5r; (■) C273A; (▲) G274A; (▼) P275A; (♦) P276A; (**x**) P277A; and (+) M278A.

degree of positive shift in the midpoint potential, resulting in midpoint potentials near that of free flavin. The three proline substitutions did result in a positive shift, having midpoint potentials within 10 mV of that for WT in the presence of NAD^+. Midpoint values are reported in Table 22.

Characterization of the C273M/S, G274P/S A-insertion, and G-insertion variants.

Mutant constructs encoding the C273S, C273M, G274P, G274S, P277–alanine insertion (A-insertion), and P277–glycine insertion (G-insertion) cb5r variants, were generated using site-directed mutagenesis using the oligonucleotide primers listed in Appendix C. Evaluation of the expression yield of the variants indicated an expression efficiency comparable to that of the WT cb5r domain for most of the variants indicating production of a stable protein product which could be purified to apparent homogeneity as indicated by the presence of a single protein band following SDS–PAGE analysis (results not shown). Variants C273M and C273S displayed lower expression efficiency, but were still purified to apparent homogeneity as indicated by a single band following SDS-PAGE.

UV/visible absorbance spectra were obtained for both the oxidized variants and WT cb5r as a control and are presented in Figure 65A. All of the variants exhibited spectra comparable to that of the WT enzyme with an aromatic absorption maximum observed at 273 nm in the UV region of the spectrum, and a peak at 461 nm with an associated pronounced shoulder in the range of 485–500 nm in the visible region of the spectrum, attributable to protein-bound flavin.

To compare the secondary structural arrangement of the variants with that of the WT protein, circular dichroism (CD) spectra were recorded in the UV wavelength range (190–300 nm). As shown in Figure 65B, the variants exhibited positive CD from 190 to 210 nm and negative CD from 210 to 250 nm with the spectra retaining a line shape very similar to that of the WT domain. The intensities of the negative CD maxima at 222 nm were increased in the case of the C273S and A insertion variants, indicating potential

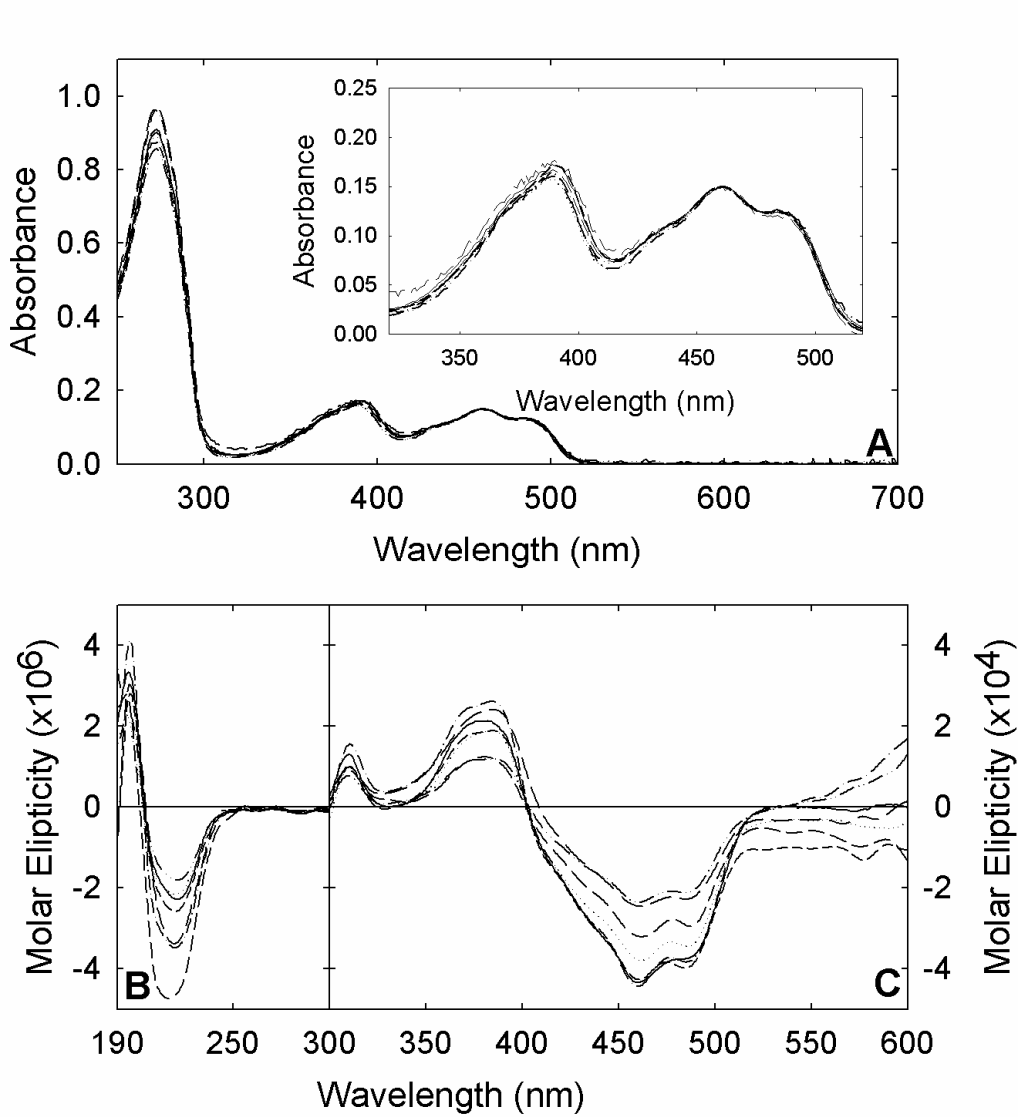

Figure 65. Ultra-Violet, Visible, and Circular Dichroism Spectra Obtained for the WT cb5r and the cb5r Variants C273S, C273M, G274P, G274S, A insertion, and G insertion. (A) UV/Visible absorption spectra were obtained for oxidized samples of cb5r and the various mutants at equivalent flavin concentrations (1.7 μM FAD) in 10 mM phosphate buffer, containing 0.1 mM EDTA at pH 7.0. The inset shows an expanded region of the visible spectrum where the flavin prosthetic group makes a major contribution. Individual spectra correspond to WT cb5r (—), C273S (— — —), C273M (– – – –), G274P (------), G274S (·····), A insertion (– · – · –), G insertion (-·-·-·-.) (B) UV CD spectra were recorded using enzyme samples (7 μM FAD) in 10 mM phosphate buffer, containing 0.1 mM EDTA at pH 7.0. (C) Visible CD spectra were recorded using enzyme samples (50 μM FAD) in 10 mM phosphate buffer, containing 0.1 mM EDTA at pH 7.0. Line styles shown in B and C are the same as those depicted in A.

minor alterations of secondary structure. The absence of any significant differences between the line shape of the spectra of the WT and the remaining mutant proteins suggested the conservation of secondary structure and that the residue substitutions had no significant deleterious effects on the folding of the diaphorase domain.

Circular dichroism measurements were performed in the near-UV/visible range (300–600 nm) in order to probe possible effects of the mutation on both flavin conformation and polarity of the prosthetic group microenvironment. As shown in Figure 65C, the mutants maintained a line shape similar to that of WT cb5r, exhibiting positive maxima at 310 and 390 nm and negative maxima at approximately 460 and 485 nm. The intensities of these maxima, however, differed from that of the WT domain, indicating potential alterations in either the polarity of the flavin environment or the conformation of the bound prosthetic group.

To examine the influence of the residue substitutions on the stability of the resulting protein, thermal denaturation profiles were generated for both variants and WT cb5r (Figure 66). Each variant displayed a reduced thermal stability relative to that of WT (Table 23). G274S, A insertion, and G insertion maintaining T_{50} values of 54 °C, 53 °C., and 55 °C respectively, comparable to that of WT cb5r, The C273M, G274P, and C273S variants were on average 4 °C lower than that of WT, suggesting that these residue substitutions had a slight effect on the thermal stability. The T_{50} values for each variant are given in Table 23.

As a measure of catalytic efficiency, NADH:FR activities were determined for the WT cb5r and all variants. Kinetic constants derived from these assays are reported in Table 23, and indicated that all the variants exhibited a marked decrease in NADH:FR

turn-over compared to that of WT cb5r, with G274P being the most severely affected, showing a 1200-fold decrease when compared to WT cb5r. The remaining variants exhibited increasing k_{cat} values on the order of: G274P<C273S<A-insertion<G-insertion<G274S<C273M<WT.

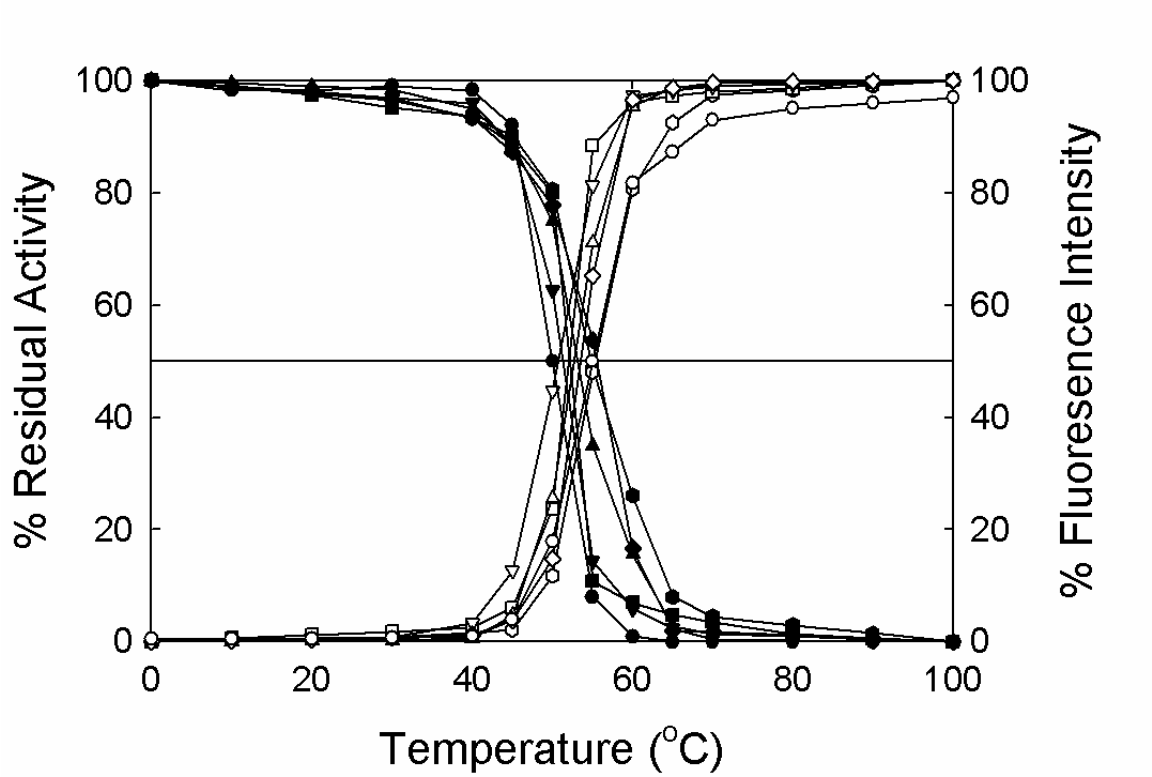

Figure 66. Thermal Stabilty Profiles Obtained for the WT cb5r and cb5r Variants C273S, C273M, G274P, G274S, A-insertion, and G-insertion. Oxidized samples of C273S, C273M, G274P, G274S, A-insertion, G-insertion, and WT H_4cb5r (5μM FAD) were incubated at the indicated temperatures, and aliquots were withdrawn and assayed for both residual NADH:FR activity and intrinsic flavin fluorescence in 10 mM phosphate buffer, containing 0.1 mM EDTA, pH 7.0 using excitation and emission wavelengths of 450 nm and 523 nm, respectively. Points correspond to: (●) H_4cb5r; (■) C273M; (▲) C273S; (▼) G274P; (♦) G274S; (x) A insertion; (+) G insertion.

The K_m value for the G insertion demonstrated the most significant decrease in affinity, having increased 97-fold with respect to WT NADH utilization, from 7 μM to 689 μM. The additional variants exhibited K_m values as shown in Table 23. The C273M

demonstrated a Km near that of WT at 10 um, suggesting substrate affinity was not significantly affected. The Michaelis constant for the artificial electron acceptor, ferricyanide, was similar to that of WT cb5r for all variants, suggesting that the mutation did not affect the binding of the oxidizing substrate.

Table 23. NADH:FR Kinetic Constants and Thermal Stability (T_{50}) Values Obtained for the C273M/S, G274P/S, A-insertion and G-insertion Variants of the "CGpppM" Motif.

cb5r Variant	NADH:FR				T_{50}
	k_{cat} (s^{-1})	K_m^{NADH} (μM)	K_m^{FeCN6} (μM)	k_{cat}/K_m^{NADH} (s^{-1} M^{-1})	(°C)
WT H_4cb5r	800 ± 17	6.0 ± 1	8 ± 1	1.4 ± 0.3 x 10^8	56.1
C273M	213 ± 4.1	10 ± 1	7 ± 1	2.1 ± 0.2 x 10^7	52.0
C273S	10 ± 4.1	17 ± 2	8 ± 1	6.0 ± 0.7 x 10^5	52.2
G274P	0.62 ± 0.1	74 ± 4	8 ± 1	8.5 ± 0.2 x 10^3	51.1
G274S	67± 3.2	76 ± 2	7 ± 1	8.8 ± 0.6 x 10^5	54.1
A-insert	17 ± 1.4	571 ± 22	8 ± 1	2.9 ± 0.4 x 10^4	53.8
G-insert	22 ± 1.1	689 ± 33	7 ± 1	3.2 ± 0.4 x 10^4	55.3

Catalytic efficiency, reflected in the k_{cat}/K_m^{NADH} value, was markedly decreased in all variants as compared to WT cb5r, with the exception of C273M which retained 15% of WT cb5r NADH:FR catalytic efficiency. The effect of the glycine to proline substitution at residue 274 on the overall NADH:FR catalytic efficiency of the enzyme was most significant, retaining only 0.006% of WT cb5r NADH:FR catalytic efficiency. These results suggested that the lower catalytic efficiency observed for the mutants was the result of both the decreased affinity for, and decreased utilization of NADH.

To determine the effects of the mutations on NADH and NAD^+ binding, spectral binding constants (K_s) were determined using differential spectroscopy as discussed

above. Representative spectra obtained from the titrations of the variants and the WT enzyme with either H_4NAD or NAD^+ are shown in Figures 67 and 68 respectively. With the exception of C273M, none of the variants demonstrated spectral changes following the addition of H_4NAD, as shown in Figure 67. C273M demonstrated a line shape similar to that of WT, with diminished intensities. The remaining variants had insufficient changes for analysis. The binding constants for H_4NAD suggest that C273M binds the substrate in a comparable manner to WT, with a K_s values of 70 μM H_4NAD.

Perturbations of the flavin visible absorbance spectrum were only detectable for the WT enzyme, C273M, the A-insertion, and the G-insertion variants in the presence of NAD^+ (Figure 68). For each of these variants, complex formation with NAD^+ resulted in spectra with severely decreased intensity with reference to WT cb5r. The C273S, G274P, and G274S variants exhibited insufficient spectral change to determine spectroscopic binding constants for the various pyridine nucleotides. The binding constants, shown in Table 24, obtained for NAD^+ suggested all variants that exhibited spectral changes bind product better than WT.

Potential effects of structural changes on the properties of the flavin prosthetic group were examined by determining the oxidation-reduction potentials for the FAD cofactor as described in the "Methods" section. Flavin midpoint potentials ($E°'$, n = 2) for the $FAD/FADH_2$ couple were determined for the variants alone and in the presence of NAD^+. The flavin redox potentials (n = 2) for the WT cytochrome b_5 reductase and generated variants for the $FAD/FADH_2$ couple were determined from the Nernst semi-log plots of the log $([oxidized]/[reduced])_{FAD}$ versus potential (mV) and are shown in Figure 69. In the absence of NAD^+, all variants demonstrated midpoint potentials equivalent to

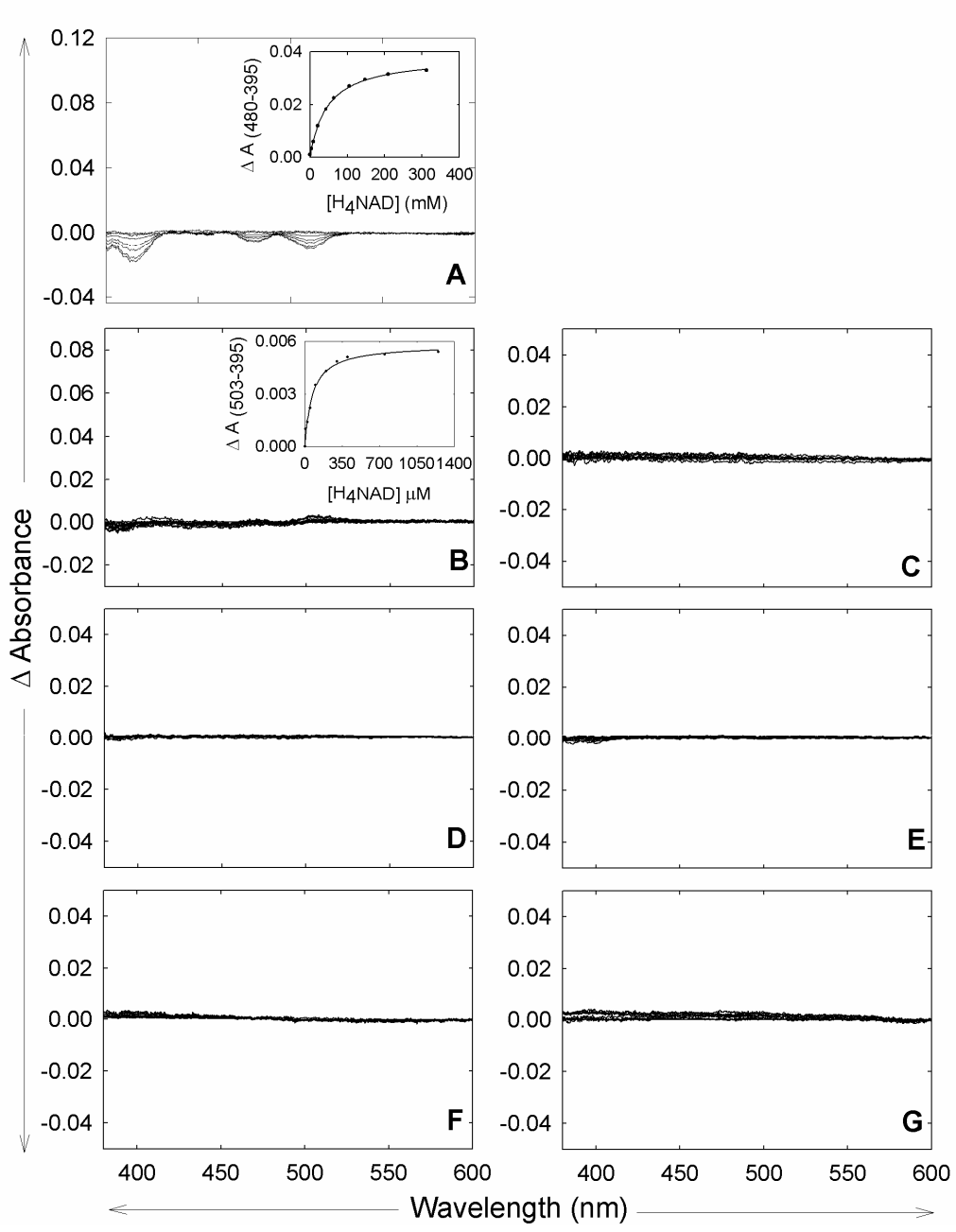

Figure 67. Spectroscopic Titrations Obtained for the WT cb5r and cb5r Variants C273S, C273M, G274P, G274S, A insertion, and G insertion in the Presence of H_4NAD. Difference spectra were obtained for the various C273S, C273M, G274P, G274S, A insertion, and G insertion - cb_5 mutants at equivalent flavin concentrations of (50 μM FAD) in 20 mM MOPS buffer, containing 0.1 m EDTA, pH 7.0 following titrations with H_4NAD as described in "Methods". The insert panels correspond to plots of the magnitudes of the observed spectral perturbations (peak to trough measurements at the indicated wavelengths) versus ligand concentration. The corresponding K_s values are given in Table 24.

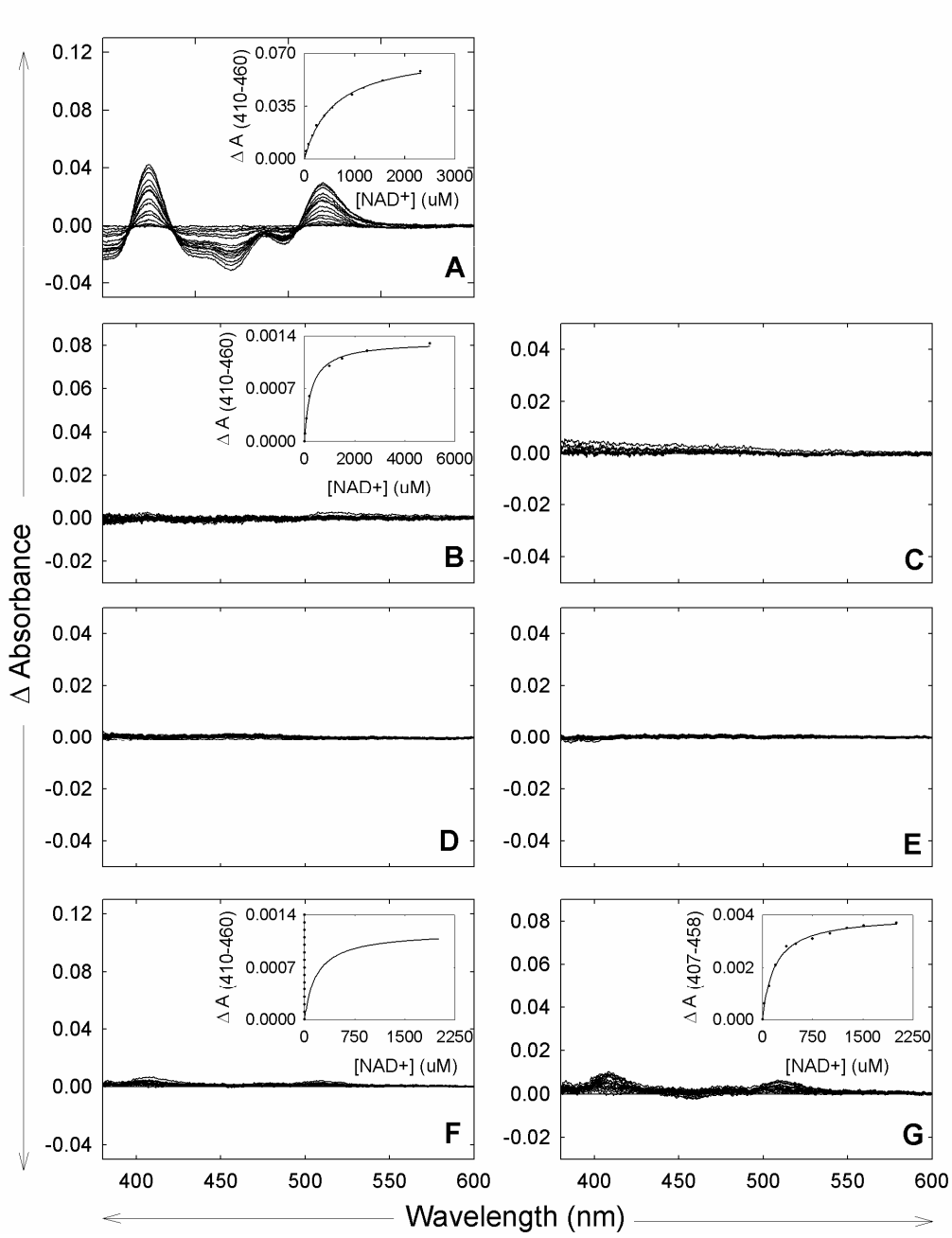

Figure 68. Spectroscopic Titrations Obtained for the WT cb5r and cb5r Variants C273S, C273M, G274P, G274S, A insertion, and G insertion in the Presence of NAD^+. Difference spectra were obtained for the various C273S, C273M, G274P, G274S, A insertion, and G insertion - cb_5 mutants at equivalent flavin concentrations of (50μM FAD) in 20 mM MOPS buffer, containing 0.1 m EDTA, pH 7.0 following titrations with NAD^+ as described in "Methods". The insert panels correspond to plots of the magnitudes of the observed spectral perturbations (peak to trough measurements at the indicated wavelengths) versus ligand concentration. The corresponding K_s values are given in Table 24.

that of WT, with values of ranging from -272 to -265 mV. In the presence of NAD^+ however, all the mutations failed to have a significant positive shift in the midpoint potential, resulting in midpoint potentials near or more negative than that of free flavin. These results clearly indicated that these amino acid substitutions significantly affect the ability of NADH to bind in the proper orientation for efficient electron transfer. The

Table 24. Spectral Binding Constant (K_s) and Standard Midpoint Potentials (E°′) Obtained for the C273M/S, G274P/S, A-insertion and G-insertion Variants of the CGpppM Motif.

cb5r Variant	K_s (μM)		$E°'_{FAD/FADH_2}$ (mV)	
	$K_s^{H_4NAD}$	K_s^{NAD+}	$-NAD^+$	$+NAD^+$
WT H_4cb5r	45 ± 10	554 ± 30	-271	-191
C273M	70 ± 9	267 ± 24	-268	-254
C273S	ND*	ND*	-272	-255
G274P	ND*	ND*	-272	-232
G274S	ND*	ND*	-272	-257
A-insert	ND*	170 ± 37	-269	-243
G-insert	ND*	182 ± 31	-265	-234

*ND indicates that the spectroscopic binding constant could not be determined, due to insufficient spectral change.

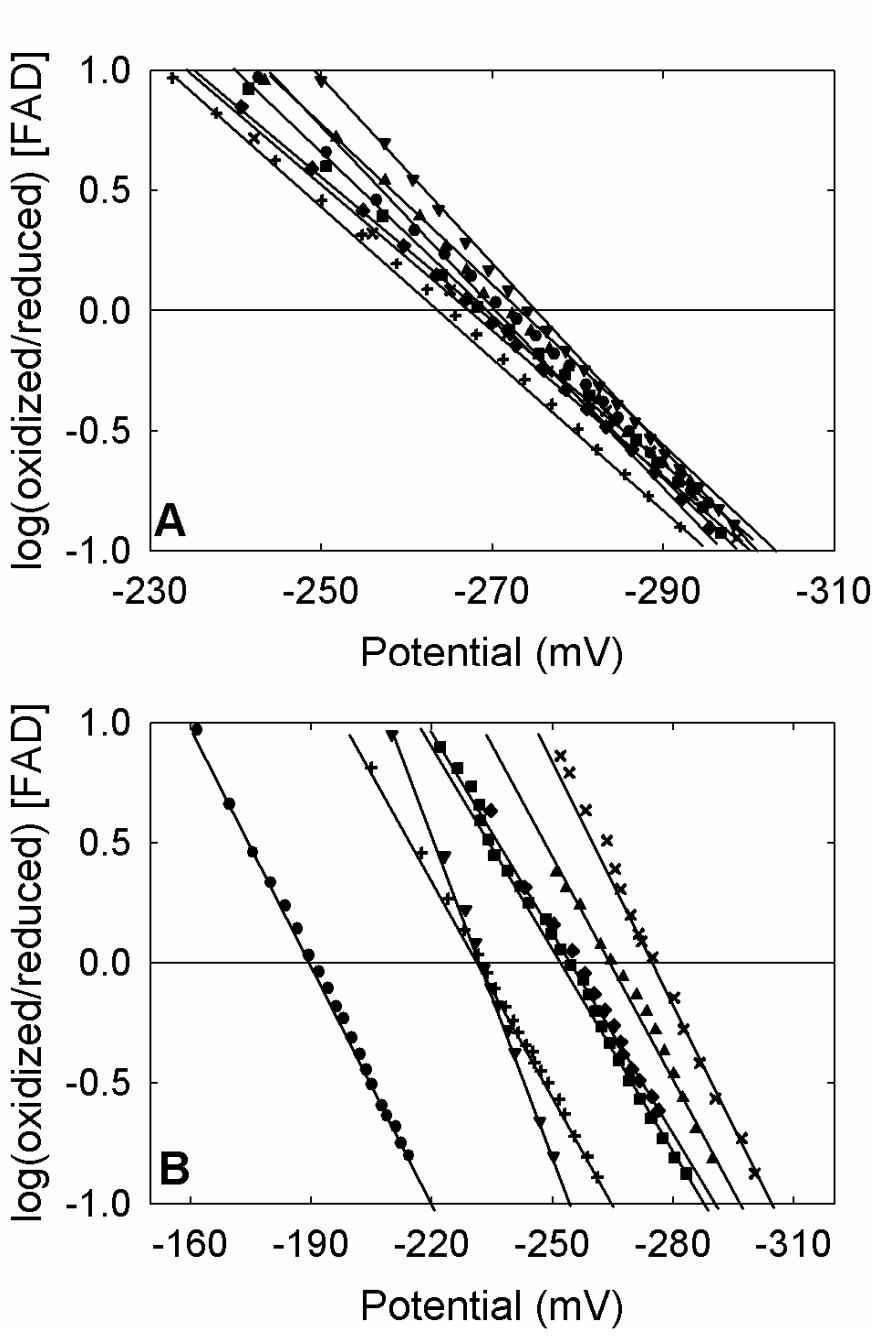

Figure 69. Oxidation-Reduction Midpoint Potentials for the FAD Prosthetic Group in the WT cb5r and cb5r Variants C273S, C273M, G274P, G274S, A insertion, and G insertion. Reductive dye titrations were performed at 25 °C as described in "Materials and Methods" using phenosafranine as the indicator dye in 100 mM phosphate buffer containing 0.1 mM EDTA, pH 7.0. Nernst plots in the absence (A) and presence (B) of 2 mM NAD^+. Plots correspond to (●) H_4cb5r; (■) C273M; (▲) C273S; (▼) G274P; (♦) G274S; (**x**) A-insertion; and (+) G-insertion.

values obtained for the midpoint potentials of the variants are reported in Table 24.

The differential spectroscopy studies in the presence of NAD^+ for both insertion variants as well as the M278A demonstrated a marked increase in the affinity for NAD^+. Based on this, and the decrease in catalytic efficiency and rate of turnover of substrate seen in the three variants, we proposed that these mutants are deleterious due to product inhibition. To further probe the properties of product inhibition, initial rate enzyme kinetics were performed in the presence of varying concentrations of NAD^+ to determine if the competitive inhibition properties of the NAD^+ product was capable of giving rise to the alterations observed in the overall catalytic efficiencies and K_s values of these variants. As shown in Figure 70, the Lineweaver-Burke plots obtained for WT cb5r and the M278A, A-insertion and G-insertion mutants all displayed a model of competitive inhibition represented by a single intercept at the *y*-axis showing no change in V_{max} in the presence of varying concentrations of NAD^+. K_i values [*x*-intercept = $-(K_i)$] were established for the WT cytochrome b_5 reductase and corresponding variants through the secondary plot of the K_m values for each assay against that of the concentration of the NAD^+ inhibitor. The K_i values obtained which corresponded to 675, 349, 193, and 120 μM for the WT domain, M278A, A-insertion and G-insertion variants, respectively. The results were in good agreement with the catalytic efficiencies and K_s values obtained and confirmed that NAD^+ is not able to disassociate from the complex efficiently and thus acts as an inhibitor in the cb5r reaction pathway.

Figure 70. Enzyme Inhibition Assessment in the Presence of NAD^+ for the M278A, A-insertion, and G-insertion Variants. Panels A-D represent the Lineweaver-Burke plots obtained from the initial rate kinetic analyses in the presence of various concentrations of NAD^+. Concentrations of NAD^+ correspond to (●) 0 μM; (■) 50 μM; (▲) 100 μM; (▼) 250 μM; (♦) 500 μM; and (+) 1000 μM for panel (A) [WT cb5r]; (●) 0 μM; (■) 25 μM; (▲) 50 μM; (▼) 100 μM; (♦) 250 μM; and (+) 500 μM for panels [B and C] [M278A and A-insertion], respectively, and (●) 0 μM; (■) 25 μM; (▲) 50 μM; (▼) 100 μM; and (♦) 500 μM for panel (D) [G-insertion]. Panel (E) represents a replot of the observed K_m^{NADH} determined from each Lineweaver-Burke plot in (A-D) versus the concentration of inhibitor (NAD^+) where the inhibition constant (K_i) can be determined by the equation: *x*-intercept = -(K_i), and the *y*-intercept = K_m.

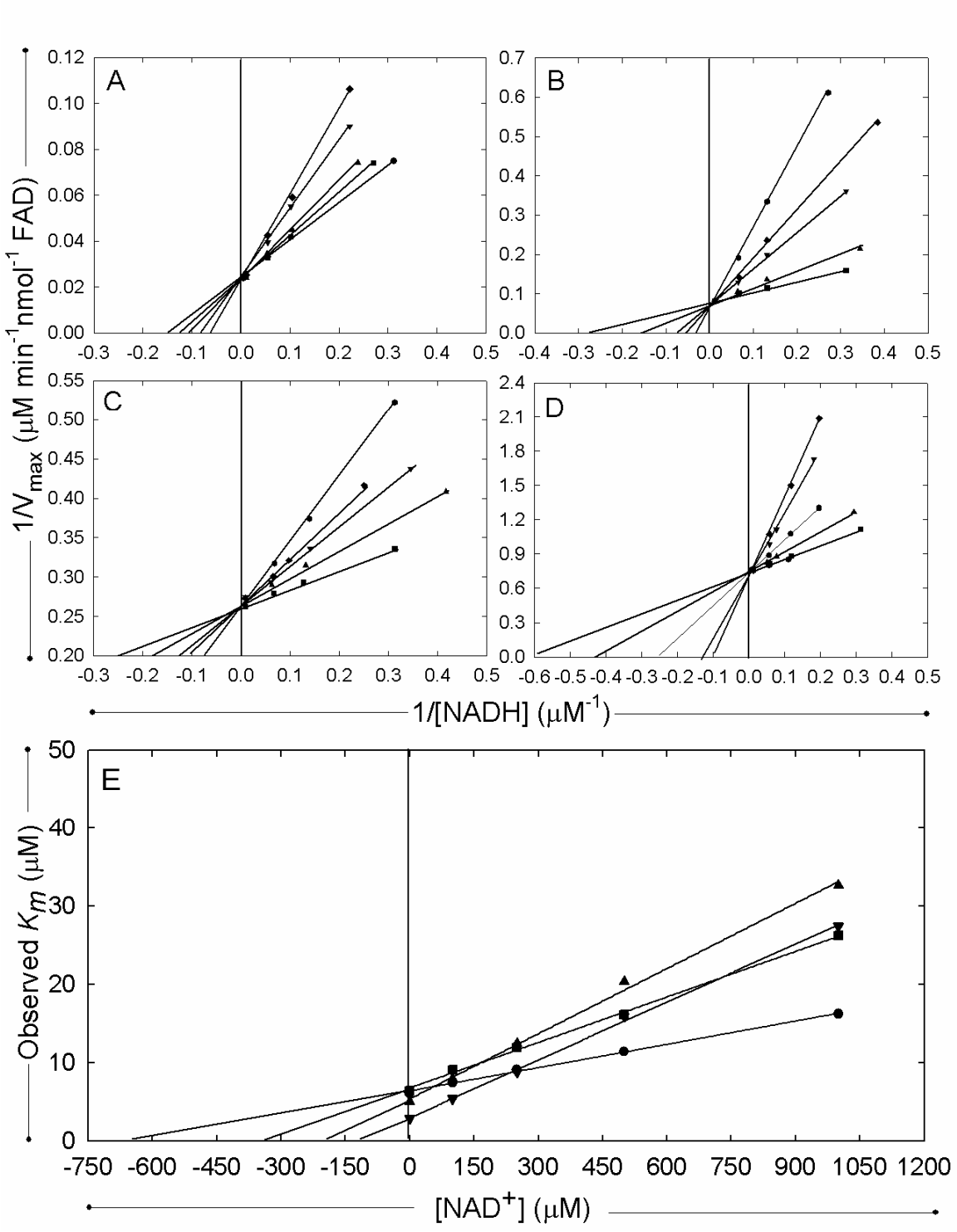
A
B
C
D
E
1/V_{max} (μM min^{-1}nmol^{-1} FAD)
1/[NADH] (μM^{-1})
Observed K_m (μM)
[NAD$^+$] (μM)

Summary of the Role of NADH binding motif ^{273}CGxxxM^{278}

The product of the *DIA1* gene, the flavoprotein cytochrome b_5 reductase, has been shown to be a critical enzyme in mammalian metabolism since an extensive number of mutations have been identified in the gene that result in the disease recessive congenital methemoglobinemia. Of the over forty mutations that have been identified, the majority correspond to individual amino acid substitutions or deletions, in addition to a number of nucleotide alterations that result in the presence of either premature stop codons (truncation mutants) or incorrect gene processing. These mutations in the *DIA1* gene have been classified as producing either the type I or type II forms of RCM. The former are the more benign form of the disease with cyanosis representing the dominant symptom, while in contrast, the latter variant is physiologically more severe resulting in impaired neurological development and finally death. Previous studies of the majority of the known cb5r methemoglobinemia mutants that utilized a novel cb_5/cb5r fusion protein (NCR) have indicated that the variants that impact the NADH-binding site are some of the most compromised mutants in terms of the level of retained specific activity.

Of the four primary sequence motifs that have been found to be characteristic of the pyridine nucleotide transhydrogenase family of flavoproteins, the carboxy-terminal "CGxxxM" motif is one of two motifs involved in pyridine nucleotide binding. It is clear from the x-ray structure obtained for the WT cb5r that adverse effects involving the "CGxxxM" motif are unavoidable if substitutions of the conserved "C", "G" or "M" residues occur. Alterations in the nature of the amino acid side chains of residues in the "CGxxxM" motif have been shown to account for the substantially-weakened binding of NADH to the various alanine variants, when compared to the NADH-affinities of the WT

proteins. If the combination of hydrogen-bonding to the nicotinamide moiety and hydrophobic interactions between NAD(H) and this motif are a significant factor in modulating NADH binding, then any perturbation of the molecular structure surrounding this binding site would adversely affect the affinity for NADH, and prediction that is verified by the results obtained for the various alanine-scanning variants.

In the WT protein, the hydrophobic C273 side chain is positioned approximately 4.2 A^o from the *si* face of the FAD isoalloxazine ring system, and is in van der Waals contact with the nicotinamide moiety of NAD^+. This suggested the possibility that C273 is involved in controlling the equilibrium between the unstacked configuration of bound NADH and the charge transfer complex. In the C273A variant, the absence of a thiol side chain would be expected to result in an incorrect orientation of the bound NADH that would decrease the rate of electron transfer and reduce catalytic efficiency. Furthermore, the presence of the sulfur group in the C273M was unable to recover the activity seen in the C273A, indicating that the positioning of the sulfur is key to allowing the NADH to adopt the correct orientation for efficient enzymatic activity.

The G274 residue of the native cb5r is found participating in hydrogen bonding between the backbone oxygen of the residue with the nitrogen N7 of the nicotinamide moiety. Substitutions of this residue would result in minor deviations of the backbone which would affect this hydrogen bond formation. The introduction of even the small side chain methyl group of alanine to this position could result in a physical hindrance to the binding of NADH, or cause the NADH to misalign in the binding pocket, placing the nicotinamide moiety in a position incompatible with electron transfer. The substitution of the various amino acids described in the data indicated that these newly introduced

side chains of increasing size and, in the case of proline and serine, additional characteristics, such as rigidity and polarity, may result in a sterically hindered environment, consequently disrupting the hydrogen bonding. Figure 71 illustrates these effects. G274P introduces a high level of conformational rigidity via the secondary amine structure of its side chain. This causes a kink in the peptide backbone affecting the downstream orientation of the protein. In the immediate vicinity, it also introduces a physical hindrance to the binding of NADH, though to a lesser extent than previously seen in the G180P and G182P mutations. The position of the proline oxygen backbone would also likely shift slightly further away from the N7 nitrogen of the nicotinamide ring, altering the hydrogen bond formation between the two atoms. The severe deleterious effect of the mutation on the catalytic efficiency demonstrates the impact that these collective effects have. In addition, the G274A and G274S substitutions cause equally severe deleterious effects on the catalytic activity through decreasing turnover efficiency and diminishing binding affinity of the substrate through similar processes of altering the hydrogen bonding distance and introducing physical obstructions to the binding area. Moreover, the inability to maintain spectral differences for each of the substitutions further indicates a disruption of the hydrogen bonding essential for substrate binding.

The role of the three sequential proline residues proved to be important, but not vital, to the proper function of the enzyme, in as far as that the removal of the proline without replacement by a large side chain, in this case the alanine substitutions, did not drastically impact the catalytic, spectroscopic, thermal stability, or electron transfer properties of the protein. It is important to note, however, that residue P275, though in

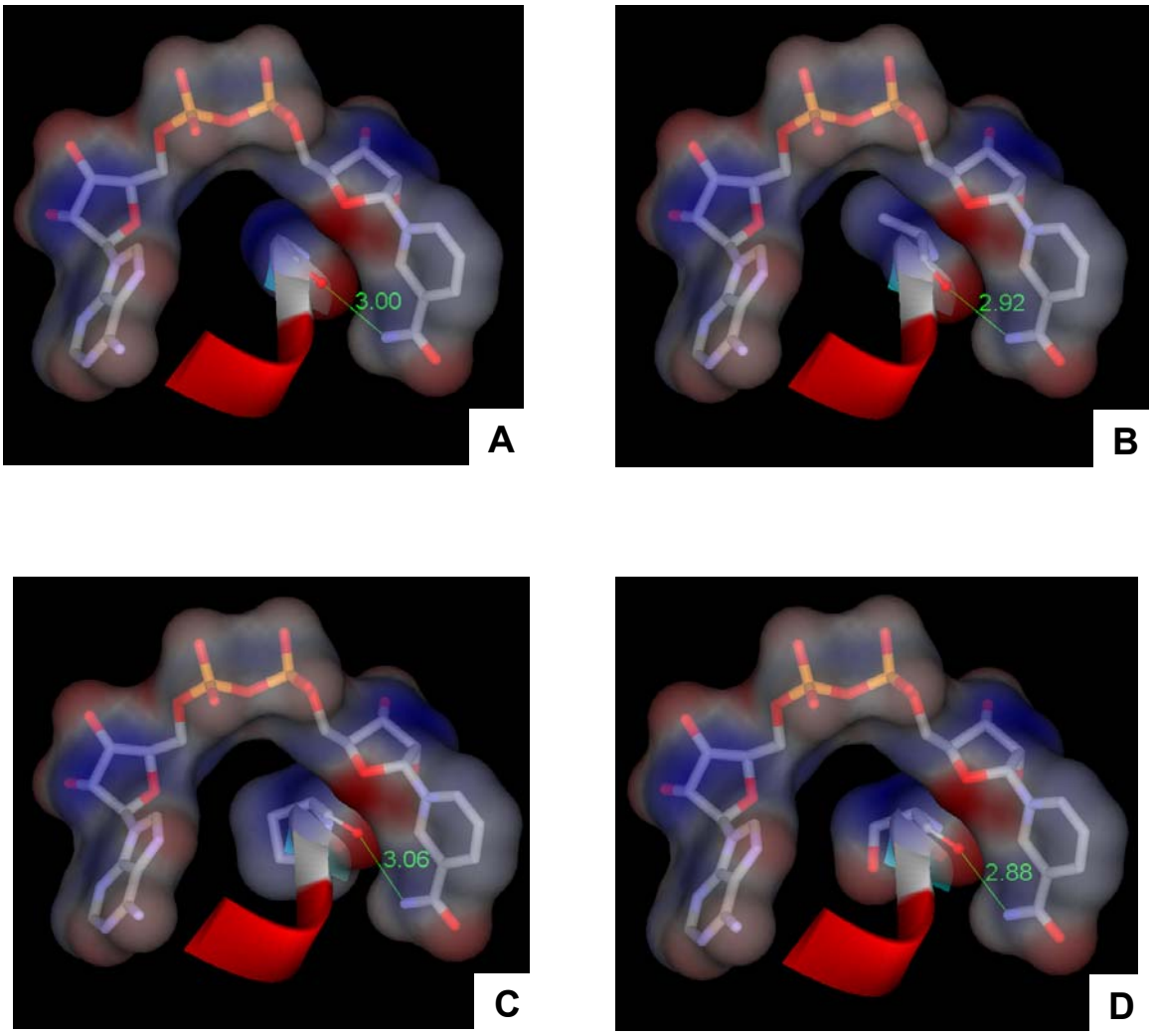

Figure 71. Structures of WT cb5r and cb5r variants G274A, G274P and G274S with NAD^+ Generated *in silica*. The molecular model of cb5r displaying the charged surfaces of (A) residue G274 (B) cb5r variant G274A (C) cb5r variant G274Pand (D) cb5r variant G274S in association with NAD^+ generated utilizing the automated comparative protein modeling server SWISS-MODEL [111] and analyzed using the molecular modeling software Web Lab Viewer Pro [134]. Model depicts surface representation of the residue and NAD^+ in transparent display style. Distance between N7 nitrogen of the nicotinamide and the backbone oxygen of each residue are shown in green. Models generated from cb5r in complex with FAD and NAD^+ (1IB0).

this study the least affected by substitution, has been identified as a site of a mutation leading to type I RCM. The proline to leucine substitution was observed to have no

detectable effects on either the spectroscopic or thermodynamic properties of the flavin prosthetic group in the absence of NAD^+. In addition, protein folding and stability were unaffected by the mutation. In contrast, the proline to leucine substitution exhibited a profound effect on both the affinity of cb5r for the reducing substrate and its catalytic efficiency. The substitution P275L was shown through homology modeling to create a "hump" leading to steric hindrance preventing NADH from properly seating into the binding pocket [105].

The role methonine 278 plays in enzyme activity and substrate binding can be appreciated by examining the effects of a substitution of the residue. M278A exhibits a moderate decrease in rate of turnover. The increased K_m for NADH coupled with a increase in K_s for H_4NAD suggested that M278 plays a role in modulating the binding of substrate. Further, the lack of decrease of intensity of spectral changes upon the addition of NAD^+, coupled with an increased spectral binding constant, indicated a change in binding affinity caused by substitution of M278.

To further examine the role of the residue, insertion mutants were generated which caused M278 to be shifted downstream one residue, placing it out of its native register. Regardless of the inserted residue, the effect of the insertion was to decrease the rate of turnover to approximately 3% of WT, as well as decrease the affinity for substrate by 90 fold on average. While no noticeable changes were observed upon the addition of H_4NAD, the addition of NAD^+ yielded spectral changes at lower concentrations of NAD^+ than in the case of WT, indicating a preference for the product in the case of both insertion mutants. Additionally, NADH:FR assays in the presence of NAD^+ demonstrated that all three mutants had increased inhibition constants for NAD^+ as

compared to WT, indicating that the decreased turnover rate is, at least in part, the result of product inhibition. Thus, it is possible that M278 functions in release of NAD^+ after transfer of electrons to the flavin prosthetic group.

Secondary effects could also play a role in the reduced affinity of the various "CGxxxM" variants for NADH. Such effects could be propagated through small displacements in the neighboring loops which make up nearby sections of the NADH binding site. For example, a small reorientation of the α-helical region following the "CGxxxM" motif could reduce the space available for binding the adenine moiety, forcing some reorganization of the loop containing F251, the stacking residue for adenine in the WT.

The possible contribution of secondary effects of this kind could be investigated by measuring the affinity of phosphorylated adenenines for the site. In cb5r homologues, such as cytochrome P450 reductase and ferredoxin:$NADP^+$ reductase, partial NADPH analogs such as 2'-AMP and 2',5'-ADP are inhibitors (and in some cases activators) because they compete with NADPH. The FAD and pyridine nucleotide binding sites in these enzymes have features which cb5r lacks, including a stacking residue supplied by the carboxyl-terminal region for the FAD isoalloxazine and interdomain hydrogen bonds to the pyridine nucleotide.

While the substitution of the individual residues in the "CGxxxM" motif were anticipated to have a substantial impact on the K_m for NADH owing to the perturbation of the position of the subsequent residues that correspond to C273 to M278, they were not anticipated to have any substantial impact on the spectroscopic or thermodynamic properties of the flavin prosthetic group. As expected, none of the "CGxxxM" motif

substitution mutants adversely affected the wavelength maxima determined for the FAD prosthetic group in either the visible absorption or CD spectra. This result demonstrated that altering the nature of amino acid residues situated opposite the isoalloxazine ring would not be expected to have a significant effect on the redox properties of the flavin prosthetic group, a prediction that was tested by performing oxidation-reduction titrations for the various mutants, and is also reflected in the turn-over value of the variants.

Overall, the results of these studies indicate the important contribution of the residues that comprise the "CGxxxM" reduced pyridine nucleotide-binding motif and suggest that any naturally occurring mutations in these residues are likely to be manifest in RCM with different degrees of severity.

4. CONCLUSIONS AND FUTURE DIRECTIONS

These studies were designed to provide additional structural and functional insight into the highly conserved motifs found within cytochrome b_5 reductase, and other members of the FNR super-family with respect to the mode of NADH-binding and the enzymes catalytic function. This objective was accomplished using two approaches. The first approach involved the generation of an array of cb5r variants with substitutions of amino acid residues found within the conserved motifs based on alternative residues observed to occur at the same position in other members of the FNR family as well as within other species, structural difference among between residues, removal or addition of polar groups, and the introduction of positive charges. The second approach incorporated the analyses of naturally occurring recessive congenital methemoglobinemia mutants that are located within, or in close proximity to, the conserved motifs. Through this method of characterization, we were able to establish a role for each of the previously uncharacterized amino acid residues found in the NADH-binding motifs in addition to suggest the molecular basis for the disease for each of the RCM variants. The construction and characterization of the canine cytochrome b_5 reductase protein was also designed in order to compare and contrast the differences and similarities in structure and function among mammalian protein variants.

Previous studies on the human, bovine, and porcine variants of cb5r have elucidated discrepancies in the kinetic constants of proteins that would otherwise appear to be nearly identical in nature. The primary structure of these different variants retained a high level of sequence similarity among the residues, and demonstrated conserved sequence motifs involved in binding of its flavin cofactor and the reduced substrate, NADH.

With the sequencing of the dog genome, potential gene transcripts had been identified that maintained sequence similarity to the cb5r sequence. The theoretical sequences for the canine cb5r variant indicated a high level of dissimilarity in the amino terminal portion of the sequence. This work was designed to examine these dissimilarities as well as provide a comparison of the characterization of the gene products from two mammalian species, under identical conditions, in an effort to determine the differences and similarities in their structural and functional parameters.

In constructing the canine variant, it was shown that the dissimilarity in the amino terminus reported in the original GenBank sequence was in error, and likely due to incorrect sequencing. The canine variant retained a primary structure nearly identical to that of the rat and human variants, with a small degree of disagreement with each sequence at a limited number of residues. Comparison of the results obtained from the spectroscopic, kinetic, and thermal stability studies confirmed predictions generated from the pair-wise sequence alignments that the structural and functional properties of the recombinant canine cb5r diaphorase domain should be directly comparable to those of the corresponding rat domain. The similarity in the kinetic properties is particularly

significant and suggests that other cb5r variants exhibiting similarly conserved sequences should exhibit comparable kinetic properties.

Analysis of the crystal structure of cb5r reveled that two residues, Y112 and Q210, formed hydrogen bonds with the pyrophosphate backbone of NAD^+, forming an anchoring attachment from the external surface of the protein. This, combined with the high level of conservation of these residues within FNR family members and other cb5r sequences, suggested that these residues may play a vital role in the correct binding with NADH and, consequently, efficient electron transfer with cb5r. This work examined several substitutions of each residue to determine the importance of the residues and their potential roles in enzyme structure and function. Characterization of the variants indicated that the hydroxyl group of Y112 was necessary for binding NADH in the proper orientation. Substitution of this residue resulted in moderately decreased kinetic constants, indicating inefficient transfer of reducing equivalents. The Q210 variants also showed a decrease in function, however to a lesser degree, indicating that Y112 is more critical in orienting the reduced substrate than Q210.

Proximal to the two pyrophosphate associating residues are two residues shown to be mutated in patients presenting with type I RCM. The two mutations, corresponding to T116S and E212K, were detected in the same patient presenting with cyanosis and increased serum methemoglobin concentrations. The T116S mutation had previously been demonstrated to occur in approximately 27% of the African American population, and thus was identified as a polymorphism. These individual variants were investigated to determine the causative nature of each mutant leading to the presentation of disease. Additionally, the double mutant, T116S/E212K, was generated and characterized to

further elucidate the condition of the patient. Subsequent characterization revealed that both mutations affected the function of the protein. For the T116S variant, the affects were mild, but still significant enough to cause a disease condition. Catalytic efficiency was decreased by half, and the ability to transfer electrons was shown to be somewhat impaired. Similarly, E212K showed impaired function, to a slightly greater extent than the T116S variant. Most notable was the decrease in stability of the E212K mutation, which is likely the causative agent in the presentation of RCM for the patient, as protein in the circulating erythrocytes gradually breaks down overtime and cannot be replaced. The double mutant showed an even great decrease in functionality, indicating that the T116S does indeed add to the effects of the E212K mutation.

Multiple sequence alignments of FNR family members and cb5r sequences revealed that several structural motifs exist that are vital for the binding and association of flavin cofactors and pyridine nucleotide substrates. One of these motifs, corresponding to "^{180}GtGitP^{185}" in cb5r, is located in the NADH-binding lobe of cb5r. Based on analysis of the x-ray crystal structure, these residues are shown to form hydrophobic interactions and direct connections with both the FAD cofactor and the NAD^+ molecule associated with cb5r. The general structural nature of the conserved residues of this motif suggested that a vital role for this motif is to form a scaffold onto which the NADH can bind to properly align for subsequent electron transfer. Additionally, the two threonine residues located in the motif, T181 and T184, bind to NAD^+ and FAD, respectively, aiding in the proper positioning of each group. Furthermore, T184 binds to N5 of the isoalloxazine ring of FAD, the location of one of the electrons in the reduced FAD. Substitution of the residue of this region with

structural alternatives as well as naturally occurring alternate residues in the FNR family members confirmed the importance of each residue. Both G180 and G182 are necessary to provide a relatively clear area around which the NADH can bind in order to properly position the nicotinamide portion of the molecule. Proline substitution of each of these residues resulted in displacement of the nicotinamide moiety, decreasing catalytic efficiency. Likewise, the proline residue, P185, confers structural rigidity in the middle of the helix Nα1. Removal of the residue removes the necessary structural needs to maintain the proper folding in the immediate region of the residue. A higher degree of "openness" is generated as a result, allowing for better association of NADH, but not in the proper orientation. The structural importance is further demonstrated in the reduced thermal stability seen in the variants of this residue. I183, likewise, causes structural integrity, with substitution leading to decreased stability while maintaining a moderate level of catalytic ability of WT. This was expected, as this residue does not participate in any direct interaction with the FAD or NAD^+ groups, but is located in a structural component leading to the stability of the protein and the proper orientation of both groups. The –OH group of T181 was shown to be vital in anchoring the NADH in the proper orientation to align the N7 nitrogen of the nicotinamide ring for the subsequent electron transfer. This was demonstrated by differential spectroscopy of the variants T181A and T181I adopting a line shape similar to $PAAD^+$ which lacks this nitrogen. Substitution of T184 demonstrated a great impact upon the association of FAD and on the function of the protein. T184 interacts with FAD in two locations, one of which is the site of a hydrogen added during the reduction reaction. Removal of the –OH group caused a destabilizing effect on the semiquinone intermediate, decreasing catalytic

efficiency. Replacement with histidine caused even more severe impairment, causing the mutant to have a midpoint potential about equal to that of free flavin.

Preceding the GxGxxP motif is another highly conserved glycine residue G179. This residue helps to form the transition in the helical structure of the motif. It is highly conserved among FNR family members and across species sequences. The function of this residue was investigated by replacement with naturally occurring alternate residues and characterized for kinetic, spectral and thermal stability properties. It was shown that replacement of this residue lead to decreased affinity for substrate and decreased catalytic function. Substitution with alanine caused the least deleterious effects on the function of the protein while the other substitutions, (P, T, and V) effectively caused NADH to be unable to efficiently bind. Interestingly though, substitution with valine lead to increased affinity of NADPH over NADH, indicating that this residue plays a role in substrate specificity.

Immediately preceding G179 is another residue, A178, which has been shown to be occur as two distinct mutations, A178T and A178V, that result in presentation of type I RCM. Presentation in each patient was mostly restricted to cyanosis with elevated methemoglobin levels. Both were shown to be distinct mutations and not polymorphisms. Previous studies of A178V demonstrated that the variant maintained near WT catalytic function, and only differed by having a lower thermal stability than WT. To further explore the effects of these mutations on the function of cb5r, the two mutants were generated and characterized based on kinetic, spectral, and thermal stability properties and compared to WT. It was shown that, as previously reported, the A178V mutant maintained near WT activity, though not to the extent as previously reported.

Additionally, the only alteration was a decreased stability to temperature, indicating that the causative nature of disease of this mutant is a result of degradation of protein in the circulating erythrocytes. A178T, on the other hand, demonstrated equivalent stability, yet showed a more significant decrease in kinetic function. The presence of the –OH group of A178T causes electrostatic and/or steric interference of the neighboring GxGxxP motif, leading to dysfunction. This interference leads to decreased ability to bind NADH properly and thus decreases catalytic activity. Though greater than the effects of A178V, the A178T mutation is itself mild, and thus would likely not cause severe consequences in the patient.

The second conserved motif present in the FNR family members and specifically in cb5r is the "^{273}CGpppM^{278}" motif. As shown from x-ray crystallography this motif, while not directly associating with NAD^+, generates an extensive framework of hydrophobic interactions with the bound NAD^+ properly orienting it into the binding pocket. The only direct bonding occurs between the backbone of residue G274 and the N7 of the nicotinamide of NAD^+. To investigate the importance of this motif, variants were generated based upon side chain properties of each residue to determine what role each play. Additionally, two insertion mutants were created to investigate the presence of an additional residue in this motif that occurs in several member of the FNR family. Characterization of these residues indicated that each of the three sequential proline residues are necessary to generate the correct orientation of the tertiary structure of the protein in the proximal vicinity, allowing the necessary rigidity to generate a kink in the protein changing its direction and initiating a helical structure. Alterations of these residues yield mildly decreased function of the protein, but not to a significant extent as

other mutations did. The presence and position of the sulfur group of C273 was shown to be important to the function of the enzyme as removal or repositioning of the group, as done by C273A and C273M variants respectively, yielded drastically diminished activity. Likewise, the presence of G274 was shown to be vital to the proper orientation of NADH. Introduction of any side chain to this region resulted in the inability of NADH to effectively bind to cb5r, and in effect prevented the protein from functioning, with the G274P mutant retaining less that .01% catalytic efficiency of WT. The effect seems to result from three different effects. First, the movement of the backbone altered the position of the oxygen involved in hydrogen bonding with the NAD^+ nicotinamide N7. Secondly, the presence of additional atoms on the side chains of any residue substituted in this region could generate a physical obstacle toward the binding of NADH. Finally, in the case of proline, introduction of rigidity at this position would result in alteration of the folding of the protein in the immediate region, generating potential downstream effects that lead to decreased function, as well as affecting the nearby structural motifs GxGxxP also involved in the binding of NADH and the proper placement of the nicotinamide moiety.

The alanine substitution combined with the two insertion mutants shed light on the function of M278. The results demonstrated that the decrease in catalytic efficiency was coupled with an increased affinity for binding of NAD^+. Inhibition studies indicated that these mutants had lower inhibition constants than WT, indicating that NAD^+ was not dissociating form the enzyme as well as it does in WT. This suggests that M278 potentially plays gate keeping role in the process of associating with substrate and dissociating product.

These data provide valuable insight into the structural and functional properties of the highly conserved motifs of cytochrome b_5 reductase that are involved in NADH-binding and orientation as well as a determination of the molecular basis of the disease recessive congenital methemoglobinemia. These results support logical conclusions based on the kinetic, spectral, thermodynamic, and molecular modeling properties of each of the generated variants. The data presented in this research provided a broad analysis of the motif using alanine scanning as well as specifically tailored substitutions to provide information on the structural and catalytic role of each individual residue. However, in order to complete this work and support our conclusions crystal structures of several of the variants, both in the absence and presence of NAD^+ should be obtained. This would provide the most concrete evidence to support the conclusions presented in this work.

REFERENCES

1. Gupta, S.K.; Gupta, R.C.; Gupta, A.B.; Seth, A.K.; Bassin, J.K.; Gupta, A. and Sharma, M.L. (2001) Recurrent diarrhea in children living in areas with high levels of nitrate in drinking water. *Arch. Environ. Health.* **56**: pp. 369-73.
2. Rehman, H.U. (2001) Methemoglobinemia. *West. J. Med.* **175**: pp. 193-96.
3. Jaffe, E.R and Hultquist, D.E. (2001) The Molecular and Molecular Basis of Inherited Disease 8th Ed. C.R. Scriver, A.L. Beaudet, W.S. Sly, and D. Valle (eds.) McGraw Hill, New York. pp. 4555-70.
4. Da Silva S.S.; Sajan I.S.; and Underwood III, J. P. (2003) Congenital methemoglobinemia: a rare cause of cyanosis in the newborn--a case report. *Pediatrics* **112**: pp.158-61.
5. Hegesh E.; Hegesh, J. and Kaftory, A. (1986) Congenital methemoglobinemia with a deficiency of cytochrome b_5. *N. Engl. J. Med.* **314**: pp. 757.
6. Francios (1845) Cas de cyanose congenitale sans causeapparante. *Bull. Acad. Roy. Med. Belg*. **4**: pp. 698.
7. Diitrich, P. (1891) Ueber methamoglobinbildende Gifte Naunyn-Schmiedbergs. *Arch. Exp. athol. Pharmocol*. **29**: pp. 247.
8. Hitzenberger, K. (1932) Autotoxische zyanose (intraglubulare methamoglobinamie). *Wien. Arch. Inn. Med.* **23**: pp. 85.
9. Deeney, J.; Murdock, E.T. and Rogan, J.J.. (1943) Familial idopathic methaemoglobinemia. *British Medical Journal*. **I**: pp. 721-23.
10. Barcroft, H.; Gibson, Q.H.; Harrison, D.C. and McMurray, J. (1945) Familil idiopathic methemoglobinemia and its treatment with ascorbic acid. *Clin.Sci*. **5**: pp. 145
11. Gibson, Q.H. (1948) The reduction of methaemoglobin in red blood cells and studies on the cause of idiopathic methaemoglobinaemia. *Biochem. J.* **42**: pp. 13-23.
12. Scott, E.M. and Griffith, I.V. (1959) The enzyme defect of hereditary methemoglobinemia: Diaphorase. *Biochim. Biophys. Acta*. **34**: pp. 584.
13. Scott, E.M. (1960) The relation of diaphorase of human erythrocytes to inheritance of methemoglobinemia. *J. Clin. Invest*. **39**: pp. 1176.
14. Balsamo, P.; Hardy, W.R.; and Scott, E.M. (1964) Hereditary methemoglobinemia due to diaphorase deficiency in Navajo Indians. *J. Pediatr.* **65**: pp. 298.
15. Cawein, Madison, et. al. (1964) Hereditary diaphorase deficiency and methemoglobinemia. *Arch. of Int. Med.*

16. Leroux, A.; Junien C.; Kaplan, J. and Bamberger J. (1975) Generalised deficiency of cytochrome b5 reductase in congenital methaemoglobinaemia with mental retardation. *Nature*. **258**: pp. 619-20.
17. Hultquist, D.E. and Passon, P.G. (1971) Catalysis of methaemoglobin reduction by erythrocyte cytochrome b_5 and cytochrome b_5 reductase. *Nat. New Biol.* **229**: pp. 252-54.
18. Hyde, G.E.; Crawford N.M. and W.H. Campbell. (1991) The sequence of squash NADH:nitrate reductase and its relationship to the sequences of other flavoprotein oxidoreductases. A family of flavoprotein pyridine nucleotide cytochrome reductases. *J Biol Chem*. **266**: pp. 23542-7.
19. Karplus, P.A. and C.M. Bruns. (1994) Structure-function relations for ferredoxin reductase. *J Bioenerg Biomembr*. **26**: pp. 89-99.
20. Campbell, W.H. and K.R. Kinghorn. (1990) Functional domains of assimilatory nitrate reductases and nitrite reductases. *Trends Biochem Sci.* **15**: pp. 315-9.
21. Wang, M.; Roberts D.L.; Paschke R.; Shea, T. M.; Masters B.S. and Kim, J. J. (1997) Three-dimensional structure of NADPH-cytochrome P450 reductase: prototype for FMN- and FAD-containing enzymes. *Proc Natl Acad Sci U S A*. **94**: pp. 8411-6.
22. Correll, C.C.; Ludwig, M.L.; Burns, C.M. and Karplus P.A. (1993) Structural prototypes for an extended family of flavoprotein reductases: comparison of phthalate dioxygenase reductase with ferredoxin reductase and ferredoxin. *Protein Sci*. **2**: pp. 2112-33.
23. Lu, G.; Campbell, W.H.; Schneider, G. and Lindqvist, Y. (1994) Crystal structure of the FAD-containing fragment of corn nitrate reductase at 2.5 A resolution: relationship to other flavoprotein reductases. *Structur*. **2**: pp. 809-21.
24. Strittmatter, P. (1965) The reaction sequence in electron transfer in the reduced nicotinamide adenine dinucleotide-cytochrome b5 reductase system. *J Biol Chem*. **240**: pp. 4481-7.
25. Kitao, T.; Sugita, Y.; Yoneyama, Y.; and Hattori, K. (1974) Methemoglobin reductase (cytochrome b_5 reductase) deficiency in congenital methemoglobinemia. *Blood* **44**: pp. 879-84
26. Oshino, N.; Imai, Y. and Sato, R. (1971) A function of cytochrome b_5 in fatty acid desaturation by rat liver microsomes, *J. Biochem. (Tokyo)* **69**: pp. 155-67.
27. Reddy, V.V.; Kupfer, D. and Caspi E. (1977) Mechanism of C-5 double bond introduction in the biosynthesis of cholesterol by rat liver microsomes. *J Biol Chem*. **252**: pp. 2797-801.
28. Hildebrandt, A. and R.W. Estabrook. (1971) Evidence for the participation of cytochrome b 5 in hepatic microsomal mixed-function oxidation reactions. *Arch Biochem Biophys*. **143**: pp. 66-79.
29. Loughran, P.A.; Roman, L.J.; Miller, R.T. and Masters, B.S.S. (2001) The kinetic and spectral characterization of the E. coli-expressed mammalian CYP4A7: cytochrome b_5 effects vary with substrate, *Arch. Biochem. Biophys*. **385**: pp. 311-21.
30. Pugh, E.L. and Kates, M. (1977) Direct desaturation of eicosatrienoyl lecithin to arachidonoyl lecithin by rat liver microsomes, *J. Biol. Chem*. **252**: pp. 68-73.

31. Kurian, J.R.; Chin, N.A.; Longlais, B.J.; Hayes, K.L. and Trepanier L.A. (2006) Reductive detoxification of arylhydroxylamine carcinogens by human NADH cytochrome b5 reductase and cytochrome b5. *Chem Res Toxicol*. **19**: pp. 1366-73.
32. Tomatsu, S.; Kobayashi, Y.; Fukumaki, Y.; Yubisui, T.; Orii, T. and Sakaki, Y. (1989) The organization and the complete nucleotide sequence of the human NADH-cytochrome b5 reductase gene. *Gene.* **80**: p. 353-61.
33. Bull, P.C.; Shepard E.A.; Povey, S.; Santisteban I. and Phillips I.R. (1988) Cloning and chromosomal mapping of human cytochrome b5 reductase (DIA1). *Ann Hum Genet*. **52**: pp. 263-8.
34. Pietrini, G.; Carrera, P. and Borgese, N. (1988) Two transcripts encode rat cytochrome b5 reductase. *Proc Natl Acad Sci U S A*. **85**: pp. 7246-50.
35. Kobayashi, Y.; Fukumaki, Y.; Yubisui, T.; Inoue, J. and Sakaki, Y. (1990) Serine-proline replacement at residue 127 of NADH-cytochrome b5 reductase causes hereditary methemoglobinemia, generalized type. *Blood*. **75**: p. 1408-13.
36. Spatz, L. and Strittmatter, P. (1971) A form of cytochrome b_5 that contains an additional hydrophobic sequence of 40 amino acid residues. *Proc. Natl. Acad. Sci. U S A*. **68**: pp. 1042-6.
37. Strittmatter, P.; Rogers, M.J. and Spatz, L. (1972) The binding of cytochrome b_5 to liver microsomes. *J. Biol. Chem*. **247**: pp. 7188-94.
38. Ozols, J.; Carr, S.A. and Stritmatter, P. (1984) Identification of the NH2-terminal blocking group of NADH-cytochrome b5 reductase as myristic acid and the complete amino acid sequence of the membrane-binding domain, *J. Biol. Chem*. **259**, pp. 13340-54.
39. Kuma, F. (1981) Properties of methemoglobin reductase and kinetic study of methemoglobin reduction. *J Biol Chem*. **256**: pp. 5518-23.
40. Pietrini, G.; Aggujaro, D.; Carrera, P.; Malyszko, J.; Vitale, A. and Borgese, N. (1992) A single mRNA, transcribed from an alternative, erythroid-specific, promoter, codes for two non-myristylated forms of NADH-cytochrome b_5 reductase. *J. Cell. Biol.* **117**: pp. 975-86.
41. Du, M.; Shirabe, K. and Takeshita, M. (1997) Identification of alternative first exons of NADH-cytochrome b5 reductase gene expressed ubiquitously in human cells. *Biochem. Biophys. Res. Commun.* **235**: pp. 779-83.
42. Shirabe, K.; Yubisui, T.; Borgese, N.; Tang, C.Y.; Hultquist, D.E. and Takeshita, M. (1992) Enzymatic instability of NADH-cytochrome b5 reductase as a cause of hereditary methemoglobinemia type I (red cell type). *J Biol Chem*. **267**: pp. 20416-21.
43. Kimura, S.; Kawamura, M. and Iyanagi, T. (2003) Role of Thr(66) in porcine NADH-cytochrome b5 reductase in catalysis and control of the rate-limiting step in electron transfer. *J Biol Chem*. **278**: pp. 3580-89.
44. Strittmatter, P. (1962) Direct hydrogen transfer from reduced pyridine nucleotides to microsomal cytochrome b5 reductase. *J Biol Chem*. **237**: pp. 3250-54.
45. Strittmatter, P. (1963) The interaction of reduced pyridine-aldehyde adenine dinucleotide with cytochrome b-5 reductase. *J Biol Chem*. **238**: pp. 2213-19.

46. Strittmatter, P. (1965) The reaction sequence in electron transfer in the reduced nicotinamide adenine dinucleotide-cytochrome b5 reductase system. *J Biol Chem*. **240**: pp. 4481-7.
47. Iyanagi, T. (1977) Redox properties of microsomal reduced nicotinamide adenine dinucleotide-cytochrome b5 reductase and cytochrome b5, *Biochemistry* **16**: pp. 2725-30.
48. Iyanagi, T.; Watanabe, S. and Anan K.F. (1984) One-electron oxidation-reduction properties of hepatic NADH-cytochrome b5 reductase. *Biochemistry*. **23**: pp. 1418-25.
49. Meyer, T.E.; Shirabe, K.; Yubisui, T.; Takeshita, M.; Bes, M.T.; Cusanovich, M.A. and Tollin, G. (1995) Transient kinetics of intracomplex electron transfer in the human cytochrome b5 reductase-cytochrome b5 system: NAD+ modulates protein-protein binding and electron transfer. *Arch Biochem Biophys*. **318**: pp. 457-64.
50. McCarty, K. (2001) Methemoglobinemia: Feeling Blue? http://www.mc.uky.edu/ahec/skyahec/methem-CE.htm
51. Kell, S. (2003) University of Virginia Health System "Clinical Service" http://www.healthsystem.virginia.edu/internet/medtox/images/methemoglobinemia.jpg
52. Gibson, Q.H. (1948) The reduction of methaemoglobin in red blood cells and studies on the cause of idiopathic methaemoglobinaemia. *Biochem. J*. **42**: pp. 13-23.
53. Worster-Drought, C.; White, J. C. and Sargent, F. (1953) Familial, idiopathic methaemoglobinaemia associated with mental deficiency and neurological abnormalities. *Brit. Med. J.* **2**: pp. 114-8.
54. Aalfs, C. M.; Salieb-Beugelaar, G. B.; Wanders, R. J. A.; Mannens, M.M.A.M. and Wijburg, F. A. (2000) A case of methemoglobinemia type II due to NADH-cytochrome b5 reductase deficiency: determination of the molecular basis. *Hum. Mutat.* **16:** pp. 18-22,.
55. Katsube, T.; Sakamoto, N.; Kobayahis, Y.; Seki, R.; Hirano, M.; Tanishima, K.; Tomada, A.; Takazakura, E.; Yubisui, T.; Takeshita, M; Sakaki, Y. and Fukumaki, Y. (1991) Exonic point mutations in NADH-cytochrome B5 reductase genes of homozygotes for hereditary methemoglobinemia, types I and III: putative mechanisms of tissue-dependent enzyme deficiency. *Am J Hum Genet*. **48**: pp. 799-808.
56. Yubisui, T.; Shirabe, K.; Takeshita, M.; Kobayashi, Y.; Fukumaki, Y.; Sakaki, Y. and Takano, T. (1991) Structural role of serine 127 in the NADH-binding site of human NADH-cytochrome b5 reductase. *J Biol Chem*. **266**: pp. 66-70.
57. Jenkins, M.M. and Prchal, J.T. (1996) A novel mutation found in the 3' domain of NADH-cytochrome b5 reductase in an African-American family with type I congenital methemoglobinemia. *Blood*. **87**: pp. 2993-99.
58. Bewley, M.C.; Marohnic, C.C. and Barber, M.J. (2001) The structure and biochemistry of NADH-dependent cytochrome b5 reductase are now consistent. *Biochemistry*. **40**: pp. 13574-82.

59. Nishida, H.; Inaka, K. and Miki, K. (1995) Specific arrangement of three amino acid residues for flavin-binding barrel structures in NADH-cytochrome b5 reductase and the other flavin-dependent reductases. *FEBS Lett*. **361**: pp. 97-100.
60. Davis, C.A. (2004) Sytematic Analysis of Recessive Congenital Methemoglobinemia: Molecular Basis for Disease. Ph.D. dissertation, University of South Florida.
61. Rossmann, M.G.; Moras, D. and Olsen, K.W. (1974) Chemical and biological evolution of nucleotide-binding protein. *Nature*. **250**: pp. 194-9.
62. Sakuradani, E.; Kobayashi, M. and Shimizu, S. (1999) Identification of an NADH-cytochrome b(5) reductase gene from an arachidonic acid-producing fungus, *Mortierella alpina* 1S-4, by sequencing of the encoding cDNA and heterologous expression in a fungus, *Aspergillus oryzae*. *Appl. Environ. Microbiol.* **65**: 3873-79.
63. Barrell, B. and Rajandream, M.A. (1994) *GenBank* Direct Submission CAA86908.
64. Fukuchi-Mizutani, M.; Mizutani, M.; Tanaka, Y.; Kusumi, T. and Ohta, D. (1999) Microsomal electron transfer in higher plants: cloning and heterologous expression of NADH-cytochrome b_5 reductase from *Arabidopsis*, *Plant Physiol*. **119**: pp.353-62.
65. Kamath, R.S.; Fraser, A.G.; Dong, Y.; Poulin, G.; Durbin, R.; Gotta, M.; Kanapin, A.; Le Bot, N.; Moreno, S.; Sohrmann, M.; Welchman, D.P.; Zipperlen, P. and Ahringer, J. (2003) Systematic functional analysis of the *Caenorhabditis elegans* genome using RNAi, *Nature* **421**: pp. 231-7.
66. Adams, M.D.; Celniker, S.E.; Gibbs, R.A.; Rubin, G.M. and Venter, C.J. (2000) *GenBank* Direct Submission NM_168479.
67. Strausberg, R. (2003) *GenBank* Direct Submission BC045880.
68. Klein, S.L.; Strausberg, R.L.; Wagner, L.; Pontius, J.; Clifton, S.W. and Richardson, P. (2002) Genetic and genomic tools for *Xenopus* research: The NIH *Xenopus* initiative, *Dev. Dyn.* **225**: pp. 384-91.
69. Boardman, P.E.; Bonfield, J.K.; Brown, W.R.A.; Carder, C.; Chalk, S.E.; Croning, M.D.R.; Davies, R.M.; Francis, M.D.; Grafham, D.V.; Hubbard, S.J.; Humphray, S.J.; Hunt, P.J.; Maddison, M.; McLaren, S.R.; Niblett, D.; Overton, I.M.; Rogers, J.; Scott, C.E.; Taylor, R.G.; Tickle, C. and Wilson, S.A. (2004) *GenBank* Direct Submission BX950830.
70. Pietrini, G.; Carrera, P. and Borgese, N. (1988) Two transcripts encode rat cytochrome b_5 reductase, *Proc. Natl. Acad. Sci. U.S.A.* **85**: pp. 7246-50.
71. Yubisui, T.; Naitoh, Y.; Zenno, S.; Tamura, M.; Takeshita, M. and Sakaki, Y. (1987) Molecular cloning of cDNAs of human liver and placenta NADH-cytochrome b_5 reductase, *Proc. Natl. Acad. Sci. U.S.A.* **84**: pp. 3609-13.
72. Carlton, J.M.; Angiuoli; S.V.; Carucci, D.J.; et. al. (2002) Genome sequence and comparative analysis of the model rodent malaria parasite *Plasmodium yoelii yoelii*, *Nature* **419**: pp. 512-9.
73. Shirabe, K.; Yubisui, T. and Takeshita, M. (1989) Expression of human erythrocyte NADH-cytochrome b5 reductase as an alpha-thrombin-cleavable fused protein in *Escherichia coli*, *Biochem. Biophys. Acta*. **1008**: pp. 189-92.

74. Strittmatter, P.; Kittler, J.M.; Coghill, J.E. and Ozols, J. (1992) Characterization of lysyl residues of NADH-cytochrome b5 reductase implicated in charge-pairing with active-site carboxyl residues of cytochrome b5 by site-directed mutagenesis of an expression vector for the flavoprotein, *J Biol Chem* **267**: pp. 2519-23.
75. Barber, M. J. and Quinn, G. B. (1996) High-level expression in *Escherichia coli* of the soluble, catalytic domain of rat hepatic cytochrome b5 reductase, *Protein Expr. Purif.* **8**: pp. 41-7.
76. Higasa, K.; Manabe, J-I.; Yubisui, T.; Sumimoto, H.; Pung-Amritt, P.; Tanphaichitr, V.S.; and Fukumaki, Y. (1998) Molecular basis of hereditary methaemoglobinaemia, types I and II: two novel mutations in the NADH-cytochrome b5 reductase gene, *Br. J. Haematol*. **103**: pp. 922-30.
77. Karplus, P.A.; Daniels, M.J. and Herriott, J.R. (1991) Atomic structure of ferredoxin-NADP+ reductase: prototype for a structurally novel flavoenzyme family. *Science*. **251**: pp. 60-6.
78. Benson, D.A., et al. (1994) GenBank. *Nucleic Acids Res*. 1994. **22**: pp. 3441-4.
79. Prosser, I.M. and C.M. Lazarus. (1990) Nucleotide sequence of a spinach nitrate reductase cDNA. *Plant Mol Bio*l. **15**: pp. 187-90.
80. Newman, D.J.; Ihle, J.N. and Dure, L 3rd; (1969) Chemical composition of a ferredoxin isolated from cotton. *Biochem Biophys Res Commun*. **36**: pp. 947-50.
81. Haniu, M.; McManus, M.E.; Birkett, D.J.; Lee, T.D. and Shively J.E.. (1989) Structural and functional analysis of NADPH-cytochrome P-450 reductase from human liver: complete sequence of human enzyme and NADPH-binding sites. *Biochemistry*. **28**: pp. 8639-45.
82. Nakane, M.; Schmidt, H.H.; Pollock, J.S.; Förstermann, U. and Murad, F. (1993) Cloned human brain nitric oxide synthase is highly expressed in skeletal muscle. *FEBS Lett*. **316**: pp. 175-80.
83. Leclerc, D.; Wilson, A.; Dumas, R.; Gafuik, C.; Song, D.; Watkins, D.; Heng, H.H.; Rommens, J.M.; Scherer, S.W.; Rosenblatt, D.S. and Gravel, R.A. (1998) Cloning and mapping of a cDNA for methionine synthase reductase, a flavoprotein defective in patients with homocystinuria. *Proc Natl Acad Sci U S A*. **95**: pp. 3059-64.
84. Ostrowski, J.; Wu, J.Y.; Rueger, D.C.; Miller, B.E.; Siegel, L.M. and Kredich, N.M.. (1989) Characterization of the cysJIH regions of *Salmonella typhimurium* and *Escherichia coli* B. DNA sequences of cysI and cysH and a model for the siroheme-Fe4S4 active center of sulfite reductase hemoprotein based on amino acid homoloy with spinach nitrite reductase. *J Biol Chem*. **264**: pp. 15726-37.
85. Plamann, M.D. and G.V. Stauffer, (1983) Characterization of the *Escherichia coli* gene for serine hydroxymethyltransferase. *Gene*. **22**: pp. 9-18.
86. Davis, C.A.; Dhawan, I.K.; Johnson, M.K. and Barber, M.J. (2002) Heterologous expression of an endogenous rat cytochrome b(5)/cytochrome b(5) reductase fusion protein: identification of histidines 62 and 85 as the heme axial ligands. *Arch Biochem Biophys*. **400**: pp. 63-75.
87. Bosch, R.; Garcia-Valdes, E. and Moore E.R. (1999) Genetic characterization and evolutionary implications of a chromosomally encoded naphthalene-degradation upper pathway from *Pseudomonas stutzeri* AN10. *Gene*. **236**: pp. 149-57.

88. Nordlund, I., Powlowski, J. and Shingler, V. (1990) Complete nucleotide sequence and polypeptide analysis of multicomponent phenol hydroxylase from *Pseudomonas* sp. strain CF600. *J Bacteriol*. **172**: p. 6826-33.
89. Welch, R.A.; Burland V.; Blattner, F.R.; et al. (2002) Extensive mosaic structure revealed by the complete genome sequence of uropathogenic *Escherichia coli. Proc Natl Acad Sci U S A*. **99**: p. 17020-24.
90. Jiang, X.M.; Neal, B.; Santiago, F.; Lee, S.J.; Romana, L.K. and Reeves P.R. (1991) Structure and sequence of the rfb (O antigen) gene cluster of *Salmonella serovar typhimurium (strain LT2). Mol Microbiol*, 1991. **5**: pp. 695-713.
91. Eaton, R.W. (1996) p-Cumate catabolic pathway in *Pseudomonas putida* Fl: cloning and characterization of DNA carrying the *cmt* operon. *J Bacteriol*. **178**: pp. 1351-62.
92. James, K.D. and P.A. Williams. (1998) *ntn* genes determining the early steps in the divergent catabolism of 4-nitrotoluene and toluene in *Pseudomonas sp.* strain TW3. *J Bacteriol*. **180**: pp. 2043-49.
93. Trimboli, A.J.; Quinn, G.B.; Smith, E.T. and Barber, M.J. (1996) Thiol modification and site directed mutagenesis of the flavin domain of spinach NADH:nitrate reductase. *Arch Biochem Biophys*. **331**: pp. 117-26.
94. Stainthorpe, A.C., Lees, V.; Salmond, G.P.; Dalton, H. and Murrell, J.C. (1990) The methane monooxygenase gene cluster of *Methylococcus capsulatus* (Bath). *Gene*. **91**: pp. 27-34.
95. Bundy, B.M.; Campbell, A.L. and Neidle E.L. (1998) Similarities between the antABC-encoded anthranilate dioxygenase and the benABC-encoded benzoate dioxygenase of *Acinetobacter sp.* strain ADP1. *J Bacteriol*. **180**: pp. 4466-74.
96. Neidle, E.L.; Hartnett, C.; Ornston, L.N.; Bairoch, A.; Rekik, M. and Harayama, S. (1991) Nucleotide sequences of the *Acinetobacter calcoaceticus benABC* genes for benzoate 1,2-dioxygenase reveal evolutionary relationships among multicomponent oxygenases. *J Bacteriol*. **173**: pp. 5385-95.
97. Haak, B.; Fetzner, S. and Lingens, F. (1995) Cloning, nucleotide sequence, and expression of the plasmid-encoded genes for the two-component 2-halobenzoate 1,2-dioxygenase from *Pseudomonas cepacia* 2CBS. *J Bacteriol*. **177**: pp. 667-5.
98. Kalman, S.; Mitchell, W.; Marathe, R.; Lammel, C.; Fan, J.; Hyman, R.W.; Olinger, L.; Grimwood, J.; Davis, R.W.; and Stephens, R.S. (1999) Comparative genomes of *Chlamydia pneumoniae* and *C. trachomatis. Nat Genet.* **21**: pp. 385-9.
99. Kaneko, T.; et al. (2000) Complete genome structure of the nitrogen-fixing symbiotic bacterium *Mesorhizobium loti. DNA Res*. **7**: pp. 331-8.
100. Ng, W.V., et al., Genome sequence of *Halobacterium species* NRC-1. *Proc Natl Acad Sci U S A*. **97**: pp. 12176-81.
101. Zhou, N.Y.; Jenkins, A.; Chan Kwo Chio, C.K. and Leak, D.J. **(**1999). The alkene monooxygenase from *Xanthobacter* strain Py2 is closely related to aromatic monooxygenases and catalyzes aromatic monohydroxylation of benzene, toluene, and phenol. *Appl Environ Microbiol*. **65**: pp. 1589-95.
102. Marohnic, C.C. and Barber M.J. (2001) Arginine 91 is not essential for flavin incorporation in hepatic cytochrome b(5) reductase. *Arch Biochem Biophys*. **389**: pp. 223-33.

103. Kirkness, E.F.; Bafna, V.; Halpern, A.L.; Levy, S.; Remington, K.; Rusch, D.B.; Delcher, A.L.; Pop, M.; Wang, W.; Fraser, C.M. and Venter, J.C. (2003) The Dog Genome: Survey Sequencing and Comparative Analysis, *Science* **301**: pp. 1898-903.
104. Shirabe, K.; Yubisui, T.; Nishino, T. and Takeshita, M. (1991) Role of cysteine residues in human NADH-cytochrome b_5 reductase studied by site-directed mutagenesis. Cys-273 and Cys-283 are located close to the NADH-binding site but are not catalytically essential. *J. Biol. Chem*. **266**: pp. 7531-36.
105. Crowley, Louis J. (2007) Structure-function studies of conserved sequence motifs of cytochrome b5 reductase. Ph.D. dissertation, University of South Florida. (Publication No. AAT 3260053).
106. Murataliev, M.B. and R. Feyereisen, (2000) Interaction of NADP(H) with oxidized and reduced P450 reductase during catalysis. Studies with nucleotide analogues. *Biochemistry*. **39**: pp 5066-74
107. Beck von Bodman, S., et al., (1986) Synthesis, bacterial expression, and mutagenesis of the gene coding for mammalian cytochrome b5. *Proc Natl Acad Sci U S A*. **83**: pp. 9443-7.
108. Laemmli, U.K. (1970) Cleavage of structural proteins during the assembly of the head of bacteriophage T4. *Nature*. **227**: pp. 680-5.
109. Turchin, A. and Lawler, J.F. Jr. (1999) The primer generator: a program that facilitates the selection of oligonucleotides for site-directed mutagenesis. *Biotechniques*. **26**: pp. 672-6.
110. Yuckenberg, P.D.; Witney, F.; Geisselsoder, J. and McClary, J. (1991) Site-directed in vitro mutagenesis using uracil-containing DNA and phagemid vectors. *Directed Mutagenesis: A Pratical Approach*, ed. M.J. McPherson. New York: Oxford University Press.
111. Schwede, T.; Kopp, J.; Guex, N. and Peitsch, M.C. (2003) SWISS-MODEL: an automated protein homology-modeling server. *Nucl. Acids Res*. **31**: pp. 3381-5.
112. Bando, S.; Takano, T.; Yubisui, T.; Shirabe, K.; Takeshita, M. and Nakagawa, A. (2004) Structure of human erythrocyte NADH-cytochrome b5 reductase, *Acta Crystallogr. D Biol. Crystallogr*. **60**: pp. 1929-1934.
113. Vriend, G. (1990) WHAT IF: A molecular modeling and drug design program, *J. Mol. Graph*. **8**: pp. 52-56.
114. Accelrys. *DS Viewer Pro Software suite*. 2004 [cited; http://www.accelrys.com].
115. Chen, G.C. and Yang, J.T. (1977) Two-point calibration of circular dichrometerwith d-10 camphorsulfonnic acid. *Anal. Letter*. **10**: pp. 1195-1207.
116. Sancho, J. and Gomez-Moreno, C. (1991) Interaction of ferredoxin-$NADP^+$ reductase from Anabaena with its substrates. *Arch Biochem Biophys*. **288**: pp.231-8.
117. Barber, M.J. and G.B. (2001) Quinn, Production of a recombinant hybrid hemoflavoprotein: engineering a functional NADH:cytochrome c reductase. *Protein Expr Purif*. **23**: pp. 348-58.
118. Massey, V. (1991) A simple method for the determination of redox potentials. *Flavins and Flavoproteins*, S.R. B. Curti, and G. Zanetti, Editor. de Gruyter: Berlin. pp. 59-66.

119. Kirkness, E.F.; Bafna, V.; Halpern, A.L.; Levy, S.; Remington, K.; Rusch, D.B.; Delcher, A.L.; Pop, M.; Wang, W.; Fraser, C.M. and Venter, J.C. (2003) The Dog Genome: Survey Sequencing and Comparative Analysis, *Science* **301**: pp. 1898-1903.
120. Benson, D.A.; Karsch-Mizrachi, I.; Lipman, D.J.; Ostell, J. and Wheeler, D.L. (2005) *Nucl. Acids Res.* **33**: pp. D34-D38.
121. Davis, C.A.; Crowley, L.J. and Barber, M.J. (2004) Cytochrome b5 reductase: the roles of the recessive congenital methemoglobinemia mutants, L148P, and R159*. *Arch Biochem Biophys*. **431**: pp. 233-44.
122. Marohnic, C.C.; Crowley, L.J.; Davis, C.A.; Smith, E.T. and Barber, M.J. (2005) Cytochrome b_5 reductase: Role of the *si*-face residues, proline 92 and tyrosine 93, in structure and catalysis, *Biochemistry* **44**: pp. 2449-61.
123. Bewley, M.C.; Davis, C.A.; Marohnic, C.C; Taormina, D. and Barber, M.J. (2003) The Structure of the S127P Mutant of Cytochrome *b*5 Reductase that Causes Methemoglobinemia Shows the AMP Moiety of the Flavin Occupying the Substrate Binding Site, *Biochemistry* **42**: pp. 13145-51.
124. Marohnic, C.C.; Bewley, M.C. and Barber, M.J. (2003) Engineering and characterization of a NADPH-utilizing cytochrome b5 reductase. *Biochemistry*. **42**: pp. 11170-82.
125. Roma, G.W.; Crowley, L.J.; Davis, C.A. and Barber, M.J. (2005), Mutagenesis of glycine 179 modulates both catalytic efficiency and reduced pyridine nucleotide specificity in cytochrome b_5 reductase, *Biochemistry* **44**: pp. 13467-76.
126. Trimboli, A.J. and Barber, M.J. (1994) Assimilatory nitrate reductase: Reduction and inhibition by NADH/NAD^+ analogs, *Arch. Biochem. Biophys*. **315**: pp. 48-53.
127. Hulo N.; Sigrist C.J.A.; Le Saux V.; Langendijk-Genevaux P.S.; Bordoli L.; Gattiker A.; De Castro E., Bucher P. and Bairoch A. (2004) Recent improvements to the PROSITE database. *Nucl. Acids Res*. **32**: pp. 134-7
128. Correll, C.C.; Ludwig, M.L.; Bruns, C.M. and Karplus, P.A. (1993) Structural prototypes for an extended family of flavoprotein reductases: Comparison of phthalate dioxygenase reductase with ferredoxin reductase and ferredoxin, *Prot. Sci.* **2**, 2112-2131.
129. M.J. Percy; McFerran, N.V. and Lappin, T.R.J. (2005) Disorders of oxidized haemoglobin *Blood Revs*. **19**: pp. 61–8.
130. Agar, N.S. and Harley, J.D. (1972) Erythrocitic methemoglobin reductases of various mammalian species *Experientia* **28:** pp. 1248–9.
131 Lo S.C.L. and Agar N.S. (1986) NADH-methemoglobulin reductase activity in the erythrocytes of newborn and adult mammals. *Experientia* **42**: pp. 1264–5.
132 Whittington, A.T.; Parkinson, A.L.; Spencer, P.B.S.; Grigg, G.; Hinds, L.; Gallagher, C.H.; Kuchel, P.W. and Agar, N.S. (1995) Comparitive study of the antioxidant defense systems in the erythrocytes of Australian marsupials and montremes *Comp. Biochem. Physiol*. **10C**: pp. 267–72.
133 Srivastava, S.; Alhomida, A.S.; Siddiqi, N.J.; Puri, S.K. and Pandey, V.C. (2002) Methemoglobin reductase activity and *in vitro* sensitivity towards oxidant induced methemoglobinemia in Swiss mice and Beagle dogs erythrocytes, *Mole. Cell. Biochem.* **232**: pp. 81-85.

134. Chen, L., et al. (1993) Purification and characterization of an NADH-rubredoxin oxidoreductase involved in the utilization of oxygen by Desulfovibrio gigas. *Eur J Biochem*. **216**: pp. 443-8.
135. Jenkins, M.M. and Prchal, J.T. (1996) A novel mutation found in the 3' domain of NADH-cytochrome b5 reductase in an African-American family with type I congenital methemoglobinemia. *Blood* **87**: pp. 2993–9
136. Dym, O. and Eisenberg, D. (2001) Sequence-structure analysis of FAD-containing proteins, *Prot. Sci.* **10**: pp. 1712-28.
137. Hahne,K.; Haucke,V.; Ramage,L. and Schatz,G. (1994) Incomplete arrest in the outer membrane sorts NADH-cytochrome b_5 reductase to two different submitochondrial compartments, *Cell* **79**: pp. 829-39.
138. Medina, M.; Luquita, A.; Tejero, J.; Hermoso, J.; Mayoral, T.; Sanz-Aparicio, J.; Grever, K. and Gomez-Moreno, C. (2001) Probing the determinants of coenzyme specificity in ferredoxin-$NADP^+$ reductase by site-directed mutagenesis, *J. Biol. Chem*. **276**: pp. 11902-12.
139. Müller, F. (1991) Free flavins: Syntheses, chemical and physical properties, *Chemistry and Biochemistry of Flavoenzymes Vol. 1*, (F. Müller editor), CRC Press, Boca Raton, 1-60
140. Kuchler, B.; Abdel-Ghany, A.G.; Bross, P.; Nandy, A.; Rasched, I. and Ghisla, S. (1999) Biochemical characterization of a variant human medium-chain acyl-CoA dehydrogenase with a disease-associated mutation localized in the active site, *Biochem. J.* **337**: pp. 225-30
141. Bateman, A., Coin, L., Durbin, R., Finn, R.D., Hollich, V., Griffiths-Jones, S., Khanna, A., Marshall, M., Moxon, S., Sonnhammer, E.L.L., Studholme, D.J., Yeats, C. and Eddy, S.R. (2004) The Pfam protein families database, *Nucl. Acids Res*. **32**: pp. D138-D141
142. Hermoso, J.A.; Mayoral, T.; Faro, M.; Gomez-Moreno, C.; Sanz-Aparicio, J. and Medina, M. (2002) Mechanisms of coenzyme recognition and binding revealed by crystal structural analysis of ferredoxin-$NADP^+$ reductase complexed with $NADP^+$, *J. Mol. Biol*. **319**: pp. 1133-42
143. Elmore, C. L. and Porter, T. D. (2002) Modification of the nucleotide cofactor-binding site of cytochrome P-450 reductase to enhance turnover with NADH *in vivo*, *J. Biol. Chem.* **277**: pp. 48960-4
144. Shiraishi, N.; Croy, C.; Kaur, J. and Campbell, W. H. (1998) Engineering of pyridine nucleotide specificity of nitrate reductase: Mutagenesis of recombinant cytochrome *b* reductase fragment of *Neurospora crassa* NADPH:Nitrate reductase, *Arch. Biochem. Biophys*. **358**: pp. 104-15
145. Barber, M. J. (2000) Altered pyridine nucleotide specificity of spinach nitrate reductase, *FASEB J.* **14**: pp. A1416
146. Serov, A. E., Popova, A. S., Fedorchuk, V. V. and Tishkov, V. I. (2002) Engineering of coenzyme specificity of formate dehydrogenase from *Saccharomyces cerevisiae*, *Biochem. J.* **367**: pp. 841-7
147. Dekker J., et. al. (2001) Seven new mutations in the nicotinamide adenine dinucleotide reduced–cytochrome *b*5 reductase gene leading to methemoglobinemia type I. *Blood.* **97**: pp1106-14

148. Kugler W., Pekrun A., Laspe P., Erdlenbruch B. and Lakomek M. (2001) Molecular Basis of Recessive Congenital Methemoglobinemia, Types I and II: Exon Skipping and Three Novel Missense Mutations in the NADH-Cytochrome b_5 Reductase (Diaphorase 1) Gene . *Human Mutation: Mutation in Brief.* pp. **402**
149. Higasa K., Manabe J. Yubisui T., Sumimoto H., Pung-Amritt P., Tanphaichitr V. S. and Fukumaki Y. (1998) Molecular basis of hereditary methaemoglobinaemia, types I and II: two novel mutations in the NADH-cytochrome b_5 reductase gene. *British Journal of Haematology.* **103**: pp. 922-30

APPENDICES

Appendix A

List of oligonucleotide primers used to generate the Y112, T116, Q210, and E212K variants. Nucleotides underlined and in bold encode the mutated bases generated to introduce the proper mutation. Silent mutations in italics add (+) or eliminate (-) the indicated restriction site.

Mutation	Primer Sequence (5'→ 3')	Restriction Site
Y112A*	GTG GTC AAG GTT ***GCA*** TTC AAG GAC ACG	+*Bsm* I
Y112D	GTG GTC AAG GTT ***G***AC TTC AAG GAC ACG	+*Hinc* II
Y112F*	GTG GTC AAG GTT T***T***C TTC AAG GAC ACG	+*Mbo* II
Y112H	GTG GTC AAG GTT ***C***AC TT*T* AA*A* GAC ACG	+*Dra* I
Y112L*	GTG GTC AAG GTT ***CT***C TTC AAG GAC ACG	+*Mbo* II
T116A	C TTC AAG GAC ***G***CG CAT CCC AAG	+*Hga* I
T116S*	GTT TAC TTC AAG GA*T* ***T***CG CAT CCC AAG	+*Tfi* I
Q210A*	CTT TTC GCC AAC ***GC***G TCC GAG AAA GAC	+*Afl* III
Q210R*	CTT TTC GCC AAC C***G***G TCC GAG AAA GAC	+*Age* I
Q210V*	CTT TTC GCC AAC ***GT***G TCC GAG AAA GAC	+*Afl* III
E212A	CC AAC CAG TCC G***C***G AAA GAC ATC C	+*Bst*U I
E212K*	GCC AAC CAG TCC ***A***A***A*** AAA GAC ATC CTG	-*Hpy*188I

Appendix B

List of oligonucleotide primers used to generate the A178, G179, G180, T181, G182, I183, T184, and P185 variants Nucleotides underlined and in bold encode the mutated bases generated to introduce the proper mutation. Silent mutations in italics add (+) or eliminate (-) the indicated restriction site.

Mutation	Primer Sequence (5'→ 3')	Restriction Site
A178T*	GTA GGC ATG ATC ACT GGA GGG ACA GGC	+*Bcl* I
A178V*	GTA GGC ATG ATT GTG GGA GGG ACA GGC	-*Hpy*CH4 V
G179A*	ATG ATT GCA GCT GGG ACA GGC ATC ACC	+*Pvu* II
G179P*	ATG ATT GCT CCA GGG ACA GGC ATC ACC	+*Bpm* I
G179T*	ATG ATT GCA ACC GGG ACA GGC ATC ACC	+*Nci* I
G179V*	ATG ATT GCC GTG GGG ACA GGC ATC ACC	+*Btg* I
G180A*	ATG ATT GCA GGA GCG ACA GGC ATC ACC	-*Mnl* I
G180P*	ATG ATT GCA GGA CCG ACA GGC ATC AC	+*Ava* II
T181A*	ATG ATT GCA GGA GGG GCA GGC ATC ACC	+*Mwo* I
T181I*	ATG ATT GCC GGA GGG TUC GGC ATC ACC	+*Msp* I
T181S*	ATG ATT GCC GGA GGG TCA GGC ATC ACC	+*Msp* I
G182A*	GCA GGA GGG ACA GCC ATC ACC CCA ATG	-*Sfa*N I
G182P	GCA GGA GGG ACA CCC ATC ACC CCA ATG	-*Sfa*N I
I183A*	GGA GGG ACA GGC GCC ACC CCA ATG CTG	-*Sfa*N I
I183F	GGA GGG ACA GGC TTC ACC CCA ATG CTG	-*Sfa*N I
I183L	GGA GGG ACA GGC CTC ACC CCA ATG CTG	-*Sfa*N I
I183M	GGA GGG ACA GGC ATG ACC CCA ATG CTG	-*Sfa*N I
T184A*	GGG ACA GGC ATC GCC CCA ATG CTG CAG	-*Msl* I
T184H	GG ACA GGC ATC CAC CCA ATG CTG C	-*Msl* I
T184S*	GGG ACA GGC ATC TCC CCA ATG CTG CAG	-*Msl* I
T184V	GGG ACA GGC ATC GTC CCA ATG CTG CAG	-*Msl* I
P185A*	GGG ACA GGC ATC ACC GCA ATG CTG CAG	+*Bsr*D I
P185G	GGG ACA GGC ATC ACC GGA ATG CTG CAG	+*Bsa*W I

Appendix C

List of oligonucleotide primers used to generate the C273, G274, P275, P276, P277, M278, A-insertion, and G-insertion variants Nucleotides underlined and in bold encode the mutated bases generated to introduce the proper mutation. Silent mutations in italics add (+) or eliminate (-) the indicated restriction site.

Mutation	Primer Sequence (5'→ 3')	Restriction Site
C273A*	CTG ATA CTG ATG **GC*G*** GGA CCC CCA CCG	+*Bsm*F I
C273M*	CTG ATA CTG ATG **AT*G*** GG*C* CC*A* CCA CCG	+*Apa* II
C273S*	CTG ATA CTG ATG ***A***G***C*** GGA CCC CCA CCG	+*Bsr*B I
G274A*	CTG ATA CTG ATG TGT G***C***A CCC CCA CCG	-*Ava* II
G274P*	CTG ATA CTG ATG TGT **CC**A CCC CC*G* CCG	-*Fau* I
G274S*	CTG AT*T* CTG ATG TGT **TC**A CCC CCA CCG	+*Tfi* I
P275A*	CTG ATG TGT GG*G* ***G***CC CCA CCG ATG ATC	+*Apa* I
P276A*	ATG TGT GGA CC*G* ***G***CA CCG ATG ATC CAG	-*Ban* I
P277A*	TGT GGA CCC CCA ***G***C***A*** ATG ATC CAG TTT	+*BsrD* I
M278A*	GGA CCC CCA CCG **GC**G AT*T* CAG TTT GCC	-*Tfi* I
A ins*	GGA CCC CCA CCG ***GCC*** ATG ATC CAG TTT	+*Eae* I
G ins*	GGA CCC CCA CCG ***GGC*** ATG ATC CAG TTT	+*Nci* I

ABOUT THE AUTHOR

Glenn William Roma was born Mount Vernon, NY and was raised in Hudson, Florida. With a predisposition to understanding science, Glenn embarked on a successful academic career, with the end goal of studying veterinary medicine. After graduating at the head of his high school class, Glenn attend the University of Florida in 1997 majoring in Microbiology and Cell Sciences. During his time there, he developed a strong interest in biochemistry as well as in education. He received a Bachelor of Science degree in Microbiology and Cell Science from the University of Florida in 2000, with minors in Chemistry and Zoology. Shortly after gradutating, Glenn began teaching high school chemistry and biology. He then decided to return to the world of academia and pursue his doctorate degree. He enrolled in the Graduate Program in Medical Sciences at the University of South Florida, College of Medicine in the Department of Biochemistry and Molecular Biology in 2003. He found a home in the lab of Michael Barber, D.Phil and has enjoyed a productive career as a graduate student under Dr. Barber's tutelage. Glenn hopes to attain an appointed position in a major university in the Pacific Northwest, or work in the developmental field of biotechnology.